

Harnessing Human Milk Oligosaccharides and Ellagic Acid Glycosides to Combat

Group B *Streptococcus*

By

Schuyler Ann Chambers

Dissertation

Submitted to the Faculty of the
Graduate School of Vanderbilt University
in partial fulfillment of the requirements

for the degree of

DOCTOR OF PHILOSOPHY

in

Chemistry

March 31st, 2021

Nashville, Tennessee

Approved:

Steven D. Townsend, Ph.D.

Brian O. Bachmann, Ph.D.

Gary A. Sulikowski, Ph.D.

Jennifer A. Gaddy, Ph.D.

For my grandparents Dudley, Jean, Richard, and Marilyn

And my parents Ron and Kristi

You all paved the way.

Acknowledgments

Scientific research advances our knowledge of the natural world and is only made possible through a vast network of curious and passionate scientists. I have been fortunate to work with so many of these individuals during my time at Vanderbilt and the completion of this dissertation is largely indebted to them. Over the last 5 years, my closest mentor and guide, Steve Townsend, has provided every opportunity and resource to enable my unfettered scientific inquisition. I am grateful for the relationship that we have developed; one of true scientific collaboration, wherein we can spit-ball, troubleshoot, and terminate experimental ideas that are good, bad, or ugly. My time within this lab has enabled some of the most intellectually independent and unencumbered scientific research I will ever conduct and I am truly thankful for this opportunity. My appreciation also extends to another close mentor and friend, Jennifer Gaddy, who has been integral in shaping much of my identity as a female STEM scientist. From her expertise, I have not only learned dozens of new scientific skills but have more importantly expanded the way in which I think about scientific problems and how to best support the scientists around me. I will sincerely miss our late-night discussions while counting GBS colonies, but remain grateful to have such a supportive and formidable mentor in my research family.

For each of the mentors I have studied alongside, there are dozens of other students who have also shaped my development as a chemist. First and foremost, one's personal advancement often comes due to challenge and encouragement from individuals more skilled. When I began my graduate program, Jamin Keith was precisely that force; a

scientist who challenged my knowledge and expectations, and skillfully taught me intricacies about carbohydrates and NMR. His expertise provided motivation and encouragement to improve my synthetic abilities and expand my knowledge. Especially in moments of failure or distress, Jamin always offered a helpful suggestion or just a pertinent hard rock song to play throughout the lab. I have overcome many challenges during my graduate studies due to his companionship and guidance. In a similar vein, Dorothy Ackerman, Kelly Craft, and Rebecca Moore have also been integral to my development and training as a microbiologist. The work developed within this dissertation would not be possible without their guidance and I am lucky to have learned so much from them. I will also look fondly on my time sharing a bench with the genius of Eric Huseman, another scientist and friend that has taught me an immeasurable amount. We have progressed through the struggles of graduate school alongside one another and because of that our relationship is one I will value long into the future. I know that I can seek his expertise out if I need a debrief of the most recent published literature or just the most recent Taylor Swift CD. The breadth of space between those two topics is what makes me grateful for our continued friendship.

There is also an unchallenged amount of support that has come from those in surrounding research areas and during my studies, the contributions of Jenna DeSousa and Callie Dulin have been immense. Together we have prepared for exams, lifted each other over research hurdles, and shared in academic triumphs, but all of this was only made possible due to our close friendship outside of Stevenson Center. I will cherish our adventures throughout the city of Nashville; from birthday celebrations, concerts, and girls' nights, to Halloween excursions and Christmas celebrations. Our friendship has hallmarked my

time in the city of Nashville and rest assured, we will be meeting here again in the near future to celebrate the completion of all of our doctoral studies.

While the support of scientists and friends has made my graduate studies a success, all of this work has been underpinned by the love of my family. My parents have enabled my continued education and unequivocally encouraged me to ask questions about my surroundings and do things that make me happy. Their guidance has cultivated my thoughtfulness and skills as a leader; two traits that have been integral to my perseverance and success in scientific research. Because of them and countless others, I look upon my time within graduate school as a wonderful experience of independent research and personal growth.

For all of the support, love, guidance, and mentorship, I sincerely thank you all.

Table of Contents

	Page
Dedication.....	ii
Acknowledgments.....	iii
List of Tables	xii
List of Figures	xiv
List of Schemes	xix
List of Abbreviations.....	xx
 Chapter	
1. Group B <i>Streptococcus</i> : clinical manifestations, virulence, and preventative treatments	1
1.1 Abstract.....	1
1.2 <i>Streptococcus</i> : a bacterium ubiquitous in human health	1
1.3 Group B <i>Streptococcus</i> : an introduction.....	3
1.4 GBS transmission	4
1.4.1 Introduction.....	4
1.4.2 Infant GBS early onset disease (EOD).....	5
1.4.3 Infant GBS late onset disease (LOD)	6
1.5 Clinical burden of GBS infections.....	6
1.6 GBS virulence: key components and regulatory mechanisms	8
1.6.1 GBS virulence factors: an introduction	8

1.6.2 GBS biofilms: a contributing factor to GBS virulence.....	10
1.6.3 GBS virulence regulation via two-component systems.....	11
1.7 Antibiotic preventions for GBS infections	13
1.7.1 Introduction: relevant antibiotic structures and mechanisms of action	13
1.7.2 Antibiotic prophylaxis to prevent GBS transmission	16
1.7.3 Current limitations of antibiotic treatments.....	17
1.8 Purpose of dissertation	18
1.9 References.....	19
2. Synthesis and application of ellagic acid glycosides in preventing group B <i>Streptococcus</i> biofilm formation	28
2.1 Abstract.....	28
2.2 Ellagitannin natural products	28
2.3 Biological activity of ellagitannins	32
2.3.1 Introduction.....	32
2.3.2 Antibacterial activity of ellagitannins	33
2.3.3 Fontaine synthesis of EA glycosides	35
2.4 Synthesis of EA glycosides	36
2.4.1 Rationale and retrosynthesis	36
2.4.2 Total synthesis of EA glycosides	37
2.5 Biological activity of synthetic EA glycosides	42
2.5.1 Antibacterial activity of EA glycosides against GBS	42
2.5.2 Visualization of EA glycoside-mediated effects on GBS biofilms.....	44

2.5.3 Antibacterial activity of EA glycosides against ESKAPE pathogens	46
2.6 Conclusion and future directions	48
2.7 Experimental methods	49
2.8 References	64
Appendix A2: Data and NMR spectra relevant to Chapter 2	69
3. Human milk oligosaccharides as antibiotic adjuvants against group B <i>Streptococcus</i>	101
3.1 Abstract	101
3.2 Human milk oligosaccharides	101
3.2.1 Macromolecular composition of human breast milk	101
3.2.2 Chemical structure and biosynthesis of HMOs	102
3.3 Biological activity of HMOs: previous studies	106
3.3.1 HMOs as prebiotics	106
3.3.2 HMOs as antimicrobials	108
3.3.3 Antibacterial activity of HMOs against GBS	109
3.4 HMOs as antibiotic adjuvants	109
3.4.1 Previous studies	109
3.4.2 Expanded study	111
3.5 HMO-TMP combination as a powerful tool to combat antifolate resistance	113
3.5.1 Bacterial folate biosynthesis	113
3.5.2 Bacterial resistance to TMP	116

3.5.3 HMO-TMP combination treatment is efficacious across GBS serotypes.....	117
3.5.4 HMO-TMP is a synergistic antibiotic combination.....	118
3.5.5 HMO-TMP and the folate biosynthetic pathway.....	118
3.6 HMO-TMP activity is facilitated through CovRS TCS.....	119
3.6.1 CovRS: an introduction.....	119
3.6.2 CovRS is implicated in the antibiotic synergy of HMO-TMP	120
3.7 Conclusion and future directions.....	122
3.8 Experimental methods	124
3.9 References.....	128
4. Metabolomic interrogation of HMO-mediated antibacterial activity in group B Streptococcus.....	134
4.1 Abstract.....	134
4.2 Bacterial metabolism: an overview.....	134
4.3 Metabolomic analyses as methods for determining antibiotic mechanism of action	135
4.4 Metabolomic analysis of HMO-induced perturbations in GBS: experimental design and rational.....	136
4.5 GBS metabolic pathways perturbed upon HMO treatment	138
4.5.1 Global metabolic pathway analysis.....	138
4.5.2 HMO-mediated perturbations to linoleic acid metabolites.....	139
4.5.2.1 Introduction: bacterial fatty acid synthesis and utilization of linoleic acid	139
4.5.2.2 Impact of HMOs on linoleic acid metabolites	140

4.5.3 HMO-induced perturbations to GBS glycerophospholipid metabolism	143
4.5.3.1 Introduction: bacterial glycerophospholipid metabolism...	143
4.5.3.2 Impact of HMOs on GBS glycerophospholipid metabolism	145
4.5.4 Other HMO-induced changes to GBS metabolism	148
4.6 Conclusion and future directions	149
4.7 Experimental methods	151
4.8 References	155
Appendix A4: Supplementary metabolomics figures relevant to Chapter 4	159
5. Chemoproteomic target identification of human milk oligosaccharides in group B <i>Streptococcus</i>	167
5.1 Abstract	167
5.2 Chemoproteomic target identification	167
5.2.1 Using chemical biology to interrogate antibiotic mechanism of action: an introduction	167
5.2.2 Molecular probes for target ID	168
5.3 Proposed workflow for using target ID to identify HMO interactions with GBS	171
5.4 Rationale and design of HMO bioorthogonal probes	173
5.4.1 Identification of antibacterial single-entity HMOs	173
5.4.2 Design of bioorthogonal HMO probes	175
5.5 Kochetkov amination of HMOs	177
5.6 Synthesis of diazirine-containing HMO bioorthogonal probes	179

5.7 Expansion of methodology: synthesis of additional HMO bioorthogonal tool compounds.....	182
5.8 Validation of antibacterial properties of HMO probes	183
5.9 Conclusion and future directions	185
5.10 Experimental methods	187
5.11 References.....	201
Appendix A5: Data and NMR spectra relevant to Chapter 5.....	207
6. Summary: dissertation findings and future perspectives	253

List of Tables

	Page
1.1 Clinically relevant <i>Streptococcus</i> strains and affiliated infections	2
1.2 Disease outcomes for maternal GBS colonization, 2015	7
1.3 Key GBS virulence factors	9
1.4 General antibiotic classes and respective bacterial targets	13
2.1 MIC and MBIC of EA glycosides in GBS strains	43
2.2 Growth inhibition of EA glycosides against additional pathogens	47
2.3 Bacterial strains	59
3.1 Select HMO structures and corresponding SNFG	104
3.2 Inhibitory activity of pooled HMOs against GBS	109
3.3 Initial HMO-antibiotic combination study	110
3.4 Expanded HMO-antibiotic combination study	112
3.5 HMO-TMP combination treatment across GBS strains.....	117
3.6 HMO-TMP treatment in the presence of thymidine	119
3.7 HMO and HMO-TMP activity within Δ CovRS mutants	121
3.8 Bacterial strains	124
4.1 Pathway analysis of perturbed GBS metabolites	139

A4.1 Quality metrics obtained for the heavy labeled standard molecules used for this study to assess the metabolite extraction, instrument performance and injection volume reproducibility.....	160
A4.2 Data table of linoleic acid metabolites	161
A4.3 Data table of glycerophospholipid metabolites	163
A4.4 Data table of cell wall metabolites	166
5.1 Single-entity HMO antibacterial activity.....	174

List of Figures

	Page
1.1 Chemical structures of GBS CPS repeating units.....	4
1.2 Worldwide distribution of GBS disease and burden.....	8
1.3 Lifecycle of <i>Streptococcus</i> biofilm.....	11
1.4 Conceptual model of bacterial TCS.....	12
1.5 Antibiotic structures and molecular class.....	14
1.6 IAP treatment decision making workflow.....	17
2.1 Ellagitannin structures.....	29
2.2 Impact of 220D-F2 on <i>S. aureus</i> biofilm as assessed by confocal microscopy.....	34
2.3 Proposed structures of active constituents in isolate 220D-F2.....	34
2.4 Antibiofilm activity of EA glycosides.....	44
2.5 Scanning electron micrographs GB590 biofilm formation in THB after 24 h.....	45
A2.1 ¹ H NMR (400 MHz, CDCl ₃) of 2.39	70
A2.2 ¹³ C NMR (101 MHz, CDCl ₃) of 2.39	71
A2.3 ¹ H NMR (400 MHz, CDCl ₃) of 2.40	72
A2.4 ¹³ C NMR (101 MHz, CDCl ₃) of 2.40	73
A2.5 ¹ H NMR (400 MHz, CDCl ₃) of 2.41	74
A2.6 ¹³ C NMR (101 MHz, CDCl ₃) of 2.41	75
A2.7 ¹ H NMR (400 MHz, CDCl ₃) of 2.44	76
A2.8 ¹³ C NMR (151 MHz, CDCl ₃) of 2.44	77
A2.9 ¹ H NMR (400 MHz, CDCl ₃) of 2.45	78

A2.10 ^{13}C NMR (151 MHz, CDCl_3) of 2.45	79
A2.11 ^1H NMR (400 MHz, CDCl_3) of 2.46	80
A2.12 ^{13}C NMR (151 MHz, CDCl_3) of 2.46	81
A2.13 ^1H NMR (600 MHz, $\text{d}_6\text{-DMSO}$) of 2.34	82
A2.14 ^{13}C NMR (151 MHz, $\text{d}_6\text{-DMSO}$) of 2.34	83
A2.15 HSQC (600 MHz, $\text{d}_6\text{-DMSO}$) of 2.34	84
A2.16 COSY (600 MHz, $\text{d}_6\text{-DMSO}$) of 2.34	85
A2.17 HMBC (600 MHz, $\text{d}_6\text{-DMSO}$) of 2.34	86
A2.18 ^1H NMR (600 MHz, $\text{d}_6\text{-DMSO}$) of 2.47	87
A2.19 ^{13}C NMR (151 MHz, $\text{d}_6\text{-DMSO}$) of 2.47	88
A2.20 HSQC (600 MHz, $\text{d}_6\text{-DMSO}$) of 2.47	89
A2.21 COSY (600 MHz, $\text{d}_6\text{-DMSO}$) of 2.47	90
A2.22 HMBC (600 MHz, $\text{d}_6\text{-DMSO}$) of 2.47	91
A2.23 ^1H NMR (600 MHz, $\text{d}_6\text{-DMSO}$) of 2.35	92
A2.24 ^{13}C NMR (151 MHz, $\text{d}_6\text{-DMSO}$) of 2.35	93
A2.25 HSQC (600 MHz, $\text{d}_6\text{-DMSO}$) of 2.35	94
A2.26 COSY (600 MHz, $\text{d}_6\text{-DMSO}$) of 2.35	95
A2.27 HMBC (600 MHz, $\text{d}_6\text{-DMSO}$) of 2.35	96
A2.28 CIF/PLATON report for 2.44	97
3.1 Macromolecular composition of human breast milk	102
3.2 Monosaccharides used in HMO biosynthesis and corresponding SNFG.....	103
3.3 Schematic representation of HMO biosynthesis	103
3.4 CovRS conceptual model	120

4.1 Accumulations of pentose phosphate pathway metabolites caused by pretomanid	136
4.2 Pairwise comparisons of experimental conditions and significantly perturbed metabolites	138
4.3 Heat-map representation of linoleic acid metabolites.....	142
4.4 Representative structures of relevant LNA metabolites	143
4.5 Representative structures of relevant glycerophospholipid metabolites.....	146
4.6 Heat map representation of glycerophospholipid metabolites.....	147
4.7 Heat map representation of cell wall metabolites from HILIC positive LC- MS/MS analysis.....	149
A4.1 Global principal component analysis of the two different experimental sample groups.....	160
A4.2 Linoleic acid pathway	162
A4.3 Glycerophospholipid pathway.....	164
A4.4 Sphingolipid pathway.....	165
5.1 General molecular scaffold and functional groups useful in target ID studies.....	169
5.2 Proposed general workflow for chemoproteomic target ID of HMOs in GBS.....	172
5.3 General proposed HMO probe scaffold including HMOs and bioorthogonal tags of interest.....	177
5.4 Growth curves of single-entity HMOs and HMO probes in GB590 when dosed at ~5 mg mL ⁻¹	184
A5.1 ¹ H NMR (600 MHz, D ₂ O) of 5.28	208
A5.2 ¹³ C NMR (151 MHz, D ₂ O) of 5.28	209
A5.3 ¹ H NMR (600 MHz, D ₂ O) of 5.29	210

A5.4 ^{13}C NMR (151 MHz, D_2O) of 5.29	211
A5.5 ^1H NMR (600 MHz, D_2O) of 5.30	212
A5.6 ^{13}C NMR (151 MHz, D_2O) of 5.30	213
A5.7 ^1H NMR (600 MHz, D_2O) of 5.31	214
A5.8 ^{13}C NMR (151 MHz, D_2O) of 5.31	215
A5.9 ^1H NMR (600 MHz, D_2O) of 5.32	216
A5.10 ^{13}C NMR (151 MHz, D_2O) of 5.32	217
A5.11 ^1H NMR (600 MHz, D_2O) of 5.39	218
A5.12 ^{13}C NMR (151 MHz, D_2O) of 5.39	219
A5.13 HSQC (600 MHz, D_2O) of 5.39	220
A5.14 COSY (600 MHz, D_2O) of 5.39	221
A5.15 HMBC (600 MHz, D_2O) of 5.39	222
A5.16 ^1H NMR (600 MHz, D_2O) of 5.40	223
A5.17 ^{13}C NMR (151 MHz, D_2O) of 5.40	224
A5.18 HSQC (600 MHz, D_2O) of 5.40	225
A5.19 COSY (600 MHz, D_2O) of 5.40	226
A5.20 HMBC (600 MHz, D_2O) of 5.40	227
A5.21 ^1H NMR (600 MHz, D_2O) of 5.41	228
A5.22 ^{13}C NMR (151 MHz, D_2O) of 5.41	229
A5.23 HSQC (600 MHz, D_2O) of 5.41	230
A5.24 COSY (600 MHz, D_2O) of 5.41	231
A5.25 HMBC (600 MHz, D_2O) of 5.41	232
A5.26 ^1H NMR (600 MHz, D_2O) of 5.42	233
A5.27 ^{13}C NMR (151 MHz, D_2O) of 5.42	234

A5.28 HSQC (600 MHz, D ₂ O) of 5.42	235
A5.29 COSY (600 MHz, D ₂ O) of 5.42	236
A5.30 HMBC (600 MHz, D ₂ O) of 5.42	237
A5.31 ¹ H NMR (600 MHz, D ₂ O) of 5.43	238
A5.32 ¹³ C NMR (151 MHz, D ₂ O) of 5.43	239
A5.33 HSQC (600 MHz, D ₂ O) of 5.43	240
A5.34 COSY (600 MHz, D ₂ O) of 5.43	241
A5.35 HMBC (600 MHz, D ₂ O) of 5.43	242
A5.36 ¹ H NMR (600 MHz, MeOD) of 5.44	243
A5.37 ¹³ C NMR (151 MHz, MeOD) of 5.44	244
A5.38 ¹ H NMR (600 MHz, MeOD) of 5.45	245
A5.39 ¹³ C NMR (151 MHz, MeOD) of 5.45	246
A5.40 ¹ H NMR (600 MHz, MeOD) of 5.46	247
A5.41 ¹³ C NMR (151 MHz, MeOD) of 5.46	248
A5.42 ¹ H NMR (600 MHz, MeOD) of 5.47	249
A5.43 HSQC (600 MHz, MeOD) of 5.47	250
A5.44 Viability was assessed by enumeration of CFU mL ⁻¹ performed at 0, 2, 4, 6, 8, and 24 h.....	251
A5.45 Effects of single-entity HMO and HMO probes at ~5 mg mL ⁻¹ on GBS biofilm production in THB after 24 h of growth.....	252

List of Schemes

	Page
2.1 Representative biosynthesis of gallotannin and ellagitannin natural products	31
2.2 Metabolism of EA to urolithins	33
2.3 Fontaine synthesis of EA glycosides.....	35
2.4 Retrosynthetic analysis of EA glycosides.....	37
2.5 Synthesis of EA acceptor 2.41	38
2.6 Initial glycosylation screen with xylosyl donors and EA acceptor 2.41	39
2.7 Successful glycosylation of EA glycosides and X-ray crystallography verification of 1,2- <i>trans</i> stereochemistry	41
2.8 Final deprotection of EA glycosides	42
3.1 HMO metabolism and conversion to SCFAs by <i>Bifidobacterium</i>	107
3.2 Bacterial folate biosynthetic pathway	114
3.3 Tetrahydrofolate as a cofactor in dTMP biosynthesis	115
4.1 Biosynthesis of phosphoglycerides	144
5.1 Activation of various photoactivatable groups	170
5.2 Mechanism of the Kochetkov amination	178
5.3 Kochetkov amination of HMOs	179
5.4 Synthesis of minimalistic diazirine tag 5.37	180
5.5 Synthesis of diazirine-appended bioorthogonal HMO probes	181
5.6 Synthesis of additional HMO bioorthogonal tool compounds.....	183

List of Abbreviations

2'-FL	2'-fucosyllactose
3-FL	3-fucosyllactose
3'-SL	3'-sialyllactose
6'-SL	6'-sialyllactose
AckA	acetate kinase
ACN / MeCN	acetonitrile
AcOH	acetic acid
Adh2	aldehyde-alcohol dehydrogenase 2
ADP	adenosine diphosphate
AMP	antimicrobial peptide / adenosine monophosphate
ANOVA	analysis of variance
Ara	arabinose
ATCC	American Tissue Culture Collection
ATP	adenosine triphosphate
BCA	bicinchoninic acid
BODIPY	4,4-difluoro-4-bora-3a,4a-diaza-s-indacene
CAMBH	cation-adjusted Mueller Hinton broth
CAMP, cAMP	cyclic adenosine monophosphate
CFU	colony forming units
CHDS	CDP-diglyceride synthase
CIT	Vanderbilt Center for Innovative Technology
CL	cardiolipin
CLS	cardiolipin synthase
CLSI	Clinical and Laboratory Standards Institute
COADD	Community for Open Antimicrobial Drug Discovery
Cov	control of virulence
CPS	capsular polysaccharide
CV	coefficient of variance

DCM	dichloromethane
DDA	data dependent acquisition
Ddn	deazaflavin dependent nitroreductase
DFL	difucosyllactose
DHAP	dihydroxyacetone phosphate
DHFR	dihydrofolate reductase
DHFS	dihydrofolate synthase
DHPS	dihydropteroate synthase
DHQ	3-dehydroquinic acid
DiHOME	dihydroxyoctadecanoic acids
DIPEA	diisopropylethylamine
DMAP	4-dimethylaminopyridine
DMF	dimethylformamide
DMSO	dimethyl sulfoxide
DNA	deoxyribonucleic acid
DQD	dehydroquininate dehydratase
DSLNT	disialyllacto- <i>N</i> -tetraose
dTMP	deoxythymidine monophosphate
dUMP	deoxyuridine monophosphate
EA	ellagic acid
ECM	extracellular matrix
EDC	1-ethyl-3-(3-dimethylaminopropyl)carbodiimide
Eno	enolase
EOD	early onset disease
EpOMe	epoxyoctadecanoic acids
EPS	exopolysaccharide
erm	erythromycin ribosome methylation
EtOAc	ethyl acetate
F6PPK	fructose-6-phosphoketolase
FA	formic acid
FAS-II	fatty acid synthase type II

Fbs	fibrinogen-binding protein
FC	fold change
FIC	fractional inhibitory concentration
FR	fold reduction
Fuc	fucose
FucA	L-fuculose-1P aldolase
Fucl	fucose isomerase
FucK	fucose kinase
FUT	fucosyltransferase
G6DP	glucose-6-phosphate dehydrogenase
GA	gallic acid
Gal	galactose
GalK	galactokinase
GalM	galactose mutarotase
GAPDH	glyceraldehyde-3-phosphate dehydrogenase C
GBS	group B <i>Streptococcus</i> , <i>Streptococcus agalactiae</i> , Group B Strep
Glc	glucose
GlcNAc	<i>N</i> -acetylglucosamine
Glu	glutamate
GPAT	glycerol phosphate acyltransferase
Gpi	glucose 6-phosphate isomerase
Gpm	phosphoglycerate mutase
GT	glycosyl transferase
HATU	1-[bis(dimethylamino)methylene]-1H-1,2,3-triazolo[4,5- b]pyridinium 3-oxide hexafluorophosphate
HHDP	hexahydroxydiphenoyl
HILIC	hydrophilic interaction liquid chromatography
HIV	human immunodeficiency virus
HMDB	Human Metabolome Data Base
HMO	human milk oligosaccharide

HMO-TMP	HMO-trimethoprim
HOBT	hydroxybenzotriazole
HPLC	high-pressure liquid chromatography
HPPK	6-hydroxymethyl-7,8-dihydropterin pyrophosphokinase
HRMS	high-resolution mass spectrometry
i-PrOH	isopropanol
IAP	intrapartum antibiotic prophylaxis
IC	inhibitory concentration
ID	identification
ISC	intersystem crossing
Lac	lactose
LDA	lithium diisopropylamine
Ldh	lactate dehydrogenase
Le	Lewis
Lmb	laminin binding protein
LNA	linoleic acid
LNB	lacto- <i>N</i> -biose
LNBP	lacto- <i>N</i> -biose phosphorylase
LNFP-I	lacto- <i>N</i> -fucopentaose I
LNFP-II	lacto- <i>N</i> -fucopentaose II
LNFP-III	lacto- <i>N</i> -fucopentaose III
LNnT	lacto- <i>N</i> -neotetraose
LNT	lacto- <i>N</i> -tetraose
LNT-II	lacto- <i>N</i> -triose II
LOD	late onset disease
LRMS	low-resolution mass spectrometry
LSTa	LS-tetrasaccharide A
LSTb	LS-tetrasaccharide b
LTA	lipoteichoic acid
m.p.	melting point
MBIC	minimum biofilm inhibitory concentration

mef	macrolide efflux
MeOH	methanol
MIC	minimum inhibitory concentration
MOI	multiplicity of infection
MRSA	methicillin-resistant <i>Staphylococcus aureus</i>
MS/MS	tandem mass spectrometry / mass fragmentation
MSSA	methicillin-sensitive <i>Staphylococcus aureus</i>
MudPIT	multi-dimensional protein identification technology
NADPH	reduced nicotinamide adenine dinucleotide phosphate
NADPH+	oxidized nicotinamide adenine dinucleotide phosphate
NBS	<i>N</i> -bromosuccinimide
NEt ₃	triethylamine
NeuNAc	N-acetylneuraminic acid
NIST	National Institute of Standards and Technology
NMR	nuclear magnetic resonance
OD	optical density
OR	optical rotation
P / Pi	phosphate
PA	phosphatidic acid
pABA	<i>para</i> -aminobenzoic acid
PBP	penicillin-binding protein
PBS	phosphate buffered saline
PC	principal component
PE	phosphatidyl ethanolamine
Pfl	phosphate acetyl transferase
Pgk	phosphoglyceric kinase
Pgm	phosphoglucomutase
PGP	phosphatidylglycerolphosphate
PHSS	phosphatidylserine synthase
PPi	pyrophosphate
PPP	pentose phosphate pathway

PS	phosphatidyl serine
PSD	phosphatidylserine decarboxylase
PyClock	6-chloro-benzotriazole-1-yloxy-tris-pyrrolidinophosphonium hexafluorophosphate
Pyk	pyruvate kinase
QC	quality control
RAE	reverse anomeric effect
Rha	rhamnose
RNA	ribonucleic acid
RPLC	reverse-phase liquid chromatography
RPM	rotations per minute
RT	room temperature
SCFA	short chain fatty acids
SDH	shikimate dehydrogenase
SDS	sodium dodecyl sulfate
SEM	scanning electron microscopy
SEM	standard error of the mean / scanning electron microscopy
SHMT	serine hydroxymethyltransferase
Sia	sialic acid
siglecs	sialic acid-binding immunoglobulin-like lectins
SILAC	stable isotope labeling with amino acids in cell culture
SNFG	symbol nomenclature for glycans
SodA	superoxide dismutase
Tal	transaldolase
TAMRA	tetramethylrhodamine
TASF	tris(dimethylamino)sulfonium difluorotrimethylsilicate
TBAB	tetra- <i>N</i> -butylammonium bromide
TBAF	tetra- <i>N</i> -butylammonium fluoride
TBAI	tetra- <i>N</i> -butylammonium iodide
TBS	<i>tert</i> -butyl dimethylsilyl
TCS	two-component signal transductions system

THB	Todd-Hewitt broth
TIPS	triisopropylsilyl
TLC	thin layer chromatography
TMP	trimethoprim
TMSOTf	trimethylsilyl trifluoromethanesulfonate
TpiA	triosephosphate isomerase
UgpA	UTP-glucose-1-phosphate uridylyltransferase
UTP	uridine 5'-triphosphate
UV	ultra-violet
Xyl	xylose
YPD	yeast extract-peptone dextrose
β-H	β-hemolysin

Chapter 1

Group B *Streptococcus*: clinical manifestations, virulence, and preventative treatments

1.1 Abstract

Group B *Streptococcus* is a bacterial pathogen associated with adverse pregnancy outcomes and is the leading cause of neonatal sepsis and meningitis. While this bacterium presents significant risk to infants, healthy adults are often passively colonized with Group B *Streptococcus* and this dual nature complicates prevention and treatment strategies associated with Group B streptococcal infections. This chapter will detail the healthcare burden of GBS infections, mechanisms by which GBS maintains virulence, and current antibiotic treatments and limitations.

1.2 *Streptococcus*: a bacterium ubiquitous in human health

The genus *Streptococcus* describes a subset of gram-positive bacteria that are integral to human health and capable of acting as both pathogen and commensal.^{1,2} Streptococci are non-motile, non-spore forming cocci that grow in pairs or chains. *Streptococcus* can be facultative or obligate anaerobes, adept at survival in low or no oxygen environments. Most streptococcal strains require enriched media for growth and some are prolific biofilm producers, that is they form dense extracellular matrix (ECM) to increase virulence. *Streptococcus* are classified according to Lancefield group, wherein strains are categorized according to cell wall affiliated carbohydrate composition.³ Clinically relevant streptococci and corresponding Lancefield serogroups are listed in **Table 1.1** where, most

notably, Group A *Streptococcus* is the leading contributor to upper-respiratory infections in humans and the common source for the diagnosis of “strep throat”. *S. pneumoniae* is frequently associated with lower-respiratory infections, particularly in the development of pneumonia. Group B *Streptococcus* predominantly acts as a commensal bacterium within healthy adults, but significantly contributes to neonatal infections. The increased burden of GBS infections within infants, makes it a primary interest of research within the area of neonatal health and wellness.

Table 1.1 Clinically relevant *Streptococcus* strains and affiliated infections

Type Species	Lancefield Serogroup	Typical Human Disease
<i>S. pyogenes</i>	A	pharyngitis
<i>S. agalactiae</i>	B	neonatal sepsis and meningitis
<i>S. equisimilis</i>	C	endocarditis, pneumonia, upper respiratory infection
<i>S. anginosus</i>	F,G ^a	subcutaneous or organ abscesses, endocarditis, upper respiratory infection
<i>S. sanguis</i>	H	endocarditis, caries
<i>S. salivarius</i>	K	endocarditis, caries
<i>S. mitis</i> , <i>S. mutans</i> “viridans” streptococci	non-Lancefield cocci	endocarditis, caries
<i>S. pneumoniae</i>	non-Lancefield cocci	pneumonia

^aHeterogeneous phenotypes

1.3 Group B Streptococcus: an introduction

Group B *Streptococcus* (*Streptococcus agalactiae*, Group B Strep, GBS) is a biofilm-producing facultative anaerobe. It is β -hemolytic, meaning these cocci produce streptolysin, an enzyme responsible for the complete lysis of red blood cells. This full hemolytic activity separates GBS from other streptococcal species and is also believed to be an important virulence factor for GBS (see section 1.6). From initial categorization according to hemolytic activity, GBS strains are further separated according to capsular polysaccharide (CPS) serotyping. Serotype is determined via the experimental reactivity of CPSs with antigens in immunological assays.⁴⁻⁷ There are currently nine known GBS serotypes, denoted as serotypes I-IX, with an additional classification between serotypes Ia and Ib. Structurally, these CPSs vary in monosaccharide composition, branching pattern, and types of glycosidic linkages (**Figure 1.1**). Of special note, is serotype VIII, that contains an L-rhamnose monosaccharide, unique among all other GBS serotypes.

Clinically, in North America, invasive GBS disease is primarily associated with serotypes I, III, and V, wherein these serotypes represent approximately 60-80% of isolates from clinical infections.^{7, 8} Prevalent serotypes can also differ across geographic regions. By example, serotypes II and IV were found to be among the most common within clinical isolates from Iran.^{9, 10} The CPS of GBS strains is believed to be a virulence factor for GBS infection (see section 1.6).

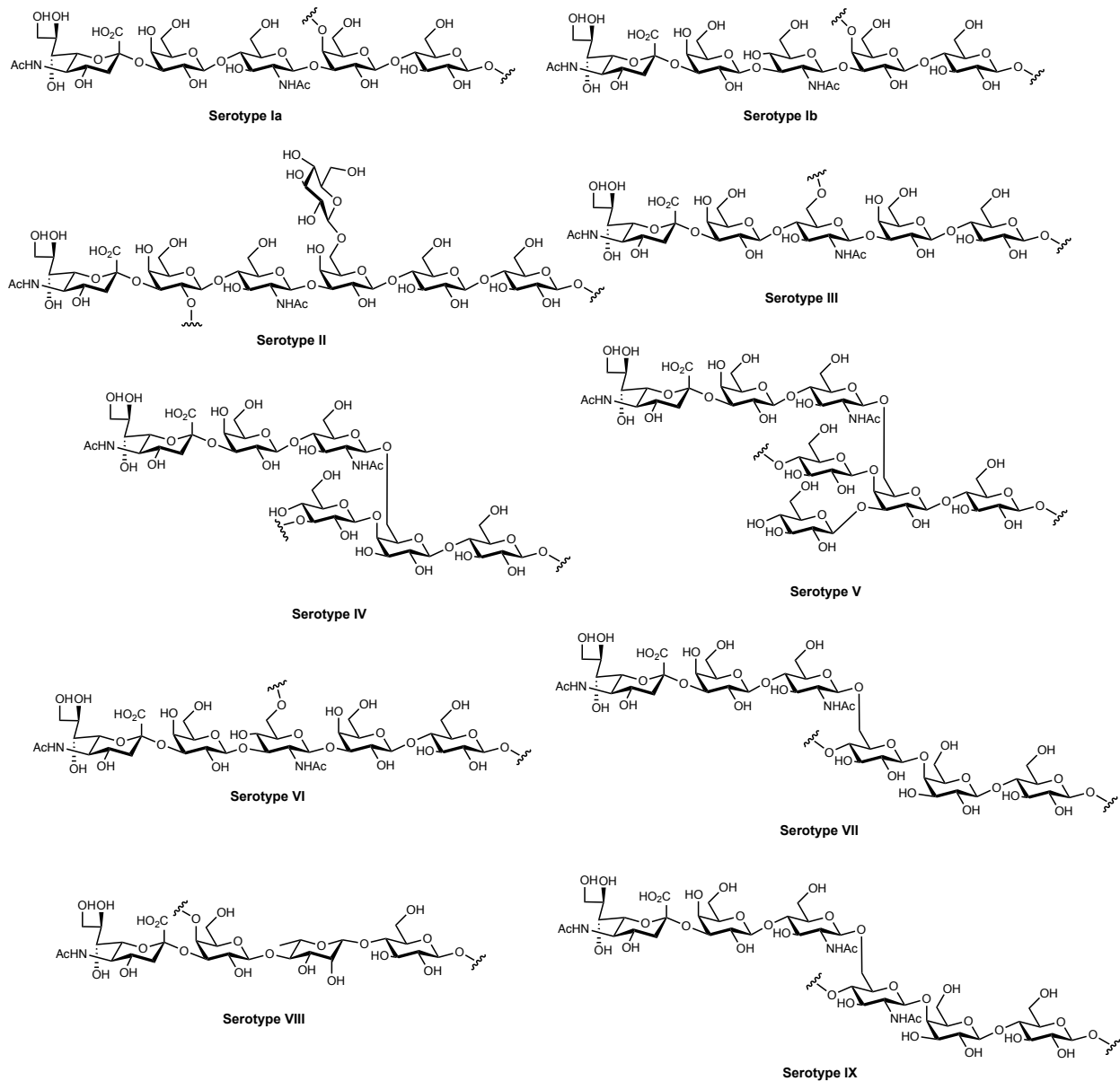


Figure 1.1 Chemical structures of GBS CPS repeating units

1.4 GBS transmission

1.4.1 Introduction

As GBS predominantly behaves as a commensal, many adults are passively colonized with GBS at some point in their lifetime without ever developing signs of infection.¹¹ Those adults most at risk for serious GBS infections include individuals who are

immunocompromised, are HIV-positive and/or have diabetes.^{12, 13} In contrast, infants are particularly susceptible to GBS infections due to their undeveloped immune system.

Critically, GBS transmission from adults to infants, both through vertical and horizontal mechanisms, significantly increases the risk of neonatal infection.¹⁴⁻¹⁶ GBS is a frequent colonizer of the maternal gastrointestinal and genital tracts, and approximately 20-30% of pregnant women will be vaginally colonized with GBS at some point during pregnancy.^{6,}

¹⁷ It is estimated that if untreated, 50% of their infants will then be colonized with GBS at birth and 1% will continue on to develop invasive GBS disease. Consequently, rectovaginal maternal colonization is the leading risk factor for infant GBS disease. This highlights a critical challenge in combating neonatal GBS infections. That is, detection and prevention of GBS transmission must be achieved amidst the commensal ubiquity of GBS in adults.

1.4.2 Infant GBS early onset disease (EOD)

Infant GBS early onset disease (EOD) is denoted by GBS infection acquired less than seven days after parturition. EOD represents approximately 60-70% of cases of GBS disease in infants and is predominantly associated with infections from GBS serotypes Ia, III, and V.¹⁸ EOD is typically acquired from GBS within the vaginal cavity that an infant is exposed to during labor or through ruptured membranes.¹⁹ These infections can ultimately lead to chorioamnionitis, meningitis, and neonatal sepsis. As such, EOD is associated with the highest rates of mortality for GBS infections.

1.4.3 Infant GBS late onset disease (LOD)

Late onset disease (LOD) is specific to GBS infection acquired anywhere from seven days to three months after birth. LOD is typically less fatal than EOD. LOD is predominantly associated with GBS serotype III, and LOD can be acquired multiple ways.²⁰⁻²² Skin-to-skin contact with mothers during breast feeding can contribute to LOD. Infants can also acquire GBS from external sources, such as infected surfaces, hospital settings, and contact with other adults and infants. There is also reason to believe that GBS can be transmitted through breast milk itself.²³⁻²⁶ However, only 1-3% of mothers have GBS within their breast milk and the relationship between GBS-containing breast milk and GBS colonization of infants is not fully understood.

1.5 Clinical burden of GBS infections

Globally, maternal GBS colonization is associated with approximately 3.5 million preterm births every year (**Table 1.2**).²⁷ Additionally, around 300,000 cases result in invasive GBS disease, with approximately 55,000 cases ultimately leading to stillbirth. Invasive GBS disease can cause chorioamnionitis, meningitis, and neonatal sepsis.²⁸⁻³² These outcomes can be fatal to infants or cause lasting neurological and developmental damage.

The highest rates of GBS-related adverse pregnancy outcomes are seen in low- to middle- income countries such as Africa and south Asia (**Figure 1.2**). These regions see higher rates of fetal infection, indicating clear geographical disparities in the prevention of GBS transmission. This is most likely attributed to lower rates of maternal GBS screening and use of antibiotic prophylaxis within these regions (see section 1.7). As such, there is

a need to develop preventative strategies that can be implemented more effectively in countries with limited healthcare resources.

Table 1.2 Disease outcomes for maternal GBS colonization, 2015 ²⁷

Factor	Details	Estimated Cases
GBS maternal colonization	isolation by culture of GBS from vagina, rectum or peri-anal region during pregnancy	21,734,000
preterm birth associated with maternal GBS colonization	delivery prior to 37 weeks' gestation were mother had GBS isolates	Up to 3.5 million
maternal GBS disease	isolation of GBS in pregnant or postpartum women with sepsis	33,000
stillbirth	birth of fetus with no signs of life and evidence of invasive GBs disease	57,000
infant GBS invasive disease	isolation of GBS from infant with signs of clinical disease	319,000

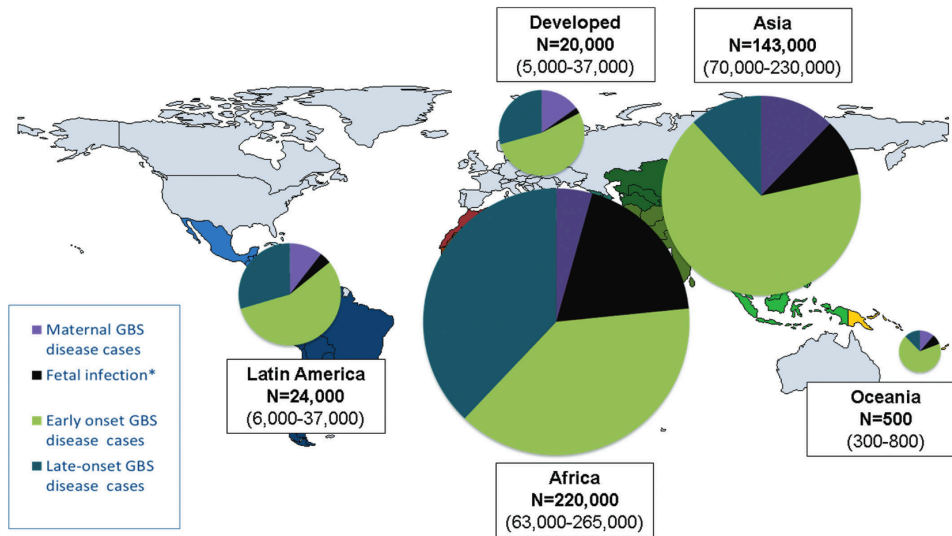


Figure 1.2 Worldwide distribution of GBS disease and burden²⁷

1.6 GBS virulence: key components and regulatory mechanisms

1.6.1 GBS virulence factors: an introduction

GBS has several key virulence factors that enable infectivity in humans (**Table 1.3**).^{33, 34}

A subset of GBS virulence factors are used to combat host-cells and the host immune response. Some GBS virulence factors promote host cell lysis, like β -hemolysin (β -H) and cyclic adenosine monophosphate (CAMP, cAMP) factor (Cfb). Other virulence factors directly engage the host immune response. By example, penicillin-binding protein 1a (PBP1a) promotes resistance to antimicrobial peptides (AMPs), and C5a peptidase impairs neutrophil recruitment.³⁵⁻⁴⁰

Another large category of GBS virulence factors are used to increase GBS adherence to host cells. Pili structures are one key component of GBS biofilm architecture (see section 1.6.2). These protein-derived fibers extend from the cell surface to catch and adhere to other bacteria or host cells. Additionally, the CPS itself can bind to host-derived sialic

acid-binding immunoglobulin-like lectins (siglecs) to promote adhesion.⁴¹⁻⁴³ These CPS-siglec interactions are one likely reason that some GBS serotypes cause more infections than others.

Table 1.3 Key GBS virulence factors

Virulence Factor Category	GBS examples	Function
pore forming toxins	β -hemolysin (β -H)	trigger host cell lysis
	CAMP factor (Cfb)	
resistance to AMPs	alanylation of LTA	decreases negative charge to repel AMPs
	PBP1a	creates resistance
host-cell adherence	pili	promotes adherence and biofilm
	fibrinogen-binding protein A and B (FbsA/FbsB)	binds to ECM fibrinogen
	laminin-binding protein (Lmb)	binds to ECM laminin
	immunogenic bacterial adhesin (BibA)	binds complement regulatory protein C4BP
	CPS	adheres to host cell siglecs
other	superoxide dismutase (SodA)	detoxifies singlet oxygen
	C5a peptidase (ScpB)	impairs neutrophil recruitment through cleavage of C5a

Fibrinogen-binding proteins A/B (FbsA/FbsB) and laminin binding proteins (Lmb) also contribute to GBS adhesion and virulence. These proteins bind to respective host-derived components and allow for direct interaction between microbe and host.^{33, 34, 44-47} Taken together, these virulence factors increase the ability of GBS to interact and adhere within a host, making it a dangerous pathogen to neonates.

1.6.2 GBS biofilms: a contributing factor to GBS virulence

Virulence components involved in GBS adherence are also integral in the formation of GBS biofilms.⁴⁸⁻⁵² Biofilm is a multi-bacterial architecture that is developed as planktonic cells adhere to host cells or abiotic surfaces (**Figure 1.3**). After initial surface adhesion, cells then use quorum sensing to aid in self-adherence and the development of three-dimensional bacterial architecture.^{49, 53} From here, cells generate ECM through the production and secretion of proteins, lipids, eDNA, and carbohydrates. In GBS, this includes the production of pili, CPS, and additional adhesin proteins. This ECM confers protection from antibiotic treatment and prevents clearance from host-derived immune cells. GBS biofilms are thought to play a key role in GBS infection and have been shown to become more robust in acidic environments such as the vaginal cavity.⁵⁴ Additionally, due to their heightened difficulty in elimination from medical devices, biofilm matrices are particularly associated with hospital-acquired infections and might have implications in the transmission of GBS to infants during labor and delivery in hospital settings.⁵⁵

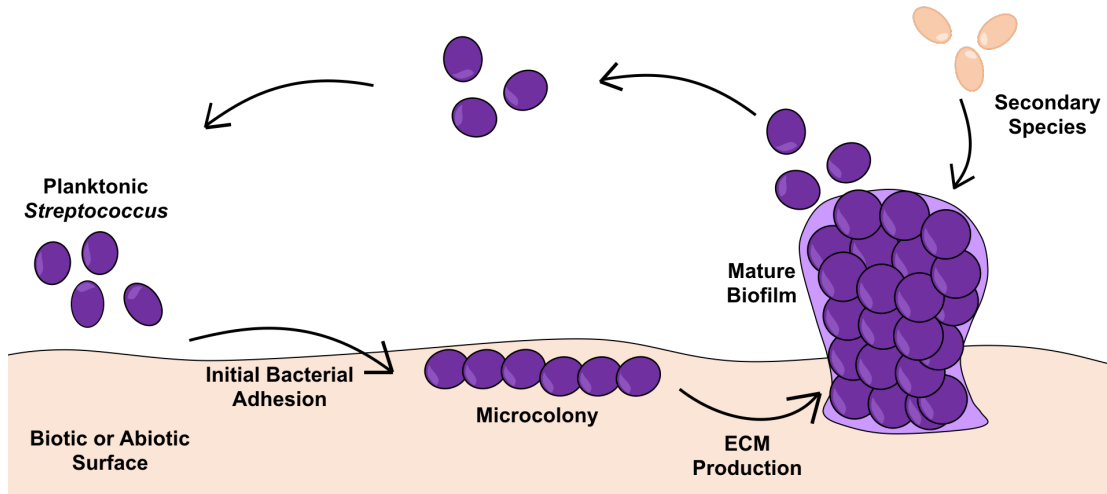


Figure 1.3 Lifecycle of *Streptococcus* biofilm

1.6.3 GBS virulence regulation via two-component systems

Virulence factors are regulated at the cellular level through multiple methods, but the most predominant regulatory mechanism in GBS is the use of two-component signal transduction systems (TCSs) (**Figure 1.4**).⁵⁶⁻⁵⁸ TCSs are responsible for sensing and responding to external signals. TCSs contain a trans-membrane histidine kinase component responsible for detecting external signal inputs. Common signals that are sensed by TCSs include availability of nutrients, external pH, antibiotic pressure, or other foreign bacterial metabolites. Upon detection of a signal, histidine phosphorylation then engages a response regulator component.⁵⁹ This component then facilitates changes in bacterial transcription, thereby, changing bacterial physiology as a response to the initial external signal.

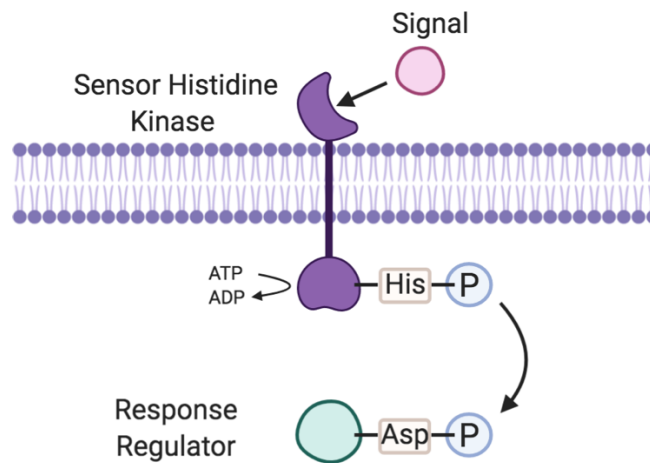


Figure 1.4 Conceptual model of bacterial TCS

Within GBS there are an estimated twenty TCSs, with the functions of only five having been thoroughly studied; CovRS (CsrRS), DltRS, RgfBC, FspRS, and CiaRH.^{58, 60-64} Of particular interest, is the CovRS system that is thought to be a global regulatory system for GBS, heavily involved in cellular regulation in both acidic and high-carbohydrate environments.⁶⁵⁻⁶⁸ Transcriptionally, CovRS regulation has been shown to impact over 100 genes, with predominant changes occurring to those that regulate cell envelope processes.^{60, 69, 70} These include genes implicated in cell wall processes, transport proteins and lipopeptides, as well as cell membrane bioenergetics. CovRS deletion mutants see significant downregulation in transcription of these genes. For these reasons, CovRS is believed to be a key TCS used to promote GBS virulence and pathogenesis.

1.7 Antibiotic preventions for GBS infections

1.7.1 Introduction: relevant antibiotic structures and mechanisms of action

Antibiotics are essential in the treatment of bacterial infections. For about a century, scientists have worked diligently to identify potent antibacterial compounds, their respective bacterial targets, and how to circumvent mechanisms of antibiotic resistance.

The most predominant classes of clinically used antibiotics today target or inhibit the biogenesis of essential bacterial components, such as the cell wall, cell membrane, proteins, DNA, RNA, and folate (**Table 1.4/Figure 1.5**).^{71, 72}

Table 1.4 General antibiotic classes and respective bacterial targets

Antibiotic Class	Example	Antibiotic Target
β -lactam	penicillin	penicillin-binding protein (cell wall)
glycopeptide	vancomycin	peptidoglycan and lipid II (cell wall)
antimicrobial peptide	polymyxin B	cell membrane
aminoglycoside	gentamicin	30S ribosomal subunit (protein synthesis)
macrolide	erythromycin	50S ribosomal subunit (protein synthesis)
oxazolidinone	linezolid	
tetracycline	minocycline	
lincosamide	clindamycin	
quinolone	ciprofloxacin	topoisomerase II (DNA replication)
sulfonamide	sulfadiazine	folate biosynthesis
rifamycin polyketide	rifampicin	RNA polymerase (RNA synthesis)
nitrofurantoin	nitrofurantoin	DNA synthesis

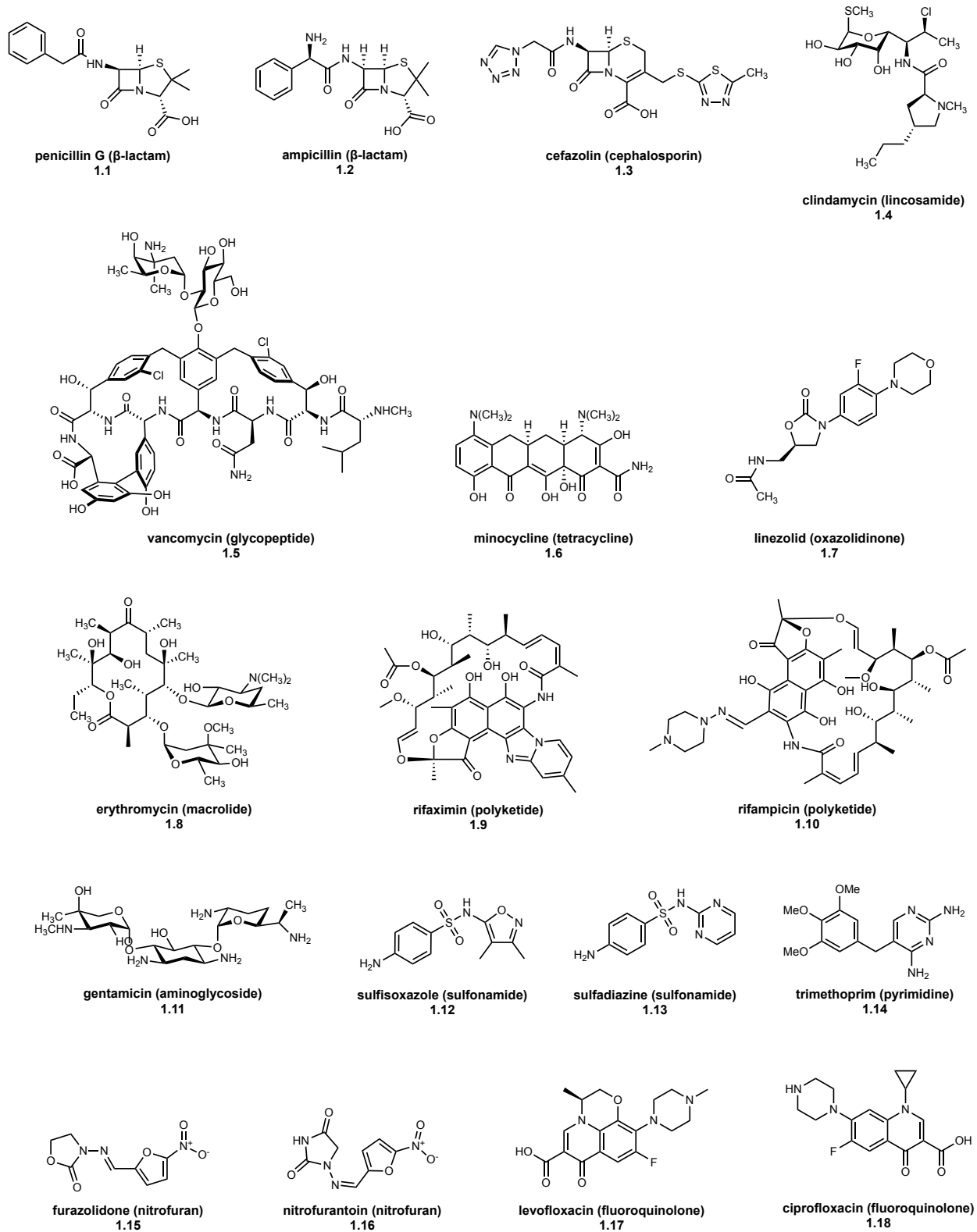


Figure 1.5 Antibiotic structures and molecular class

Briefly described, components within the cell envelope have been targeted for antibiotic interventions. Cell wall targeting antibiotics including penicillin (**1.1**), ampicillin (**1.2**), cefazolin (**1.3**), and vancomycin (**1.5**) have proved particularly efficacious in the treatment of gram-positive bacterial infections.⁷³⁻⁷⁵ Conversely, cell membrane targeting antibiotics like polymyxin B, are of specific use in combating gram-negative infections.

Another large subset of antibiotics inhibits the intracellular assembly of proteins via interactions with the bacterial ribosome.^{76, 77} Lincosamides, macrolides, oxazolidinones, and tetracyclines all interact at the 50S subunit of the ribosome. These classes include clinically used antibiotics such as clindamycin (**1.4**), minocycline (**1.6**), linezolid (**1.7**), and erythromycin (**1.8**).⁷⁸ Aminoglycosides such as gentamicin (**1.11**) impede protein synthesis through interaction with the 30S ribosomal subunit.^{79, 80} Antibiotics such as these can be used in the treatment of both gram-positive and gram-negative bacterial infections.

Aside from the ribosome, antibiotics can also target other intracellular processes. Several antibiotics target genomic materials. DNA synthesis and integrity can be altered by nitrofurans (**1.15** and **1.16**) and quinolones, such as ciprofloxacin (**1.18**).⁸¹⁻⁸³ Alternatively, RNA synthesis can be stunted by rifamycin polyketides like rifaximin (**1.9**) and rifampicin (**1.10**).⁸⁴ Another intracellular target of antibiotics is folate biosynthesis (see section 3.5).^{85, 86} Folate is required by bacterial cells to make nucleotides. Sulfonamides (**1.12** and **1.13**) and trimethoprim (**1.14**) are known to inhibit the folate biosynthetic pathway. Folate-targeting antibiotics and DNA/RNA targeting antibiotics can be used against both gram-positive and gram-negative bacterial infections. However, these classes are most

commonly used in the treatment of gram-positive species due to higher rates of cellular penetration and efficacy.

While only a brief introduction to the breadth and diversity of antibiotics, these represent some of the most important small molecules drugs of the last century. I direct interested readers further to the cited books, reviews, and perspectives for a more detailed study of antibiotic mechanisms of action and current drug development efforts.^{71, 72, 87-91}

1.7.2 Antibiotic prophylaxis to prevent GBS transmission

Antibiotics are the gold-standard of treatment for infectious GBS disease. Most commonly used are penicillin (**1.1**) and other β -lactams, clindamycin (**1.4**), and vancomycin (**1.5**). More importantly, these antibiotics are also used to prevent transmission of GBS. To prevent EOD, mothers are vaginally screened for GBS colonization during pregnancy around 36 weeks. Those that test positive for GBS are then administered intrapartum antibiotic prophylaxis (IAP) during labor to prevent transmission. The molecular nature of this treatment is decided based on maternal allergy considerations and GBS strain sequencing for resistance (**Figure 1.6**). IAP has been shown to prevent EOD with up to 90% efficiency, but there are significant limitations to these current antibiotic treatments.

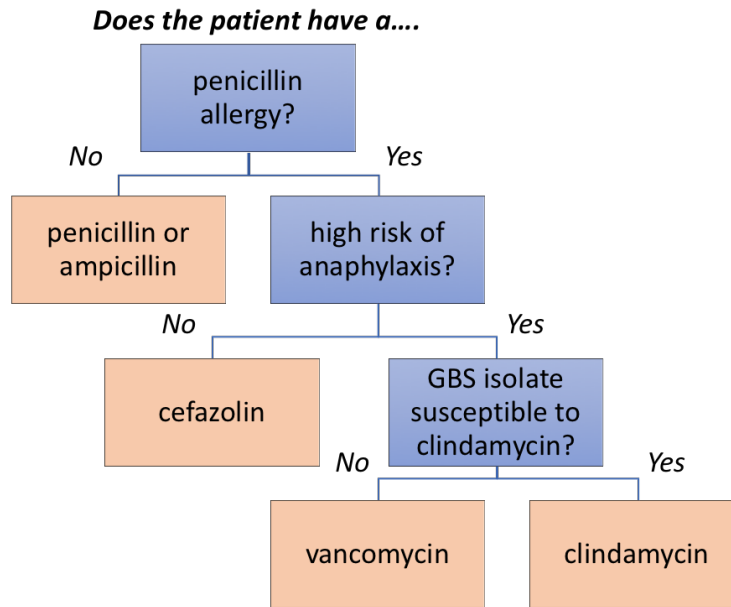


Figure 1.6 IAP treatment decision making workflow

1.7.3 Current limitations of antibiotic treatments

IAP is a powerful tool in the prevention of EOD, but it requires the universal screening of pregnant mothers for GBS colonization, followed by effective administration of an antibiotic during delivery. Both GBS screening and antibiotic administration needs to occur at their respective time-points to make IAP effective. Resultantly, resource-limited regions struggle to provide sufficient screening and treatment options to administer IAP universally and effectively. Since maternal GBS screening is also only conducted at one time-point, GBS colonization can be “missed” entirely, and therefore go untreated. Additionally, there is currently no good therapeutic method to prevent LOD.

With these considerations of therapeutic strategies, the use of antibiotics in any context is also plagued by the emergence of antibiotic resistance.⁹² Most significantly, GBS has developed resistance to clindamycin (1.4) in approximately 40% of clinical isolates and resistance to erythromycin (1.8) in approximately 50% of isolates.⁹³ This resistance can

be conferred via *erm* (erythromycin ribosome methylation) genes that decrease ribosomal binding affinity of the antibiotics, or through *mef* (macrolide efflux) genes that increase antibiotic efflux.⁹⁴ The rise of antibiotic resistance in GBS strains represents only a fraction of the global health crisis affiliated with the evolution of multi-drug resistant bacteria.^{72, 91, 95, 96}

Additionally, there is increased concern over habitual use of antibiotics due to their effects on commensal bacteria. The infant microbiome aids in the development of a healthy immune system, but there is speculation that antibiotic treatment can deter this development.⁹⁷⁻⁹⁹ IAP changes the microbiome of the mother and as a result, the infant. It has been demonstrated that neonates exposed to IAP exhibit lower colonization rates of healthy gut commensals such as bifidobacteria and lactobacilli.¹⁰⁰ Considering IAP-induced effects on the neonatal microbiome and ever-increasing rates of antibiotic resistance, there is clear and urgent need for novel GBS prevention and treatment strategies.

1.8 Purpose of dissertation

The dual nature of GBS as a harmless commensal in healthy adults, but a pathogenic danger to infants, complicates GBS detection, treatment, and prevention. Ever-increasing rates of antibiotic resistance also strengthens the necessity for novel molecular therapeutics, amenable in preventing neonatal GBS infection. This dissertation investigates novel antibiotic treatments for GBS infections. Both synthetic- and mammalian-derived carbohydrates and glycoconjugates are studied for use in inhibiting GBS growth, virulence, and biofilm formation. The synthesis and discovery of novel GBS

treatments will increase contributions towards bettering neonatal health and preventing infant mortality.

1.9 References

1. Parks, T.; Barrett, L.; Jones, N., Invasive streptococcal disease: a review for clinicians. *British Medical Bulletin* **2015**, *115* (1), 77-89.
2. Baron, S., *Medical Microbiology*. 4th Edition ed.; University of Texas Medical Branch, Department of Microbiology: 1997.
3. Facklam, R., What happened to the streptococci: overview of taxonomic and nomenclature changes. *Clinical microbiology reviews* **2002**, *15* (4), 613-30.
4. Teatero, S.; Ferrieri, P.; Martin, I.; Demczuk, W.; McGeer, A.; Fittipaldi, N., Serotype Distribution, Population Structure, and Antimicrobial Resistance of Group B Streptococcus. *Journal of Clinical Microbiology* **2017**, *55* (2), 412.
5. Manning, S. D.; Lewis, M. A.; Springman, A. C.; Lehotzky, E.; Whittam, T. S.; Davies, D., Genotypic Diversity and Serotype Distribution of Group B Streptococcus Isolated from Women Before and After Delivery. *Clin Infect Dis* **2008**, *46* (12), 1829-1837.
6. Jones, N.; Oliver, K.; Jones, Y.; Haines, A.; Crook, D., Carriage of group B streptococcus in pregnant women from Oxford, UK. *J Clin Pathol* **2006**, *59* (4), 363-6.
7. Melin, P.; Efstratiou, A., Group B streptococcal epidemiology and vaccine needs in developed countries. *Vaccine* **2013**, *31*, D31-D42.
8. Phares, C. R.; Lynfield, R.; Farley, M. M.; Mohle-Boetani, J.; Harrison, L. H.; Petit, S.; Craig, A. S.; Schaffner, W.; Zansky, S. M.; Gershman, K.; Stefonek, K. R.; Albanese, B. A.; Zell, E. R.; Schuchat, A.; Schrag, S. J., Epidemiology of Invasive Group B Streptococcal Disease in the United States, 1999-2005. *JAMA* **2008**, *299* (17), 2056-2065.
9. Jannati, E.; Roshani, M.; Arzanlou, M.; Habibzadeh, S.; Rahimi, G.; Shapuri, R., Capsular serotype and antibiotic resistance of group B streptococci isolated from pregnant women in Ardabil, Iran. *Iran J Microbiol* **2012**, *4* (3), 130-135.
10. Huang, J.; Li, S.; Li, L.; Wang, X.; Yao, Z.; Ye, X., Alarming regional differences in prevalence and antimicrobial susceptibility of group B streptococci in pregnant women: A systematic review and meta-analysis. *Journal of global antimicrobial resistance* **2016**, *7*, 169-177.

11. Le Doare, K.; Heath, P. T., An overview of global GBS epidemiology. *Vaccine* **2013**, *31 Suppl 4*, D7-12.
12. Francois Watkins, L. K.; McGee, L.; Schrag, S. J.; Beall, B.; Jain, J. H.; Pondo, T.; Farley, M. M.; Harrison, L. H.; Zansky, S. M.; Baumbach, J.; Lynfield, R.; Snippes Vagnone, P.; Miller, L. A.; Schaffner, W.; Thomas, A. R.; Watt, J. P.; Petit, S.; Langley, G. E., Epidemiology of Invasive Group B Streptococcal Infections Among Nonpregnant Adults in the United States, 2008-2016. *JAMA internal medicine* **2019**, *179* (4), 479-488.
13. Skoff, T. H.; Farley, M. M.; Petit, S.; Craig, A. S.; Schaffner, W.; Gershman, K.; Harrison, L. H.; Lynfield, R.; Mohle-Boetani, J.; Zansky, S.; Albanese, B. A.; Stefonek, K.; Zell, E. R.; Jackson, D.; Thompson, T.; Schrag, S. J., Increasing burden of invasive group B streptococcal disease in nonpregnant adults, 1990-2007. *Clin Infect Dis* **2009**, *49* (1), 85-92.
14. Foxman, B.; de Azevedo, C. L. B.; Buxton, M.; DeBusscher, J.; Pillai, P.; De Carvalho, N. S.; Barbosa-Cesnik, C., Acquisition and Transmission of Group B Streptococcus during Pregnancy. *The Journal of Infectious Diseases* **2008**, *198* (9), 1375-1378.
15. Puopolo, K. M.; Lynfield, R.; Cummings, J. J., Management of Infants at Risk for Group B Streptococcal Disease. *Pediatrics* **2019**, *144* (2), e20191881.
16. Nanduri, S. A.; Petit, S.; Smelser, C.; Apostol, M.; Alden, N. B.; Harrison, L. H.; Lynfield, R.; Vagnone, P. S.; Burzlaff, K.; Spina, N. L.; Dufort, E. M.; Schaffner, W.; Thomas, A. R.; Farley, M. M.; Jain, J. H.; Pondo, T.; McGee, L.; Beall, B. W.; Schrag, S. J., Epidemiology of Invasive Early-Onset and Late-Onset Group B Streptococcal Disease in the United States, 2006 to 2015: Multistate Laboratory and Population-Based Surveillance. *JAMA pediatrics* **2019**, *173* (3), 224-233.
17. Bergeron, M. G.; Ke, D.; Ménard, C.; François, F. J.; Gagnon, M.; Bernier, M.; Ouellette, M.; Roy, P. H.; Marcoux, S.; Fraser, W. D., Rapid Detection of Group B Streptococci in Pregnant Women at Delivery. *New England Journal of Medicine* **2000**, *343* (3), 175-179.
18. Zaleznik, D. F.; Rench, M. A.; Hillier, S.; Krohn, M. A.; Platt, R.; Lee, M. L.; Flores, A. E.; Ferrieri, P.; Baker, C. J., Invasive disease due to group B Streptococcus in pregnant women and neonates from diverse population groups. *Clin Infect Dis* **2000**, *30* (2), 276-81.
19. Boyer, K. M.; Gadzala, C. A.; Burd, L. I.; Fisher, D. E.; Paton, J. B.; Gotoff, S. P., Selective intrapartum chemoprophylaxis of neonatal group B streptococcal early-onset disease. I. Epidemiologic rationale. *J Infect Dis* **1983**, *148* (5), 795-801.
20. Weisner, A. M.; Johnson, A. P.; Lamagni, T. L.; Arnold, E.; Warner, M.; Heath, P. T.; Efstratiou, A., Characterization of Group B Streptococci Recovered from Infants

with Invasive Disease in England and Wales. *Clinical Infectious Diseases* **2004**, 38 (9), 1203-1208.

21. Easmon, C. S.; Hastings, M. J.; Clare, A. J.; Bloxham, B.; Marwood, R.; Rivers, R. P.; Stringer, J., Nosocomial transmission of group B streptococci. *Br Med J (Clin Res Ed)* **1981**, 283 (6289), 459-461.

22. Morinis, J.; Shah, J.; Murthy, P.; Fulford, M., Horizontal transmission of group B streptococcus in a neonatal intensive care unit. *Paediatr Child Health* **2011**, 16 (6), e48-e50.

23. Le Doare, K.; Kampmann, B., Breast milk and Group B streptococcal infection: vector of transmission or vehicle for protection? *Vaccine* **2014**, 32 (26), 3128-3132.

24. Zimmermann, P.; Gwee, A.; Curtis, N., The controversial role of breast milk in GBS late-onset disease. *Journal of Infection* **2017**, 74, S34-S40.

25. Burianová, I.; Paulová, M.; Cermák, P.; Janota, J., Group B streptococcus colonization of breast milk of group B streptococcus positive mothers. *Journal of human lactation : official journal of International Lactation Consultant Association* **2013**, 29 (4), 586-90.

26. Jawa, G.; Hussain, Z.; da Silva, O., Recurrent late-onset group B Streptococcus sepsis in a preterm infant acquired by expressed breastmilk transmission: a case report. *Breastfeeding medicine : the official journal of the Academy of Breastfeeding Medicine* **2013**, 8 (1), 134-6.

27. Seale, A. C.; Bianchi-Jassir, F.; Russell, N. J.; Kohli-Lynch, M.; Tann, C. J.; Hall, J.; Madrid, L.; Blencowe, H.; Cousens, S.; Baker, C. J.; Bartlett, L.; Cutland, C.; Gravett, M. G.; Heath, P. T.; Ip, M.; Le Doare, K.; Madhi, S. A.; Rubens, C. E.; Saha, S. K.; Schrag, S. J.; Sobanjo-Ter Meulen, A.; Vekemans, J.; Lawn, J. E., Estimates of the Burden of Group B Streptococcal Disease Worldwide for Pregnant Women, Stillbirths, and Children. *Clin Infect Dis* **2017**, 65 (suppl_2), S200-s219.

28. Patras, K. A.; Nizet, V., Group B Streptococcal Maternal Colonization and Neonatal Disease: Molecular Mechanisms and Preventative Approaches. *Front Pediatr* **2018**, 6 (27).

29. Fox, B. C., Delayed-onset postpartum meningitis due to group B streptococcus. *Clin Infect Dis* **1994**, 19 (2), 350.

30. Lazarus, J. M.; Sellers, D. P.; Marine, W. M., Meningitis Due to the Group B Beta-Hemolytic Streptococcus. *New England Journal of Medicine* **1965**, 272 (3), 146-147.

31. Faro, S., Group B streptococcus and puerperal sepsis. *American journal of obstetrics and gynecology* **1980**, 138 (8), 1219-20.

32. Patel, K.; Williams, S.; Guirguis, G.; Gittens-Williams, L.; Apuzzio, J., Genital tract GBS and rate of histologic chorioamnionitis in patients with preterm premature rupture of membrane. *The journal of maternal-fetal & neonatal medicine : the official journal of the European Association of Perinatal Medicine, the Federation of Asia and Oceania Perinatal Societies, the International Society of Perinatal Obstet* **2018**, *31* (19), 2624-2627.
33. Vornhagen, J.; Adams Waldorf, K. M.; Rajagopal, L., Perinatal Group B Streptococcal Infections: Virulence Factors, Immunity, and Prevention Strategies. *Trends in Microbiology* **2017**, *25* (11), 919-931.
34. Rajagopal, L., Understanding the regulation of Group B Streptococcal virulence factors. *Future Microbiol* **2009**, *4* (2), 201-221.
35. Nizet, V., Streptococcal beta-hemolysins: genetics and role in disease pathogenesis. *Trends Microbiol* **2002**, *10* (12), 575-80.
36. Lang, S.; Palmer, M., Characterization of Streptococcus agalactiae CAMP factor as a pore-forming toxin. *J Biol Chem* **2003**, *278* (40), 38167-73.
37. Jones, A. L.; Needham, R. H.; Clancy, A.; Knoll, K. M.; Rubens, C. E., Penicillin-binding proteins in Streptococcus agalactiae: a novel mechanism for evasion of immune clearance. *Molecular microbiology* **2003**, *47* (1), 247-56.
38. Poyart, C.; Pellegrini, E.; Gaillot, O.; Boumaila, C.; Baptista, M.; Trieu-Cuot, P., Contribution of Mn-cofactored superoxide dismutase (SodA) to the virulence of Streptococcus agalactiae. *Infect Immun* **2001**, *69* (8), 5098-106.
39. Takahashi, S.; Nagano, Y.; Nagano, N.; Hayashi, O.; Taguchi, F.; Okuwaki, Y., Role of C5a-ase in group B streptococcal resistance to opsonophagocytic killing. *Infect Immun* **1995**, *63* (12), 4764-9.
40. Bohnsack, J. F.; Widjaja, K.; Ghazizadeh, S.; Rubens, C. E.; Hillyard, D. R.; Parker, C. J.; Albertine, K. H.; Hill, H. R., A role for C5 and C5a-ase in the acute neutrophil response to group B streptococcal infections. *J Infect Dis* **1997**, *175* (4), 847-55.
41. Sheen, T. R.; Jimenez, A.; Wang, N. Y.; Banerjee, A.; van Sorge, N. M.; Doran, K. S., Serine-rich repeat proteins and pili promote Streptococcus agalactiae colonization of the vaginal tract. *J Bacteriol* **2011**, *193* (24), 6834-42.
42. Marques, M. B.; Kasper, D. L.; Pangburn, M. K.; Wessels, M. R., Prevention of C3 deposition by capsular polysaccharide is a virulence mechanism of type III group B streptococci. *Infect Immun* **1992**, *60* (10), 3986-93.
43. Bodaszewska-Lubas, M.; Brzychczy-Wloch, M.; Adamski, P.; Gosiewski, T.; Strus, M.; Heczko, P. B., Adherence of group B streptococci to human rectal and

vaginal epithelial cell lines in relation to capsular polysaccharides as well as alpha-like protein genes - pilot study. *Polish journal of microbiology* **2013**, 62 (1), 85-90.

44. Gutekunst, H.; Eikmanns, B. J.; Reinscheid, D. J., The novel fibrinogen-binding protein FbsB promotes *Streptococcus agalactiae* invasion into epithelial cells. *Infect Immun* **2004**, 72 (6), 3495-504.

45. Jacobsson, K., A novel family of fibrinogen-binding proteins in *Streptococcus agalactiae*. *Veterinary microbiology* **2003**, 96 (1), 103-13.

46. Spellerberg, B.; Rozdzinski, E.; Martin, S.; Weber-Heynemann, J.; Schnitzler, N.; Lütticken, R.; Podbielski, A., Lmb, a protein with similarities to the Lral adhesin family, mediates attachment of *Streptococcus agalactiae* to human laminin. *Infect Immun* **1999**, 67 (2), 871-8.

47. Santi, I.; Scarselli, M.; Mariani, M.; Pezzicoli, A.; Masignani, V.; Taddei, A.; Grandi, G.; Telford, J. L.; Soriani, M., BibA: a novel immunogenic bacterial adhesin contributing to group B *Streptococcus* survival in human blood. *Molecular microbiology* **2007**, 63 (3), 754-67.

48. Høiby, N.; Bjarnsholt, T.; Givskov, M.; Molin, S.; Ciofu, O., Antibiotic resistance of bacterial biofilms. *Int J Antimicrob Agents* **2010**, 35 (4), 322-332.

49. Cvitkovitch, D. G.; Li, Y.-H.; Ellen, R. P., Quorum sensing and biofilm formation in *Streptococcal* infections. *J Clin Invest* **2003**, 112 (11), 1626-1632.

50. Dramsi, S.; Caliot, E.; Bonne, I.; Guadagnini, S.; Prévost, M. C.; Kojadinovic, M.; Lalioui, L.; Poyart, C.; Trieu-Cuot, P., Assembly and role of pili in group B streptococci. *Molecular microbiology* **2006**, 60 (6), 1401-13.

51. Rosini, R.; Margarit, I., Biofilm formation by *Streptococcus agalactiae*: influence of environmental conditions and implicated virulence factors. *Front Cell Infect Microbiol* **2015**, 5, 6-6.

52. Parker, R. E.; Laut, C.; Gaddy, J. A.; Zadoks, R. N.; Davies, H. D.; Manning, S. D., Association between genotypic diversity and biofilm production in group B *Streptococcus*. *BMC Microbiology* **2016**, 16 (1), 86.

53. Rutherford, S. T.; Bassler, B. L., Bacterial quorum sensing: its role in virulence and possibilities for its control. *Cold Spring Harbor perspectives in medicine* **2012**, 2 (11).

54. D'Urzo, N.; Martinelli, M.; Pezzicoli, A.; De Cesare, V.; Pinto, V.; Margarit, I.; Telford, J. L.; Maione, D., Acidic pH Strongly Enhances In Vitro Biofilm Formation by a Subset of Hypervirulent ST-17 *Streptococcus agalactiae* Strains. *Applied and Environmental Microbiology* **2014**, 80 (7), 2176-2185.

55. Jamal, M.; Ahmad, W.; Andleeb, S.; Jalil, F.; Imran, M.; Nawaz, M. A.; Hussain, T.; Ali, M.; Rafiq, M.; Kamil, M. A., Bacterial biofilm and associated infections. *Journal of the Chinese Medical Association : JCMA* **2018**, *81* (1), 7-11.
56. Tiwari, S.; Jamal, S. B.; Hassan, S. S.; Carvalho, P. V. S. D.; Almeida, S.; Barh, D.; Ghosh, P.; Silva, A.; Castro, T. L. P.; Azevedo, V., Two-Component Signal Transduction Systems of Pathogenic Bacteria As Targets for Antimicrobial Therapy: An Overview. *Frontiers in Microbiology* **2017**, *8* (1878).
57. Groisman, E. A., Feedback Control of Two-Component Regulatory Systems. *Annual Review of Microbiology* **2016**, *70* (1), 103-124.
58. Jiang, S.-M.; Cieslewicz, M. J.; Kasper, D. L.; Wessels, M. R., Regulation of virulence by a two-component system in group B streptococcus. *J Bacteriol* **2005**, *187* (3), 1105-1113.
59. Gao, R.; Mack, T. R.; Stock, A. M., Bacterial response regulators: versatile regulatory strategies from common domains. *Trends in biochemical sciences* **2007**, *32* (5), 225-34.
60. Lamy, M. C.; Zouine, M.; Fert, J.; Vergassola, M.; Couve, E.; Pellegrini, E.; Glaser, P.; Kunst, F.; Msadek, T.; Trieu-Cuot, P.; Poyart, C., CovS/CovR of group B streptococcus: a two-component global regulatory system involved in virulence. *Molecular microbiology* **2004**, *54* (5), 1250-68.
61. Poyart, C.; Lamy, M. C.; Boumaila, C.; Fiedler, F.; Trieu-Cuot, P., Regulation of D-alanyl-lipoteichoic acid biosynthesis in *Streptococcus agalactiae* involves a novel two-component regulatory system. *J Bacteriol* **2001**, *183* (21), 6324-34.
62. Spellerberg, B.; Rozdzinski, E.; Martin, S.; Weber-Heynemann, J.; Lütticken, R., r_{gf} encodes a novel two-component signal transduction system of *Streptococcus agalactiae*. *Infect Immun* **2002**, *70* (5), 2434-40.
63. Quach, D.; van Sorge, N. M.; Kristian, S. A.; Bryan, J. D.; Shelver, D. W.; Doran, K. S., The CiaR response regulator in group B *Streptococcus* promotes intracellular survival and resistance to innate immune defenses. *J Bacteriol* **2009**, *191* (7), 2023-32.
64. Faralla, C.; Metruccio, M. M.; De Chiara, M.; Mu, R.; Patras, K. A.; Muzzi, A.; Grandi, G.; Margarit, I.; Doran, K. S.; Janulczyk, R., Analysis of Two-Component Systems in Group B *Streptococcus* Shows That RgfAC and the Novel FspSR Modulate Virulence and Bacterial Fitness. *mBio* **2014**, *5* (3), e00870-14.
65. Di Palo, B.; Rippha, V.; Santi, I.; Brettoni, C.; Muzzi, A.; Metruccio, M. M. E.; Grifantini, R.; Telford, J. L.; Paccani, S. R.; Soriani, M., Adaptive Response of Group B *Streptococcus* to High Glucose Conditions: New Insights on the CovRS Regulation Network. *PLOS ONE* **2013**, *8* (4), e61294.

66. Shabayek, S.; Spellerberg, B., Acid Stress Response Mechanisms of Group B Streptococci. *Front Cell Infect Microbiol* **2017**, *7* (395).
67. Santi, I.; Grifantini, R.; Jiang, S.-M.; Brettoni, C.; Grandi, G.; Wessels, M. R.; Soriani, M., CsrRS regulates group B Streptococcus virulence gene expression in response to environmental pH: a new perspective on vaccine development. *J Bacteriol* **2009**, *191* (17), 5387-5397.
68. Shelburne, S. A.; Davenport, M. T.; Keith, D. B.; Musser, J. M., The role of complex carbohydrate catabolism in the pathogenesis of invasive streptococci. *Trends Microbiol* **2008**, *16* (7), 318-25.
69. Jiang, S.-M.; Ishmael, N.; Hotopp, J. D.; Puliti, M.; Tissi, L.; Kumar, N.; Cieslewicz, M. J.; Tettelin, H.; Wessels, M. R., Variation in the Group B Streptococcus CsrRS Regulon and Effects on Pathogenicity. *J Bacteriol* **2008**, *190* (6), 1956-1965.
70. Patras, K. A.; Wang, N.-Y.; Fletcher, E. M.; Cavaco, C. K.; Jimenez, A.; Garg, M.; Fierer, J.; Sheen, T. R.; Rajagopal, L.; Doran, K. S., Group B Streptococcus CovR regulation modulates host immune signalling pathways to promote vaginal colonization. *Cell Microbiol* **2013**, *15* (7), 1154-1167.
71. Walsh, C., *Antibiotics*. American Society of Microbiology: 2003.
72. Walsh, C.; Wencewicz, T., *Antibiotics: Challenges, Mechanisms, Opportunities*. American Society of Microbiology: 2016.
73. Penicillins and other Betalactams. In *Antibiotics and Antibiotic Resistance*, 2011; pp 69-94.
74. Sarkar, P.; Yarlagadda, V.; Ghosh, C.; Haldar, J., A review on cell wall synthesis inhibitors with an emphasis on glycopeptide antibiotics. *Medchemcomm* **2017**, *8* (3), 516-533.
75. Glycopeptides. In *Antibiotics and Antibiotic Resistance*, 2011; pp 95-102.
76. Arenz, S.; Wilson, D. N., Bacterial Protein Synthesis as a Target for Antibiotic Inhibition. *Cold Spring Harbor perspectives in medicine* **2016**, *6* (9), a025361.
77. McCoy, L. S.; Xie, Y.; Tor, Y., Antibiotics that target protein synthesis. *WIREs RNA* **2011**, *2* (2), 209-232.
78. Dhawan, V. K.; Thadepalli, H., Clindamycin: a review of fifteen years of experience. *Reviews of infectious diseases* **1982**, *4* (6), 1133-53.
79. Aminoglycosides. In *Antibiotics and Antibiotic Resistance*, 2011; pp 103-113.
80. Gonzalez, L. S., 3rd; Spencer, J. P., Aminoglycosides: a practical review. *Am Fam Physician* **1998**, *58* (8), 1811-20.

81. Aldred, K. J.; Kerns, R. J.; Osheroff, N., Mechanism of quinolone action and resistance. *Biochemistry* **2014**, *53* (10), 1565-1574.
82. Hooper, D. C., Mechanisms of Action of Antimicrobials: Focus on Fluoroquinolones. *Clinical Infectious Diseases* **2001**, *32* (Supplement_1), S9-S15.
83. Quinolones. In *Antibiotics and Antibiotic Resistance*, 2011; pp 133-145.
84. Rothstein, D. M., Rifamycins, Alone and in Combination. *Cold Spring Harbor perspectives in medicine* **2016**, *6* (7), a027011.
85. Sulfonamides and Trimethoprim. In *Antibiotics and Antibiotic Resistance*, 2011; pp 29-68.
86. Gleckman, R.; Blagg, N.; Joubert, D. W., Trimethoprim: mechanisms of action, antimicrobial activity, bacterial resistance, pharmacokinetics, adverse reactions, and therapeutic indications. *Pharmacotherapy* **1981**, *1* (1), 14-20.
87. Hsieh, L.; Amin, A., Chapter 1 - Antimicrobial Stewardship: Hospital Strategies to Curb Antibiotic Resistance. In *Antibiotic Resistance*, Kon, K.; Rai, M., Eds. Academic Press: 2016; pp 1-18.
88. de Sousa Oliveira, K.; de Lima, L. A.; Cobacho, N. B.; Dias, S. C.; Franco, O. L., Chapter 2 - Mechanisms of Antibacterial Resistance: Shedding Some Light on These Obscure Processes? In *Antibiotic Resistance*, Kon, K.; Rai, M., Eds. Academic Press: 2016; pp 19-35.
89. Nielsen, T. B.; Brass, E. P.; Gilbert, D. N.; Bartlett, J. G.; Spellberg, B., Sustainable Discovery and Development of Antibiotics — Is a Nonprofit Approach the Future? *New England Journal of Medicine* **2019**, *381* (6), 503-505.
90. Spellberg, B.; Bartlett, J.; Wunderink, R.; Gilbert, D. N., Novel approaches are needed to develop tomorrow's antibacterial therapies. *American journal of respiratory and critical care medicine* **2015**, *191* (2), 135-40.
91. Hutchings, M. I.; Truman, A. W.; Wilkinson, B., Antibiotics: past, present and future. *Current Opinion in Microbiology* **2019**, *51*, 72-80.
92. Castor, M. L.; Whitney, C. G.; Como-Sabetti, K.; Facklam, R. R.; Ferrieri, P.; Bartkus, J. M.; Juni, B. A.; Cieslak, P. R.; Farley, M. M.; Dumas, N. B.; Schrag, S. J.; Lynfield, R., Antibiotic resistance patterns in invasive group B streptococcal isolates. *Infect Dis Obstet Gynecol* **2008**, *2008*, 727505-727505.
93. Back, E. E.; Grady, E. J.; Back, J. D., High Rates of Perinatal Group B Streptococcus Clindamycin and Erythromycin Resistance in an Upstate New York Hospital. *Antimicrob Agents Chemother* **2012**, *56* (2), 739.

94. Fitoussi, F.; Loukil, C.; Gros, I.; Clermont, O.; Mariani, P.; Bonacorsi, S.; Le Thomas, I.; Deforche, D.; Bingen, E., Mechanisms of Macrolide Resistance in Clinical Group B Streptococci Isolated in France. *Antimicrob Agents Chemother* **2001**, *45* (6), 1889.
95. Wright, P. M.; Seiple, I. B.; Myers, A. G., The Evolving Role of Chemical Synthesis in Antibacterial Drug Discovery. *Angew Chem Int Ed* **2014**, *53* (34), 8840-8869.
96. Kapoor, G.; Saigal, S.; Elongavan, A., Action and resistance mechanisms of antibiotics: A guide for clinicians. *J Anaesthesiol Clin Pharmacol* **2017**, *33* (3), 300-305.
97. Milani, C.; Duranti, S.; Bottacini, F.; Casey, E.; Turrone, F.; Mahony, J.; Belzer, C.; Delgado Palacio, S.; Arboleya Montes, S.; Mancabelli, L.; Lugli, G. A.; Rodriguez, J. M.; Bode, L.; de Vos, W.; Gueimonde, M.; Margolles, A.; van Sinderen, D.; Ventura, M., The First Microbial Colonizers of the Human Gut: Composition, Activities, and Health Implications of the Infant Gut Microbiota. *Microbiology and Molecular Biology Reviews* **2017**, *81* (4), e00036-17.
98. Miqdady, M.; Al Mistarihi, J.; Azaz, A.; Rawat, D., Prebiotics in the Infant Microbiome: The Past, Present, and Future. *Pediatr Gastroenterol Hepatol Nutr* **2020**, *23* (1), 1-14.
99. Verkhnyatskaya, S.; Ferrari, M.; de Vos, P.; Walvoort, M. T. C., Shaping the Infant Microbiome With Non-digestible Carbohydrates. *Frontiers in microbiology* **2019**, *10*, 343-343.
100. Moore, R. E.; Townsend, S. D., Temporal development of the infant gut microbiome. *Open Biology* *9* (9), 190128.

Chapter 2

Synthesis and application of ellagic acid glycosides in preventing group B *Streptococcus* biofilm formation

2.1 Abstract

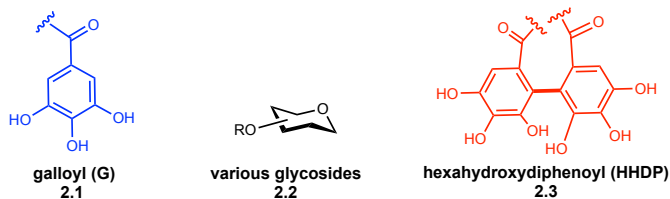
GBS is a bacterium that presents a significant health risk to infants. Unfortunately, current strategies used to prevent GBS transmission also alter the composition and development of the infant and maternal microbiome. Resultantly, continued antibiotic drug discovery efforts are needed, with emphasis on the study of selective antimicrobial compounds that minimize deleterious effects on the greater microbiome population. Herein, we investigate the synthesis and use of glycosylated ellagic acid derivatives as potential antibacterial agents against GBS. We identify that ellagic acid arabinoside has significant antibiofilm properties against GBS and inhibits early streptococcal adhesion mechanisms. We also show that synthetic ellagic acid glycosides inhibit the growth of other ESKAPE pathogens, thereby increasing interest in further development of such molecules as antibacterial therapeutics.¹

2.2 Ellagitannin natural products

Plants biosynthesize numerous types of polyphenol or tannin natural products. Gallotannins and ellagitannins are two predominant classes within these natural products and can be highly variable in structure.²⁻⁷ Most simply, these natural products are derived from only a few subunits (**Figure 2.1A**). Gallotannins are comprised of galloyl motifs (**2.1**) and various glycosides (**2.2**), while ellagitannins also feature hexahydroxydiphenoyl

moieties (HHDP, **2.3**). A few representative monomeric ellagitannins are highlighted, including sanguin H-5 (**2.4**), pariin M (**2.5**) and pedunculagin (**2.6**), but there are over 1,000 known ellagitannin natural products (**Figure 2.1B**).

A. Ellagitannin building blocks



B. Representative monomeric ellagitannins

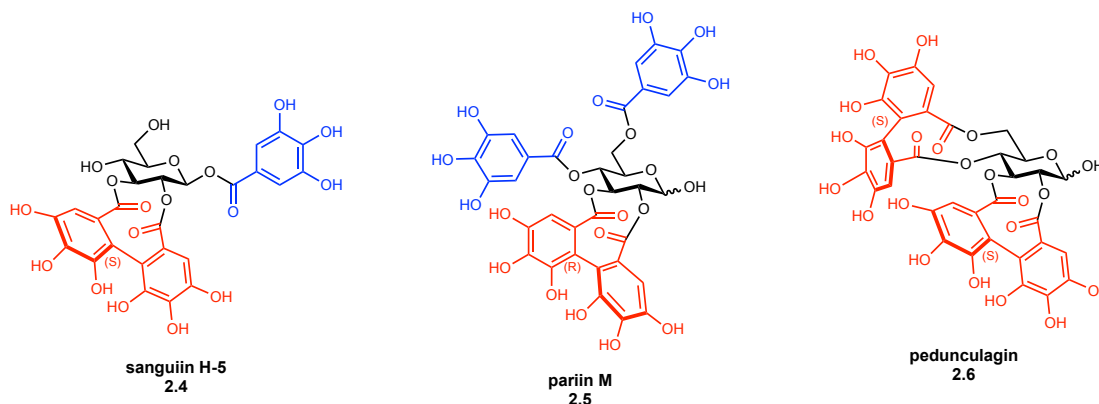


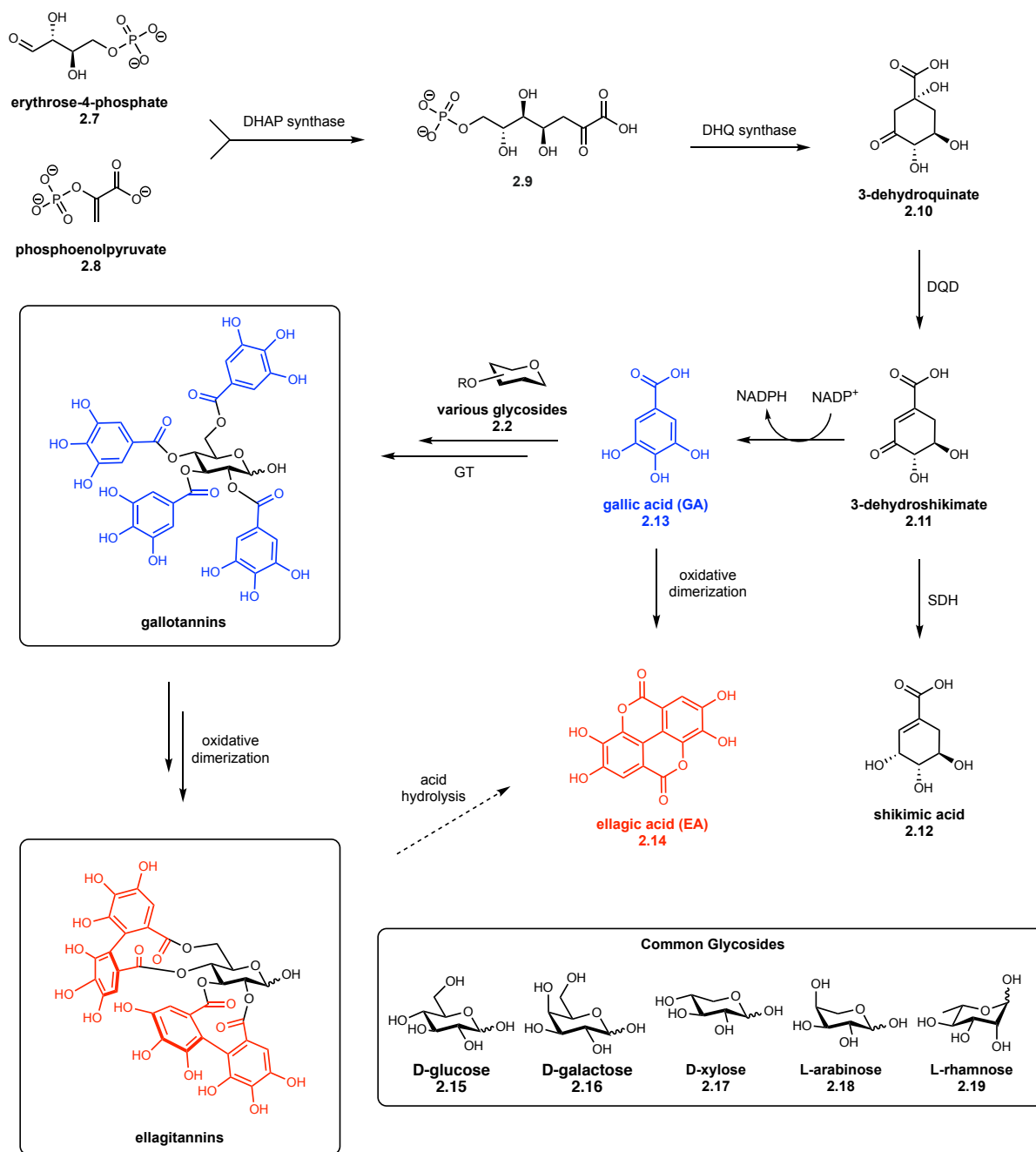
Figure 2.1 Ellagitannin structures (**A.**) Ellagitannin building blocks (**B.**) Representative monomeric ellagitannins

The structural building blocks of tannins are biosynthesized, in part, by the shikimate biosynthetic pathway (**Scheme 2.1**).^{7, 8} Beginning from erythrose **2.7** and phosphoenolpyruvate (**2.8**), formation of intermediate **2.9** and subsequent cyclization yields dehydroquinate **2.10**. From carbocycle **2.10**, dehydration gives dehydroshikimate **2.11**, which acts as a branching point within this biosynthetic pathway. Reduction of **2.11** yields shikimic acid (**2.12**), which can be further elaborated into aromatic amino acids.⁹
¹⁰ Alternatively, oxidation of **2.11** yields gallic acid (GA, **2.13**). GA (**2.13**) can also be

dimerized to afford ellagic acid (EA, **2.14**). GA and EA polyphenols are the central building blocks for the synthesis of complex gallotannins and ellagitannins, respectively.

Initially, GA (**2.13**) can be appended to a variety of glycosides to yield gallotannin natural products. D-glucose (glc, **2.15**) is the most commonly incorporated monosaccharide, but other readily available plant carbohydrates can also be incorporated. These include galactose (gal, **2.16**), xylose (xyl, **2.17**), arabinose (ara, **2.18**) and rhamnose (rha, **2.19**). The glycosyltransferase enzymes involved in these reactions are numerous and still being fully elucidated. From various monosaccharides and gallic acid, monomeric gallotannins are ultimately biosynthesized. From here, GA moieties can undergo further oxidative dimerization to generate ellagitannin natural products. These are named as such, since upon hydrolysis, ellagitannins release EA (**2.14**).¹¹ Both monomeric ellagitannins and gallotannins can undergo subsequent dimerization and oligomerization to afford higher order tannin natural products.

The complex structure of ellagitannins is of continued interest in total synthesis endeavors, and present-day research focuses on highly substituted scaffolds with ever increasing degrees of complexity.^{11, 12} Through synthetic developments by the Quideau, Khanbabaee, and Feldman labs, dozens of ellagitannin natural products have been synthesized and undergone structural confirmation. These significant contributions to ellagitannin total synthesis, have inspired present day interest in the isolation, characterization, and synthesis of novel ellagitannin natural products.

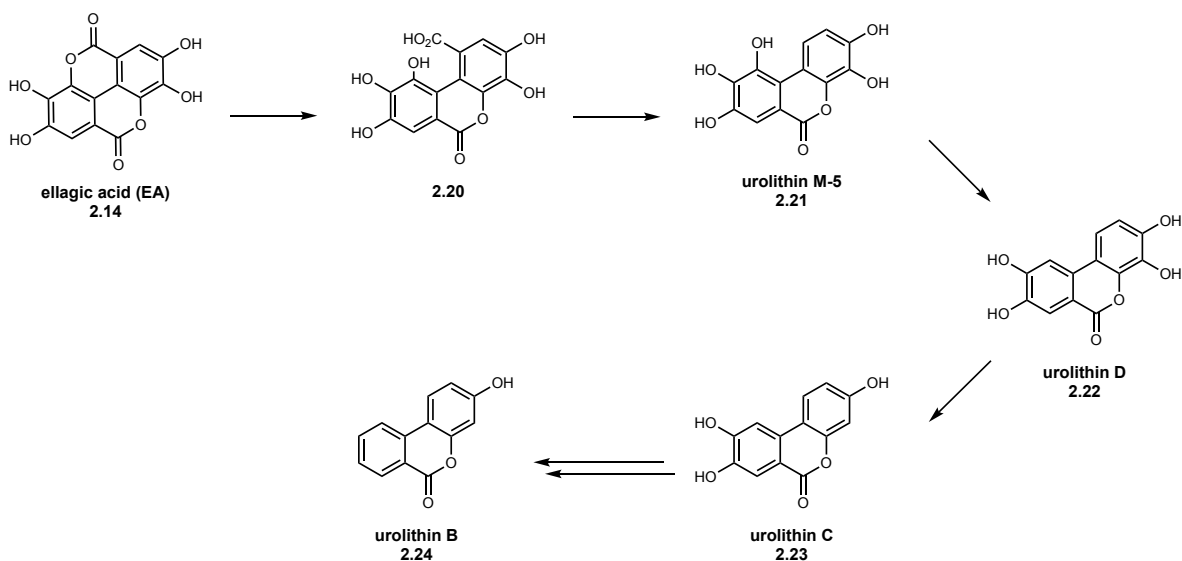


Scheme 2.1 Representative biosynthesis of gallotannin and ellagitannin natural products. Abbreviations: 3-deoxy-D-arabino-heptulosonic acid 7-phosphate (DHAP), 3-dehydroquinic acid (DHQ), dehydroquinic acid dehydratase (DQD), shikimate dehydrogenase (SDH), reduced nicotinamide adenine dinucleotide phosphate (NADPH), oxidized nicotinamide adenine dinucleotide phosphate (NADP⁺), glycosyl transferase (GT).

2.3 Biological activity of ellagitannins

2.3.1 Introduction

Ellagitannins have most extensively been studied for their dietary roles and antioxidant activity.^{13, 14} This antioxidant activity is attributed to the excess of polyphenols within these natural products that makes them prone to oxidation and increases their ability to neutralize reactive oxygen species. Additionally, as these molecules are abundant in fruits and berries, they can be metabolized by some gut microbes including strains of *Bifidobacterium* and *Gordonibacter*.¹⁵⁻¹⁷ Metabolic degradation of ellagitannins leads to the production of urolithin metabolites, that have been linked to modulation of the gut microbiome (**Scheme 2.2**).^{17, 18} EA (**2.14**), is hydrolyzed to intermediate **2.20**, which undergoes initial decarboxylation to urolithin M-5 (**2.21**). From here, it is believed that subsequent reduction generates a variety of urolithin metabolites with varying degrees of polyphenolic character (**2.22-2.24**). The enzymes involved in these processes remain largely unknown, but this removal of phenolic moieties helps to increase lipophilicity and absorption of urolithin metabolites in the gut. Resultantly, the beneficial effects of these metabolites are of continued interest to researchers.



Scheme 2.2 Metabolism of EA to urolithins

2.3.2 Antibacterial activity of ellagitannins

With studies into the antioxidant and probiotic effects of ellagitannins, alternative roles as potential antibacterial agents have been largely unexplored. One recent study conducted by Quave and coworkers, identified an extract from the *Rubus ulmifolius* blackberry plant had significant antibacterial and antibiofilm activity against *Staphylococcus aureus*.¹⁹ Across multiple *S. aureus* strains, the fraction, denoted 220D-F2, had an MIC₉₀ ranging from 530-1040 $\mu\text{g mL}^{-1}$ and an MBIC₉₀ ranging from 50-100 $\mu\text{g mL}^{-1}$. This significant antibiofilm activity was further supported by confocal microscopy visualization of *S. aureus* biofilms (**Figure 2.2**). When dosed at 50 $\mu\text{g mL}^{-1}$, the extract 220D-F2 was able to completely prevent observable biofilm formation in both methicillin-sensitive and methicillin-resistant *S. aureus* (MSSA, MRSA respectively).

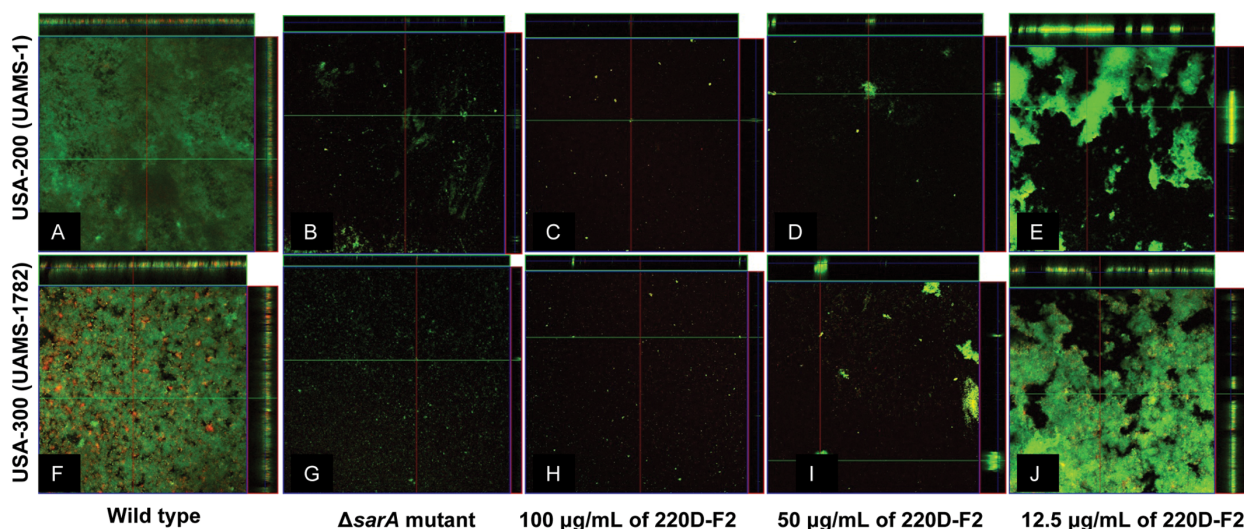


Figure 2.2 Impact of 220D-F2 on *S. aureus* biofilm as assessed by confocal microscopy. Microtiter plate biofilm assays were undertaken with UAMS-1 (top, MSSA) or UAMS-1782 (bottom, MRSA) after the addition of either 220D-F2 at the indicated concentrations or excipient (DMSO) to the growth medium. Confocal images were obtained after 20 hours of incubation. An orthogonal view is included to illustrate overall biofilm architecture at a magnification of 10 \times . Isogenic *sarA* mutants grown in BM with DMSO were included as negative controls.¹⁹

Further mass fragmentation (MS/MS) studies on extract 220D-F2 revealed the active constituents were ellagitannins, specifically mono-glycosylated EA derivatives (**Figure 2.3**). Based off the MS/MS data, the monosaccharide residues were proposed to be that of rhamnose (**2.25-2.26**) and xylose (**2.27-2.28**), however, the site and stereochemistry of glycosylation was not initially determined.

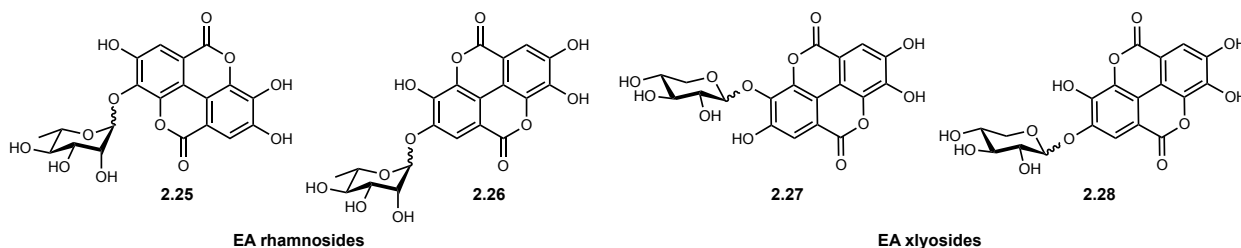
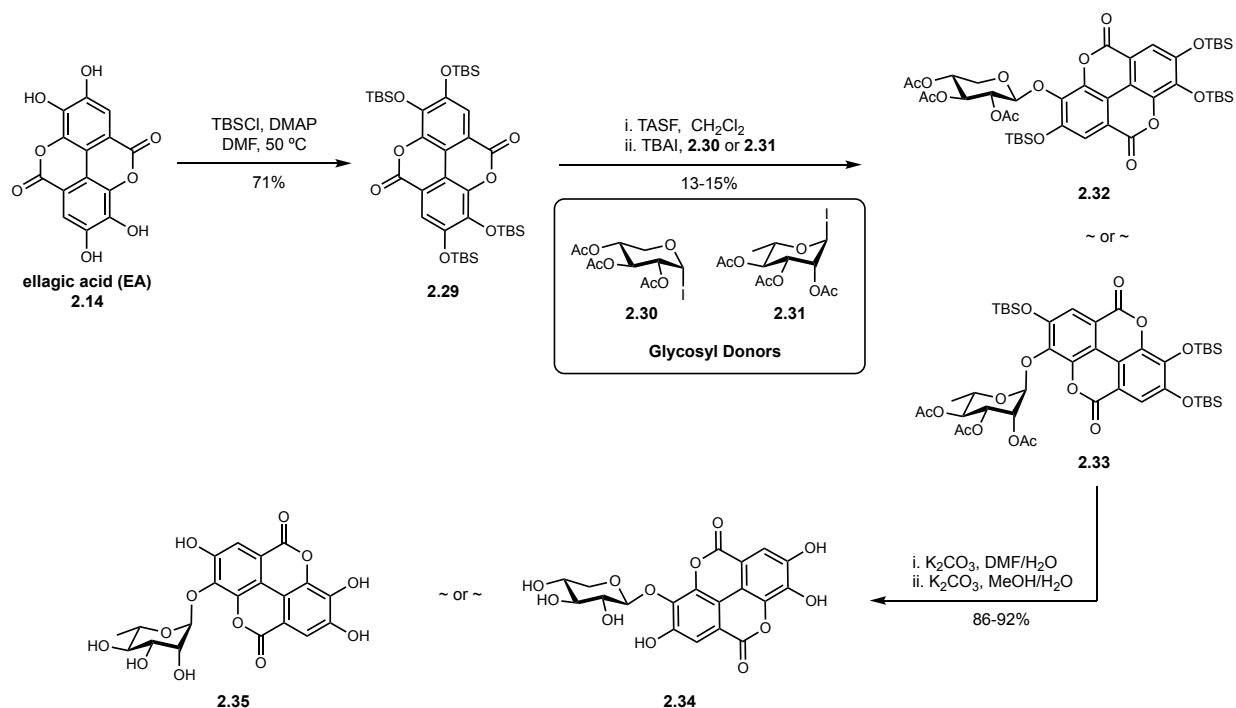


Figure 2.3 Proposed structures of active constituents in isolate 220D-F2

2.3.3 Fontaine synthesis of EA glycosides

A follow up study from Fontaine and coworkers was conducted to verify the structures of the active components in 220D-F2.²⁰ They synthesized two EA glycosides, an EA xyloside **2.34** and EA rhamnoside **2.35**, to investigate which molecule might be responsible for antibiofilm activity against MRSA (**Scheme 2.3**). Their synthesis began from EA (**2.14**), whereby per-TBS protection afforded the TBS-protected EA **2.29**. From here *in situ* deprotection of the C-3 TBS ether and glycosylation with a xylosyl (**2.30**) or rhamnosyl (**2.31**) iodide donor, yielded protected EA glycosides **2.32** and **2.33** respectively.²¹ Notably, this glycosylation proceeds in only 13-15% yield. Desilylation and deacetylation then afforded the final EA glycosides **2.34** and **2.35**.



Scheme 2.3 Fontaine synthesis of EA glycosides²⁰

Initial biological investigation in MSSA strain UAMS-1 identified that the EA xyloside **2.34** had antibacterial activity (MIC_{90} - $32 \mu\text{g mL}^{-1}$) and the EA rhamnoside **2.35** had antibiofilm activity (MBIC_{90} - $128 \mu\text{g mL}^{-1}$). Neither of these molecules were as potent as the original natural product extract 220D-F2 and as a result there were still several unaddressed questions regarding the biological activity of EA glycosides.

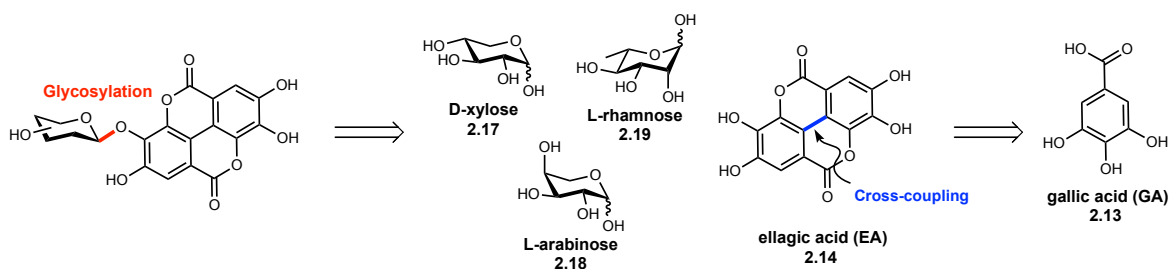
While these studies demonstrated the antibiofilm activity of EA rhamnoside **2.35**, little was understood about how the compounds elicit antibiofilm effects and the reasons for monosaccharide specific-antibiofilm activity.²² Additionally, Fontaine's work did not investigate the effects of the synthetic EA glycosides against MRSA or any other bacterial strains. Other previous total syntheses of EA glycosides also failed to investigate the range of antibacterial effects of such compounds.^{20, 23-25} Resultantly, we became interested in developing a synthetic strategy to access EA glycosides that would enable a broader evaluation of their biological activity and mechanism of action.

2.4 Synthesis of EA glycosides

2.4.1 Rationale and retrosynthesis

Based off these earlier studies into EA glycosides and biological activity, we became interest in testing these ellagitannins for activity against GBS. As GBS is disproportionately pathogenic in infants, the prevention of GBS transmission from adults to infants is crucial (see section 1.5). We hypothesized that the natural abundance of EA glycosides in normal dietary fruits would limit deleterious effects on healthy commensal bacteria, while inhibiting the proliferation of pathogenic microbes. For these reasons, we decided to design our own total synthesis campaign to produce glycosylated EA derivatives.²⁶

Retrosynthetically, we envisioned a late stage *O*-glycosylation to allow for diversification of monosaccharide substituents (**Scheme 2.4**). We initially chose xylose (**2.17**), arabinose (**2.18**), and rhamnose (**2.19**) as monosaccharide targets owing to their previously demonstrated activity and abundance within phenolic natural products.²⁰ We also wanted to synthetically access EA (**2.14**) from cross-coupling of the monomeric precursor GA (**2.13**). This would enable derivatization of the EA core and increase accessibility to starting materials.

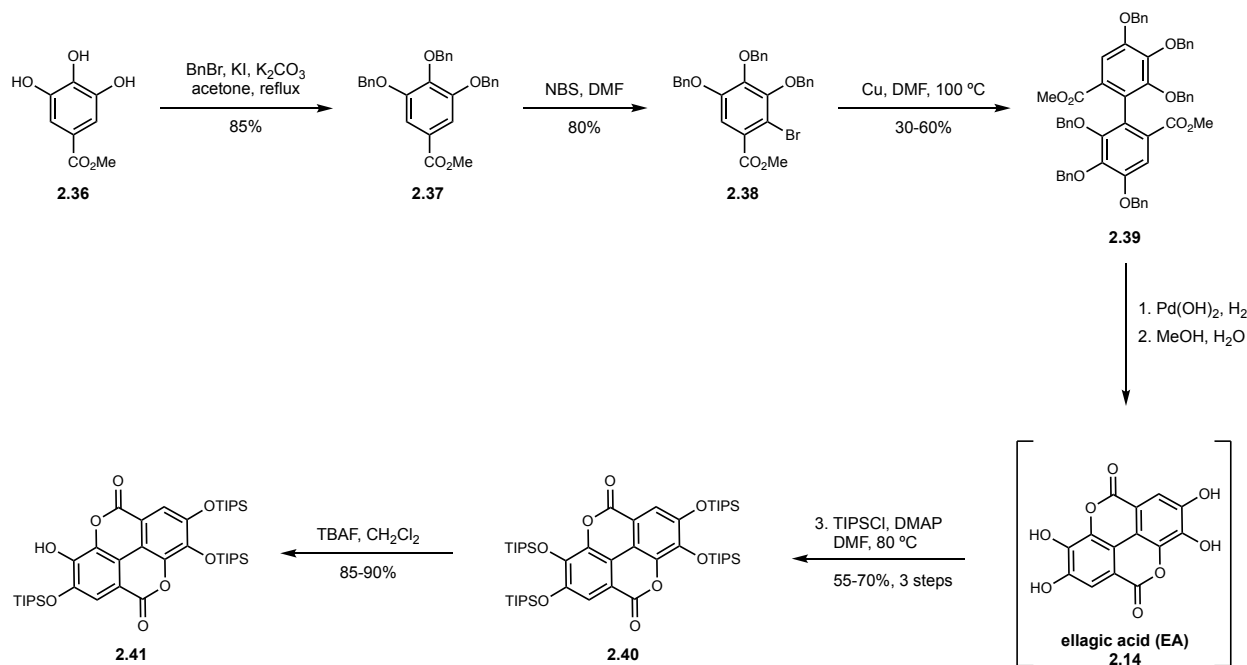


Scheme 2.4 Retrosynthetic analysis of EA glycosides

2.4.2 Total synthesis of EA glycosides

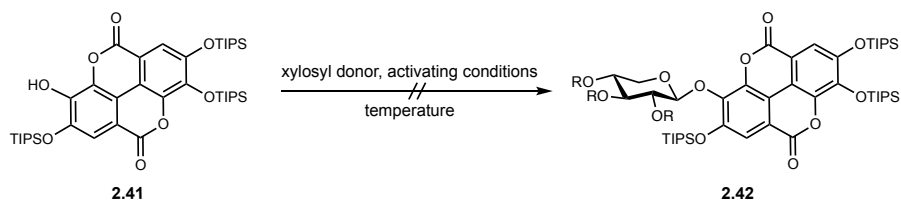
With these considerations in mind, we began our total synthesis from methyl gallate (**2.36**) (**Scheme 2.5**). Finkelstein per-*O*-benzylation and subsequent electrophilic bromination provided intermediate aryl bromide **2.38**.²⁵ This aryl bromide was then coupled under Ullmann conditions to provide biaryl **2.39**. This sterically-encumbered biaryl bond formation proceeds in relatively high yields when compared to those of similar methyl ester substituted systems.²⁷ The use of palladium and nickel additives did not improve the cross-coupling yield, however the only reaction byproduct is the dehalogenated starting material **2.37**, which can be recovered and resubjected.²⁷⁻²⁹

From biaryl **2.39**, debenzoylation and subsequent dilactonization gave EA (**2.14**), which has extremely poor solubility in most organic solvents.³⁰ By example, EA is soluble at 9.7 $\mu\text{g mL}^{-1}$ water, 671 $\mu\text{g mL}^{-1}$ methanol, and 2.5 mg mL^{-1} DMSO. These poor solubilities make EA unideal for use in direct glycosylation reactions. As a result, we immediately per-O-silylated EA (**2.14**) to arrive at **2.40** in 55-70% yield over three steps. TIPS-EA **2.40** is soluble in conventional organic solvents such as chloroform and ethyl acetate; a consideration that was critical for designing future glycosylation efforts. From **2.40**, selective TBAF-mediated mono-deprotection afforded the C-3 phenol **2.41**, providing an EA acceptor for initial glycosylation attempts.²³



From acceptor **2.41**, we then envisioned a phenolic O-glycosylation to form the key glycosidic linkage. The previous method used by Fontaine and coworkers was extremely

low yielding and we wanted to significantly improve upon it.²⁰ We used xylosyl donors in an initial glycosylation screen with acceptor **2.41**, in an attempt to form the general EA xyloside **2.42** (**Scheme 2.6**).



Entry	Xylosyl Donor	Activating Conditions	Temperature Range
I		TMSOTf	-78 °C → RT
II		BF ₃ ·OEt ₂	-78 °C → RT
III		TMSOTf	-78 °C → RT
IV		TMSOTf	-78 °C → RT
V		Ag ₂ CO ₃	RT
VI		Cs ₂ CO ₃ / TBAB / H ₂ O	RT

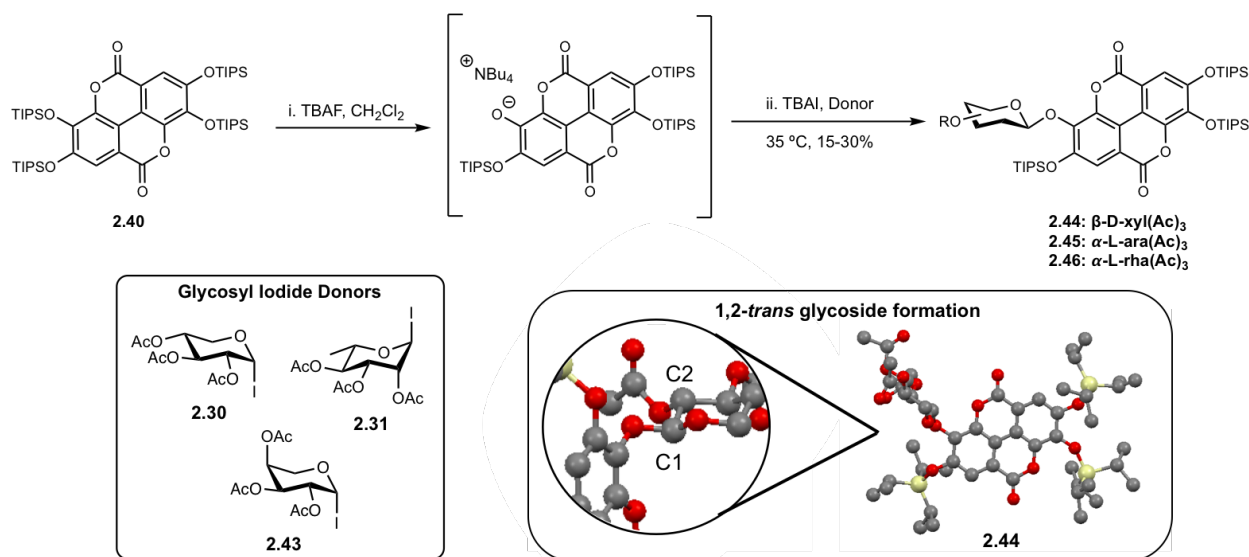
Scheme 2.6 Initial glycosylation screen with xylosyl donors and EA acceptor **2.41**

Our first attempts focused on the use of trichloroacetimidate xylosyl donors due to their highly reactive nature and ability to be activated with catalytic amounts of Lewis acid.^{31, 32} Resultantly, we screened the use of acetylated α -xylosyl trichloroacetimidate donors activated with Lewis acids over a range of temperatures (**Scheme 2.6, Entries I-II**). We

also attempted glycosylation with the acetylated β -xylosyl trichloroacetimidate (**Scheme 2.6, Entry III**), however, none of these attempts yielded the desired EA xyloside **2.42**. Due to a non-productive coupling, we used an armed benzyl-protected xylosyl trichloroacetimidate donor, in glycosylation with **2.41** (**Scheme 2.6, Entry IV**).^{33, 34} Unfortunately, this strategy was also unsuccessful in forming the glycosidic linkage. As these imidate donors proved ineffective, we then attempted to use a xylosyl bromide donor in Koenigs-Knorr glycosylation conditions (**Scheme 2.6, Entry V**) but these reaction conditions also failed.^{35, 36} We then used the xylosyl bromide donor under basic phase-transfer glycosylation conditions with **2.41** in an attempt to promote S_N2 -type glycosylation (**Scheme 2.6, Entry VI**). However, this reaction and others like it also failed to yield the desired glycoside **2.42**. In each of these conditions (**Scheme 2.6**), the EA acceptor **2.41** remained unreacted and the xylosyl donors underwent eventual quenching or hydrolysis. These results, and other previous reports, indicated that the phenolic EA acceptor **2.41** is an extremely poor nucleophile and sterically hindered, leaving conventional glycosylation strategies ineffective.²³

For these reasons, we decided to use a similar glycosylation strategy as Fontaine and coworkers (**Scheme 2.7**).^{20, 37, 38} TIPS-EA **2.40** was regioselectively desilylated at the C-3 EA phenol using TBAF to generate an intermediate quaternary ammonium salt *in situ*. This was then treated with glycosyl iodide donors (**2.30, 2.31, 2.43**) and TBAI, at which point the reaction slurry was heated over two days to yield the desired glycosylated products **2.44-2.46**.^{37, 38} These glycosylation conditions ranged from 15-30% yields, and while this was still very low, it was double that of previous methods. The diminished yields of these glycosylations are attributed to the loss of excess TIPS protecting groups, which

decreases solubility of the acceptor and hinders further reactivity. These reasons and the poor reactivity of other EA acceptors, ultimately necessitated the use of these unique glycosylation conditions.

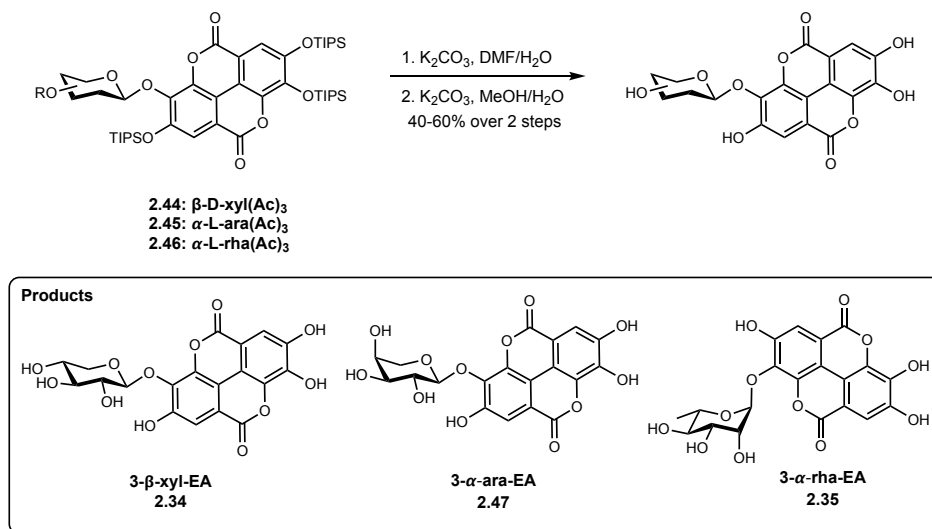


Scheme 2.7 Successful glycosylation of EA glycosides and X-ray crystallography verification of 1,2-*trans* stereochemistry

Of benefit, the glycosylation reaction proceeds stereoselectively, giving exclusively the 1,2-*trans* glycoside. Initial NMR analysis of **2.44** and **2.45** showed ³J_{1,2} coupling constants ranging from 4.6-4.8 Hz (see **Figures A2.7** and **A2.9**). This small coupling constant caused us to speculate that we had formed the 1,2-*cis* glycoside. However, further investigation and use of X-ray crystallography revealed we had actually formed the 1,2-*trans* EA glycosides (**Scheme 2.7**, **2.44**).³⁹ This is mechanistically hypothesized to occur via S_N2-like displacement of the α-glycosyl iodide with the EA phenolic acceptor.

Following successful glycosylation, **2.44-2.46** were subjected to two-step global deprotection, affording glycosides **2.34**, **2.47**, and **2.35** (**Scheme 2.8**). These glycosylated

EA variants had significantly improved solubility properties than those of free EA, and demonstrated increased solubility in DMSO and buffered aqueous solutions ranging from pH 8-9. Through our synthetic efforts, we generated approximately 500 mg of each of the desired EA glycosides **2.34**, **2.47**, and **2.35** for use in biological assays.



Scheme 2.8 Final deprotection of EA glycosides

2.5 Biological activity of synthetic EA glycosides

2.5.1 Antibacterial activity of EA glycosides against GBS

After successful synthesis of EA glycosides **2.34**, **2.47**, and **2.35**, we wanted to test their potential antibacterial effects against GBS. We hypothesized that the compounds would inhibit biofilm formation as was seen in the analogous gram-positive pathogen *S. aureus*.²⁰ We tested the glycosides **2.34**, **2.47**, and **2.35** in two strains of GBS, GB590 and GB2 (**Table 2.1**).⁴⁰⁻⁴²

Table 2.1 MIC and MBIC of EA glycosides in GBS strains^a

Compound	GB590				GB2			
	MIC ₅₀	MIC ₉₀	MBIC ₅₀	MBIC ₉₀	MIC ₅₀	MIC ₉₀	MBIC ₅₀	MBIC ₉₀
2.34	1024	ND ^b	1024	1024	ND ^b	ND ^b	512	1024
2.47	1024	1024	512	1024	1024	1024	512	1024
2.35	1024	1024	1024	1024	1024	ND ^b	1024	ND ^b

^aall values reported in $\mu\text{g mL}^{-1}$, ^bND – not determined; >1024

These initial antimicrobial assays indicated that the EA glycosides were weakly antibacterial against GBS. Across both GBS strains, the EA arabinoside **2.47** was the most antibacterial with an MIC₉₀ of 1024 $\mu\text{g mL}^{-1}$. It should be noted that we attempted to use EA as a control compound, but due to its low solubility, could only reach a maximum dose of 256 $\mu\text{g mL}^{-1}$. No changes to bacterial growth or biofilm formation were seen at this highest concentration of EA.

Most interestingly, the EA xyloside **2.34** and EA arabinoside **2.47** had antibiofilm properties against GBS. To investigate these results further, we analyzed the changes in biofilm as a ratio of biofilm to biomass (biofilm/biomass, OD₅₆₀/OD₆₀₀) (**Figure 2.4**). This parameter allows us to verify whether or not a phenotypic change in biofilm is simply due to lower cellular growth or inherent stunting of biofilm generation. We demonstrated that both EA glycosides **2.34** and **2.47** inhibit GBS biofilm formation independent of bacterial growth. Interestingly, the EA rhamnoside **2.35** did not have antibiofilm activity against GBS, even though it had the most predominant antibiofilm activity in *S. aureus*.²⁰ These results indicate there is carbohydrate specificity in the effects of EA glycosides against

gram-positive biofilm formation and further investigation into the mechanism of action is necessary.

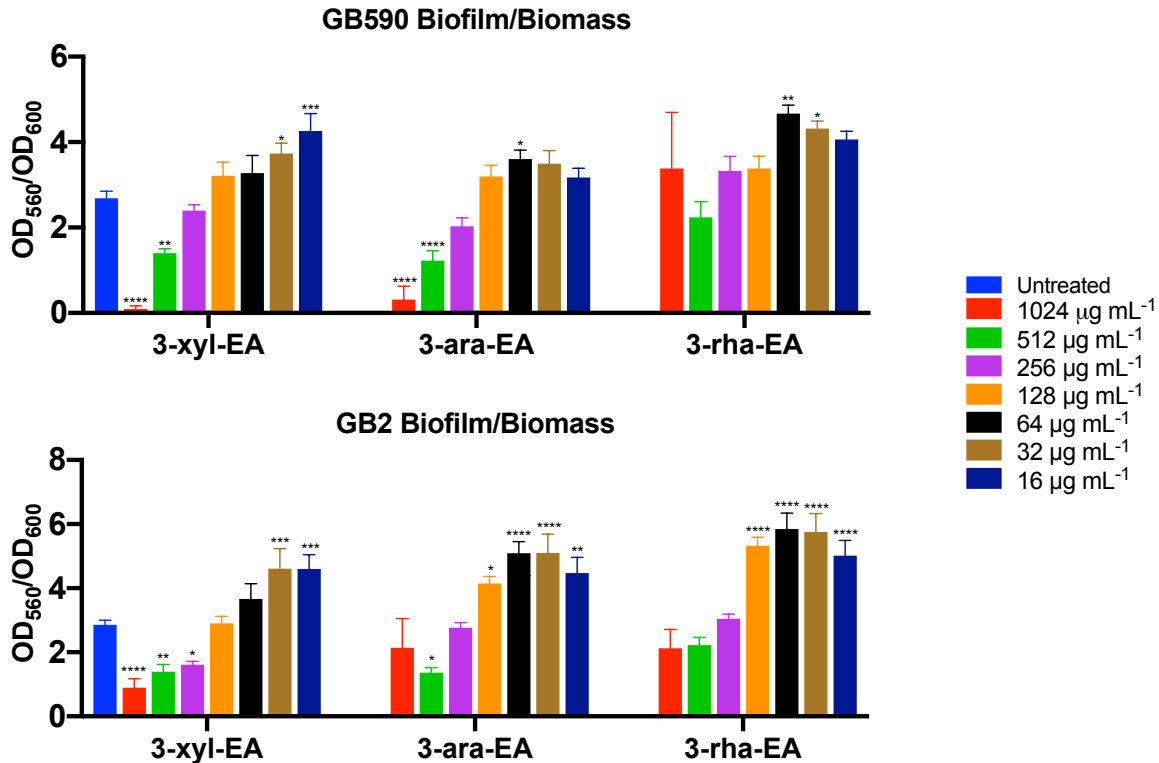


Figure 2.4 Antibiofilm activity of EA glycosides. Biofilm production as denoted by the ratio of biofilm/biomass (OD_{560}/OD_{600}) in GB590 and GB2 in the presence glycosylated EA derivatives relative to biofilm production in THB alone (untreated). Data displayed represent the relative mean biofilm/biomass ratio \pm SEM of at least three independent experiments, each with three technical replicates. * represents $p < 0.05$, ** represents $p < 0.01$, *** represents $p < 0.001$, and **** represents $p < 0.0001$ by one-way ANOVA comparing biofilm production of GBS in each EA glycoside supplementation condition to biofilm production of GBS in media alone (untreated).⁴³

2.5.2 Visualization of EA glycoside-mediated effects on GBS biofilms

To investigate how EA glycosides impact GBS biofilm formation, we sought to use microscopy imaging techniques. Scanning electron microscopy (SEM) has been used previously to identify changes to biofilm architectures and extracellular matrices (ECM).⁴⁴

⁴⁵ We conducted imaging in GB590, since it was the most significantly impacted GBS strain upon treatment with synthetic EA glycosides. Additionally, since EA arabinoside **2.47** had not been previously synthesized, we imaged its effects on GBS biofilm formation when dosed at $512 \mu\text{g mL}^{-1}$ (**Figure 2.5**).

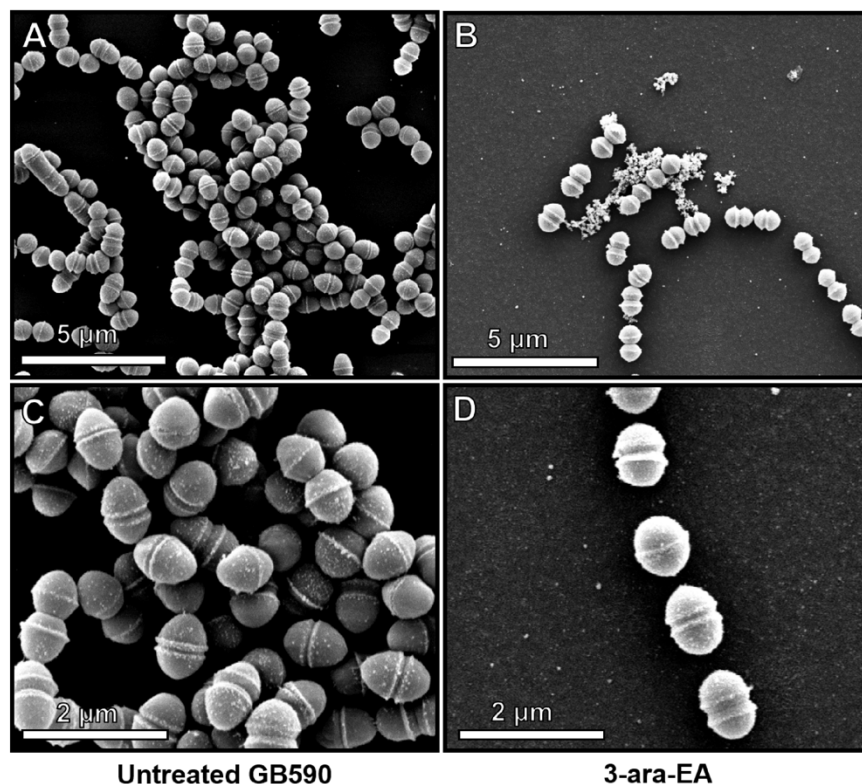


Figure 2.5 Scanning electron micrographs GB590 biofilm formation in THB after 24 h. (A.) GB590 at 20,000x magnification. (B.) GB590 when treated with $512 \mu\text{g mL}^{-1}$ of **2.47** at 20,000x magnification. (C.) GB590 at 50,000x magnification. (D.) GB590 when treated with $512 \mu\text{g mL}^{-1}$ of **2.47** at 50,000x magnification.⁴⁶

The SEM images revealed that EA arabinoside **2.47** impacts general adhesion of Group B streptococcal cells to the slide surface. In the untreated GBS samples, the cells adhere uniformly to the abiotic surface and begin to stack against one another. This monolayer formation is seen at low magnification (**Figure 2.5A**) and is the beginning bacterial

adhesion from which robust three-dimensional biofilm architectures will continue to build. Alternatively, in the GBS sample treated with EA arabinoside **2.47**, there is a lack of cellular adhesion and monolayer formation at the slide surface. At low magnification (**Figure 2.5B**) we see sparse adhesion of streptococcal cells and no cellular clumping or stacking is observed. Since the cellular adhesion is significantly stunted, this likely impedes any further biofilm structures from assembling. As these results indicate, EA glycosides impede early adhesion mechanisms of GBS biofilms. Antibiofilm activity such as this, is broadly applicable to the prevention of biofilm formation on surfaces and medical devices, and offers opportunities in combating antibiotic-resistant infections.

2.5.3 Antibacterial activity of EA glycosides against ESKAPE pathogens

Our studies demonstrated that EA glycosides have antibacterial and antibiofilm effects against GBS, and previous work has shown these ellagitannins also inhibit the growth of MSSA. This indicates EA glycosides inhibit gram-positive pathogens, but EA glycosides had not yet been investigated for activity against gram-negative pathogens. To investigate this, we collaborated with the Community for Open Antimicrobial Drug Discovery (COADD) to screen the synthetic EA glycosides **2.34**, **2.47**, and **2.35** against several ESKAPE pathogens (**Table 2.2**).⁴⁷ These assays tested for growth inhibitory effects against *Staphylococcus aureus* (MRSA), *Escherichia coli*, *Klebsiella pneumoniae*, *Pseudomonas aeruginosa*, *Acinetobacter baumannii*, and two fungal pathogens, *Candida albicans* and *Cryptococcus neoformans*. For these assays, each EA glycoside (**2.34**, **2.47**, **2.35**) and EA (**2.14**) were dosed at a constant concentration of 32 $\mu\text{g mL}^{-1}$ and growth inhibition was recorded.

Table 2.2 Growth inhibition of EA glycosides against additional pathogens^{a,b}

Compound	<i>S. aureus</i>	<i>E. coli</i>	<i>K. pneumoniae</i>	<i>P. aeruginosa</i>	<i>A. baumannii</i>	<i>C. albicans</i>	<i>C. neoformans</i> ^c
2.34	50	44	39	8	43	12	-86
2.47	42	25	26	23	25	14	-6
2.35	42	38	45	18	35	25	-2
EA (2.14)	65	5	11	3	8	21	3

^aAssay conditions performed according to COADD standard operating procedures⁴⁷

^bAll values expressed in percent ($\pm 10\%$) ^cNegative number is attributed to growth of fungus

These antimicrobial assays against several ESKAPE pathogens indicated that EA glycosides **2.34**, **2.47**, and **2.35** have antibacterial activity against gram-negative bacteria in addition to gram-positive species. As anticipated, the highest antibacterial effects were seen against *S. aureus* (MRSA), ranging from 42-50% growth inhibition across EA glycosides. EA (**2.14**) alone also significantly inhibited MRSA growth by 65%, suggesting the glycoside is not necessary for these growth inhibitory effects. Notably, the EA glycosides showed unique activity across the gram-negative ESKAPE pathogens, where **2.34** inhibited *A. baumannii* by 43% and **2.35** inhibited growth of *K. pneumoniae* by 45%. In these pathogens, the EA glycosides largely outperformed free EA (**2.14**), indicating a carbohydrate-specific antibacterial effect.

Uniquely, while most EA glycosides did not inhibit growth of the fungal pathogens *C. albicans* or *C. neoformans*, **2.34** did significantly promote the growth of *C. neoformans*. Closer interrogation revealed that the capsular polysaccharide (CPS) of *C. neoformans* is a primary virulence factor and contains xylose within its repeating unit structure.⁴⁸ We

hypothesize that *C. neoformans* can utilize the xylose residue from **2.34** within the synthesis of its capsular polysaccharide and this ultimately promotes *C. neoformans* growth. These results have illustrated the broad-spectrum antibacterial activity of EA glycosides and encourages further studies into the antibiofilm effects of such molecules on gram-negative biofilms.

2.6 Conclusion and future directions

Through this work, we synthesized a variety of glycosylated EA derivatives and investigated their biological activity against GBS. Our work showed the EA arabinoside **2.47** had significant antibiofilm activity against multiple strains of GBS and this antibiofilm activity was due to a stunting of initial bacterial adhesion mechanisms. We also demonstrated synthetic EA glycosides prevent the growth of gram-negative pathogens such as *K. pneumoniae* and *A. baumannii*. In summation, this work has demonstrated the ability of ellagitannin natural products to inhibit the growth and biofilm formation of pathogenic bacteria, but other studies would contribute to the development of such molecules as antimicrobial therapeutics.

While we showed EA glycosides could inhibit the growth of gram-negative pathogens, we have not yet studied if the glycosides inhibit biofilm formation within these strains. We hypothesize the glycosides will have similar antibiofilm properties as seen in gram-positive pathogens, but this remains to be investigated. Conducting similar antibiofilm assays and microscopy visualizations would provide support for the broad-spectrum utility of the synthetic EA glycosides in biofilm prevention.

Additionally, the studies herein have largely focused on the antibacterial effects of EA glycosides on pathogenic bacteria, but we are also interested if these compounds impact

healthy commensals. Naturally occurring EA glycosides are ingested through normal diet in the form of fruits and berries, and as such they are thought to play a healthy regulatory role within the microbiome.^{15-18, 49} As we have evidence that EA glycosides can inhibit the growth and adhesion of pathogenic microbes, it would be worth investigating if treatment with EA glycosides might conversely increase commensal proliferation and act as a probiotic. To investigate this further, strains of varying commensals including *Bifidobacterium*, *Lactobacillus*, *Streptococcus*, and *Bacteroides* species should be evaluated for growth effects of EA glycoside treatment. We would anticipate the EA glycosides would not inhibit the growth of these bacteria and might even promote the growth of some commensals. This activity would identify EA glycosides as potential molecules for maintaining microbiome symbiosis. Studies such as these would continue to identify novel use for EA glycosides in regulating a healthy microbiome and combating infectious disease.

2.7 Experimental methods

General synthetic procedures and materials

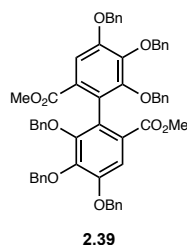
All moisture-sensitive reactions were performed in flame-dried or oven-dried glassware under an atmosphere of argon. Oven-dried stainless-steel syringes or cannula were used to transfer moisture- and air-sensitive liquids. Reaction temperatures were controlled and monitored using a hot plate stirrer with a thermocouple thermometer. Analytical thin-layer chromatography (TLC) was performed on Sorbtech Silica XHL UV-254, glass-backed, 250 μm plated, and visualized using UV, cerium ammonium molybdate stain, anisaldehyde stain, or potassium permanganate stain. Flash column chromatography

was performed as described by Still et al. using silica gel 230-400 mesh.⁵⁰ Yields were reported as purified, isolated compounds. Solvents were dried through a Braun MB-SPS solvent system and used immediately or stored over 3 Å or 4 Å molecular sieves. N-bromosuccinamide was recrystallized from water. Copper powder was activated as described by Kleiderer et al.⁵¹ Glycosyl iodide donors were prepared as reported by Mukhopadhyay et al.³⁸ Compounds **2.37** and **2.38** were prepared as reported by Hirokane et al.²⁵ Other commercial reagents were used as received.

NMR spectra were obtained on Bruker 400 MHz and Bruker 600 MHz spectrometers and are reported relative to deuterated solvent signals. Data for ¹H NMR spectra are presented as follows: chemical shift (δ ppm), multiplicity (s = singlet, d = doublet, t = triplet, q = quartet, p = pentet, m = multiplet, td = triplet of doublet, dp = doublet of pentet, dq = doublet of quartet, br = broad, app = apparent), coupling constants (Hz) and integration. Deuterated chloroform was standardized to 7.26 ppm. Deuterated methanol was standardized to 3.31 ppm. Deuterated DMSO was standardized to 2.50 ppm. ¹³C NMR spectra were obtained on Bruker 101 MHz and 151 MHz spectrometers and are reported relative to deuterated solvent signals. Deuterated chloroform was standardized to 77.0 ppm. Deuterated methanol was standardized to 49.0 ppm. Deuterated DMSO was standardized to 39.52 ppm. High-resolution mass spectra (HRMS) were obtained from the Vanderbilt Mass Spectrometry Research Center using a Synapt G2-S HDMS (Milford, Ma, USA) mass spectrometer. Low-resolution mass spectra (LRMS) were collected using a Thermo Fisher MSQ-Plus-40000 mass spectrometer. Melting points were recorded on a Fisher-Johns 12-144 melting point apparatus. Optical rotations (OR) were measured

with an Autopol IV Automatic Polarimeter at a concentration of 1 mg mL⁻¹. IR spectra were recorded neat via ATR on a Nicolet iS 5 FTIR spectrometer.

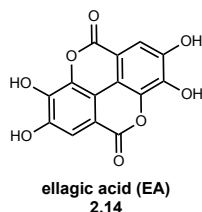
Compound preparation and characterization



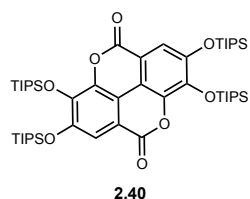
Dimethyl 4,4',5,5',6,6'-hexakis(benzyloxy)-[1,1'-biphenyl]-2,2'-dicarboxylate (2.39)

To activated Cu (0.33 g, 5.19 mmol, 8.39 equiv.) was added **2.38** (330 mg, 0.619 mmol, 1 equiv.) and DMF (0.10 mL, 6 M). and the resulting slurry heated at 110 °C for three hours. After this time, additional DMF (0.65 mL, 1 M) was added, and the reaction was heated at 150 °C overnight. After cooling to room temperature, the reaction was diluted with EtOAc (5 mL) and passed through Celite. The filtrate was washed with 1 N HCl (2 x 10 mL) and brine (5 mL) before being dried over Na₂SO₄ and concentrated *in vacuo*. The crude oil was then purified via flash column chromatography (SiO₂, 20-40% EtOAc/hexanes) to afford **2.39** (120 mg, 0.31 mmol, 43%) as an oil. R_f = 0.17 (20% EtOAc/hexanes); m.p. 60 °C; ¹H NMR (400 MHz, CDCl₃) δ 7.55 (s, 2H), 7.52 (d, *J* = 6.5 Hz, 4H), 7.46 – 7.32 (m, 10H), 7.28 – 7.21 (m, 7H), 7.17 – 7.10 (m, 6H), 6.88 (dd, *J* = 7.8, 1.8 Hz, 4H), 5.20 (dd, 4H), 4.98 (dd, 4H), 4.91 (d, *J* = 11.1 Hz, 2H), 4.77 (d, *J* = 11.1 Hz, 2H), 3.59 (s, 6H).; ¹³C NMR (101 MHz, CDCl₃) δ 166.9, 151.8, 151.1, 145.6, 137.9, 137.4, 136.8, 128.7, 128.7, 128.4, 128.2, 128.1, 127.8, 127.8, 127.6, 127.5, 125.6, 111.1, 75.5, 74.7, 71.2, 52.0; IR ν_{\max} cm⁻¹: 1727, 1431, 1367, 1329, 1188, 1100, 1054, 1021, 999,

981, 909, 765, 744, 731, 696, 617, 608; LR-ESI-MS (m/z): calcd for C₅₆H₅₀O₁₀⁺ (M+H)⁺ 907.3, found 907.2.

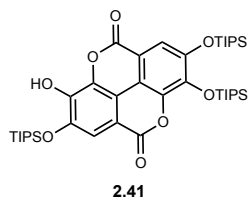


Ellagic acid (EA), (2.14) To Pd(OH)₂ (960 mg, 1.37 mmol, 20 mol %), **2.39** (6.23 g, 6.87 mmol, 1 equiv.) in EtOAc (70 mL, 0.1M) was added and the solution sparged with argon for 5 min. The solution was then sparged with H₂ gas for 5 min before being allowed to sit under a H₂ balloon for 18 h. The completed reaction was then sparged with argon for 15 min to remove any residual H₂. The slurry was dissolved in pyridine (40 mL) and the solution filtered through a pad of Celite to remove Pd(OH)₂. The filtrate was concentrated *in vacuo* and the crude material (2.52 g, 6.87 mmol) was slurried in 1:1 MeOH:H₂O (0.2 M, 30 mL), and heated at 85 °C for 4 h. The resulting green solid was then concentrated *in vacuo* and was taken forward to the next step.



2,3,7,8-tetrakis((triisopropylsilyl)oxy)chromeno[5,4,3-cde]chromene-5,10-dione (2.40) To DMF (0.25 M, 27 mL), **2.14** (2.08 g, 6.87 mmol, 1 equiv.) was added and stirred as a slurry. DMAP (839 mg, 6.87 mmol, 1 equiv.) was added, followed by imidazole (2.81 g, 41.21 mmol, 6 equiv.) and TIPSCI (6.62 g, 34.34 mmol, 5 equiv.). The slurry was then

heated at 80 °C for 18 h. The resulting mixture was cooled to room temperature and DCM (30 mL) was added to dissolve the remaining solid. The solution was filtered through Celite and the filtrate washed with 1N HCl (2 x 20 mL) and brine (20 mL). The organics were then dried over Na₂SO₄ and concentrated *in vacuo* to yield a crude solid. This solid was then triturated with hot *i*-PrOH and filtered to yield pure **2.40** as a white solid (3.91 g, 4.22 mmol, 61% over three steps). R_f = 0.80 (10% EtOAc/hexanes); m.p. >250 °C; ¹H NMR (400 MHz, CDCl₃) δ 7.63 (s, 2H), 1.58 (p, *J* = 7.6 Hz, 6H), 1.42 (p, *J* = 7.5 Hz, 6H), 1.15 (overlapping d, *J* = 2.7 Hz, 72H); ¹³C NMR (101 MHz, CDCl₃) δ 159.4, 150.1, 141.5, 139.9, 115.0, 113.4, 109.6, 18.2, 18.1, 14.3, 13.4; IR ν_{max} cm⁻¹: 2944, 2866, 1747, 1600, 1489, 1414, 1359, 1266, 1187, 1085, 1015, 994, 927, 882, 816, 759, 720, 680, 646, 618, 608; LR-ESI-MS (m/z): calcd for C₅₀H₈₆O₈Si₄⁺ (M+H)⁺ 927.5, found 927.4. The spectral data was consistent with literature values.²³



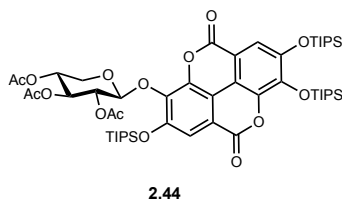
3-hydroxy-2,7,8-tris((triisopropylsilyl)oxy)chromeno[5,4,3-cde]chromene-5,10-

dione (2.41) To per-TIPS protected EA **2.40** (250 mg, 0.27 mmol, 1 equiv.) in DCM (0.1 M, 2.7 mL) at 0 °C, TBAF was added (1 M in THF, 0.9 equiv.) and the solution allowed to stir for 10 min. The reaction was quenched by addition of 1 M HCl and then extracted with DCM (2 x 10 mL) and washed with brine (5 mL). The organics were then dried over Na₂SO₄ and concentrated *in vacuo* to yield a crude solid which was purified via flash column chromatography (SiO₂, 0-10% MeOH/DCM) to afford **2.41** (175 mg, 0.23 mmol,

85%). $R_f = 0.10$ (10% EtOAc/hexanes; $^1\text{H NMR}$ (400 MHz, CDCl_3) δ 7.65 (s, 1H), 7.63 (s, 1H), 1.56 (p, $J = 7.5$ Hz, 3H), 1.42 (p, $J = 7.5$ Hz, 6H), 1.16 (s, 18H), 1.14 (s, 18H), 1.05 (s, 18H). $^{13}\text{C NMR}$ (101 MHz, CDCl_3) δ 159.2, 159.1, 159.0, 150.4, 150.1, 149.7, 145.4, 141.6, 140.7, 140.0, 136.7, 136.2, 115.5, 115.1, 114.4, 113.7, 113.0, 111.0, 109.9, 109.3, 18.2, 14.2, 13.5, 12.8.

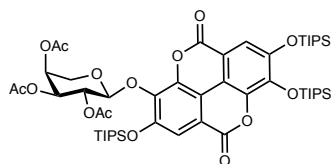
General Glycosylation Procedure²⁰

TIPS-EA (**2.40**, 1 equiv.) was dissolved in DCM (0.1 M) and the solution stirred over activated 4 Å molecular sieves for 1 hour. To this dried solution, TBAF was added (1 M in THF, 0.9 equiv.) and the reaction monitored by TLC for completion. A solution of glycosyl iodide (4 equiv.) in DCM (1 mL) was added, followed by TBAI (1 equiv.) and the slurry was heated at 35 °C in the dark for two days or until glycosyl iodide disappearance via TLC. The reaction was cooled to room temperature and then concentrated *in vacuo*. The concentrated oil was treated with cold EtOAc and filtered to remove excess TBAI. The filtrate was re-concentrated to afford a crude oil which was then purified via flash column chromatography (SiO_2 , 10-30% EtOAc/hexanes) to afford pure glycosylated products **2.44-2.46**.



(2S,3R,4S,5R)-2-((5,10-dioxo-2,7,8-tris((triisopropylsilyl)oxy)-5,10-dihydrochromeno[5,4,3-cde]chromen-3-yl)oxy)tetrahydro-2H-pyran-3,4,5-triyl

triacetate (2.44) 322 mg, 29%; $R_f = 0.33$ (20% EtOAc/hexanes); m.p. 120°C; $[\alpha]^{20}_D - 50.0^\circ$ (1 mg mL⁻¹, CHCl₃); ¹H NMR (600 MHz, CDCl₃) δ 7.63 (overlapping s, 2H), 5.81 (d, $J = 4.8$ Hz, 1H), 5.32 (dd, $J = 7.0, 4.8$ Hz, 1H), 5.23 (t, $J = 6.7$ Hz, 1H), 5.02 (td, $J = 6.0, 4.0$ Hz, 1H), 4.46 (dd, $J = 12.4, 4.1$ Hz, 1H), 3.55 (dd, $J = 12.5, 5.7$ Hz, 1H), 2.15 (s, 3H), 2.14 (s, 3H), 2.07 (s, 3H), 1.56 (p, $J = 7.6$ Hz, 3H), 1.40 (dp, $J = 24.3, 7.6$ Hz, 6H), 1.13 (overlapping d, $J = 7.5$ Hz, 54H); ¹³C NMR (151 MHz, CDCl₃) δ 170.0, 170.0, 169.3, 158.9, 158.8, 151.3, 150.4, 142.8, 141.6, 139.7, 138.9, 115.5, 115.4, 113.8, 113.5, 113.0, 109.5, 99.7, 69.7, 69.6, 68.5, 61.9, 21.0, 20.9, 20.8, 18.1, 18.0, 18.0, 14.2, 13.4, 13.0; IR ν_{max} cm⁻¹: 2945, 2867, 1749, 1603, 1479, 1411, 1360, 1241, 1219, 1187, 1085, 1017, 916, 881, 814, 760, 717, 688, 646, 624, 614, 600; LR-ESI-MS (m/z): calcd for C₅₂H₈₀O₁₅Si³⁺ (M+H)⁺ 1029.5, found 1030.2.

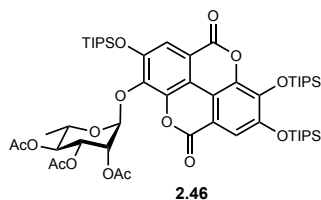


2.45

(2S,3R,4S,5S)-2-((5,10-dioxo-2,7,8-tris((triisopropylsilyl)oxy)-5,10-dihydrochromeno[5,4,3-cde]chromen-3-yl)oxy)tetrahydro-2H-pyran-3,4,5-triyl

triacetate (2.45) 180 mg, 23%; $R_f = 0.33$ (20% EtOAc/hexanes); m.p. 120°C; $[\alpha]^{20}_D - 26.0^\circ$ (1 mg mL⁻¹, CHCl₃); ¹H NMR (600 MHz, CDCl₃) δ 7.64 (s, 1H), 7.63 (s, 1H), 5.68 (d, $J = 4.7$ Hz, 1H), 5.50 (dd, $J = 7.0, 4.7$ Hz, 1H), 5.26-5.34 (m, 2H), 4.28 (dd, $J = 12.2, 5.9$ Hz, 1H), 3.62 (dd, $J = 12.1, 2.9$ Hz, 1H), 2.17 (overlapping s, 6H), 2.12 (s, 3H), 1.56 (p, $J = 7.6$ Hz, 3H), 1.40 (dp, $J = 21.0, 7.6$ Hz, 6H), 1.14 (overlapping d, $J = 7.5$ Hz 54H); ¹³C NMR (151 MHz, CDCl₃) δ 170.4, 170.3, 169.4, 159.0, 158.9, 151.5, 150.4, 142.9,

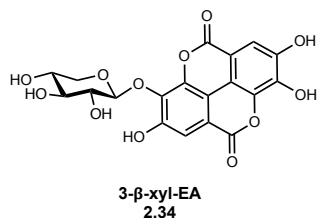
141.7, 139.8, 139.1, 115.6, 115.3, 113.9, 113.5, 113.0, 109.5, 99.8, 69.2, 68.8, 66.6, 61.5, 21.0, 20.9, 18.1, 18.0, 18.0, 14.2, 13.4, 13.0; IR ν_{\max} cm^{-1} : 2944, 2866, 1747, 1602, 1478, 1411, 1359, 1241, 1218, 1187, 1084, 1017, 995, 966, 917, 880, 861, 814, 760, 717, 685, 647; LR-ESI-MS (m/z): calcd for $\text{C}_{52}\text{H}_{80}\text{O}_{15}\text{Si}_3^+$ ($\text{M}+\text{H}$) $^+$ 1029.5, found 1029.4.



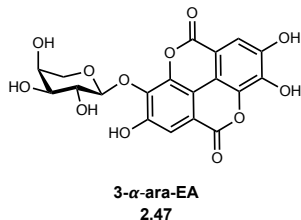
(2*S*,3*R*,4*R*,5*S*,6*S*)-2-((5,10-dioxo-2,7,8-tris((triisopropylsilyl)oxy)-5,10-dihydrochromeno[5,4,3-*cde*]chromen-3-yl)oxy)-6-methyltetrahydro-2*H*-pyran-3,4,5-triyl triacetate (2.46) 119 mg, 21%; R_f = 0.40 (20% EtOAc/hexanes); m.p. 124 °C; $[\alpha]_D^{20}$ -8.0° (1 mg mL^{-1} , CHCl_3); ^1H NMR (600 MHz, CDCl_3) δ 7.65 (s, 1H), 7.63 (s, 1H), 5.74 (dd, J = 3.5, 1.8 Hz, 1H), 5.66 (d, J = 1.7 Hz, 1H), 5.59 (dd, J = 10.2, 3.4 Hz, 1H), 5.17 (t, J = 10.1 Hz, 1H), 4.83 (dq, J = 9.9, 6.3 Hz, 1H), 2.16 (s, 3H), 2.09 (s, 3H), 2.01 (s, 3H), 1.56 (p, J = 7.6 Hz, 3H), 1.42 – 1.38 (m, 6H), 1.16 – 1.09 (m, 57H); ^{13}C NMR (151 MHz, CDCl_3) δ 170.3, 170.0, 169.7, 158.9, 158.7, 151.3, 150.4, 143.5, 141.6, 139.7, 139.1, 115.4, 115.2, 114.2, 113.5, 112.9, 109.5, 99.7, 70.5, 69.3, 68.7, 21.0, 20.9, 20.8, 18.1, 18.0, 17.9, 17.3, 14.2, 13.4, 13.1; IR ν_{\max} cm^{-1} : 2944, 2866, 1747, 1602, 1478, 1411, 1358, 1239, 1216, 1186, 1139, 1083, 1016, 996, 963, 916, 880, 861, 813, 760, 716, 686, 647; LR-ESI-MS (m/z): calcd for $\text{C}_{53}\text{H}_{82}\text{O}_{15}\text{Si}_3^+$ ($\text{M}+\text{H}$) $^+$ 1043.5, found 1043.5.

General Deprotection Procedure²⁰

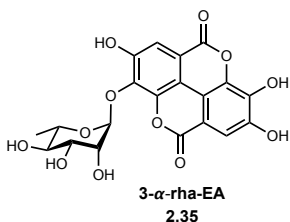
To protected EA glycosides **2.44-2.46** (1 equiv.) in 10:1 DMF/H₂O (0.1 M) was added K₂CO₃ (1.3 equiv.) and the solution allowed to for 5 h at room temperature. The reaction was diluted with toluene (5 mL) and adjusted to pH~6 with dilute AcOH. The solution was concentrated *in vacuo* and the resulting solid co-evaporated toluene (3 X 5 mL). The solid was then re-dissolved in 10:1 MeOH/H₂O (0.1 M) and K₂CO₃ (1.5 equiv.) was added. The resulting slurry was allowed to stir for 2 days at RT. To quench, Dowex H⁺ resin was added until reaction pH~4 and the resulting solution was filtered and concentrated *in vacuo*. The final solid was dissolved in H₂O and lyophilized to dryness to afford the desired deprotected ellagic acid glycosides **2.34**, **2.47** and **2.35**.



2,3,7-trihydroxy-8-(((2S,3R,4S,5R)-3,4,5-trihydroxytetrahydro-2H-pyran-2-yl)oxy)chromeno[5,4,3-cde]chromene-5,10-dione (2.34) 30 mg, 20% over two steps; m.p. >250°C; $[\alpha]^{20}_D +12.0^\circ$ (1 mg mL⁻¹, DMSO); ¹H NMR (600 MHz, d₆-DMSO) δ 7.50 (s, 1H), 7.36 (s, 1H), 5.36 (d, *J* = 6.9 Hz, 1H), 3.81 (dd, *J* = 11.4, 5.0 Hz, 1H), 3.47-3.41 (m, 2H), 3.29 (t, *J* = 8.3 Hz, 1H), 3.11 (dd, *J* = 11.6, 9.1 Hz, 1H); ¹³C NMR (151 MHz, d₆-DMSO) δ 159.3, 159.0, 151.9, 149.4, 141.9, 136.1, 135.9, 113.4, 112.5, 112.0, 111.1, 109.1, 103.0, 75.5, 73.3, 69.4, 65.8; IR ν_{\max} cm⁻¹: 3234, 1716, 1608, 1582, 1484, 1430, 1359, 1186, 1104, 1046, 919, 822, 756, 604; HR-ESI-MS (*m/z*): calcd for C₁₉H₁₄O₁₂⁻ (M-H)⁻ 433.0407, found 433.0403. The spectral data was consistent with literature values.²⁰



2,3,7-trihydroxy-8-(((2S,3R,4S,5S)-3,4,5-trihydroxytetrahydro-2H-pyran-2-yl)oxy)chromeno[5,4,3-cde]chromene-5,10-dione (2.47) 40 mg, 32% over two steps; m.p. >250°C; $[\alpha]^{20}_{\text{D}}$ -10.0° (1 mg mL⁻¹, DMSO); ¹H NMR (600 MHz, d₆-DMSO): δ 7.51 (s, 1H), 7.42 (s, 1H), 5.53 (d, J = 3.18, 1 H), rest of spectra obscured by residual H₂O. ¹³C NMR (151 MHz, d₆-DMSO) δ 159.2, 158.8, 152.1, 148.9, 141.8, 136.2, 135.6, 113.4, 112.4, 112.0, 111.0, 109.9, 101.7, 71.0, 70.1, 64.6, 62.7; IR ν_{max} cm⁻¹: 3251, 1704, 1608, 1429, 1366, 1188, 1107, 1065, 1021, 948, 920, 880, 820, 758, 618; HR-ESI-MS (m/z): calcd for C₁₉H₁₄O₁₂⁻ (M-H)⁻ 433.0407, found 433.0395.



2,3,7-trihydroxy-8-(((2S,3R,4R,5R,6S)-3,4,5-trihydroxy-6-methyltetrahydro-2H-pyran-2-yl)oxy)chromeno[5,4,3-cde]chromene-5,10-dione (2.35) 70 mg, 60%; m.p. >250°C; $[\alpha]^{20}_{\text{D}}$ -22.0° (1 mg mL⁻¹, DMSO); ¹H NMR (600 MHz, d₆-DMSO): δ 7.56 (s, 1H), 7.47 (s, 1H), 5.52 (d, J = 1.38, 1H), rest of spectra obscured by residual H₂O. ¹³C NMR (151 MHz, d₆-DMSO) δ 159.3, 159.1, 152.9, 148.8, 142.8, 140.2, 137.2, 136.7, 113.7, 112.6, 112.1, 111.7, 110.8, 107.7, 102.9, 71.9, 71.0, 70.8, 70.8, 70.6, 70.5, 18.2; IR ν_{max} cm⁻¹: 3265, 2926, 1722, 1608, 1487, 1428, 1361, 1183, 1096, 1058, 1021, 951, 914, 826,

757, 600; HR-ESI-MS (m/z): calcd for C₂₀H₁₆O₁₂⁻ (M-H)⁻ 447.0564, found 447.0567. The spectral data was consistent with literature values.²⁰

Bacterial strains and culture conditions

Table 2.3 Bacterial strains

Bacterial Strain	Source
<i>S. agalactiae</i> strain GB590 (GB00590)	Clinical isolate, Shannon Manning, Michigan State, Genome Accession Number: NZ_LGAI01000000
<i>S. agalactiae</i> strain GB2 (GB00002)	Clinical Isolate, Shannon Manning, Michigan State, Genome Accession Number: SAMN00991164
<i>S. aureus</i> strain 43300	American Tissue Culture Collection (ATCC)
<i>E. coli</i> strain 25922	American Tissue Culture Collection (ATCC)
<i>K. pneumoniae</i> strain 700603	American Tissue Culture Collection (ATCC)
<i>A. baumannii</i> strain 19606	American Tissue Culture Collection (ATCC)
<i>P. aeruginosa</i> strain 27853	American Tissue Culture Collection (ATCC)
<i>C. albicans</i> strain 90028	American Tissue Culture Collection (ATCC)
<i>C. neoformans</i> strain 208821	American Tissue Culture Collection (ATCC)

All *S. agalactiae* strains were grown on tryptic soy agar plates supplemented with 5% sheep blood (blood agar plates) at 37 °C in ambient air overnight. Strains were sub-cultured from blood agar plates into 5 mL of Todd-Hewitt broth (THB) and incubated under shaking conditions at 180 rpm at 37 °C in ambient air overnight. Following overnight incubation, bacterial density was quantified through absorbance readings at 600 nm

(OD₆₀₀) using a Promega GloMax-Multi Detection System plate reader. Bacterial numbers were determined using the predetermined coefficient of 1 OD₆₀₀ = 10⁹ CFU mL⁻¹.

Additional bacterial strains were grown and assayed by COADD according to their standard operating procedures detailed below:

COADD sample preparation

Samples were prepared in DMSO to a final testing concentration of 32 µg mL⁻¹ in 384-well, non-binding surface plate (NBS) for each bacterial/fungal strain, and in duplicate (n=2), and keeping the final DMSO concentration to a maximum of 1% DMSO. All the sample-preparation were done using liquid handling robots.

COADD antimicrobial assay

All bacteria were cultured in Cation-adjusted Mueller Hinton broth (CAMHB) at 37 °C overnight. A sample of each culture was then diluted 40-fold in fresh broth and incubated at 37 °C for 1.5-3 h. The resultant mid-log phase cultures were diluted (CFU mL⁻¹ measured by OD₆₀₀), then added to each well of the compound containing plates, giving a cell density of 5 x 10⁵ CFU mL⁻¹ and a total volume of 50 µL. All the plates were covered and incubated at 37 °C for 18 h without shaking.

Inhibition of bacterial growth was determined measuring absorbance at 600 nm (OD₆₀₀), using a Tecan M1000 Pro monochromator plate reader. The percentage of growth inhibition was calculated for each well, using the negative control (media only) and positive control (bacteria without inhibitors) on the same plate as references. The

significance of the inhibition values was determined by modified Z-scores, calculated using the median and MAD of the samples (no controls) on the same plate.

COADD antifungal assay

Fungi strains were cultured for 3 days on Yeast Extract-Peptone Dextrose (YPD) agar at 30 °C. A yeast suspension of 1×10^6 to 5×10^6 CFU mL⁻¹ (as determined by OD₅₃₀) was prepared from five colonies. The suspension was subsequently diluted and added to each well of the compound-containing plates giving a final cell density of fungi suspension of 2.5×10^3 CFU mL⁻¹ and a total volume of 50 µL. All plates were covered and incubated at 35 °C for 24 h without shaking.

Growth inhibition of *C. albicans* was determined measuring absorbance at 530 nm (OD₅₃₀), while the growth inhibition of *C. neoformans* was determined measuring the difference in absorbance between 600 and 570 nm (OD₆₀₀₋₅₇₀), after the addition of resazurin (0.001% final concentration) and incubation at 35 °C for additional 2 h. The absorbance was measured using a Biotek Synergy HTX plate reader. The percentage of growth inhibition was calculated for each well, using the negative control (media only) and positive control (fungi without inhibitors) on the same plate. The significance of the inhibition values was determined by modified Z-scores, calculated using the median and MAD of the samples (no controls) on the same plate.

COADD quality control

Colistin and vancomycin were used as positive bacterial inhibitor standards for gram-negative and gram-positive bacteria, respectively. Fluconazole was used as a positive

fungal inhibitor standard for *C. albicans* and *C. neoformans*. The antibiotics were provided in 4 concentrations, with 2 above and 2 below its MIC value, and plated into the first 8 wells of column 23 of the 384-well NBS plates. The quality control (QC) of the assays was determined by the antimicrobial controls and the Z'-factor (using positive and negative controls). Each plate was deemed to fulfil the quality criteria (pass QC), if the Z'-factor was above 0.4, and the antimicrobial standards showed full range of activity, with full growth inhibition at their highest concentration, and no growth inhibition at their lowest concentration.

Determination of minimum inhibitory concentration (MIC) and minimum biofilm inhibition concentration (MBIC) in GBS

GBS cultures were grown overnight as described above and used to inoculate fresh THB to achieve 5×10^5 CFU mL⁻¹. To 96 well tissue culture treated, sterile polystyrene plates was added the inoculated media in the presence of increasing concentrations of ellagic acid glycosides 2-4 to achieve a final volume of 100 μ L per well. Bacteria grown in THB in the presence of DMSO served as the control. The plates were incubated under static conditions at 37 °C in ambient air for 24 h. Bacterial growth was quantified through absorbance readings (OD₆₀₀). The minimum inhibitory concentrations (MICs) were assigned at the lowest concentration of compound at which a percentage of growth (50% or 90%; MIC₅₀ or MIC₉₀ respectively) was observed compared to that of the control.

To measure biofilm production, culture medium was then removed, and wells were washed gently with phosphate buffered saline (PBS, pH 7.4) to remove non-adherent cells; the remaining biofilms were stained with a 10% crystal violet solution for 5–10 min.

Following staining, wells were washed with PBS and allowed to dry at room temperature for at least 30 min. After drying, the remaining crystal violet stain was solubilized via addition of 100 μ L of 80% ethanol/20% acetone solution. Biofilm formation was quantified through absorbance readings (OD_{560}). Results were analyzed compared to controls in the absence of ellagic acid glycosides. The minimum biofilm inhibition concentrations (MBIC) were assigned at the lowest concentration of compound at which a percentage of absorbance (50% or 90%; MBIC₅₀ or MBIC₉₀ respectively) was observed compared to that of the control. Biofilm to biomass ratios were reported as the ratio OD_{560}/OD_{600} .

Statistical analysis

Unless otherwise stated, all data is representative of at least three biological replicates with three technical replicates each. Data are expressed as the mean \pm SEM. Statistical analyses were performed in GraphPad Prism Software v. 7.0c. Statistical significance for biofilm production was determined using one-way ANOVA with post hoc Dunnett's multiple comparison test comparing biofilm production in the presence of EA glycosides to biofilm production in media alone.

Scanning electron microscopy sample preparation

Bacterial cells were analyzed by scanning electron microscopy as previously described with some modifications.⁴⁴ Briefly, bacteria were cultured in Todd-Hewitt broth (THB) in wells containing 12 mm glass coverslips coated with poly-L-lysine (Corning, Bedford MA) at 37 °C for 24 h. At 24 h, supernatants were removed and samples were fixed with 2.0% paraformaldehyde and 2.5% glutaraldehyde in 0.05 M sodium cacodylate buffer for 24 h.

Secondary fixation with 0.1% osmium tetroxide was performed for 5 min prior to sequential dehydration with increasing concentrations of ethanol. After ethanol dehydration, samples were dried at the critical point using a critical point dryer machine (Tousimis), mounted onto aluminum sample stubs, and sputter-coated with 80/20 gold–palladium. Afterward, samples were painted with a thin strip of colloidal silver (Electron Microscopy Sciences) at the edge to facilitate charge dissipation. Samples were imaged with a FEI Quanta 250 field-emission gun scanning electron microscope. Images shown are representative of three technical replicates.

2.8 References

1. This chapter is adapted from "Synthetic Ellagic Acid Glycosides Inhibit Early Stage Adhesion of *Streptococcus agalactiae* Biofilms as Observed by Scanning Electron Microscopy" published in *Chemistry-A European Journal* and has been reproduced with the permission of the publisher and my co-authors, Jennifer A. Gaddy and Steven D. Townsend. S. A. Chambers, J. A. Gaddy, S. D. Townsend, Synthetic Ellagic Acid Glycosides Inhibit Early Stage Adhesion of *Streptococcus agalactiae* Biofilms as Observed by Scanning Electron Microscopy. *Chem. Eur. J.* 2020, 26, 9923.
2. Feldman, K. S.; Sambandam, A., Ellagitannin Chemistry. The First Total Chemical Synthesis of an O(2),O(3)-Galloyl-Coupled Ellagitannin, Sanguin H-5. *The Journal of Organic Chemistry* **1995**, 60 (25), 8171-8178.
3. Su, X.; Surry, D. S.; Spandl, R. J.; Spring, D. R., Total Synthesis of Sanguin H-5. *Organic Letters* **2008**, 10 (12), 2593-2596.
4. Khanbabaee, K.; Lötzerich, K., Synthesis of Enantiomerically Pure Unusual Ellagitannins 1,4,6-Tri-O-galloyl-2,3-(R)-hexahydroxydiphenoyl- β -d-glucopyranoside and 4,6-Di-O-galloyl-2,3-(R)-hexahydroxydiphenoyl-d-glucoside. The Proposed Chemical Structures for Cercidin A and B Must Be Revised. *The Journal of Organic Chemistry* **1998**, 63 (24), 8723-8728.
5. Feldman, K. S.; Smith, R. S., Ellagitannin Chemistry. First Total Synthesis of the 2,3- and 4,6-Coupled Ellagitannin Pedunculagin. *The Journal of Organic Chemistry* **1996**, 61 (8), 2606-2612.

6. Khanbabaee, K.; Großer, M., An Efficient Total Synthesis of Pedunculagin by Using a Twofold Intramolecular Double Esterification Strategy. *European Journal of Organic Chemistry* **2003**, 2003 (11), 2128-2131.
7. Khanbabaee, K.; van Ree, T., Tannins: Classification and Definition. *Natural Product Reports* **2001**, 18 (6), 641-649.
8. Russell, A., The Natural Tannins. *Chemical Reviews* **1935**, 17 (2), 155-186.
9. Tzin, V.; Galili, G., New Insights into the Shikimate and Aromatic Amino Acids Biosynthesis Pathways in Plants. *Molecular Plant* **2010**, 3 (6), 956-972.
10. Maeda, H.; Dudareva, N., The Shikimate Pathway and Aromatic Amino Acid Biosynthesis in Plants. *Annual Review of Plant Biology* **2012**, 63 (1), 73-105.
11. Quideau, S.; Feldman, K. S., Ellagitannin Chemistry. *Chem Rev* **1996**, 96 (1), 475-504.
12. Pouységu, L.; Deffieux, D.; Malik, G.; Natangelo, A.; Quideau, S., Synthesis of ellagitannin natural products. *Nat Prod Rep* **2011**, 28 (5), 853-874.
13. Quideau, S.; Deffieux, D.; Douat-Casassus, C.; Pouységu, L., Plant Polyphenols: Chemical Properties, Biological Activities, and Synthesis. *Angew Chem Int Ed* **2011**, 50 (3), 586-621.
14. Kähkönen, M. P.; Hopia, A. I.; Vuorela, H. J.; Rauha, J.-P.; Pihlaja, K.; Kujala, T. S.; Heinonen, M., Antioxidant Activity of Plant Extracts Containing Phenolic Compounds. *J Agric Food Chem* **1999**, 47 (10), 3954-3962.
15. Gaya, P.; Peirotén, Á.; Medina, M.; Álvarez, I.; Landete, J. M., Bifidobacterium pseudocatenulatum INIA P815: The first bacterium able to produce urolithins A and B from ellagic acid. *Journal of Functional Foods* **2018**, 45, 95-99.
16. Kujawska, M.; Jodynis-Liebert, J., Potential of the ellagic acid-derived gut microbiota metabolite - Urolithin A in gastrointestinal protection. *World J Gastroenterol* **2020**, 26 (23), 3170-3181.
17. García-Mantrana, I.; Calatayud, M.; Romo-Vaquero, M.; Espín, J. C.; Selma, M. V.; Collado, M. C., Urolithin Metabotypes Can Determine the Modulation of Gut Microbiota in Healthy Individuals by Tracking Walnuts Consumption over Three Days. *Nutrients* **2019**, 11 (10), 2483.
18. Tomás-Barberán, F. A.; González-Sarrías, A.; García-Villalba, R.; Núñez-Sánchez, M. A.; Selma, M. V.; García-Conesa, M. T.; Espín, J. C., Urolithins, the rescue of "old" metabolites to understand a "new" concept: Metabotypes as a nexus among phenolic metabolism, microbiota dysbiosis, and host health status. *Mol Nutr Food Res* **2017**, 61 (1).

19. Quave, C. L.; Estévez-Carmona, M.; Compadre, C. M.; Hobby, G.; Hendrickson, H.; Beenken, K. E.; Smeltzer, M. S., Ellagic Acid Derivatives from *Rubus ulmifolius* Inhibit *Staphylococcus aureus* Biofilm Formation and Improve Response to Antibiotics. *PLOS ONE* **2012**, *7* (1), e28737.
20. Fontaine, B. M.; Nelson, K.; Lyles, J. T.; Jariwala, P. B.; García-Rodríguez, J. M.; Quave, C. L.; Weinert, E. E., Identification of Ellagic Acid Rhamnoside as a Bioactive Component of a Complex Botanical Extract with Anti-biofilm Activity. *Front Microbiol* **2017**, *8* (496).
21. Gervay-Hague, J., Taming the Reactivity of Glycosyl Iodides To Achieve Stereoselective Glycosidation. *Accounts of Chemical Research* **2016**, *49* (1), 35-47.
22. Raybaudi-Massilia, R. M.; Mosqueda-Melgar, J.; Soliva-Fortuny, R.; Martín-Belloso, O., Control of Pathogenic and Spoilage Microorganisms in Fresh-cut Fruits and Fruit Juices by Traditional and Alternative Natural Antimicrobials. *Compr Rev Food Sci* **2009**, *8* (3), 157-180.
23. Kobayashi, R.; Hanaya, K.; Shoji, M.; Ohba, S.; Sugai, T., Synthesis of Okicamelliaside, a Glucoside of Ellagic Acid with Potent Anti-Degranulation Activity. *Biosci Biotechnol Biochem* **2013**, *77* (4), 810-813.
24. Asami, Y.; Ogura, T.; Otake, N.; Nishimura, T.; Xinsheng, Y.; Sakurai, T.; Nagasawa, H.; Sakuda, S.; Tatsuta, K., Isolation and Synthesis of a New Bioactive Ellagic Acid Derivative from *Combretum yunnanensis*. *J Nat Prod* **2003**, *66* (5), 729-731.
25. Hirokane, T.; Hirata, Y.; Ishimoto, T.; Nishii, K.; Yamada, H., A unified strategy for the synthesis of highly oxygenated diaryl ethers featured in ellagitannins. *Nat Commun* **2014**, *5*, 3478.
26. Chambers, S. A.; Gaddy, J.; Townsend, S., Synthetic Ellagic Acid Glycosides Inhibit Early-Stage Adhesion of *Streptococcus agalactiae* Biofilms as Observed by Scanning Electron Microscopy. *Chemistry – A European Journal* **2020**, *n/a* (n/a).
27. Chen, W.-W.; Zhao, Q.; Xu, M.-H.; Lin, G.-Q., Nickel-Catalyzed Asymmetric Ullmann Coupling for the Synthesis of Axially Chiral Tetra-ortho-Substituted Biaryl Dials. *Org Lett* **2010**, *12* (5), 1072-1075.
28. Hennings, D. D.; Iwama, T.; Rawal, V. H., Palladium-Catalyzed (Ullmann-Type) Homocoupling of Aryl Halides: A Convenient and General Synthesis of Symmetrical Biaryls via Inter- and Intramolecular Coupling Reactions. *Organic Letters* **1999**, *1* (8), 1205-1208.
29. Khan, F.; Dlugosch, M.; Liu, X.; Banwell, M. G., The Palladium-Catalyzed Ullmann Cross-Coupling Reaction: A Modern Variant on a Time-Honored Process. *Accounts of Chemical Research* **2018**, *51* (8), 1784-1795.

30. Bala, I.; Bhardwaj, V.; Hariharan, S.; Kumar, M. N. V. R., Analytical methods for assay of ellagic acid and its solubility studies. *J Pharm Biomed Anal* **2006**, *40* (1), 206-210.
31. Schmidt, R. R.; Zhu, X., Glycosyl Trichloroacetimidates. In *Glycoscience: Chemistry and Chemical Biology*, Fraser-Reid, B. O.; Tatsuta, K.; Thiem, J., Eds. Springer Berlin Heidelberg: Berlin, Heidelberg, 2008; pp 451-524.
32. Schmidt Glycosylation. In *Comprehensive Organic Name Reactions and Reagents*, pp 2498-2502.
33. Fraser-Reid, B.; López, J. C., Armed-disarmed effects in carbohydrate chemistry: history, synthetic and mechanistic studies. *Topics in current chemistry* **2011**, *301*, 1-29.
34. Fraser-Reid, B.; Wu, Z.; Udodong, U. E.; Ottosson, H., Armed/disarmed effects in glycosyl donors: rationalization and sidetracking. *The Journal of Organic Chemistry* **1990**, *55* (25), 6068-6070.
35. Igarashi, K., The Koenigs-Knorr Reaction. In *Advances in Carbohydrate Chemistry and Biochemistry*, Stuart Tipson, R.; Horton, D., Eds. Academic Press: 1977; Vol. 34, pp 243-283.
36. Koenigs, W.; Knorr, E., Ueber einige Derivate des Traubenzuckers und der Galactose. *Berichte der deutschen chemischen Gesellschaft* **1901**, *34* (1), 957-981.
37. Du, W.; Gervay-Hague, J., Efficient Synthesis of α -Galactosyl Ceramide Analogues Using Glycosyl Iodide Donors. *Org Lett* **2005**, *7* (10), 2063-2065.
38. Mukhopadhyay, B.; Kartha, K. P. R.; Russell, D. A.; Field, R. A., Streamlined Synthesis of Per-O-acetylated Sugars, Glycosyl Iodides, or Thioglycosides from Unprotected Reducing Sugars¹. *J Org Chem* **2004**, *69* (22), 7758-7760.
39. X-ray crystal structure courtesy of Professor Nathan Schley.
40. Davies, H. D.; Adair, C.; McGeer, A.; Ma, D.; Robertson, S.; Mucenski, M.; Kowalsky, L.; Tyrell, G.; Baker, Carol J., Antibodies to Capsular Polysaccharides of Group B Streptococcus in Pregnant Canadian Women: Relationship to Colonization Status and Infection in the Neonate. *J Infect Dis* **2001**, *184* (3), 285-291.
41. Manning, S. D.; Lewis, M. A.; Springman, A. C.; Lehotzky, E.; Whittam, T. S.; Davies, D., Genotypic Diversity and Serotype Distribution of Group B Streptococcus Isolated from Women Before and After Delivery. *Clin Infect Dis* **2008**, *46* (12), 1829-1837.
42. Melin, P.; Efstratiou, A., Group B streptococcal epidemiology and vaccine needs in developed countries. *Vaccine* **2013**, *31*, D31-D42.
43. Reproduced with permission. License number 4955430922528.

44. Ackerman, D. L.; Doster, R. S.; Weitkamp, J. H.; Aronoff, D. M.; Gaddy, J. A.; Townsend, S. D., Human Milk Oligosaccharides Exhibit Antimicrobial and Antibiofilm Properties against Group B Streptococcus. *ACS Infect Dis* **2017**, 3 (8), 595-605.
45. Moore, R. E.; Craft, K. M.; Xu, L. L.; Chambers, S. A.; Nguyen, J. M.; Marion, K. C.; Gaddy, J. A.; Townsend, S. D., Leveraging Stereoelectronic Effects in Biofilm Eradication: Synthetic β -Amino Human Milk Oligosaccharides Impede Microbial Adhesion As Observed by Scanning Electron Microscopy. *The Journal of Organic Chemistry* **2020**.
46. Reproduced with permission. License number 4955430922528.
47. Blaskovich, M. A. T.; Zuegg, J.; Elliott, A. G.; Cooper, M. A., Helping Chemists Discover New Antibiotics. *ACS Infect Dis* **2015**, 1 (7), 285-287.
48. Srikanta, D.; Santiago-Tirado, F. H.; Doering, T. L., Cryptococcus neoformans: historical curiosity to modern pathogen. *Yeast* **2014**, 31 (2), 47-60.
49. Espín, J. C.; Larrosa, M.; García-Conesa, M. T.; Tomás-Barberán, F., Biological significance of urolithins, the gut microbial ellagic Acid-derived metabolites: the evidence so far. *Evidence-based complementary and alternative medicine : eCAM* **2013**, 2013, 270418.
50. Still, W. C.; Kahn, M.; Mitra, A., Rapid chromatographic technique for preparative separations with moderate resolution. *The Journal of Organic Chemistry* **1978**, 43 (14), 2923-2925.
51. Kleiderer, E. C.; Adams, R., Stereochemistry of Diphenyls. XXXI.1 Preparation and Properties of 2,2',6,6'-Tetrafluoro-3,3'-dicarboxy-5,5'-dichlorodiphenyl. *Journal of the American Chemical Society* **1933**, 55 (10), 4219-4225.

Appendix A2

Data and NMR spectra relevant to Chapter 2

Figure A2.1 ¹H NMR (400 MHz, CDCl₃) of 2.39

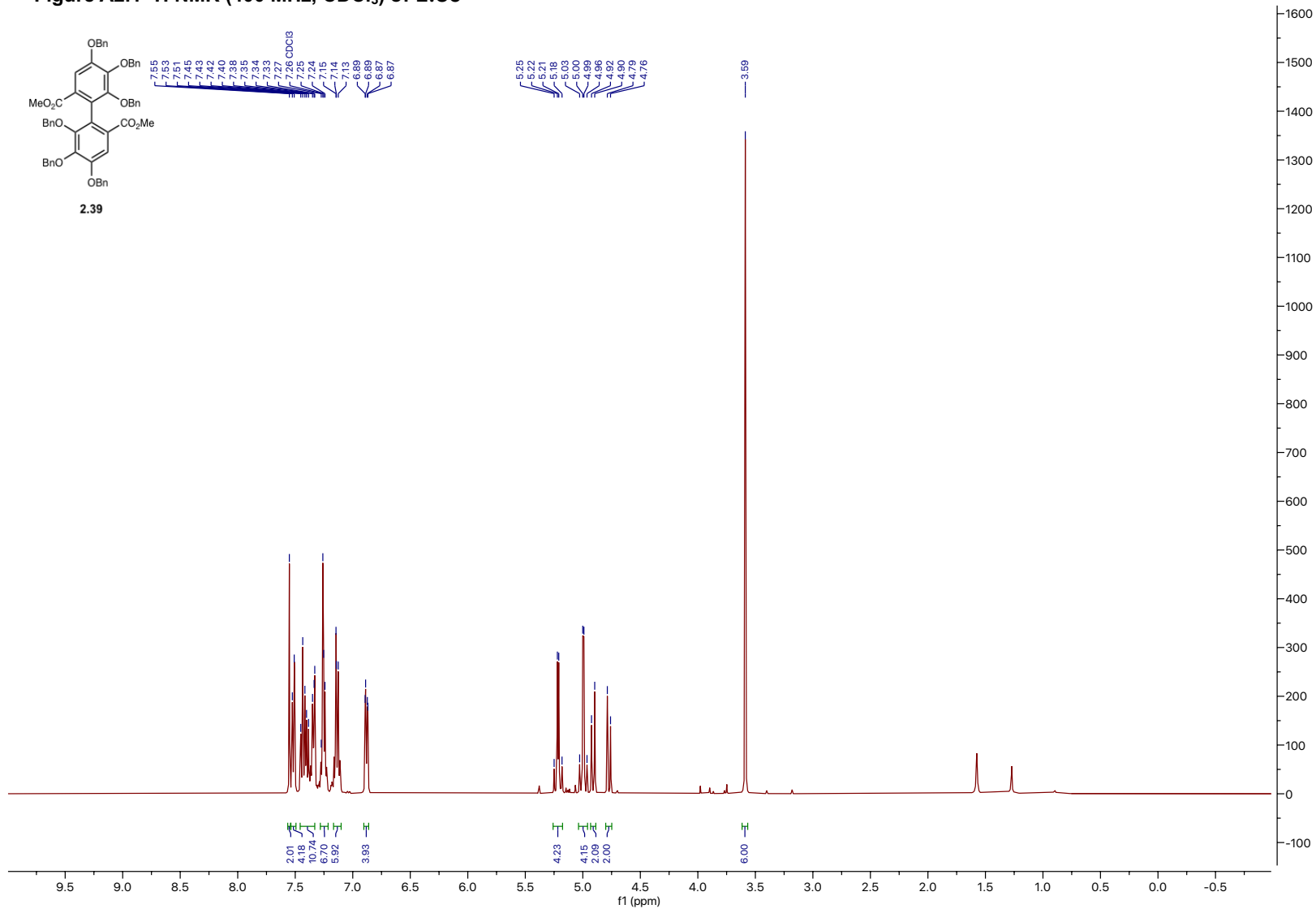


Figure A2.2 ^{13}C NMR (101 MHz, CDCl_3) of 2.39

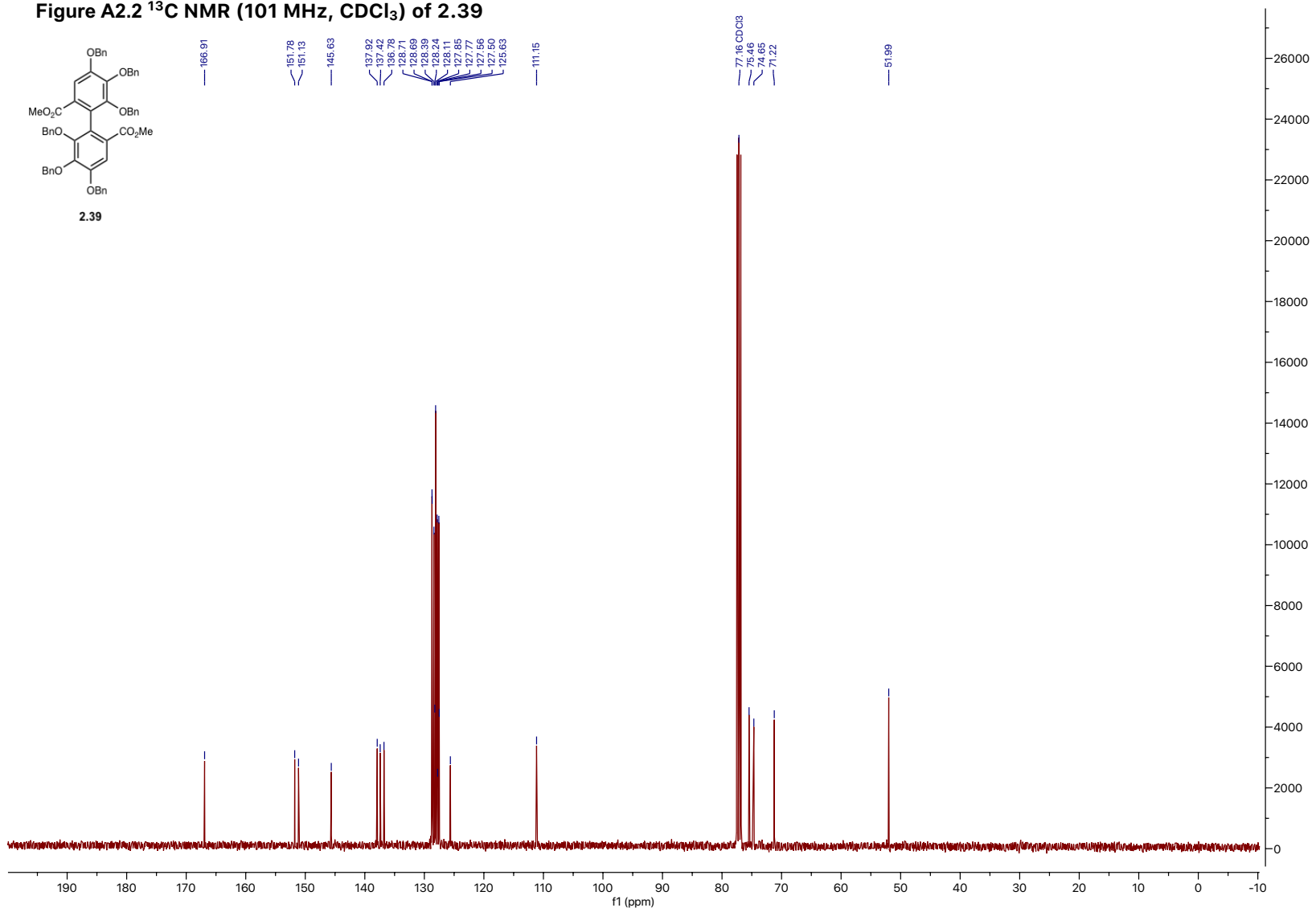


Figure A2.3 ¹H NMR (400 MHz, CDCl₃) of 2.40

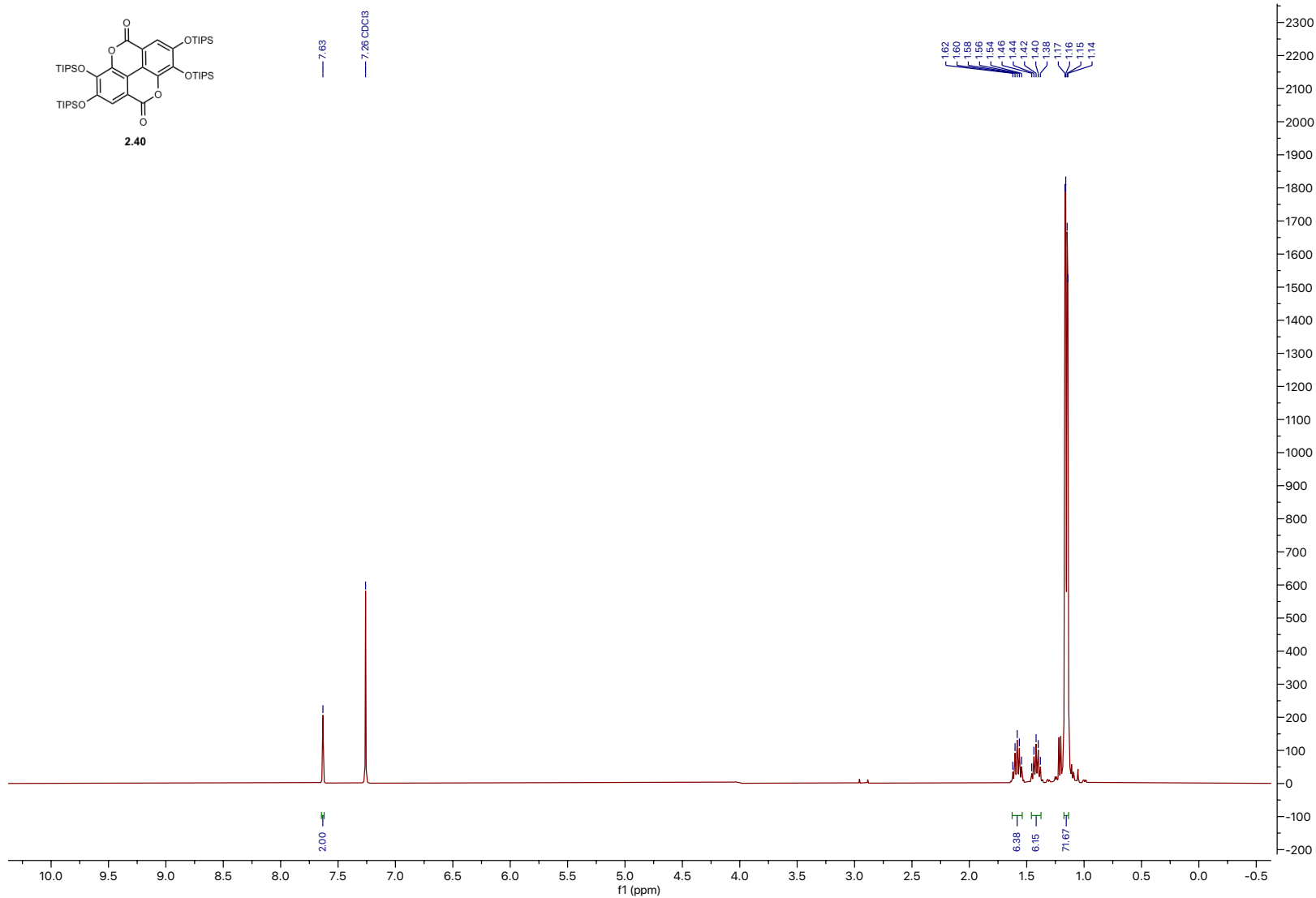


Figure A2.4 ^{13}C NMR (101 MHz, CDCl_3) of 2.40

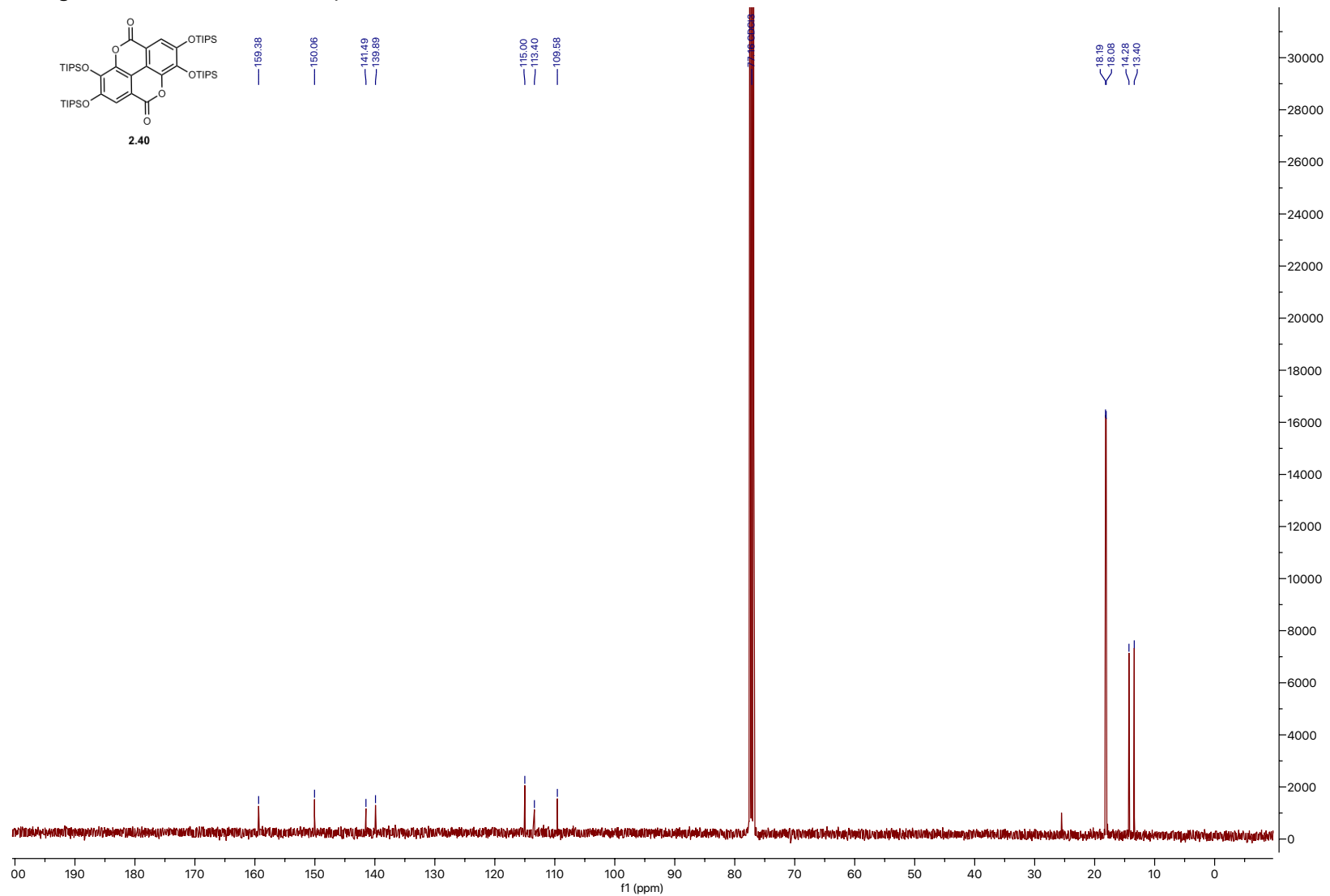


Figure A2.5 ¹H NMR (400 MHz, CDCl₃) of 2.41

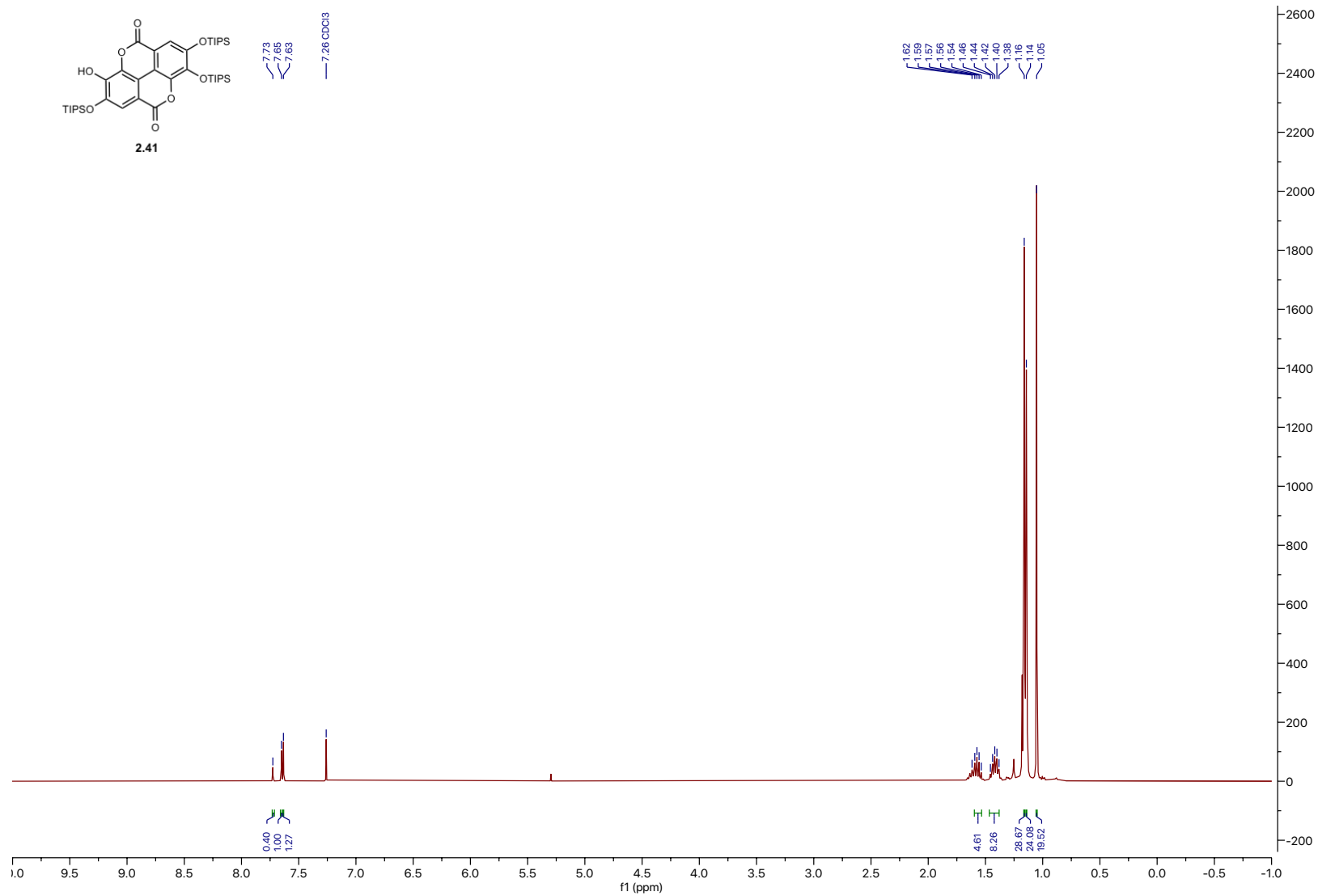


Figure A2.6 ^{13}C NMR (101 MHz, CDCl_3) of 2.41

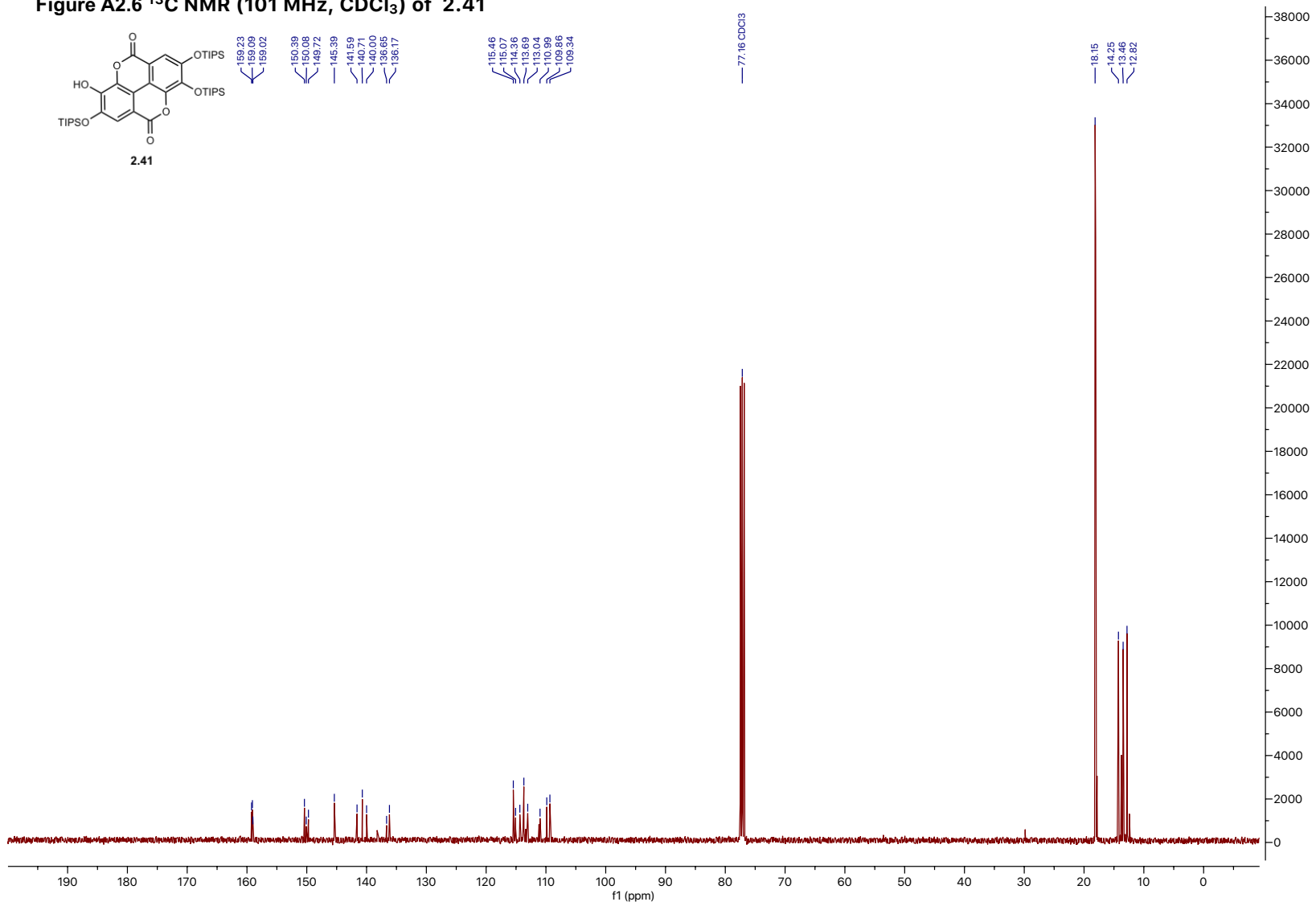


Figure A2.7 ¹H NMR (400 MHz, CDCl₃) of 2.44

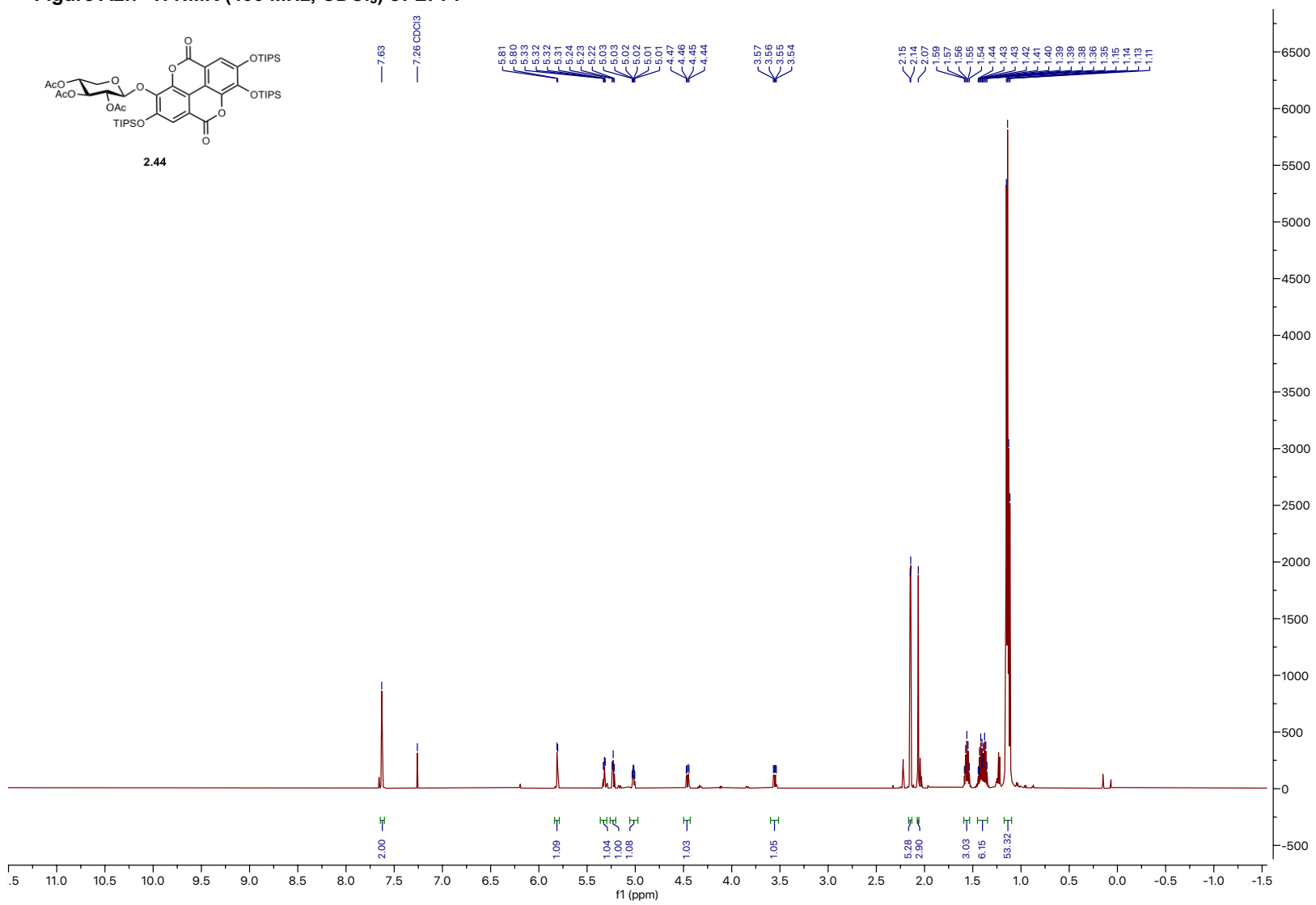


Figure A2.8 ^{13}C NMR (151 MHz, CDCl_3) of 2.44

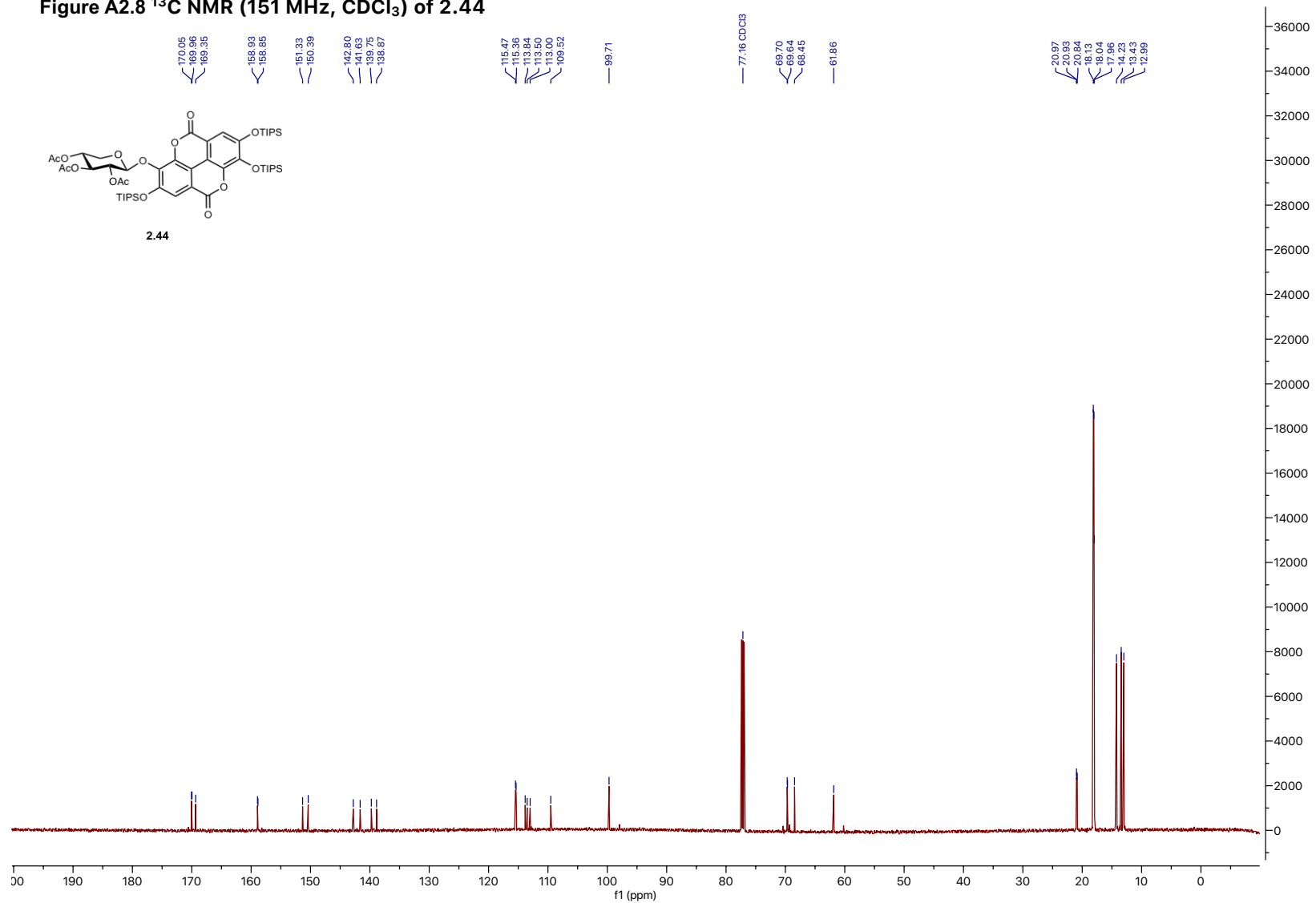


Figure A2.9 ¹H NMR (400 MHz, CDCl₃) of 2.45

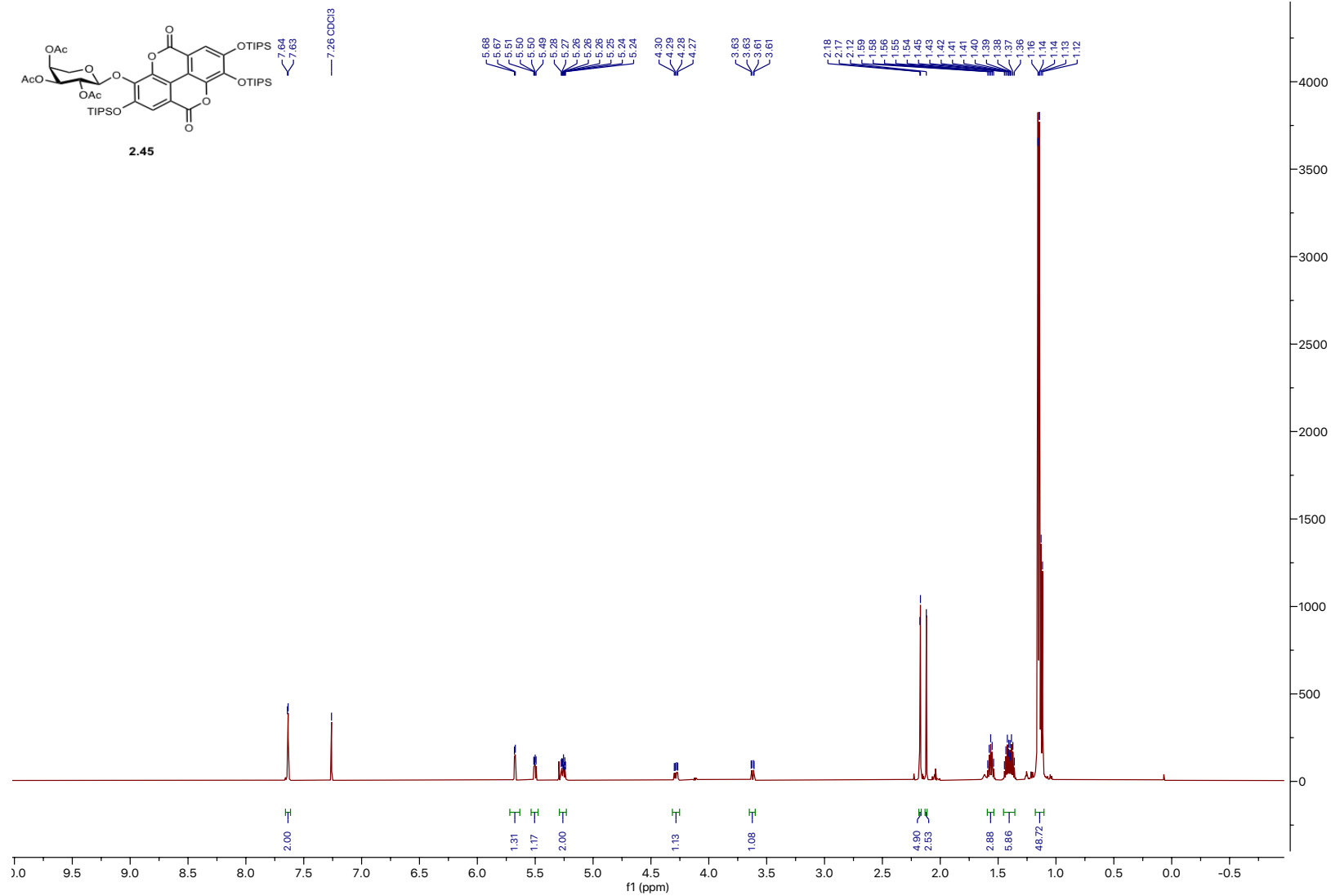


Figure A2.10 ^{13}C NMR (151 MHz, CDCl_3) of 2.45

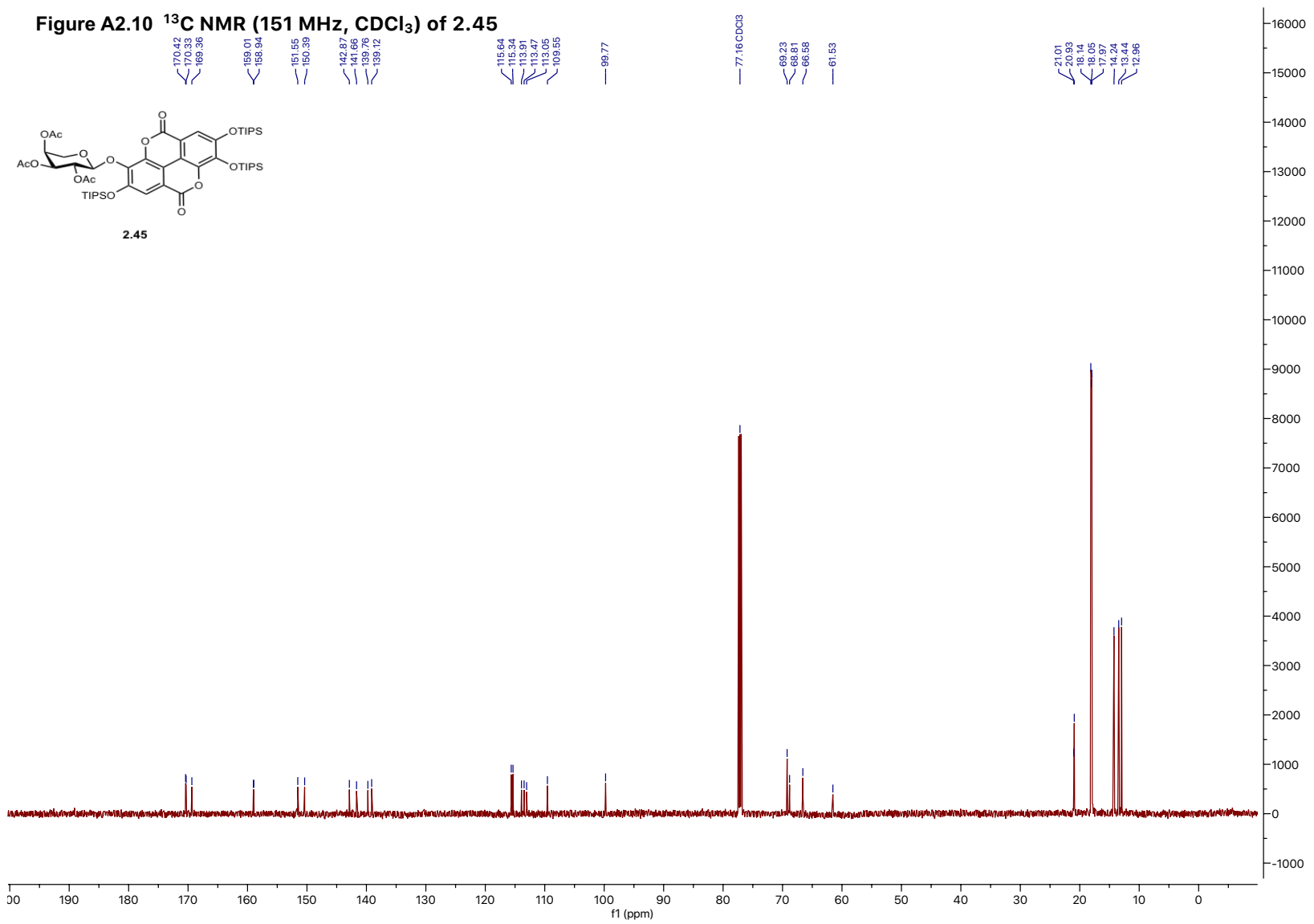


Figure A2.11 ¹H NMR (400 MHz, CDCl₃) of 2.46

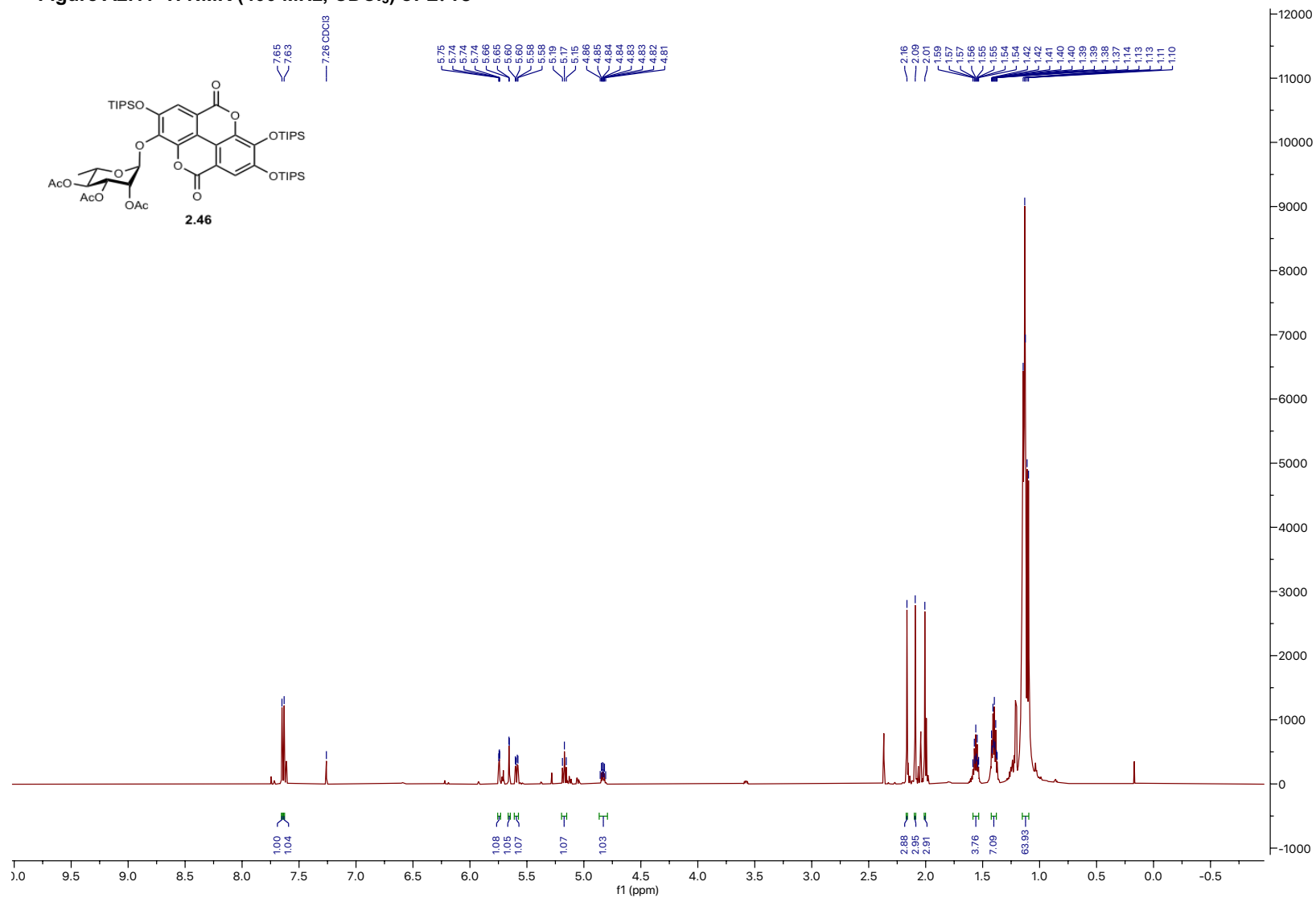


Figure A2.12 ¹³C NMR (151 MHz, CDCl₃) of 2.46

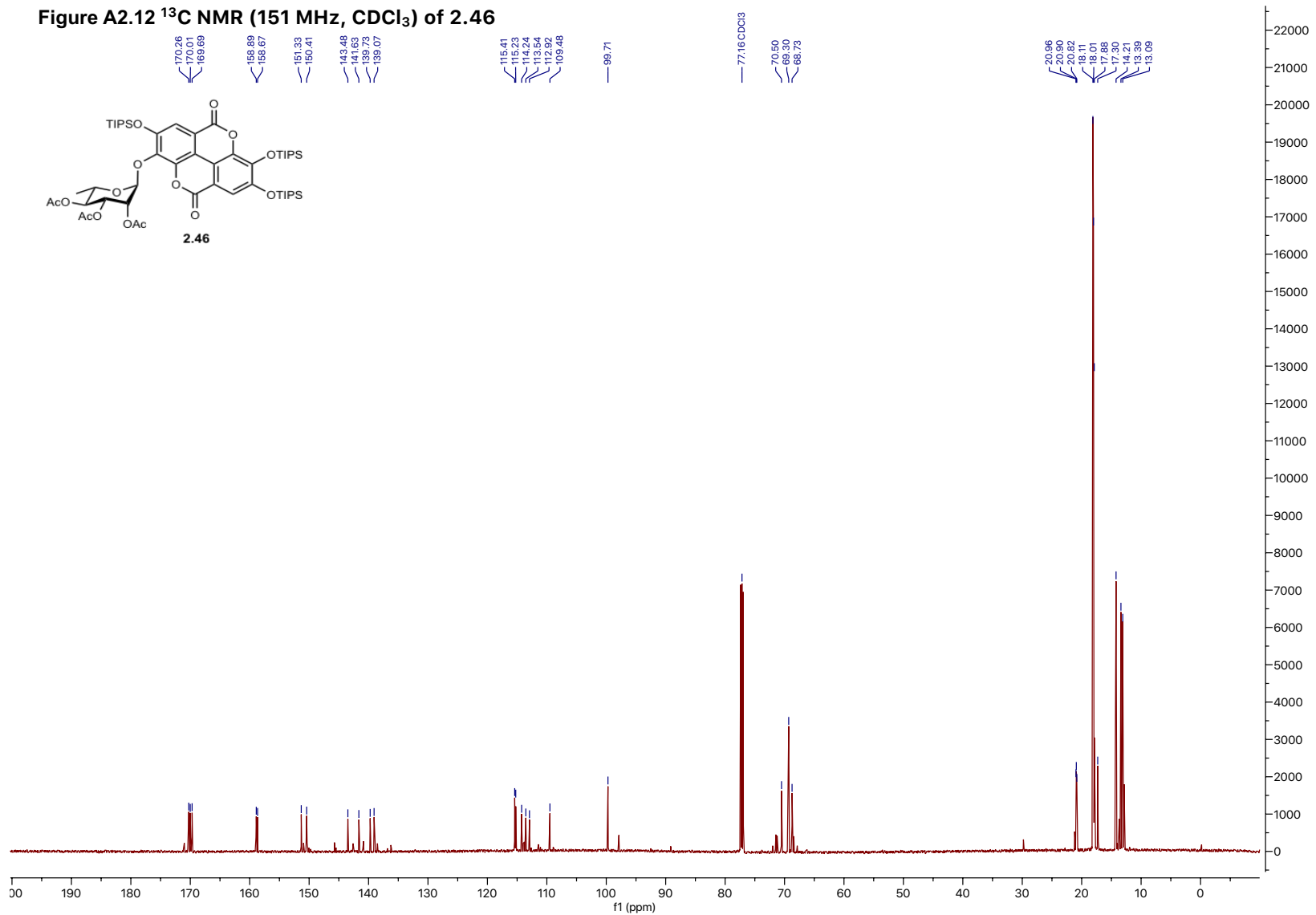


Figure A2.13 ¹H NMR (600 MHz, d₆-DMSO) of 2.34

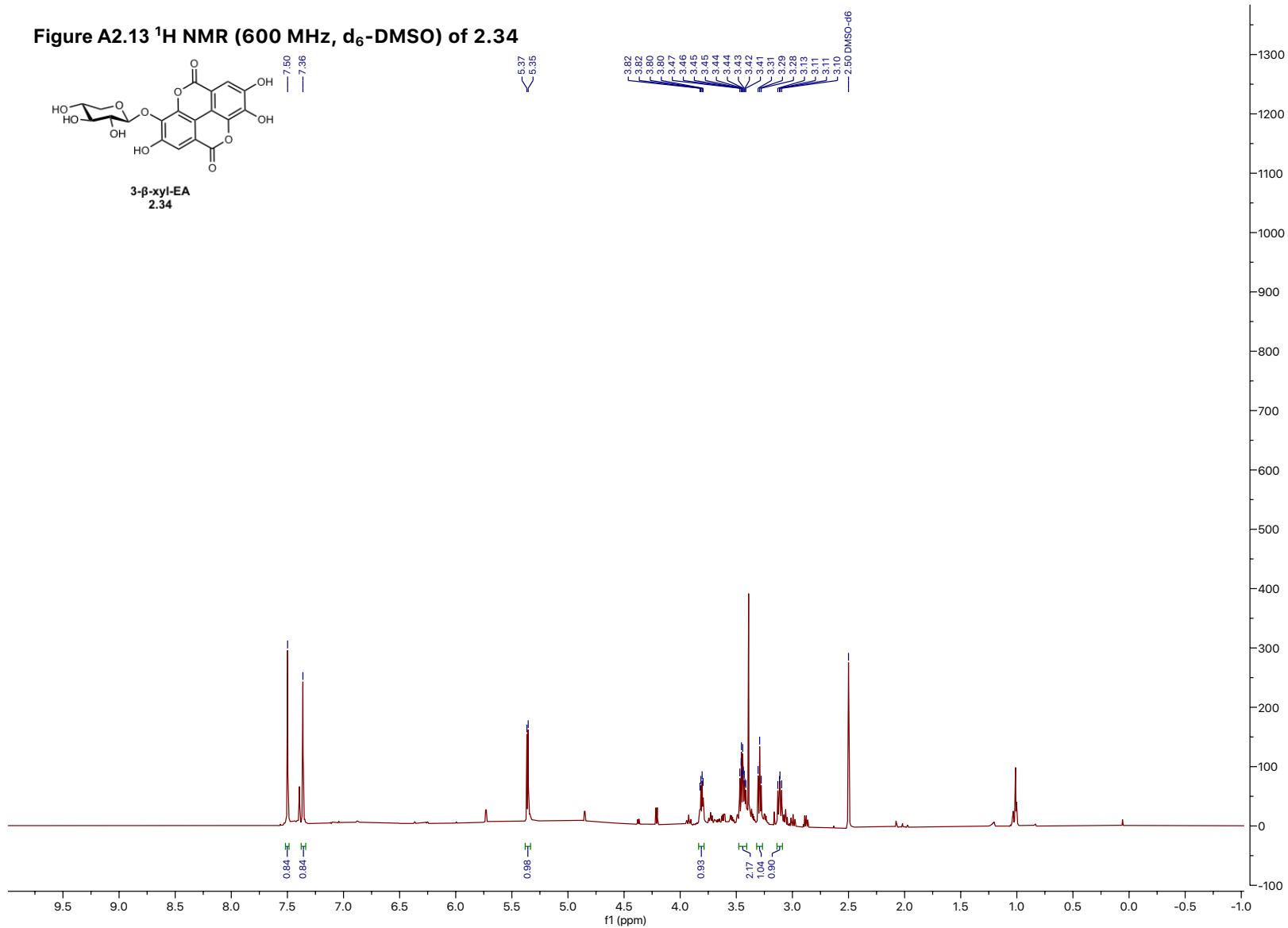


Figure A2.14 ¹³C NMR (151 MHz, d₆-DMSO) of 2.34

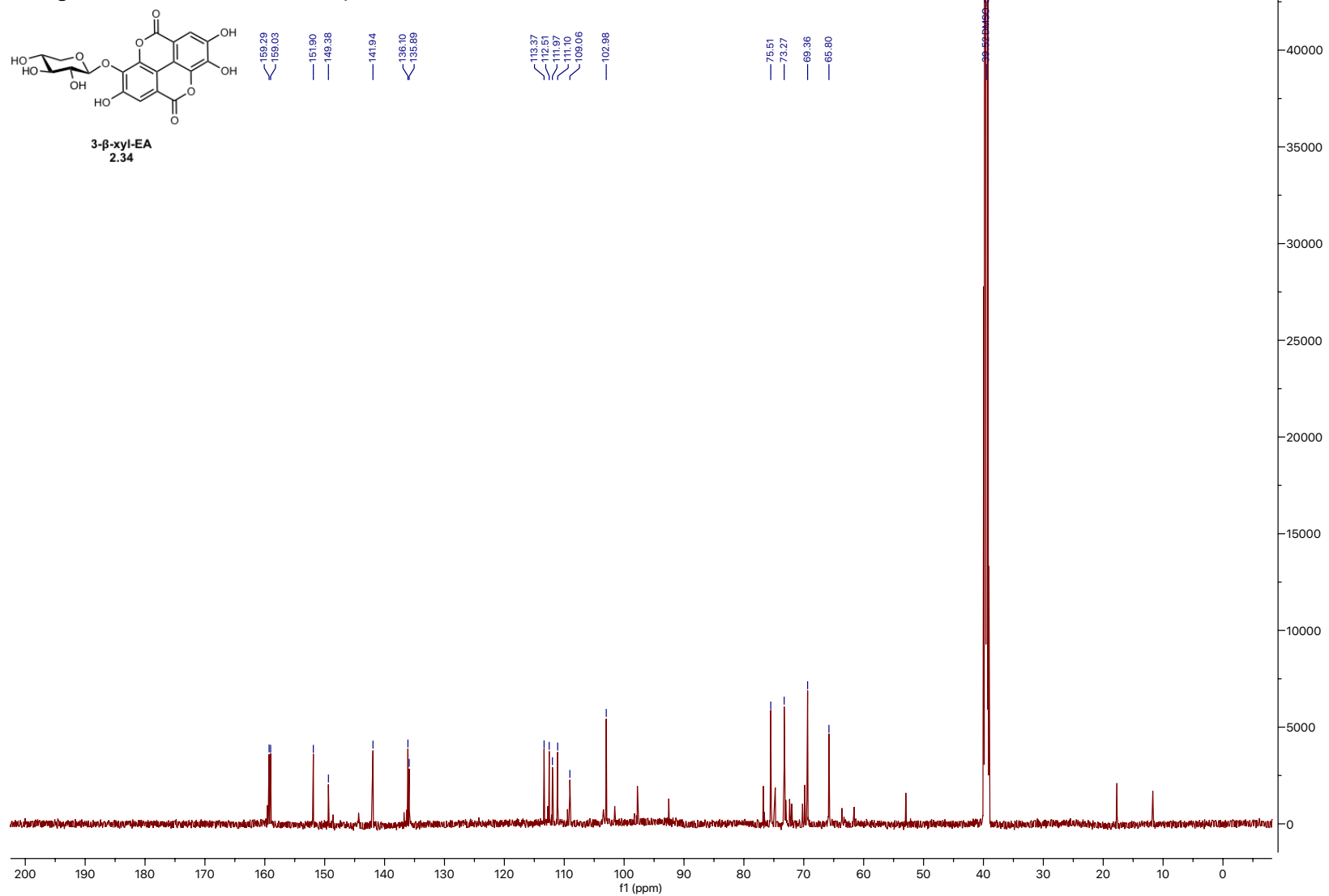


Figure A2.15 HSQC (600 MHz, d₆-DMSO) of 2.34

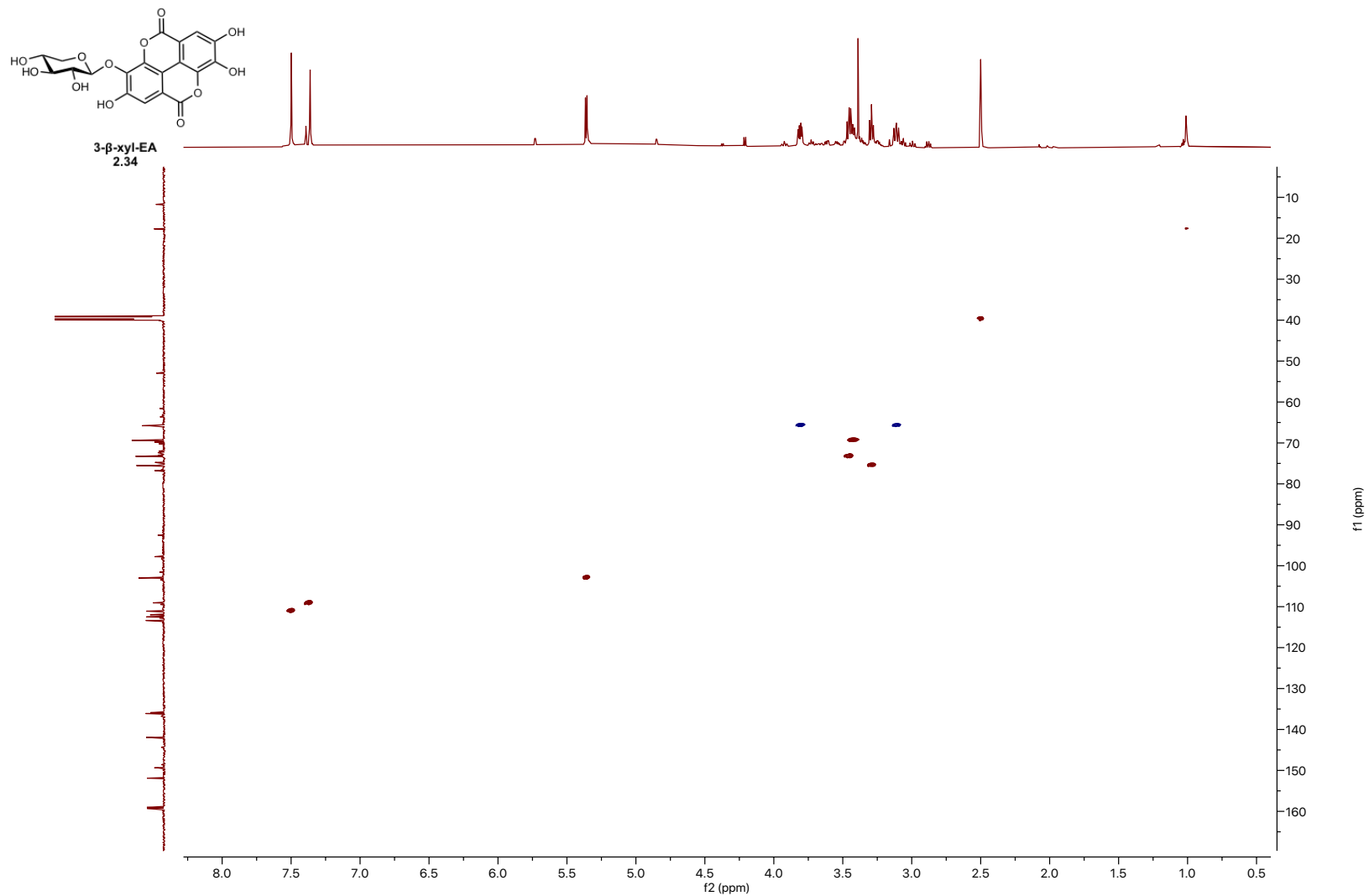


Figure A2.16 COSY (600 MHz, d₆-DMSO) of 2.34

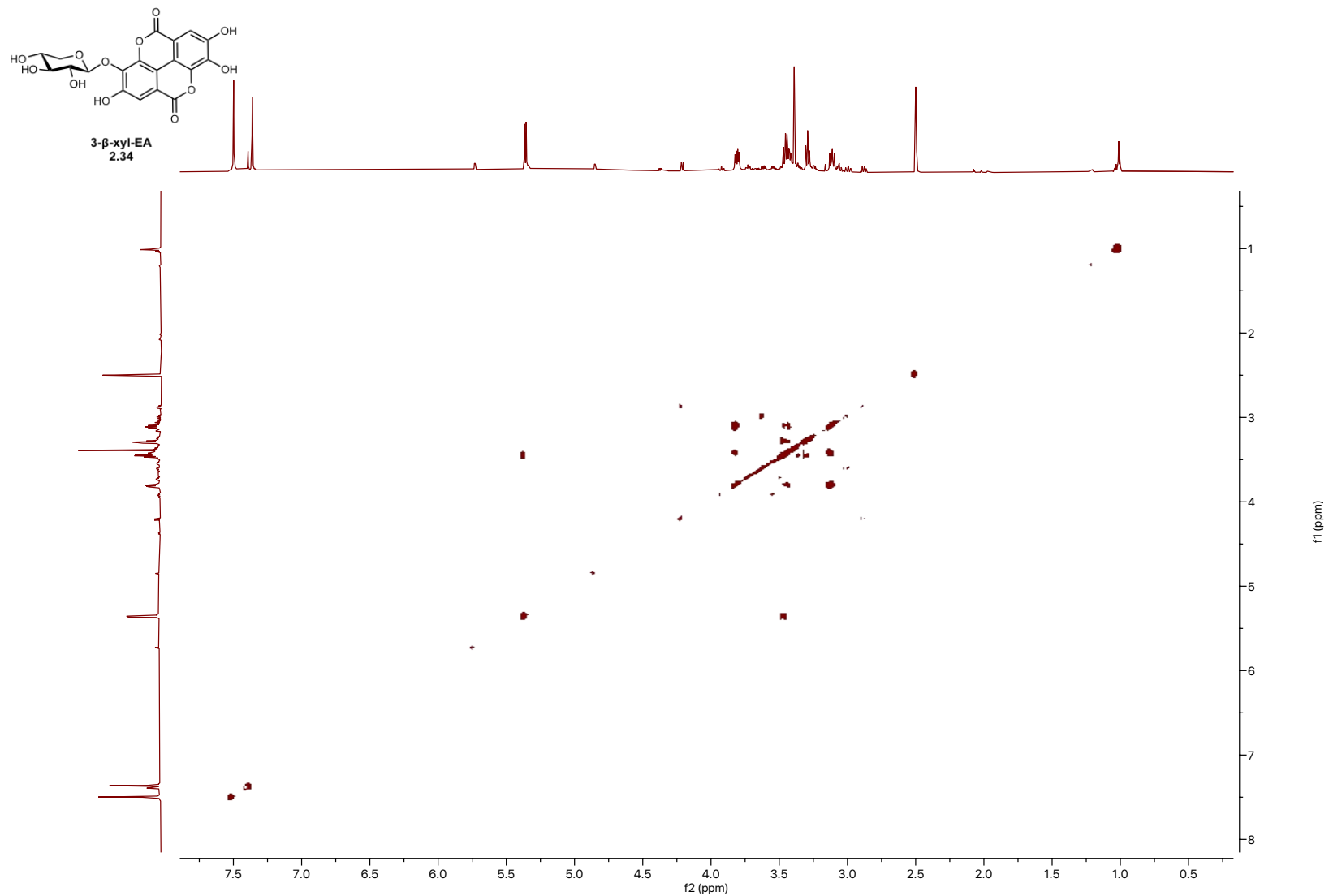
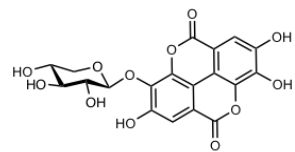


Figure A2.17 HMBC (600 MHz, d₆-DMSO) of 2.34



3-β-xyl-EA
2.34

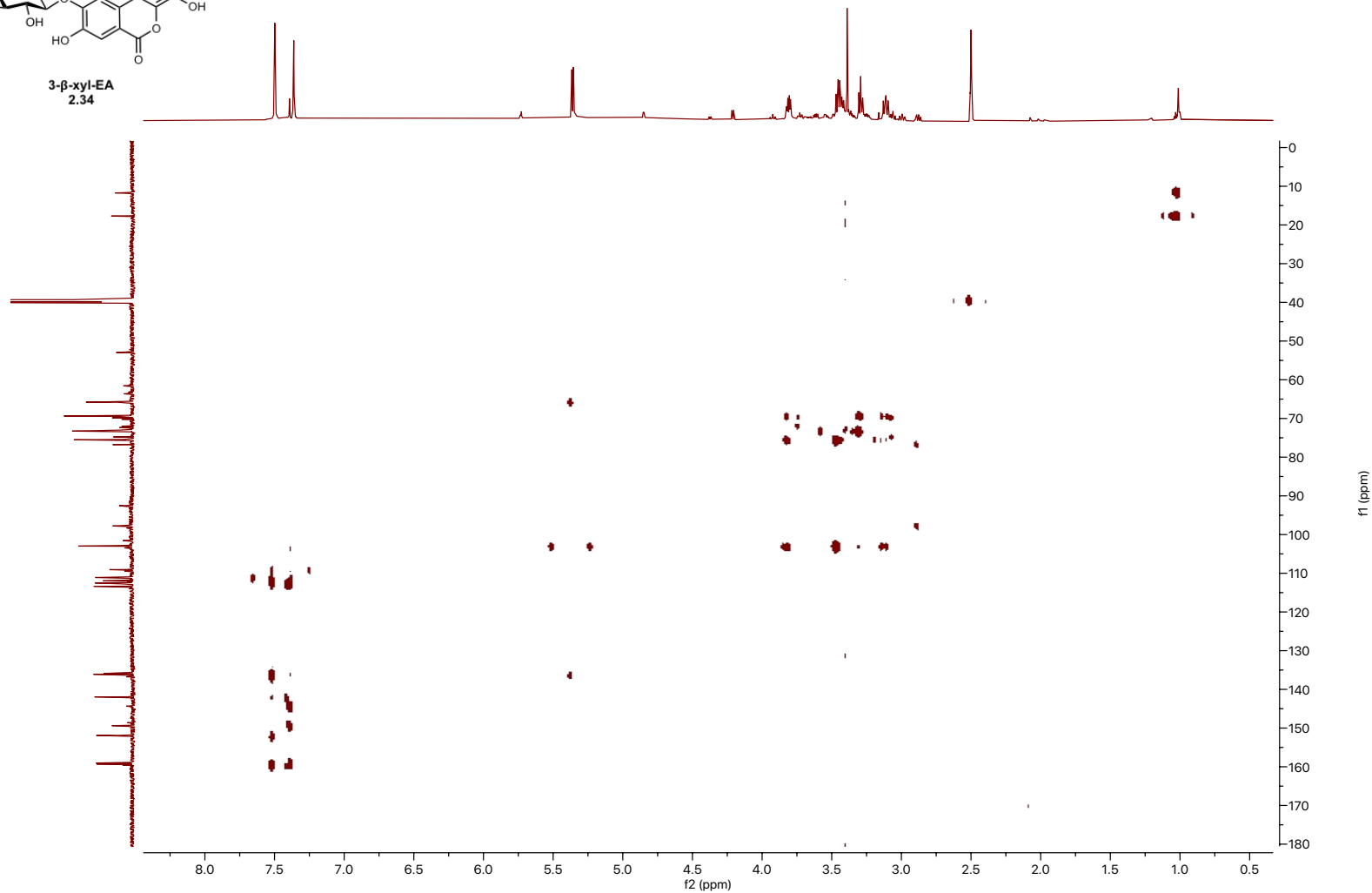


Figure A2.18 ¹H NMR (600 MHz, d₆-DMSO) of 2.47

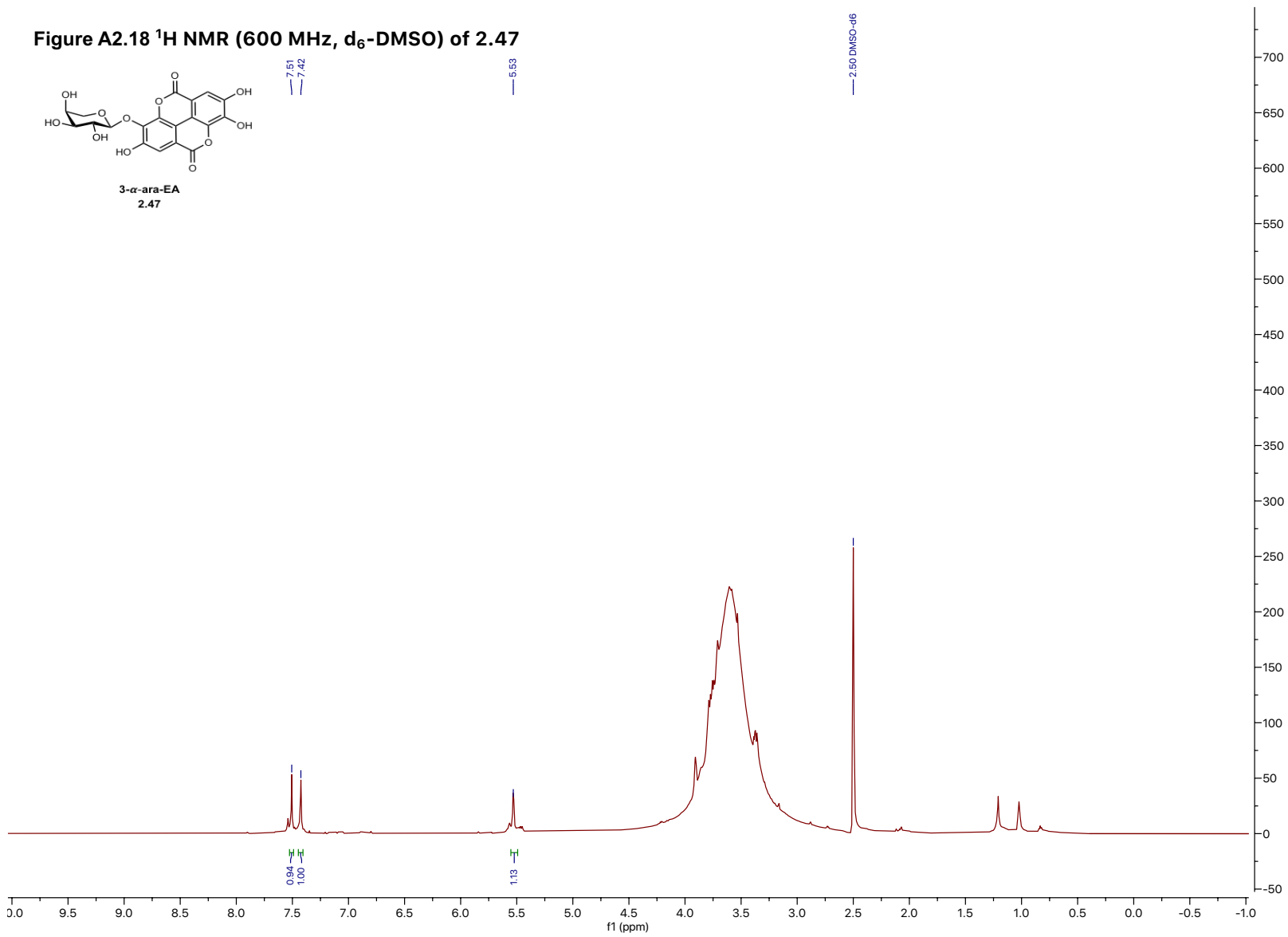


Figure A2.19 ^{13}C NMR (151 MHz, $\text{d}_6\text{-DMSO}$) of 2.47

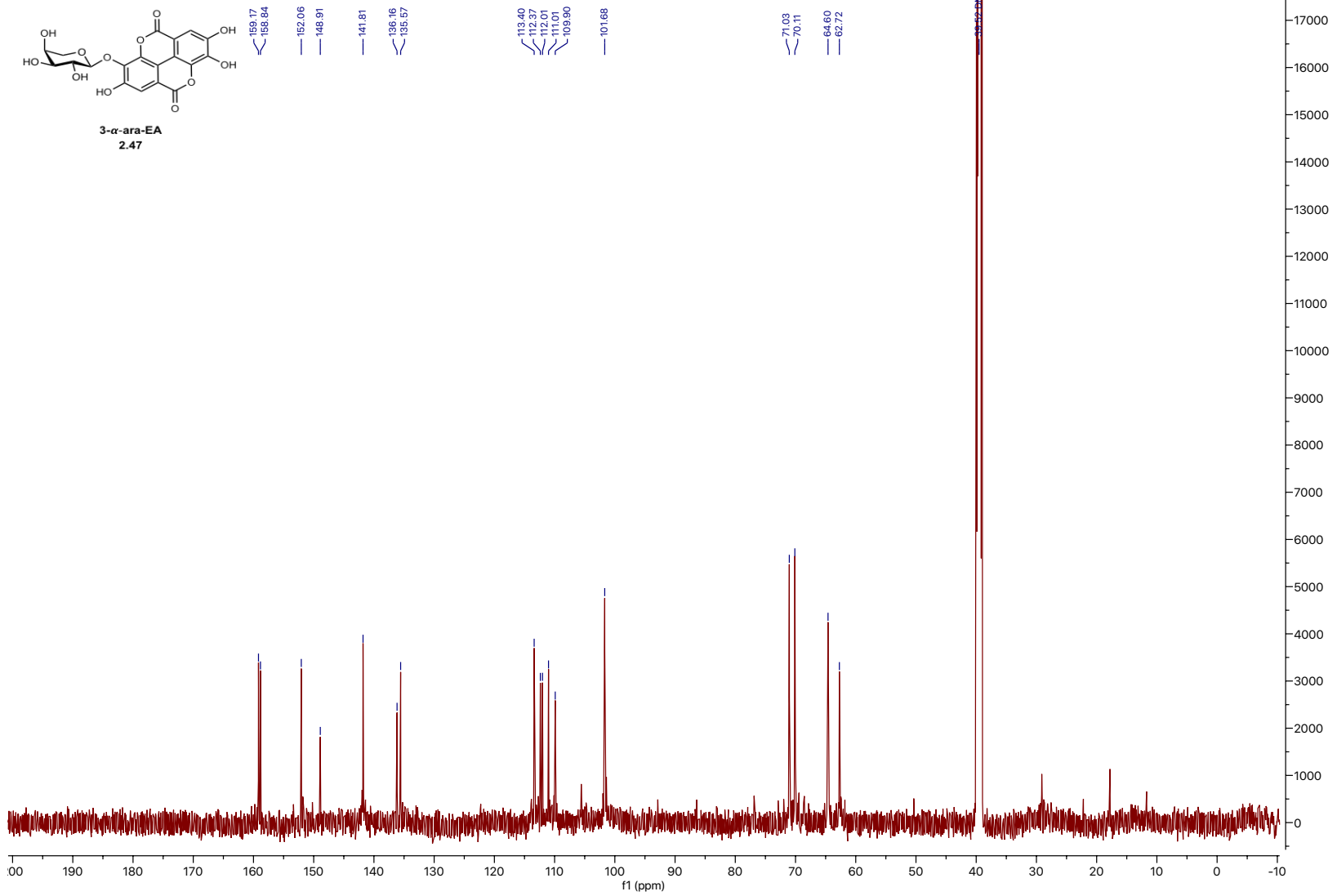
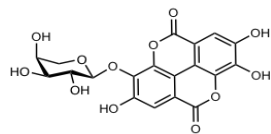


Figure A2.20 HSQC (600 MHz, d₆-DMSO) of 2.47



3- α -ara-EA
2.47

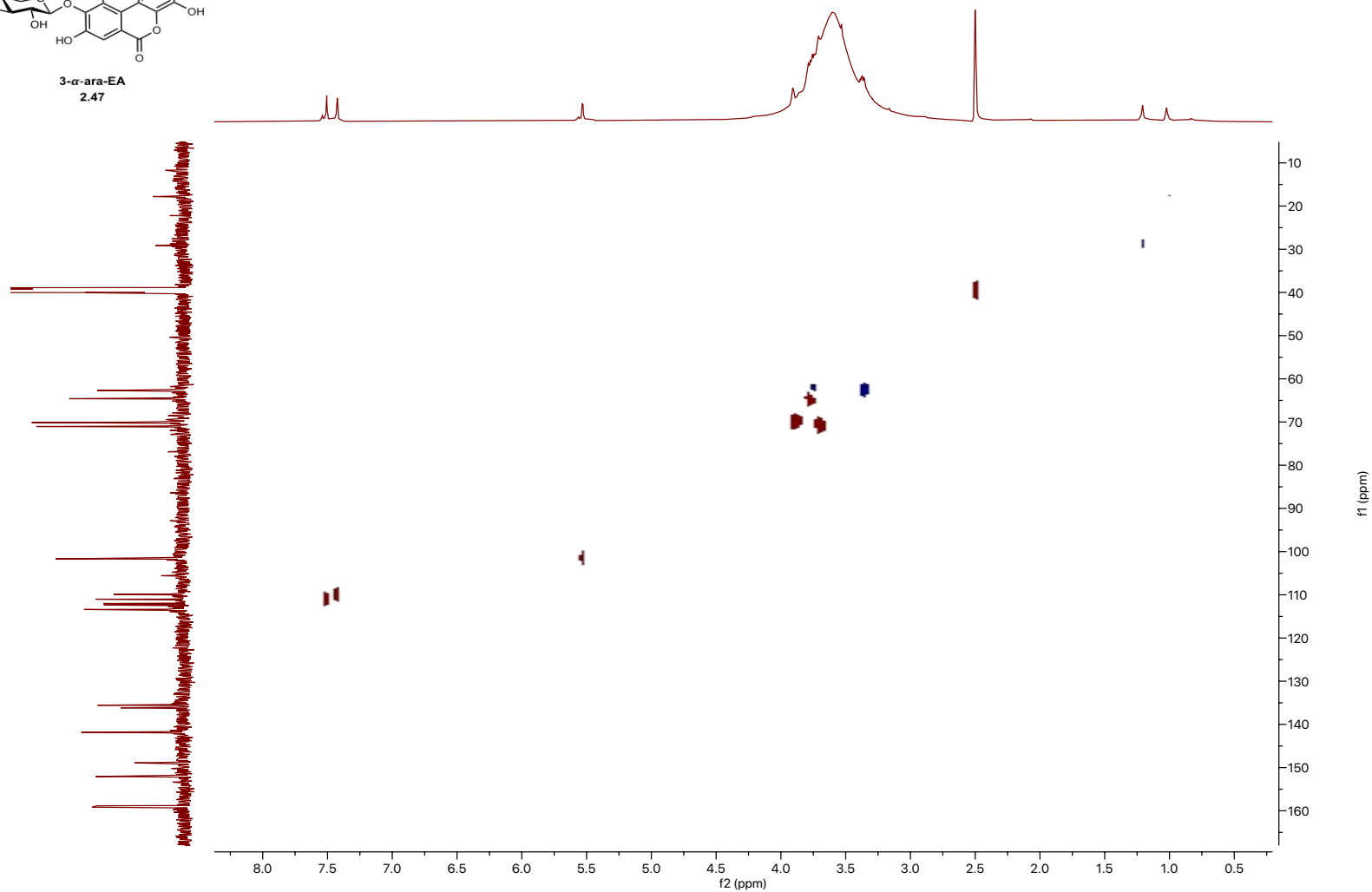
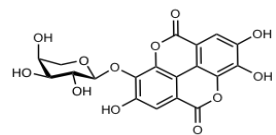


Figure A2.21 COSY (600 MHz, d₆-DMSO) of 2.47



3- α -ara-EA
2.47

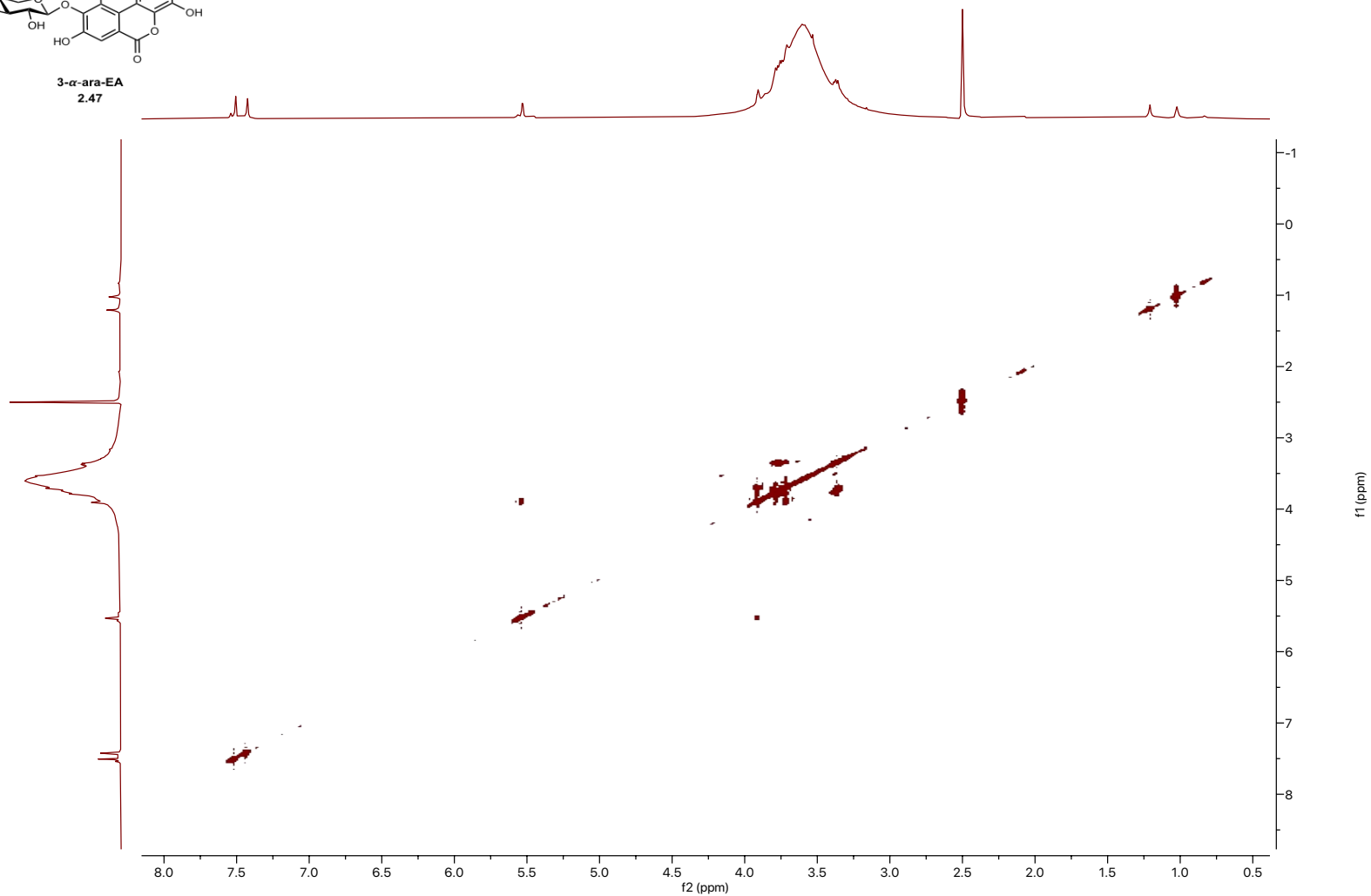
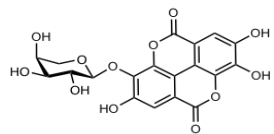


Figure A2.22 HMBC (600 MHz, d₆-DMSO) of 2.47



3- α -ara-EA
2.47

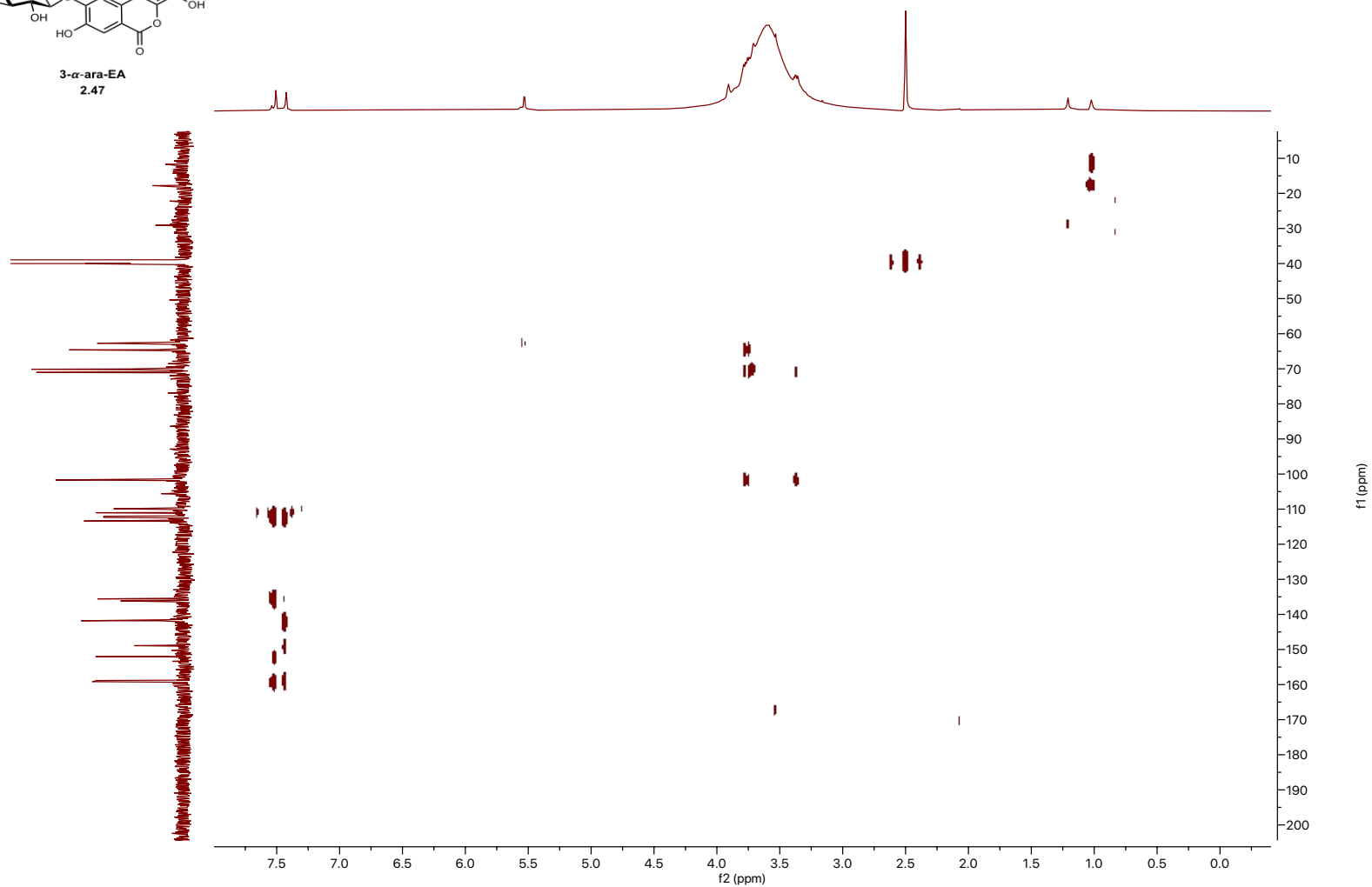


Figure A2.23 ¹H NMR (600 MHz, d₆-DMSO) of 2.35

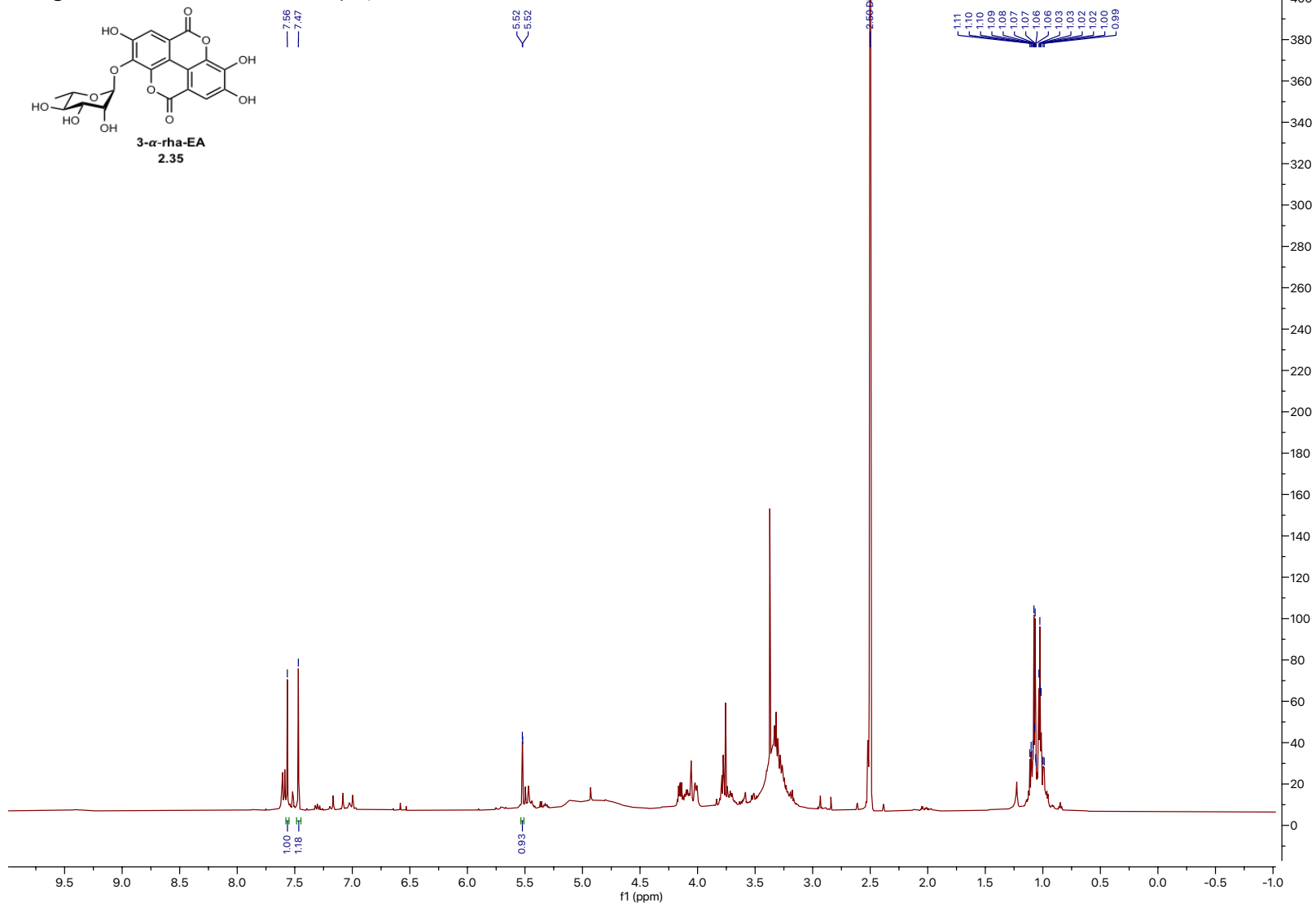


Figure A2.24 ¹³C NMR (151 MHz, d₆-DMSO) of 2.35

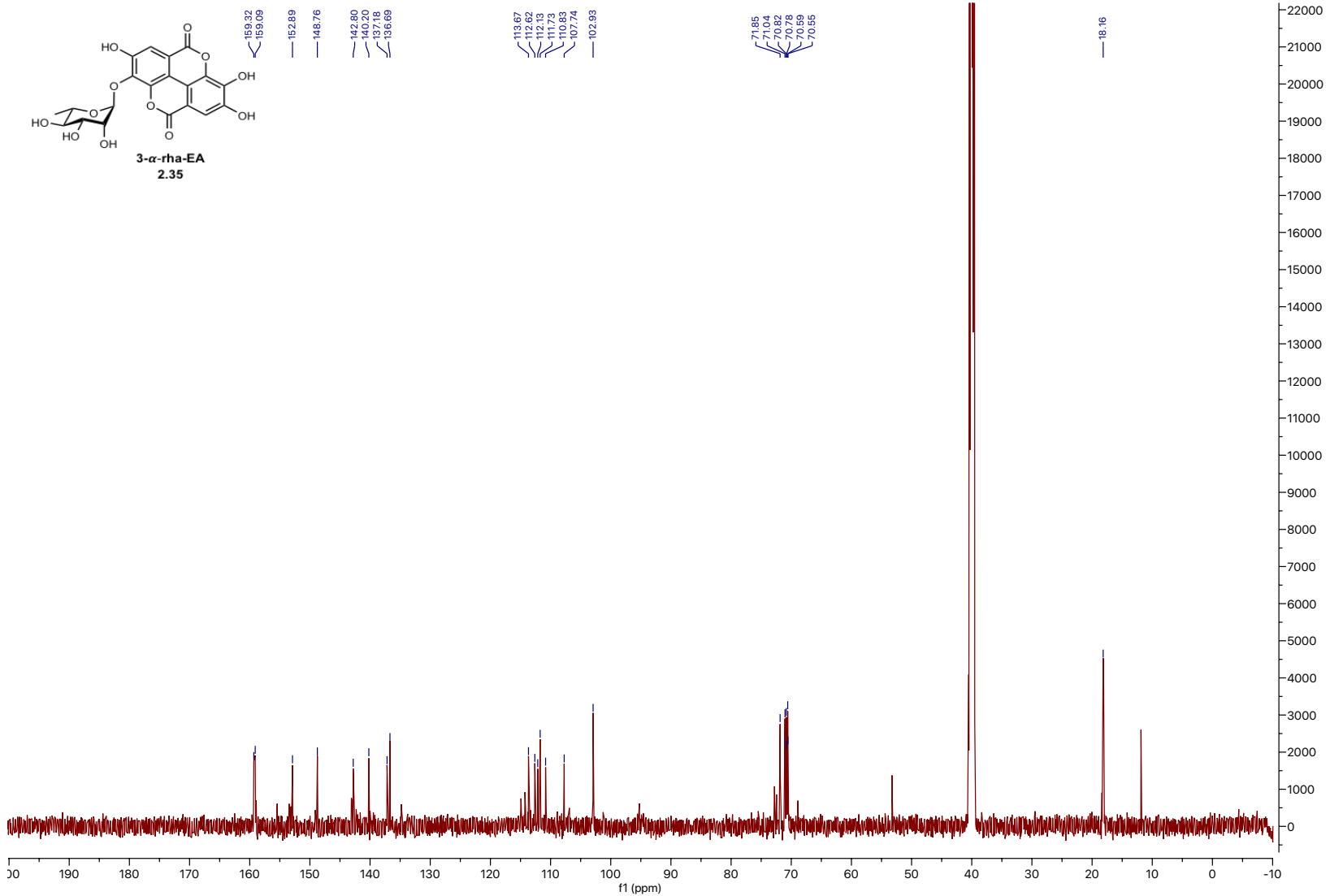


Figure A2.25 HSQC (600 MHz, d₆-DMSO) of 2.35

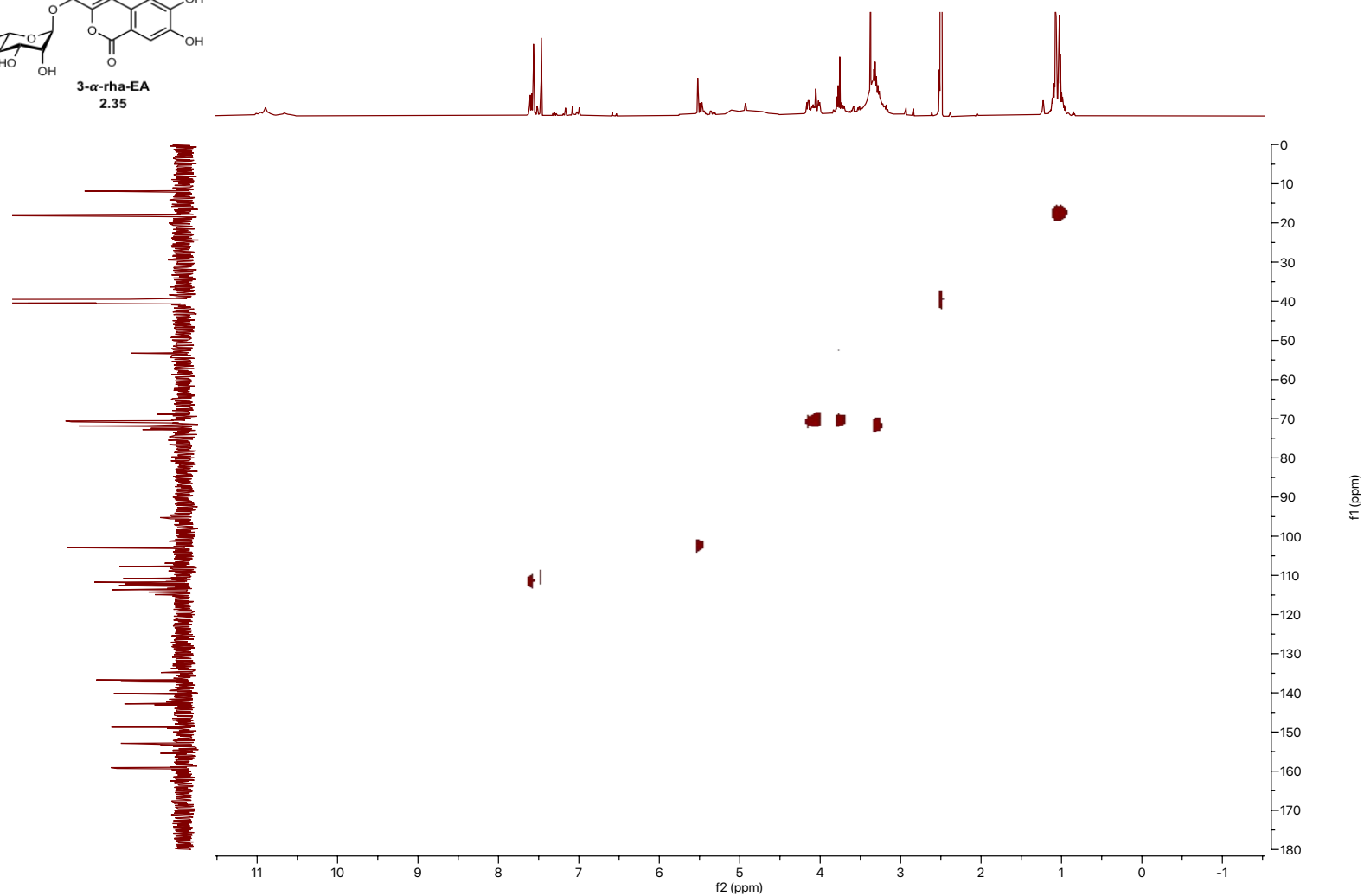
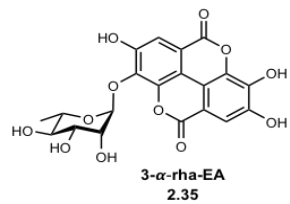


Figure A2.26 COSY (600 MHz, d₆-DMSO) of 2.35

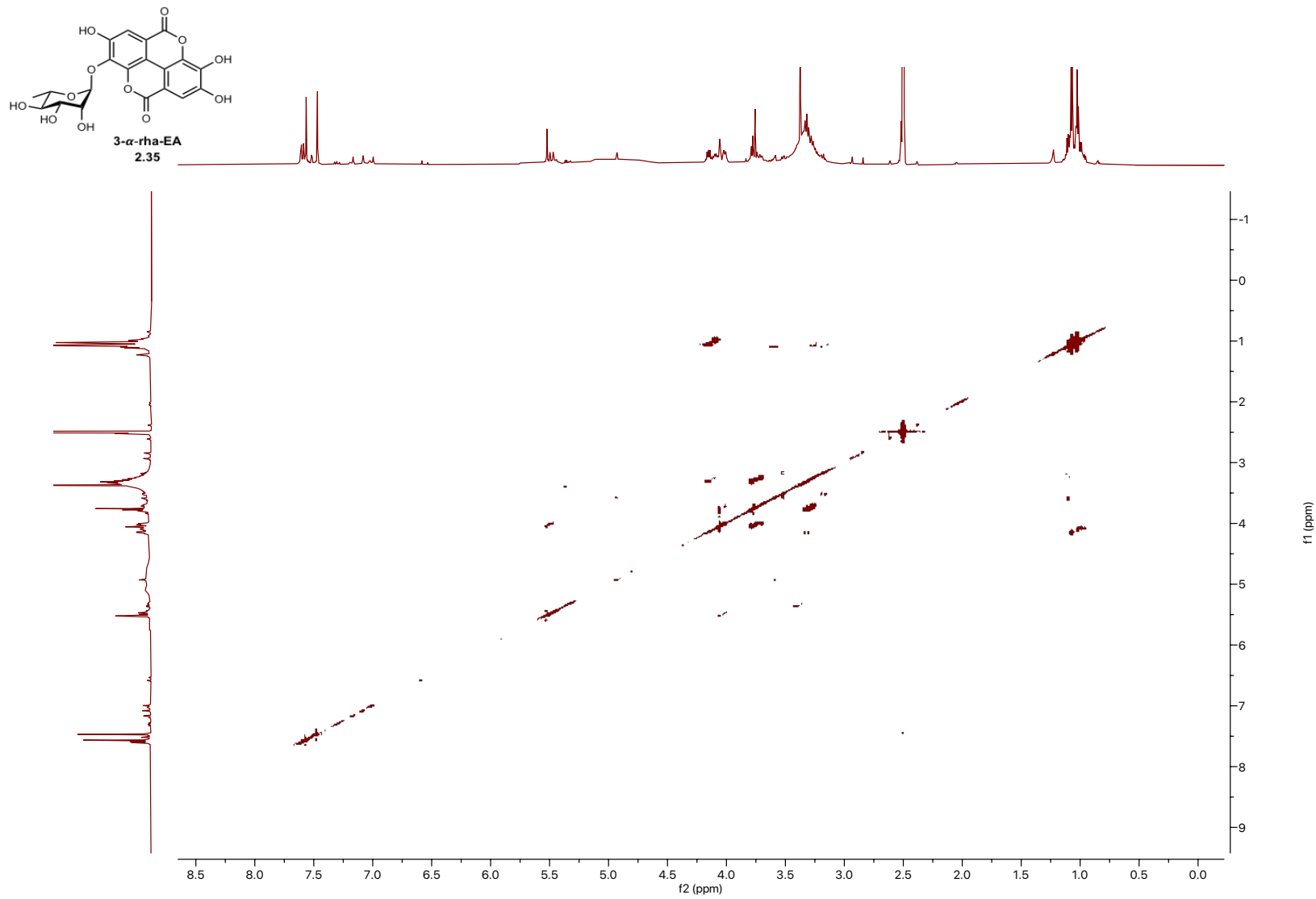


Figure A2.28 CIF/PLATON report for 2.44

checkCIF/PLATON report

Structure factors have been supplied for datablock(s) sac-0611

THIS REPORT IS FOR GUIDANCE ONLY. IF USED AS PART OF A REVIEW PROCEDURE FOR PUBLICATION, IT SHOULD NOT REPLACE THE EXPERTISE OF AN EXPERIENCED CRYSTALLOGRAPHIC REFEREE.

No syntax errors found. CIF dictionary Interpreting this report

Datablock: sac-0611

Bond precision: C-C = 0.0125 A Wavelength=1.54184
Cell: a=15.1547(2) b=11.8637(2) c=31.8968(5)
 alpha=90 beta=96.3795(14) gamma=90
Temperature: 100 K

	Calculated	Reported
Volume	5699.24(15)	5699.22(16)
Space group	P 21	P 1 21 1
Hall group	P 2yb	P 2yb
Moiety formula	C52 H80 O15 Si3	C52 H80 O15 Si3
Sum formula	C52 H80 O15 Si3	C52 H80 O15 Si3
Mr	1029.43	1029.43
Dx, g cm-3	1.200	1.200
Z	4	4
Mu (mm-1)	1.277	1.277
F000	2216.0	2216.0
F000'	2225.53	
h,k,lmax	18,14,39	18,14,39
Nref	22988[12076]	19907
Tmin,Tmax	0.850,0.955	0.732,1.000
Tmin'	0.751	

Correction method= # Reported T Limits: Tmin=0.732 Tmax=1.000
AbsCorr = GAUSSIAN

Data completeness= 1.65/0.87 Theta(max)= 73.578

R(reflections)= 0.0833(16698) wR2(reflections)= 0.2389(19907)

S = 1.030 Npar= 1303

The following ALERTS were generated. Each ALERT has the format
test-name_ALERT_alert-type_alert-level.
Click on the hyperlinks for more details of the test.

Alert level B

PLAT220_ALERT_2_B Non-Solvent Resd 1 C Ueq(max)/Ueq(min) Range 6.4 Ratio
PLAT220_ALERT_2_B Non-Solvent Resd 2 C Ueq(max)/Ueq(min) Range 6.4 Ratio
PLAT340_ALERT_3_B Low Bond Precision on C-C Bonds 0.01246 Ang.
PLAT360_ALERT_2_B Short C(sp3)-C(sp3) Bond C38B - C40B . 1.27 Ang.

Alert level C

DIFMX02_ALERT_1_C The maximum difference density is > 0.1*ZMAX*0.75
The relevant atom site should be identified.

PLAT094_ALERT_2_C Ratio of Maximum / Minimum Residual Density 2.26 Report
PLAT097_ALERT_2_C Large Reported Max. (Positive) Residual Density 1.09 eA-3
PLAT213_ALERT_2_C Atom C5 has ADP max/min Ratio 3.6 prolat
PLAT213_ALERT_2_C Atom C9 has ADP max/min Ratio 3.6 prolat
PLAT213_ALERT_2_C Atom C30B has ADP max/min Ratio 3.3 prolat
PLAT213_ALERT_2_C Atom C40B has ADP max/min Ratio 4.0 prolat
PLAT220_ALERT_2_C Non-Solvent Resd 1 O Ueq(max)/Ueq(min) Range 5.1 Ratio
PLAT222_ALERT_3_C Non-Solv. Resd 1 H Uiso(max)/Uiso(min) Range 6.1 Ratio
PLAT222_ALERT_3_C Non-Solv. Resd 2 H Uiso(max)/Uiso(min) Range 6.9 Ratio
PLAT230_ALERT_2_C Hirshfeld Test Diff for C4 --C5 . 6.5 s.u.
PLAT234_ALERT_4_C Large Hirshfeld Difference O2 --C5 . 0.22 Ang.
PLAT234_ALERT_4_C Large Hirshfeld Difference O5 --C8 . 0.21 Ang.
PLAT234_ALERT_4_C Large Hirshfeld Difference O6 --C8 . 0.24 Ang.
PLAT234_ALERT_4_C Large Hirshfeld Difference C38B --C40B . 0.22 Ang.
PLAT234_ALERT_4_C Large Hirshfeld Difference C41B --C42B . 0.17 Ang.
PLAT241_ALERT_2_C High 'MainMol' Ueq as Compared to Neighbors of C5 Check
PLAT242_ALERT_2_C Low 'MainMol' Ueq as Compared to Neighbors of O5 Check
PLAT242_ALERT_2_C Low 'MainMol' Ueq as Compared to Neighbors of C4 Check
PLAT242_ALERT_2_C Low 'MainMol' Ueq as Compared to Neighbors of C10 Check
PLAT242_ALERT_2_C Low 'MainMol' Ueq as Compared to Neighbors of C29 Check
PLAT242_ALERT_2_C Low 'MainMol' Ueq as Compared to Neighbors of Si1B Check
PLAT242_ALERT_2_C Low 'MainMol' Ueq as Compared to Neighbors of Si2B Check
PLAT242_ALERT_2_C Low 'MainMol' Ueq as Compared to Neighbors of C26B Check
PLAT242_ALERT_2_C Low 'MainMol' Ueq as Compared to Neighbors of C29B Check
PLAT242_ALERT_2_C Low 'MainMol' Ueq as Compared to Neighbors of C32B Check
PLAT242_ALERT_2_C Low 'MainMol' Ueq as Compared to Neighbors of C35B Check
PLAT242_ALERT_2_C Low 'MainMol' Ueq as Compared to Neighbors of C38B Check
PLAT412_ALERT_2_C Short Intra XH3 .. XHn H38B ..H40E . 1.87 Ang.
x,y,z = 1_555 Check

PLAT601_ALERT_2_C Structure Contains Solvent Accessible VOIDS of . 56 Ang**3
PLAT915_ALERT_3_C No Flack x Check Done: Low Friedel Pair Coverage 73 %
PLAT978_ALERT_2_C Number C-C Bonds with Positive Residual Density. 0 Info

Alert level G

PLAT072_ALERT_2_G SHELXL First Parameter in WGHT Unusually Large 0.13 Report
PLAT083_ALERT_2_G SHELXL Second Parameter in WGHT Unusually Large 7.27 Why ?
PLAT395_ALERT_2_G Deviating X-O-Y Angle From 120 for O13 128.6 Degree
PLAT395_ALERT_2_G Deviating X-O-Y Angle From 120 for O14 134.1 Degree
PLAT395_ALERT_2_G Deviating X-O-Y Angle From 120 for O15 144.5 Degree
PLAT395_ALERT_2_G Deviating X-O-Y Angle From 120 for O13B 129.4 Degree
PLAT395_ALERT_2_G Deviating X-O-Y Angle From 120 for O14B 132.1 Degree
PLAT395_ALERT_2_G Deviating X-O-Y Angle From 120 for O15B 146.2 Degree
PLAT720_ALERT_4_G Number of Unusual/Non-Standard Labels 8 Note
PLAT791_ALERT_4_G Model has Chirality at C1 (Chiral SPGR) S Verify
PLAT791_ALERT_4_G Model has Chirality at C1B (Chiral SPGR) S Verify
PLAT791_ALERT_4_G Model has Chirality at C2 (Chiral SPGR) R Verify
PLAT791_ALERT_4_G Model has Chirality at C2B (Chiral SPGR) R Verify
PLAT791_ALERT_4_G Model has Chirality at C3 (Chiral SPGR) S Verify
PLAT791_ALERT_4_G Model has Chirality at C3B (Chiral SPGR) S Verify
PLAT791_ALERT_4_G Model has Chirality at C4 (Chiral SPGR) R Verify

PLAT791_ALERT_4_G Model has Chirality at C4B (Chiral SPGR) R Verify
PLAT910_ALERT_3_G Missing # of FCF Reflection(s) Below Theta(Min). 1 Note
PLAT912_ALERT_4_G Missing # of FCF Reflections Above STh/L= 0.600 123 Note

0 **ALERT level A** = Most likely a serious problem - resolve or explain
4 **ALERT level B** = A potentially serious problem, consider carefully
32 **ALERT level C** = Check. Ensure it is not caused by an omission or oversight
19 **ALERT level G** = General information/check it is not something unexpected

1 ALERT type 1 CIF construction/syntax error, inconsistent or missing data
34 ALERT type 2 Indicator that the structure model may be wrong or deficient
5 ALERT type 3 Indicator that the structure quality may be low
15 ALERT type 4 Improvement, methodology, query or suggestion
0 ALERT type 5 Informative message, check

It is advisable to attempt to resolve as many as possible of the alerts in all categories. Often the minor alerts point to easily fixed oversights, errors and omissions in your CIF or refinement strategy, so attention to these fine details can be worthwhile. In order to resolve some of the more serious problems it may be necessary to carry out additional measurements or structure refinements. However, the purpose of your study may justify the reported deviations and the more serious of these should normally be commented upon in the discussion or experimental section of a paper or in the "special_details" fields of the CIF. checkCIF was carefully designed to identify outliers and unusual parameters, but every test has its limitations and alerts that are not important in a particular case may appear. Conversely, the absence of alerts does not guarantee there are no aspects of the results needing attention. It is up to the individual to critically assess their own results and, if necessary, seek expert advice.

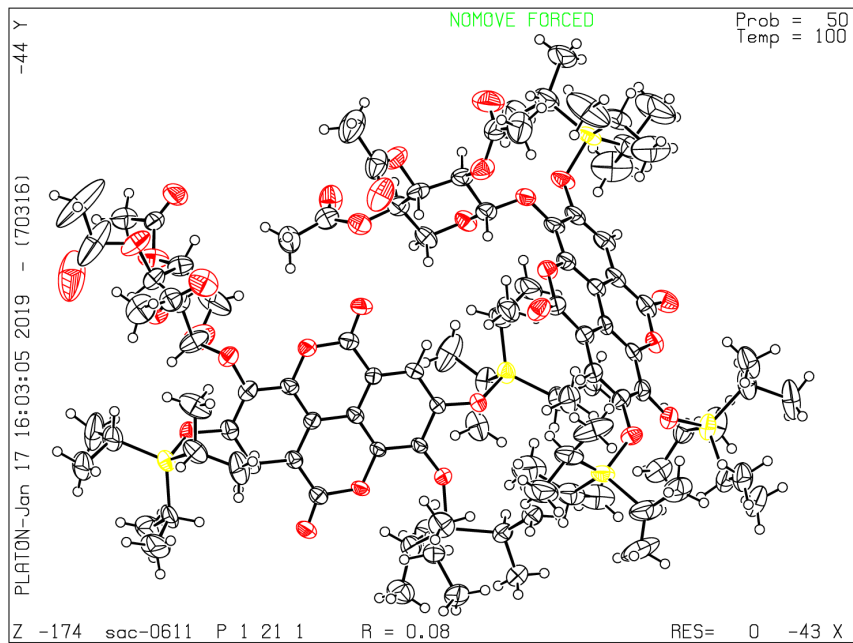
Publication of your CIF in IUCr journals

A basic structural check has been run on your CIF. These basic checks will be run on all CIFs submitted for publication in IUCr journals (*Acta Crystallographica*, *Journal of Applied Crystallography*, *Journal of Synchrotron Radiation*); however, if you intend to submit to *Acta Crystallographica Section C* or *E* or *IUCrData*, you should make sure that full publication checks are run on the final version of your CIF prior to submission.

Publication of your CIF in other journals

Please refer to the *Notes for Authors* of the relevant journal for any special instructions relating to CIF submission.

PLATON version of 06/01/2019; check.def file version of 19/12/2018



Chapter 3

Human milk oligosaccharides as antibiotic adjuvants against group B

Streptococcus

3.1 Abstract

Human milk oligosaccharides (HMOs) are a class of complex carbohydrates unique in infant nutrition. These carbohydrates have been shown to have powerful antibiotic activity against GBS, but little is known about how they facilitate this activity and how it might be harnessed in the development of new therapeutics. In this chapter, we will discuss the structure and biosynthesis of HMOs, as well as their use as antibiotic adjuvants. We identify HMOs can be used to reverse antifolate-antibiotic resistance in GBS and that two component regulatory systems are involved in HMO-antibiotic synergy.¹

3.2 Human milk oligosaccharides

3.2.1 Macromolecular composition of human breast milk

Human breast milk is considered the gold-standard in infant nutrition. Breast milk is comprised of approximately 54% lactose, 32% fat, 6% protein, and 8% human milk oligosaccharides (HMOs) (**Figure 3.1**).² HMOs are a group of complex carbohydrates unique to human breast milk. The concentration of HMOs in breast milk varies between mothers and throughout lactation. Typically, the concentration of HMOs is highest in the milk produced immediately after delivery, known as the colostrum.³ Over time, the concentration of HMOs in breast milk diminishes. This biologically supports the fact that HMOs are most important in the earliest stages of infant development. Notably, these

oligosaccharides are also not well represented by current infant formulas. As a result, there is need to better understand the biological importance of HMOs and develop better breast milk mimics.

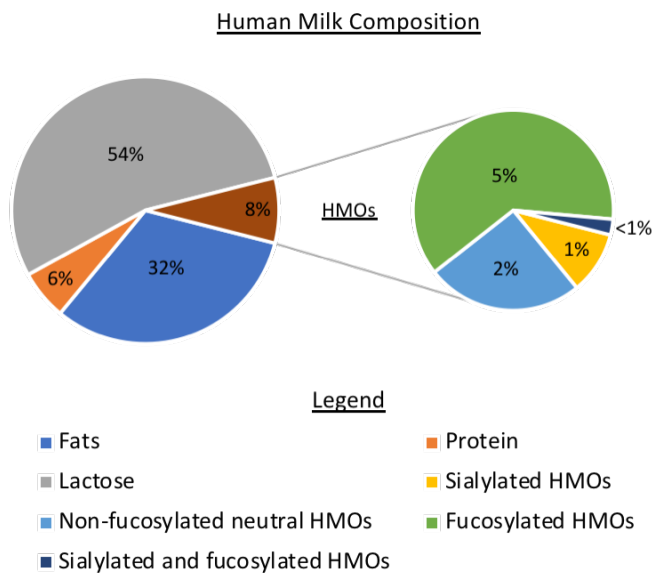


Figure 3.1 Macromolecular composition of human breast milk

3.2.2 Chemical structure and biosynthesis of HMOs

Structurally, HMOs are comprised of five pyranose monosaccharide residues; β -D-glucose (Glc, **3.1**), β -D-galactose (Gal, **3.2**), *N*-acetyl- β -D-glucosamine (GlcNAc, **3.3**), α -L-fucose (Fuc, **3.4**), and the sialic acid *N*-acetyl- α -D-neuraminic acid (NeuNAc or Sia, **3.5**) (**Figure 3.2**).⁴⁻⁶

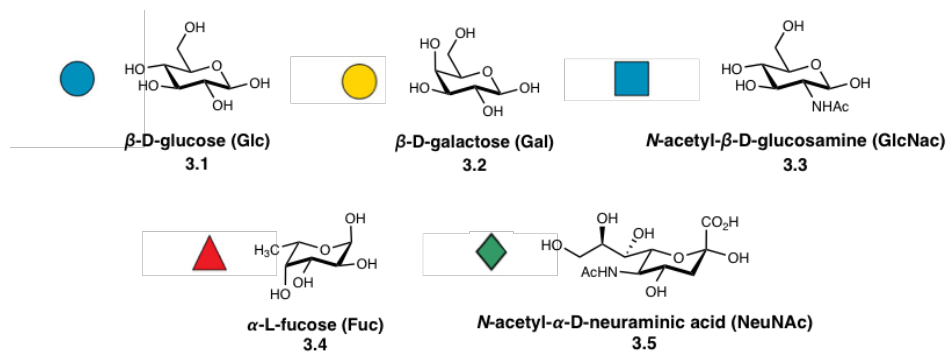


Figure 3.2 Monosaccharides used in HMO biosynthesis and corresponding SNFG

HMO biosynthesis begins in the Golgi apparatus of the mammary gland. Here, lactose is first synthesized via β -(4) connection of Gal-Glc (**Figure 3.3**). This is catalyzed by the enzyme β 1–4-galactosyltransferase 1 (β 1–4GalT1) which is bound to α -lactalbumin in a lactose synthase complex.^{7, 8} Lactose is then functionalized using *N*-acetyllactosamine as an elongation residue or lacto-*N*-biose (LNB) as a terminating residue. These elongated oligosaccharides can be either linear (*iso*-) or branched (*para*-) in nature.

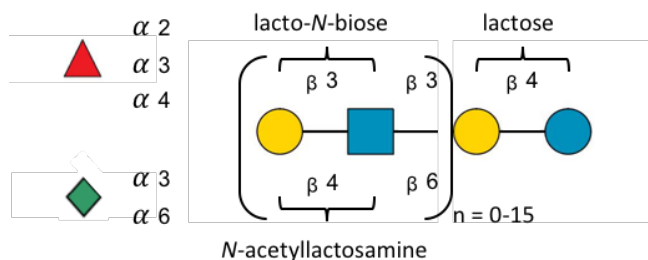


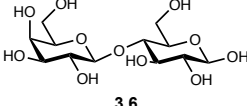
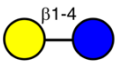
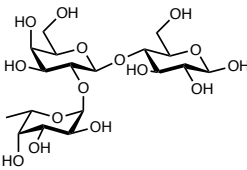
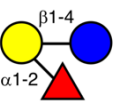
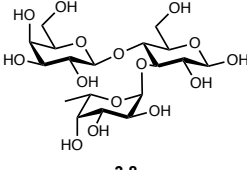
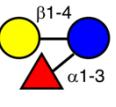
Figure 3.3 Schematic representation of HMO biosynthesis

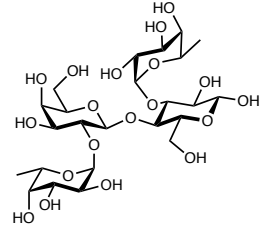
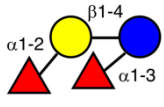
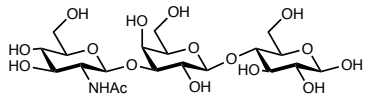
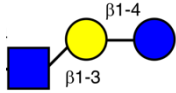
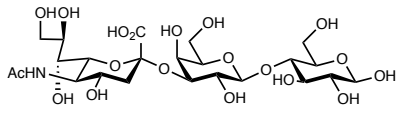
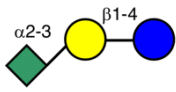
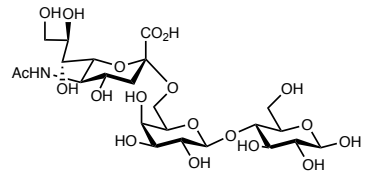
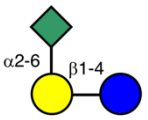
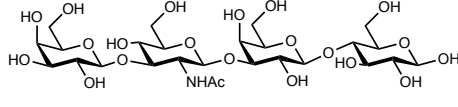
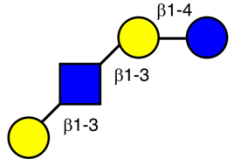
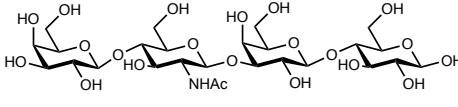
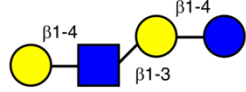
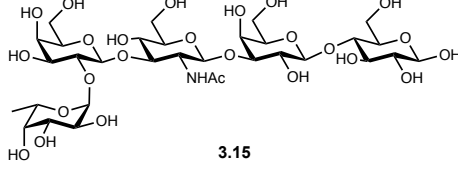
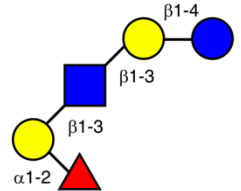
From this core oligosaccharide, subsequent fucosylation or sialylation is genetically guided based on secretor status and Lewis (Le) blood group.⁹ Secretor status is determined by the presence of a gene encoding for α -2-fucosyltransferase (FUT2), while

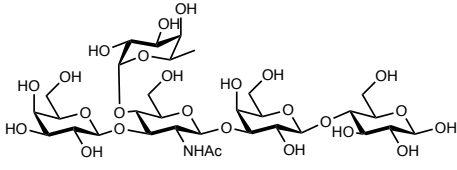
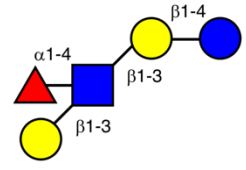
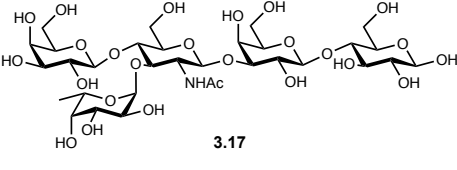
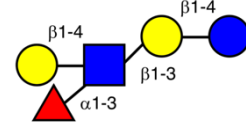
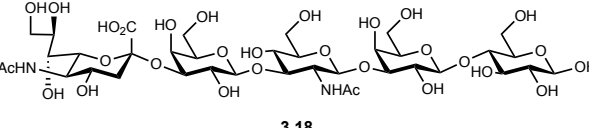
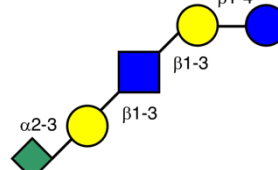
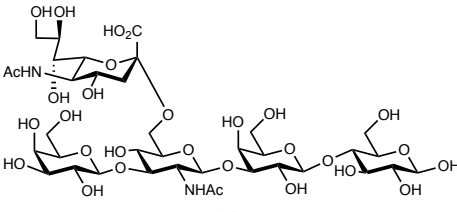
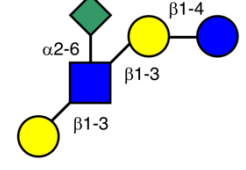
Le blood group encodes for the α 3/4-fucosyltransferase (FUT3). These enzymes are responsible for the installation of fucose onto HMO cores. Similarly, sialic acid decoration occurs after initial HMO elongation, although less is understood about the enzymes that govern the sialylation process.

Overall, of the HMOs present in human breast milk, approximately 62% are fucosylated, 25% are non-fucosylated, 12% are sialylated, and <1% are both sialylated and fucosylated (**Figure 3.1**).¹⁰ To date, over 200 unique HMO structures have been isolated and fully characterized through a combination of biological isolation, mass spectrometry, and nuclear magnetic resonance analyses.^{11, 12} **Table 3.1** contains a few representative HMO structures and the corresponding symbol nomenclature for glycans (SNFG).

Table 3.1 Select HMO structures and corresponding SNFG

HMO Name	Chemical Structure	SNFG
lactose (Lac)	 <p>3.6</p>	
2'-fucosyllactose (2'-FL)	 <p>3.7</p>	
3-fucosyllactose (3-FL)	 <p>3.8</p>	

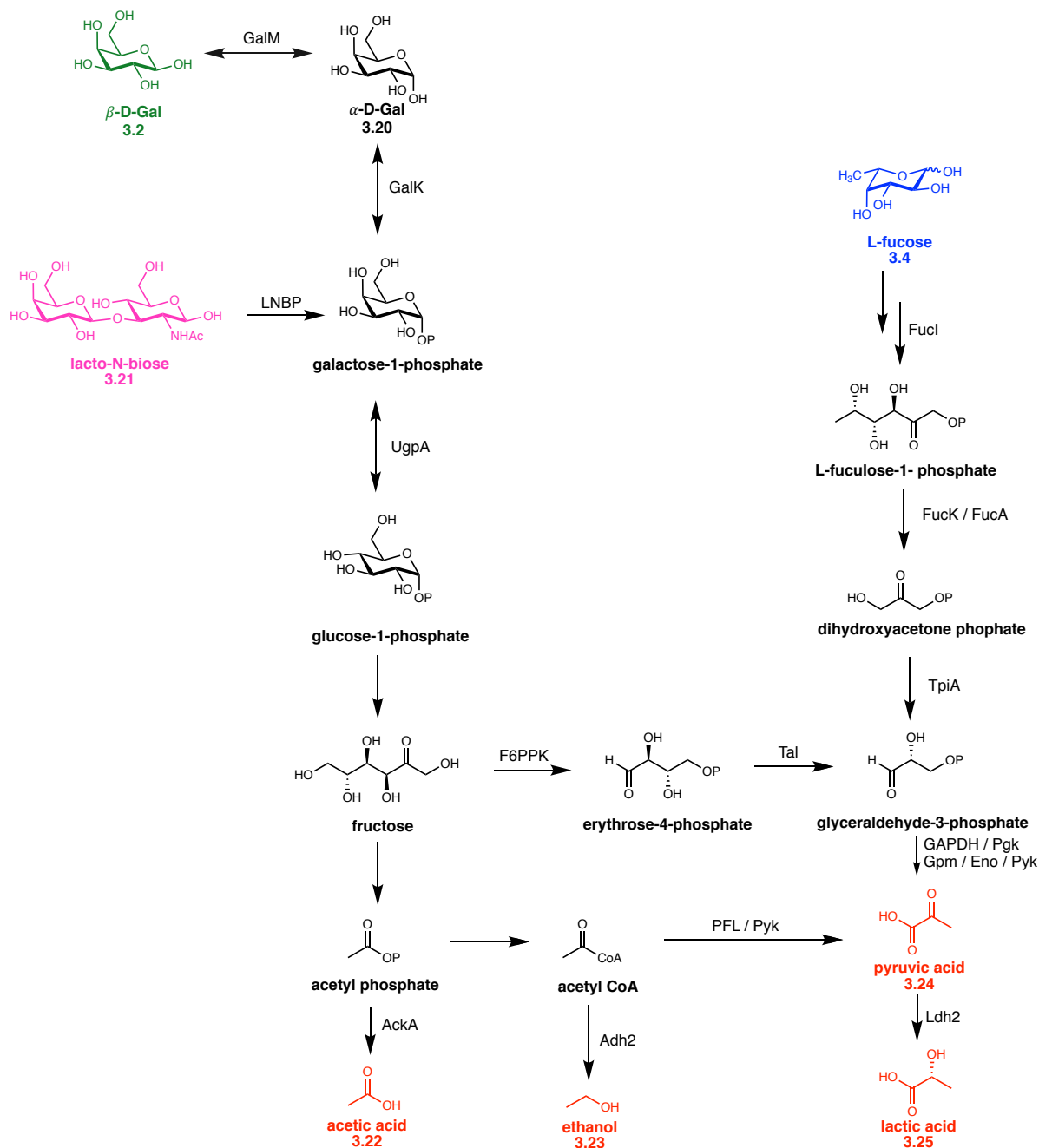
<p>difucosyllactose (DFL)</p>	 <p>3.9</p>	
<p>lacto-<i>N</i>-triose II (LNT-II)</p>	 <p>3.10</p>	
<p>3'-sialyllactose (3'-SL)</p>	 <p>3.11</p>	
<p>6'-sialyllactose (6'-SL)</p>	 <p>3.12</p>	
<p>lacto-<i>N</i>-tetraose (LNT)</p>	 <p>3.13</p>	
<p>lacto-<i>N</i>-neotetraose (LNnT)</p>	 <p>3.14</p>	
<p>lacto-<i>N</i>-fucopentaose I (LNFP-I)</p>	 <p>3.15</p>	

<p>lacto-<i>N</i>- fucopentaose II (LNFP-II)</p>	 <p>3.16</p>	
<p>lacto-<i>N</i>- fucopentaose III (LNFP-III)</p>	 <p>3.17</p>	
<p>LS- tetrasaccharide a (LSTa)</p>	 <p>3.18</p>	
<p>LS- tetrasaccharide b (LSTb)</p>	 <p>3.19</p>	

3.3 Biological activity of HMOs: previous studies

3.3.1 HMOs as prebiotics

The infant gut does not possess the enzymatic machinery to digest and use HMOs as a direct energy source.¹³ Instead, microbes have evolved to utilize HMOs during the development of the infant microbiome. Early studies revealed that HMOs act as powerful prebiotics for commensal bacteria within the infant gut.^{14, 15} Particularly, *Bifidobacterium* and *Bacteroides* species within the infant gut use HMOs almost exclusively as carbon sources, encoding robust enzymatic machinery to harness HMOs and convert them into short chain fatty acids (SCFA) (**Scheme 3.1**).¹⁶⁻²¹



Scheme 3.1 HMO metabolism and conversion to SCFAs by *Bifidobacterium*
 Abbreviations: acetate kinase (AckA), aldehyde-alcohol dehydrogenase 2 (Adh2), enolase (Eno), galactokinase (GalK), galactose mutarotase (GalM), glyceraldehyde-3-phosphate dehydrogenase C (GAPDH), glucose 6-phosphate isomerase (Gpi), phosphoglycerate mutase (Gpm), fructose-6-phosphoketolase (F6PPK), L-fucose isomerase (Fucl), L-fuculose kinase (FucK), L-fuculose-1P aldolase (FucA), lactate dehydrogenase (Ldh2), lacto-N-biose phosphorylase (LNBP), phosphate (P), phosphoglyceric kinase (Pgk), phosphoglucomutase (Pgm), formate acetyltransferase (Pfl), pyruvate kinase (Pyk), transaldolase (Tal), triosephosphate isomerase (TpiA), UTP-glucose-1-phosphate uridylyltransferase (UgpA)

Most notably, galactose (3.2) and lacto-*N*-biose (3.21) can be metabolized to yield acetic acid (3.22) and ethanol (3.23). Additionally, acetyl CoA can be further metabolized to pyruvic acid (3.24) and lactic acid (3.25). Fucose (3.4) can also be fermented to yield pyruvic acid (3.24) and lactic acid (3.25).

The production of these SCFAs serves multiple roles. First, SCFAs aid in immune system development and modulation.^{22, 23} Secondly, this fermentation promotes colonization of the producing commensals and establishes a healthy microbial population within the infant gastrointestinal tract. Finally, the abundance of healthy commensals decreases potential colonization by pathogenic bacteria and other *firmicutes* such as *Clostridia* and *Enterococcus*.²⁴⁻²⁶ As a result, HMOs maintain infant microbiome symbiosis and promote healthy downstream immunological and neuronal development.

3.3.2 HMOs as antimicrobials

While HMOs have strong prebiotic effects on commensals, they have also been demonstrated to have antimicrobial effects on pathogenic microbes. Most notably, HMOs have significant antibacterial and antibiofilm effects against GBS (see section 3.3.3). HMOs have also been shown to combat other pathogenic microbes. HMOs can inhibit both *Candida albicans* infectivity and the attachment of the parasite *Entamoeba histolytica*.^{27, 28} Antiviral effects of HMOs have also been investigated, specifically in studies with human immunodeficiency virus (HIV), rotavirus, norovirus, and influenza.²⁹⁻³² Many of these antiviral effects are attributed to competitive binding of HMOs at cell surface glycan binding proteins. This competition limits viral adhesion. This receptor-decoy mechanism is one common way that HMOs deter microbial pathogenesis.

3.3.3 Antibacterial activity of HMOs against GBS

Early work within the Townsend lab demonstrated that pooled HMOs (that is combined HMO isolates from multiple donors) have significant antibacterial effects against multiple strains of GBS (**Table 3.2**).^{33, 34} Pooled HMOs also inhibit GBS biofilm formation on abiotic surfaces. The antibacterial activity of pooled HMOs is seen in concentrations ranging from 2.56-10.25 mg mL⁻¹. This concentration of HMOs is on the order of that seen in typical breast milk samples, so these results indicate there is a natural antibacterial contribution of HMOs during breast feeding.

Table 3.2 Inhibitory activity of pooled HMOs against GBS

GBS Strain	Serotype	MIC of Pooled HMOs ^a
GB2	Ia	2.56
GB37	V	5.12
GB83	IV	5.12
GB590	III	10.25
GB651	Ib	5.12
GB653	II	5.12
10/84	V	5.12

^aMIC values in mg mL⁻¹

3.4 HMOs as antibiotic adjuvants

3.4.1 Previous studies

Due to the rise in antibiotic drug resistance within streptococcal strains (see section 1.7.3) novel antibacterial strategies are needed for continued treatment of GBS infections. One

such strategy is the use of an antibiotic adjuvant, wherein a second compound is used in cotreatment with an antibiotic to increase the overall effectiveness of a drug. This strategy has been successfully applied in antibiotic treatments such as Augmentin (amoxicillin and clavulanate) and Bactrim (trimethoprim and sulfamethoxazole).³⁵

Resultantly, early work investigated if HMOs could potentiate the activity of clinically relevant antibiotics in similar antibiotic adjuvant strategies. To do this, GBS was grown in the presence of a sub-inhibitory concentration of pooled HMOs and another clinically used antibiotic was serially diluted to determine the MIC of the combination. It was determined that pooled HMOs could potentiate the activity of several antibiotics in multiple strains of GBS (**Table 3.3**).³⁶

Table 3.3 Initial HMO-antibiotic combination study

Antibiotic	GB590			GB2		
	MIC ^a	MIC w/HMOs ^{a,b}	FR ^c	MIC ^a	MIC w/HMOs ^{a,b}	FR ^c
penicillin	0.03	0.03	0	0.03	0.016	2
ampicillin	0.063	0.063	0	0.13	0.063	2
cefazolin	0.13	0.063	2	0.13	0.063	0
vancomycin	1.0	0.5	2	1	0.5	2
clindamycin	0.031	0.016	2	0.031	0.008	4
linezolid	2	1	2	2	1	2
gentamicin	16	1	16	16	2	8
erythromycin	0.31	0.001	32	0.016	0.001	16
minocycline	4	0.5	8	2	0.25	8

^aMIC values in $\mu\text{g mL}^{-1}$ ^bHMOs dosed at IC₂₅ value ^cfold reduction

Gentamicin, erythromycin, and minocycline all saw significant potentiation when co-dosed with HMOs, with maximum fold reductions in MIC of 16, 32, and 8 for the respective combination treatments. Notably, these three antibiotics all inhibit protein synthesis through intracellular-targeting of the ribosome (see section 1.7.1). Conversely, none of the cell wall targeting antibiotics saw potentiation of activity when co-dosed with HMOs. As a result, it was hypothesized that HMOs increase GBS cell permeability and facilitate easier influx of ribosomal-targeting antibiotics.

3.4.2 Expanded study

Previous work demonstrated the utility of HMOs in increasing ribosomal-targeting antibiotic efficacy, but it was not well understood if this utility extended towards other intracellular-targeting antibiotics. To test this, we expanded our studies to investigate HMO-mediated effects on the activity of antibiotics with other intracellular targets (see section 1.7.1). We included antibiotics that impact bacterial DNA synthesis and integrity, RNA synthesis, and folate biosynthesis (**Table 3.4**).³⁷ Ciprofloxacin (**1.18**), levofloxacin (**1.17**), nitrofurantoin (**1.16**) and furazolidone (**1.15**) were chosen to represent antibiotics that target DNA synthesis. Rifampicin (**1.10**) and rifaximin (**1.9**) impair RNA synthesis, and sulfisoxazole (**1.12**), sulfadiazine (**1.13**), and trimethoprim (**1.14**) are all antifolate antibiotics. Collectively, these antibiotics all have intracellular targets and were of interest within our expanded study.

Table 3.4 Expanded HMO-antibiotic combination study

Antibiotic	GB590			GB2		
	MIC ^a	MIC w/HMOs ^{a,b}	FR ^c	MIC ^a	MIC w/HMOs ^{a,b}	FR ^c
trimethoprim	>1024	16	64	1024	2	512
rifampicin	0.0313	0.0156	2	0.125	0.0156	8
ciprofloxacin	2	1	2	2	1	2
levofloxacin	1	0.5	2	1	0.5	2
rifaximin	0.125	0.0625	2	0.125	0.0625	2
sulfisoxazole	>64	>64	0	>64	>64	0
sulfadiazine	>64	>64	0	>64	>64	0
nitrofurantoin	2	4	0	4	2	2
furazolidone	64	64	0	64	32	2

^aMIC values in $\mu\text{g mL}^{-1}$ ^bHMOs dosed at $\sim 1.42 \text{ mg mL}^{-1}$ ^cfold reduction

Through similar HMO-antibiotic combination assays in GBS, we identified that HMO-mediated antibiotic potentiation was not conserved across every intracellular-targeting antibiotic. By example, fluoroquinolone- and nitrofurantoin-derived antibiotics saw no significant potentiation when dosed with HMOs. Additionally, GBS was intrinsically resistant to the sulfonamides, sulfisoxazole (**1.12**) and sulfadiazine (**1.13**), with no significant potentiation seen when dosed with HMOs. The antibiotic activity of rifaximin (**1.9**) was also unchanged when cotreated with HMOs, but in GB2 the HMO-rifampicin combination promoted an 8-fold decrease in MIC.

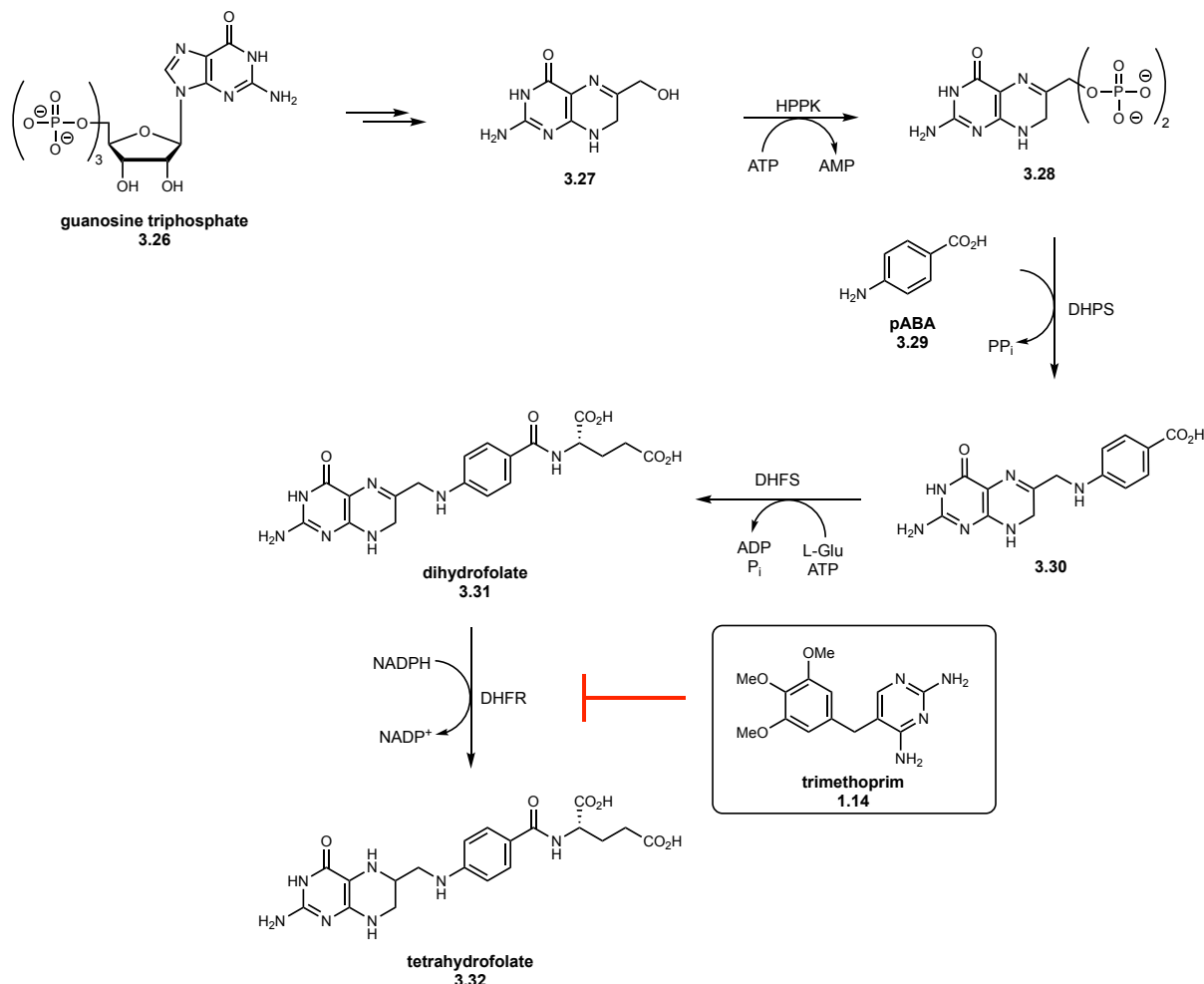
Most impressively, this work identified that HMOs can significantly improve the antibiotic activity of trimethoprim (TMP, **1.14**). TMP alone has an MIC $\geq 1024 \mu\text{g mL}^{-1}$ in GB590 and GB2, but the HMO-trimethoprim combination (HMO-TMP) increased antibiotic efficacy significantly. In GB590, the HMO-TMP MIC was $16 \mu\text{g mL}^{-1}$, which corresponded to at least a 64-fold reduction in MIC. In GB2, the HMO-TMP MIC was $2 \mu\text{g mL}^{-1}$, which corresponded to a 512-fold reduction in MIC over that of TMP alone. This represented the largest fold change in MIC observed to-date within our antibiotic adjuvant studies and is of particular importance since most GBS strains are resistant to TMP (see section 3.5.2). With significant potentiation seen for some intracellular-targeting antibiotics, but not all, these observations suggest that HMOs selectively aid in potentiating the activity of antibiotics. These unique potentiation profiles prompted us to further investigate the nuances of HMO-TMP activity and its utility against GBS.

3.5 HMO-TMP combination as a powerful tool to combat antifolate resistance

3.5.1 Bacterial folate biosynthesis

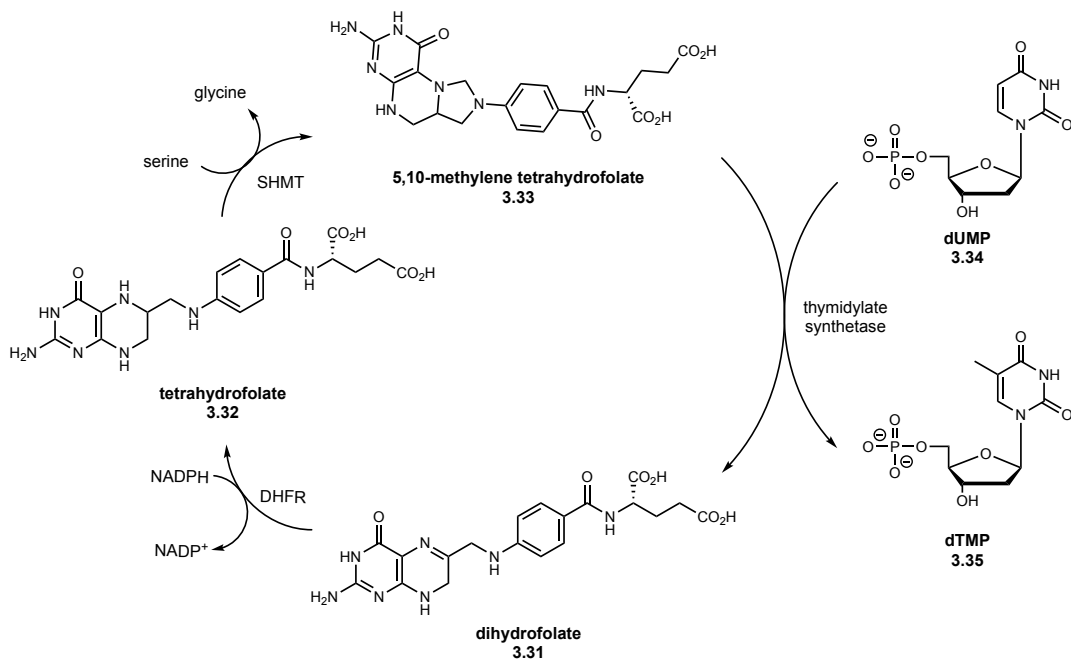
Trimethoprim (TMP, **1.14**) is an antibiotic that targets the folate biosynthetic pathway. In bacteria, the biosynthesis of folate is required to generate purines and pyrimidines used in the ultimate synthesis of DNA.³⁸ Folate biosynthesis begins from guanosine triphosphate (**3.26**), which over several steps is converted to **3.27 (Scheme 3.2)**.^{39, 40} From this, phosphorylation and subsequent installation of *para*-aminobenzoic acid (pABA, **3.29**) yields intermediate **3.30**. Coupling of **3.30** with L-glutamate gives dihydrofolate (**3.31**). Dihydrofolate reductase (DHFR) is then responsible for the final reduction of dihydrofolate (**3.31**) to yield tetrahydrofolate (**3.32**). Within the folate

biosynthetic pathway, TMP (1.14) inhibits DHFR and prevents the formation of tetrahydrofolate (3.32). TMP also has significantly increased binding affinity for bacterial DHFR over mammalian DHFR.⁴¹ This makes TMP a selective and potent antibiotic intervention strategy.



Scheme 3.2 Bacterial folate biosynthetic pathway. Abbreviations: 6- hydroxymethyl-7,8-dihydropterin pyrophosphokinase (HPPK), adenosine triphosphate (ATP), adenosine monophosphate (AMP), *para*-aminobenzoic acid (pABA), dihydropteroate synthase (DHPS), pyrophosphate (PP_i), dihydrofolate synthase (DHFS), L- glutamate (L-glu), adenosine diphosphate (ADP), inorganic phosphate (Pi), dihydrofolate reductase (DHFR), reduced nicotinamide adenine dinucleotide phosphate (NADPH), oxidized nicotinamide adenine dinucleotide phosphate (NADP⁺).

If unperturbed, the folate biosynthetic pathway yields tetrahydrofolate (**3.32**), which is then utilized as a cofactor for a variety of one-carbon metabolic processes.⁴² One notable process is the production of thymidine, a DNA base necessary for bacterial cell division (**Scheme 3.3**).



Scheme 3.3 Tetrahydrofolate as a cofactor in dTMP biosynthesis. Abbreviations: serine hydroxymethyltransferase (SHMT), deoxyuridine monophosphate (dUMP), deoxythymidine monophosphate (dTMP), dihydrofolate reductase (DHFR), reduced nicotinamide adenine dinucleotide phosphate (NADPH), oxidized nicotinamide adenine dinucleotide phosphate (NADP⁺).

Here, tetrahydrofolate (**3.32**) is first methylated via serine hydroxymethyl transferase (SHMT) to form intermediate **3.33**. Using **3.33**, thymidylate synthetase then catalyzes methyl group transfer and reduction onto deoxyuridine monophosphate (dUMP, **3.34**) to ultimately yield deoxythymidine monophosphate (dTMP, **3.35**) and dihydrofolate (**3.31**). dTMP then is fed into the nucleotide pools for DNA synthesis, and dihydrofolate (**3.31**) can be recycled via DHFR to regenerate tetrahydrofolate (**3.32**). The use of

tetrahydrofolate in the synthesis of thymidine nucleotides highlights one key role of this cofactor and the global metabolic impact of TMP within bacterial cells.

3.5.2 Bacterial resistance to TMP

Although TMP has selective inhibitory effects on bacterial folate biosynthesis, there are several mechanisms by which streptococci have developed resistance to TMP.⁴³⁻⁴⁹ For one, *Streptococcus* can limit TMP efficacy by decreasing membrane permeability to physically block entry of TMP.⁵⁰ Mutations in the inherent DHFR or the neighboring environment can also render TMP inactive. Single point mutations within the *dhfr* genes can weaken TMP binding to DHFR and thus, dampen or impede antibiotic efficacy.⁵¹ This can be also facilitated via horizontal transfer of *dhfr* genes that encode resistant DHFRs. Additionally, *Streptococcus* has been shown to upregulate *dhfr* gene expression to increase DHFR production. This overproduction of DHFR compensates for metabolic disruption by TMP and renders the antibiotic ineffective.

Through these resistance mechanisms, most GBS strains have become fully resistant to TMP treatment. In GB2 and GB590, the MIC of TMP was $\geq 1024 \mu\text{g mL}^{-1}$ (**Table 3.4**). The Clinical and Laboratory Standards Institute (CLSI) marks the antibiotic breakpoint for TMP in *Streptococcus* to be at $76 \mu\text{g mL}^{-1}$, so resultantly these strains are clinically considered “resistant”.^{52, 53} Notably, upon cotreatment with HMOs, the TMP MIC is $16 \mu\text{g mL}^{-1}$ and $2 \mu\text{g mL}^{-1}$ in GB590 and GB2 respectively. By CLSI standards, these GBS strains would in turn be categorized as “sensitive” to TMP. Considering this, the HMO-TMP treatment is particularly novel due to its ability to overcome the intrinsic TMP-resistance mechanisms of GBS.

3.5.3 HMO-TMP combination treatment is efficacious across GBS serotypes

As HMOs had been shown to restore antibiotic efficacy of TMP, we then explored the breadth these effects across GBS serotypes (**Table 3.5**). In almost all of the tested GBS strains, the MIC of TMP is $\geq 1024 \mu\text{g mL}^{-1}$. This confirms across serotypes that GBS is not susceptible to TMP treatment alone. Upon HMO-TMP treatment, all six strains of GBS saw significant potentiation, ranging from 8-fold to 512-fold reduction in MIC. The highest effect was seen in serotype IV GB2, where the MIC of HMO-TMP is $2 \mu\text{g mL}^{-1}$. This demonstrates HMOs are a powerful tool for reversing antibiotic resistance in multiple serotypes of GBS.

Table 3.5 HMO-TMP combination treatment across GBS strains

Strain	MIC of HMOs ^a	MIC of TMP w/out HMOs ^b	MIC of HMO-TMP ^{b,c}	Fold Reduction
10/84	5.12	>1024	8	≥ 256
GB2	2.56	1024	2	512
GB590	5.12	>1024	32	≥ 64
GB651	5.12	512	32	16
GB83	5.12	>1024	128	≥ 8
GB37	5.12	>1024	128	≥ 8

^aMIC values in mg mL^{-1} ^bMIC values in $\mu\text{g mL}^{-1}$ ^cHMOs dosed at $\sim 1.42 \text{ mg mL}^{-1}$

3.5.4 HMO-TMP is a synergistic antibiotic combination

Due to the powerful nature of the HMO-TMP combination, further studies were conducted to validate that HMOs and TMP engage in a synergistic manner. Antibiotic combination treatments can be either additive in nature, that is the activity of the combination is the sum of every independent antibiotic activity, or combinations can be synergistic in nature. Combinations are deemed synergistic if the combined activity exceeds the sum of the activities of each independent antibiotic.

Checkerboard assays were conducted in GB2 and GB590 strains to determine if the HMO-TMP combination was synergistic or additive in nature. Conventionally, synergy is determined by the fractional inhibitory concentration (FIC) index value, where $\Sigma\text{FIC} = \text{FICA} + \text{FICB} = (\text{MICA in combination}/\text{MICA alone}) + (\text{MICB in combination}/\text{MICB alone})$, where A is TMP and B is pooled HMOs.⁵⁴ Synergy is defined when the FIC is ≤ 0.5 for each antibiotic combination. It was demonstrated that in GB590, synergy was achieved when dosing HMOs from 1.28–2.56 mg mL⁻¹ in combination with TMP dosed at 8–128 $\mu\text{g mL}^{-1}$ (ΣFIC values 0.28–0.50). In GB2, the combination was synergistic with treatment of HMOs between 0.64–1.28 mg mL⁻¹ in conjunction with TMP from 4–32 $\mu\text{g mL}^{-1}$ (ΣFIC values 0.28–0.50). These assays firmly demonstrated the HMO-TMP combination to be truly synergistic in nature.

3.5.5 HMO-TMP and the folate biosynthetic pathway

We then investigated the effect of the HMO-TMP combination on the folate biosynthetic pathway within GBS. TMP-mediated inhibition of DHFR ultimately prevents downstream

synthesis of thymidine (**Scheme 3.3**). Considering this, we investigated if thymidine supplementation would alter the activity of HMO-TMP in GBS (**Table 3.6**).

Table 3.6 HMO-TMP treatment in the presence of thymidine

Strain	THB				THB+20 $\mu\text{g mL}^{-1}$ thymidine			
	MIC HMOs ^a	MIC TMP ^b	MIC HMO-TMP ^{b,c}	FR ^d	MIC HMOs ^a	MIC TMP ^b	MIC HMO-TMP ^{b,c}	FR ^d
GB590	10.25	>1024	32	≥ 64	10.25	>1024	128	8
GB2	2.56	1024	2	512	2.56	1024	16 ^d	64

^a.MIC values in mg mL^{-1} ^b.MIC values in $\mu\text{g mL}^{-1}$ ^c.HMOs dosed at $\sim 1.42 \text{ mg mL}^{-1}$ ^d.fold reduction

Upon supplementation with thymidine, the HMO-TMP combination treatment lost significant activity, with up to 8-fold loss of efficacy in thymidine-supplemented broth. In GB2, the HMO-TMP MIC was $2 \mu\text{g mL}^{-1}$ in THB, but increased to $16 \mu\text{g mL}^{-1}$ in thymidine-supplemented THB. Notably, thymidine supplementation had no effect on the MIC of HMOs alone. These results indicated that the HMO-TMP combination interacts within the folate biosynthetic pathway, but HMOs alone do not. This supports the hypothesis that HMOs potentiate the activity of TMP by enabling its on-target function within the folate biosynthetic pathway.

3.6 HMO-TMP activity is facilitated through CovRS

3.6.1 CovRS: an introduction

To further understand the antibiotic mechanism of action, we also investigated if two-component signal transduction systems (TCSs) (see section 1.6.3) within GBS might play

a role in HMO antibacterial activity, both when used as an antibiotic alone and in coordination with TMP. We focused our initial experiments on investigating how CovRS might be essential for HMO antibiotic activity or antibiotic synergy. CovRS is a GBS TCS responsible for sensing high-glucose environments and promoting GBS proliferation.⁵⁵ Of note, CovS is the sensory component of this TCS, while CovR is the response regulator (**Figure 3.4**). Previous work identified CovRS as essential for GBS virulence and carbohydrate sensing, so we hypothesized that this TCS was involved in GBS response to HMOs.

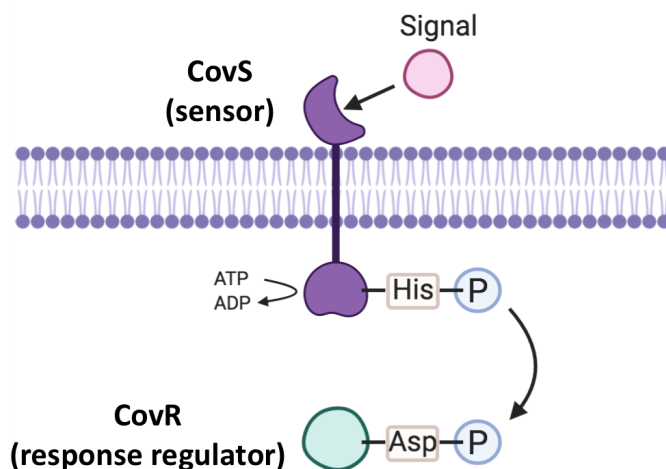


Figure 3.4 CovRS conceptual model

3.6.1 CovRS is implicated in the antibiotic synergy of HMO-TMP

We tested both HMOs and the HMO-TMP combination against CovRS deletion mutants to investigate if this TCS is responsible for the HMO antibacterial activity within GBS (**Table 3.7**). This included the wildtype strain GB37 and GB37 Δ CovR and GB37 Δ CovS mutants generated by the Gaddy lab via allelic exchange with a spectinomycin resistance

cassette. Across strains, neither the solo HMO or solo TMP MICs were impacted significantly. HMOs saw only a 2-fold difference in MIC between wildtype GB37 and either GB37 Δ CovR or GB37 Δ CovS. The MIC of TMP was >1024 $\mu\text{g mL}^{-1}$ in all of these strains. These results indicated that the CovRS system is not implicated in the independent activity of these antibiotics.

Nevertheless, there were significant changes seen when looking at the efficacy of the HMO-TMP combination across CovRS mutants. In GB37, HMO-TMP had an MIC of 128 $\mu\text{g mL}^{-1}$ and in GB37 Δ CovR the combination was also effective, with an MIC of 32 $\mu\text{g mL}^{-1}$. However, in GB37 Δ CovS, the HMO-TMP combination was no longer effective with an MIC of >1024 $\mu\text{g mL}^{-1}$. In GB37 Δ CovS, HMO-TMP activity reverts to similar potency seen for TMP alone, indicating a total loss of the desired antibiotic synergy.

Table 3.7 HMO and HMO-TMP activity within Δ CovRS mutants

Strain	MIC HMOs ^a	MIC TMP ^b	MIC HMO-TMP ^{b,c}	FR ^d
GB37	5.12	>1024	128	≥ 8
GB37 Δ CovR	2.56	>1024	32	≥ 64
GB37 Δ CovS	2.56	>1024	>1024	0

^aMIC values in mg mL^{-1} ^bMIC values in $\mu\text{g mL}^{-1}$ ^cHMOs dosed at $\sim 1.42 \text{ mg mL}^{-1}$ ^dfold reduction

These results suggest that CovS is necessary for the activity of the HMO-TMP combination. As CovS is the sensory component of this TCS, we hypothesize that CovS senses HMOs as a “high-carbohydrate” environment and the subsequent bacterial response allows for increased antibiotic efficacy of TMP. The nuances between the

interactions of this TCS and the HMO-TMP combination will need to be further explored to better understand these results.

3.7 Conclusion and future directions

Our work has demonstrated that HMOs are potent antibacterial agents against GBS and can be used in coordination with other antibiotics to restore antibiotic efficacy and combat resistance mechanisms. Our expanded study revealed additional HMO-mediated antibiotic potentiation patterns. The HMO-TMP combination is synergistic and overcomes GBS resistance mechanisms to restore the utility of TMP. The activity of this combination treatment can be lost upon genetic deletion of CovS, indicating that CovRS is involved in the antibiotic synergy of HMO-TMP. Several follow-up studies can be conducted to better understand GBS mechanisms of TMP resistance and synergy of HMO combination treatments.

Of initial interest, the basal permeability of TMP within GBS strains could be determined to study how TMP penetration is impacted upon cotreatment with HMOs. This could be conducted using subcellular fractionation of GBS at various timepoints, where subsequent quantitative mass spectrometry would indicate how much TMP has reached a particular location within the GBS cell and remained intact. We hypothesize GBS treated with TMP alone would see little to no TMP build-up within the cytoplasmic cellular fraction, due to low intrinsic permeability of TMP in GBS. We also suspect there would be much higher accumulation of TMP in the cytoplasm of the HMO-TMP treated GBS samples. An experiment such as this would detail the permeability of TMP and could also be applied

to other HMO-antibiotic combination treatments to better understand the impacts of antibiotic permeability in treating GBS infections.

CovRS could also be further investigated to determine its role in HMO-TMP synergy. We identified that CovS is necessary for HMO-TMP synergy and generally, CovS is responsible for sensing external signals to relay to CovR for further cellular regulation. The signal being sensed by CovS upon HMO-TMP treatment is still not fully understood. One hypothesis, is that the HMOs are sensed as a “high-carbohydrate” environment and might facilitate transcriptional changes to permit greater cellular flux. This increase in flux would allow TMP to enter the cell easier and elicit on-target function. This could be tested by utilizing other carbohydrate sources, such as glucose supplementation, to mimic a high-carbohydrate environment and determine if the effects of a glucose-TMP combination are similar to the HMO-TMP combination. In an alternative hypothesis, CovS could be sensing TMP, in a well evolved resistance mechanism. Sensing TMP might relay a cellular response in which HMOs become more effective and increase GBS susceptibility. A mechanism such as this might suggest CovRS is used by GBS to sense certain antibiotics and generate resistant phenotypes, so studies of other antibiotic resistant GBS strains and combinations would be particularly insightful.

Finally, we are currently using RNA sequencing to determine what transcriptional changes are occurring in GBS upon HMO-treatment. We hypothesize that transcriptional profiles for genes involved in cell envelop processes will be significantly impacted upon HMO treatment. These identified genes might also overlap with those identified by studies detailing CovRS-mediated GBS regulation.⁵⁶ Experiments such as these would explore the cellular processes that are impacted by HMOs and their continued use as antibiotic

adjuvants to combat antibiotic resistance. Indeed, this work has already provided a strong basis for antibiotic drug discovery and development. Gitai and coworkers identified a similar dual combination treatment that had increase activity against both gram-positive and gram-negative pathogens with no detectable resistance.⁵⁷ The combination was TMP and a novel cell-permeabilizing antibiotic. These coordinated results support antibiotic combination treatments as effective tools in the fight against antibiotic resistance.

3.8 Experimental methods

Bacterial strains and culture conditions

Table 3.8 Bacterial strains

Bacterial Strain	Source
<i>S. agalactiae</i> strain GB590	clinical isolate, Shannon Manning, Michigan State
<i>S. agalactiae</i> strain GB2	clinical isolate, Shannon Manning, Michigan State
<i>S. agalactiae</i> strain 10/84	ATCC
<i>S. agalactiae</i> strain GB83	clinical isolate, Shannon Manning, Michigan State
<i>S. agalactiae</i> strain GB651	clinical isolate, Shannon Manning, Michigan State
<i>S. agalactiae</i> strain GB37	clinical isolate, Shannon Manning, Michigan State
<i>S. agalactiae</i> strain GB37 Δ CovR	genetic mutant, Jennifer Gaddy, Vanderbilt University
<i>S. agalactiae</i> strain GB37 Δ CovS	genetic mutant, Jennifer Gaddy, Vanderbilt University

All strains were grown on tryptic soy agar plates supplemented with 5% sheep blood (blood agar plates) at 37 °C in ambient air overnight. All strains were subcultured from

blood agar plates into 5 mL of Todd-Hewitt broth (THB) and incubated under shaking conditions at 180 RPM at 37 °C overnight. Following overnight incubation, bacterial density was quantified through absorbance readings at 600 nm (OD₆₀₀) using a Promega GloMax-Multi Detection System plate reader. Bacterial numbers were determined using the predetermined coefficient of 1 OD₆₀₀ = 10⁹ CFU mL⁻¹.

GB37ΔCovR and GB37ΔCovS were prepared previously within the Gaddy lab via in-frame marked deletion of respective open reading frames. Briefly, 1-kbp regions upstream and downstream of the *covR* or *covS* coding region was cloned into a temperature sensitive plasmid and disrupted with a spectinomycin resistance cassette. The plasmid was electroporated into electrocompetent GB037 and colonies were selected on agar plates supplemented with 6 ug/mL of spectinomycin. To facilitate double crossover events, the cells were incubated on spectinomycin-supplemented plates at 42 °C to repress plasmid replication and force chromosomal insertion of the plasmid. Mutation was confirmed by whole genome sequencing.

HMO isolation

Human milk was obtained from healthy, lactating women between 3 days and 3 months postnatal and stored between -80 and -20°C. De-identified milk was provided by Dr. Jörn-Hendrik Weitkamp from the Vanderbilt Department of Pediatrics, under a collection protocol approved by the Vanderbilt University Institutional Review Board (IRB#100897), or Medolac. Milk samples were thawed then centrifuged for 45 minutes. Following centrifugation, the resultant top lipid layer was removed. The proteins were then removed by diluting the remaining sample with roughly 1:1 v/v 180 or 200 proof ethanol, chilling

the sample briefly, and centrifuging for 45 minutes followed by removal of the resulting HMO-containing supernatant. Following concentration of the supernatant *in vacuo*, the HMO-containing extract was dissolved in phosphate buffer (pH 6.5, 0.2 M) and heated to 37°C. β -galactosidase from *Kluveromyces lactis* was added and the reaction was stirred until lactose hydrolysis was complete. The reaction mixture was diluted with roughly 1:0.5 v/v 180 proof ethanol, chilled briefly, then centrifuged for 30 minutes. The supernatant was removed and concentrated *in vacuo*, and the remaining salts, glucose, and galactose were separated from the oligosaccharides using size exclusion chromatography with P-2 Gel (H₂O eluent). The oligosaccharides were then dried by lyophilization. Correspondingly, HMO isolates from donors were combined and solubilized in water to final concentration of 102.6 mg mL⁻¹.

Broth microdilution minimum inhibitory concentration assay

All strains were grown overnight as described above and used to inoculate fresh THB or THB + 20 μ g mL⁻¹ thymidine to achieve 5 x 10⁵ CFU mL⁻¹. To 96 well tissue culture treated, sterile polystyrene plates was added the inoculated media in the presence of increasing concentrations of antibiotic or HMO cocktail to achieve a final volume of 100 μ L per well. Bacteria grown in media in the absence of any compounds served as the controls. The plates were incubated under static conditions at 37 °C in ambient air for 24 h. Bacterial growth was quantified through absorbance readings (OD₆₀₀). The minimum inhibitory concentrations (MICs) were assigned at the lowest concentration of compound at which no bacterial growth was observed.

For HMO-antibiotic combination assays, overnight subcultures were used to inoculate fresh THB or THB + 20 $\mu\text{g mL}^{-1}$ thymidine to achieve $5 \times 10^5 \text{ CFU mL}^{-1}$. Freshly inoculated media was then supplemented with HMOs at their IC_{25} concentration ($\sim 1.24 \text{ mg mL}^{-1}$). To 96 well tissue culture treated, sterile polystyrene plates was added the inoculated media supplemented with HMOs in the presence of increasing concentrations of antibiotic. Bacteria grown in media in the absence of any compounds served as one control. Bacteria grown in media supplemented with HMOs in the absence of any antibiotic served as a second control. MICs were determined as previously described.

Checkerboard assay

Group B Streptococcus (GB2 and GB590) were grown overnight as described above and used to inoculate fresh THB to achieve $5 \times 10^5 \text{ CFU mL}^{-1}$. To 96 well tissue culture treated, sterile polystyrene plates, 100 μL per well of inoculated media was added. Trimethoprim was two-fold serially diluted descending down the plate to achieve a final volume of 100 μL per well. The final row was left without trimethoprim. The HMO cocktail was two-fold serially diluted going from right to left across the plate. The far-left column was left without HMO cocktail. Bacteria grown in media in the absence of either compound served as the controls. The plates were incubated under static conditions at 37 °C in ambient air for 24 h. Bacterial growth was quantified through absorbance readings (OD_{600}). The minimum inhibitory concentrations (MICs) were assigned at the lowest concentration of compound at which no bacterial growth was observed. The fractional inhibitory concentration (FIC) index was used to evaluate synergy. The calculation of the FIC index is as follows: $\Sigma \text{FIC} = \text{FIC A} + \text{FIC B} = (\text{MIC of drug A in the combination} / \text{MIC of drug A alone}) + (\text{MIC of drug$

B in the combination/MIC of drug B alone), where A is trimethoprim and B is the HMO cocktail. The combination is considered synergistic when the Σ FIC is ≤ 0.5 , additive or indifferent when the Σ FIC is >0.5 to <4 , and antagonistic when the Σ FIC is ≥ 4 .

Statistical analysis

HMO antimicrobial and combination assay data represent 3 biological replicates, each with 3 technical replicates. Data for synergy assays represents 3 biological replicates. Data are expressed as the mean biomass \pm SEM. Statistical analyses were performed in GraphPad Prism Software v. 7.0c.

3.9 References

1. This chapter is adapted from "A solution to antifolate resistance in group B Streptococcus: untargeted metabolomics identifies human milk oligosaccharide-induced perturbations that result in potentiation of trimethoprim" published in *mBio* and "Like mother, like microbe: human milk oligosaccharide mediated microbiome symbiosis" published in *Biochemical Society Transactions* and has been reproduced with the permission of the respective publishers and my co-authors including, Rebecca E. Moore, Kelly M. Craft, Steven D. Townsend, Jennifer A. Gaddy, Harrison C. Thomas, Rishub Das, Shannon D. Manning, Simona G. Codreanu, Stacy D. Sherrod, David M. Aronoff, and John A. McLean. Chambers SA, Moore RE, Craft KM, Thomas HC, Das R, Manning SD, Codreanu SG, Sherrod SD, Aronoff DM, McLean JA, Gaddy JA, Townsend SD. 2020. A solution to antifolate resistance in group B Streptococcus: untargeted metabolomics identifies human milk oligosaccharide-induced perturbations that result in potentiation of trimethoprim. *mBio* 11:e00076-20. Chambers SA, Townsend SD. Like mother, like microbe: human milk oligosaccharide mediated microbiome symbiosis. *Biochem Soc Trans.* 2020 48(3): 1139-1151.
2. Tao, N.; Wu, S.; Kim, J.; An, H. J.; Hinde, K.; Power, M. L.; Gagneux, P.; German, J. B.; Lebrilla, C. B., Evolutionary glycomics: characterization of milk oligosaccharides in primates. *Journal of proteome research* **2011**, 10 (4), 1548-1557.
3. Coppa, G. V.; Gabrielli, O.; Pierani, P.; Catassi, C.; Carlucci, A.; Giorgi, P. L., Changes in Carbohydrate Composition in Human Milk Over 4 Months of Lactation. *Pediatrics* **1993**, 91 (3), 637.

4. Bode, L.; Jantscher-Krenn, E., Structure-function relationships of human milk oligosaccharides. *Adv Nutr* **2012**, 3 (3), 383S-91S.
5. Lis-Kuberka, J.; Orczyk-Pawilowicz, M., Sialylated Oligosaccharides and Glycoconjugates of Human Milk. The Impact on Infant and Newborn Protection, Development and Well-Being. *Nutrients* **2019**, 11 (2), 306.
6. Zeuner, B.; Teze, D.; Muschiol, J.; Meyer, A. S., Synthesis of Human Milk Oligosaccharides: Protein Engineering Strategies for Improved Enzymatic Transglycosylation. *Molecules* **2019**, 24 (11), 2033.
7. Chen, X., Chapter Four - Human Milk Oligosaccharides (HMOS): Structure, Function, and Enzyme-Catalyzed Synthesis. In *Advances in Carbohydrate Chemistry and Biochemistry*, Baker, D. C.; Horton, D., Eds. Academic Press: 2015; Vol. 72, pp 113-190.
8. Brew, K.; Hill, R. L., Lactose biosynthesis. *Reviews of physiology, biochemistry and pharmacology* **1975**, 72, 105-58.
9. Blank, D.; Dotz, V.; Geyer, R.; Kunz, C., Human Milk Oligosaccharides and Lewis Blood Group: Individual High-Throughput Sample Profiling to Enhance Conclusions From Functional Studies. *Advances in nutrition (Bethesda, Md.)* **2012**, 3, 440S-9S.
10. Wang, M.; Li, M.; Wu, S.; Lebrilla, C. B.; Chapkin, R. S.; Ivanov, I.; Donovan, S. M., Fecal microbiota composition of breast-fed infants is correlated with human milk oligosaccharides consumed. *J Pediatr Gastroenterol Nutr* **2015**, 60 (6), 825-833.
11. Bode, L., Human milk oligosaccharides: every baby needs a sugar mama. *Glycobiology* **2012**, 22 (9), 1147-62.
12. Kobata, A., Structures and application of oligosaccharides in human milk. *Proc Jpn Acad Ser B Phys B Sci* **2010**, 86 (7), 731-747.
13. Engfer, M. B.; Stahl, B.; Finke, B.; Sawatzki, G.; Daniel, H., Human milk oligosaccharides are resistant to enzymatic hydrolysis in the upper gastrointestinal tract. *The American Journal of Clinical Nutrition* **2000**, 71 (6), 1589-1596.
14. Chambers, S. A.; Townsend, S. D., Like mother, like microbe: human milk oligosaccharide mediated microbiome symbiosis. *Biochemical Society Transactions* **2020**, 48 (3), 1139-1151.
15. Marcobal, A.; Barboza, M.; Froehlich, J. W.; Block, D. E.; German, J. B.; Lebrilla, C. B.; Mills, D. A., Consumption of Human Milk Oligosaccharides by Gut-Related Microbes. *J Agric Food Chem* **2010**, 58 (9), 5334-5340.

16. Yu, Z.-T.; Chen, C.; Newburg, D. S., Utilization of major fucosylated and sialylated human milk oligosaccharides by isolated human gut microbes. *Glycobiology* **2013**, *23* (11), 1281-1292.
17. Duranti, S.; Lugli, G. A.; Milani, C.; James, K.; Mancabelli, L.; Turrone, F.; Alessandri, G.; Mangifesta, M.; Mancino, W.; Ossiprandi, M. C.; Iori, A.; Rota, C.; Gargano, G.; Bernasconi, S.; Di Pierro, F.; van Sinderen, D.; Ventura, M., *Bifidobacterium bifidum* and the infant gut microbiota: an intriguing case of microbe-host co-evolution. *Environmental Microbiology* **2019**, *21* (10), 3683-3695.
18. Parada Venegas, D.; De la Fuente, M. K.; Landskron, G.; González, M. J.; Quera, R.; Dijkstra, G.; Harmsen, H. J. M.; Faber, K. N.; Hermoso, M. A., Short Chain Fatty Acids (SCFAs)-Mediated Gut Epithelial and Immune Regulation and Its Relevance for Inflammatory Bowel Diseases. *Front Immunol* **2019**, *10* (277).
19. O'Callaghan, A.; van Sinderen, D., Bifidobacteria and Their Role as Members of the Human Gut Microbiota. *Frontiers in Microbiology* **2016**, *7* (925).
20. Marcobal, A.; Barboza, M.; Sonnenburg, E. D.; Pudlo, N.; Martens, E. C.; Desai, P.; Lebrilla, C. B.; Weimer, B. C.; Mills, D. A.; German, J. B.; Sonnenburg, J. L., Bacteroides in the infant gut consume milk oligosaccharides via mucus-utilization pathways. *Cell Host Microbe* **2011**, *10* (5), 507-514.
21. Comstock, L. E., Importance of Glycans to the Host-*Bacteroides* Mutualism in the Mammalian Intestine. *Cell Host Microbe* **2009**, *5* (6), 522-526.
22. He, F.; Ouwehand, A. C.; Isolauri, E.; Hashimoto, H.; Benno, Y.; Salminen, S., Comparison of mucosal adhesion and species identification of bifidobacteria isolated from healthy and allergic infants. *FEMS Immunology & Medical Microbiology* **2001**, *30* (1), 43-47.
23. Bode, L.; Kunz, C.; Muhly-Reinholz, M.; Mayer, K.; Seeger, W.; Rudloff, S., Inhibition of monocyte, lymphocyte, and neutrophil adhesion to endothelial cells by human milk oligosaccharides. *Thrombosis and haemostasis* **2004**, *92* (6), 1402-10.
24. Resta-Lenert, S.; Barrett, K. E., Live probiotics protect intestinal epithelial cells from the effects of infection with enteroinvasive *Escherichia coli* (EIEC). *Gut* **2003**, *52* (7), 988.
25. Ho, N. T.; Li, F.; Lee-Sarwar, K. A.; Tun, H. M.; Brown, B. P.; Pannaraj, P. S.; Bender, J. M.; Azad, M. B.; Thompson, A. L.; Weiss, S. T.; Azcarate-Peril, M. A.; Litonjua, A. A.; Kozyrskyj, A. L.; Jaspán, H. B.; Aldrovandi, G. M.; Kuhn, L., Meta-analysis of effects of exclusive breastfeeding on infant gut microbiota across populations. *Nature Communications* **2018**, *9* (1), 4169.
26. Timmerman, H. M.; Rutten, N. B. M. M.; Boekhorst, J.; Saulnier, D. M.; Kortman, G. A. M.; Contractor, N.; Kullen, M.; Floris, E.; Harmsen, H. J. M.; Vlieger, A. M.; Kleerebezem, M.; Rijkers, G. T., Intestinal colonisation patterns in breastfed and

formula-fed infants during the first 12 weeks of life reveal sequential microbiota signatures. *Scientific reports* **2017**, 7 (1), 8327-8327.

27. Gonia, S.; Tuepker, M.; Heisel, T.; Autran, C.; Bode, L.; Gale, C. A., Human Milk Oligosaccharides Inhibit *Candida albicans* Invasion of Human Premature Intestinal Epithelial Cells. *The Journal of Nutrition* **2015**, 145 (9), 1992-1998.

28. Jantscher-Krenn, E.; Lauwaet, T.; Bliss, L. A.; Reed, S. L.; Gillin, F. D.; Bode, L., Human milk oligosaccharides reduce *Entamoeba histolytica* attachment and cytotoxicity in vitro. *British Journal of Nutrition* **2012**, 108 (10), 1839-1846.

29. Bode, L.; Kuhn, L.; Kim, H.-Y.; Hsiao, L.; Nissan, C.; Sinkala, M.; Kankasa, C.; Mwiya, M.; Thea, D. M.; Aldrovandi, G. M., Human milk oligosaccharide concentration and risk of postnatal transmission of HIV through breastfeeding. *The American journal of clinical nutrition* **2012**, 96 (4), 831-839.

30. Ramani, S.; Stewart, C. J.; Laucirica, D. R.; Ajami, N. J.; Robertson, B.; Autran, C. A.; Shinge, D.; Rani, S.; Anandan, S.; Hu, L.; Ferreon, J. C.; Kuruvilla, K. A.; Petrosino, J. F.; Venkataram Prasad, B. V.; Bode, L.; Kang, G.; Estes, M. K., Human milk oligosaccharides, milk microbiome and infant gut microbiome modulate neonatal rotavirus infection. *Nature Communications* **2018**, 9 (1), 5010.

31. Morozov, V.; Hansman, G.; Hanisch, F.-G.; Schrotten, H.; Kunz, C., Human Milk Oligosaccharides as Promising Antivirals. *Molecular Nutrition & Food Research* **2018**, 62 (6), 1700679.

32. Weichert, S.; Koromyslova, A.; Singh, B. K.; Hansman, S.; Jennewein, S.; Schrotten, H.; Hansman, G. S., Structural Basis for Norovirus Inhibition by Human Milk Oligosaccharides. *J Virol* **2016**, 90 (9), 4843-4848.

33. Ackerman, D. L.; Craft, K. M.; Doster, R. S.; Weitkamp, J. H.; Aronoff, D. M.; Gaddy, J. A.; Townsend, S. D., Antimicrobial and Antibiofilm Activity of Human Milk Oligosaccharides against *Streptococcus agalactiae*, *Staphylococcus aureus*, and *Acinetobacter baumannii*. *ACS Infect Dis* **2018**, 4 (3), 315-324.

34. Ackerman, D. L.; Doster, R. S.; Weitkamp, J. H.; Aronoff, D. M.; Gaddy, J. A.; Townsend, S. D., Human Milk Oligosaccharides Exhibit Antimicrobial and Antibiofilm Properties against Group B *Streptococcus*. *ACS Infect Dis* **2017**, 3 (8), 595-605.

35. Wright, G. D., Antibiotic Adjuvants: Rescuing Antibiotics from Resistance. *Trends in Microbiology* **2016**, 24 (11), 862-871.

36. Craft, K. M.; Gaddy, J. A.; Townsend, S. D., Human Milk Oligosaccharides (HMOs) Sensitize Group B *Streptococcus* to Clindamycin, Erythromycin, Gentamicin, and Minocycline on a Strain Specific Basis. *ACS Chem Biol* **2018**, 13 (8), 2020-2026.

37. Chambers, S. A.; Moore, R. E.; Craft, K. M.; Thomas, H. C.; Das, R.; Manning, S. D.; Codreanu, S. G.; Sherrod, S. D.; Aronoff, D. M.; McLean, J. A.;

- Gaddy, J. A.; Townsend, S. D., A Solution to Antifolate Resistance in Group B Streptococcus: Untargeted Metabolomics Identifies Human Milk Oligosaccharide-Induced Perturbations That Result in Potentiation of Trimethoprim. *mBio* **2020**, *11* (2), e00076-20.
38. Gleckman, R.; Blagg, N.; Joubert, D. W., Trimethoprim: mechanisms of action, antimicrobial activity, bacterial resistance, pharmacokinetics, adverse reactions, and therapeutic indications. *Pharmacotherapy* **1981**, *1* (1), 14-20.
39. Bermingham, A.; Derrick, J. P., The folic acid biosynthesis pathway in bacteria: evaluation of potential for antibacterial drug discovery. *BioEssays : news and reviews in molecular, cellular and developmental biology* **2002**, *24* (7), 637-48.
40. Dawadi, S.; Kordus, S. L.; Baughn, A. D.; Aldrich, C. C., Synthesis and Analysis of Bacterial Folate Metabolism Intermediates and Antifolates. *Organic Letters* **2017**, *19* (19), 5220-5223.
41. Bhosle, A.; Chandra, N., Structural analysis of dihydrofolate reductases enables rationalization of antifolate binding affinities and suggests repurposing possibilities. *The FEBS journal* **2016**, *283* (6), 1139-67.
42. Tjong, E.; Dimri, M.; Mohiuddin, S. S., Biochemistry, Tetrahydrofolate. In *StatPearls*, StatPearls Publishing Copyright © 2020, StatPearls Publishing LLC.: Treasure Island (FL), 2020.
43. Bergmann, R.; van der Linden, M.; Chhatwal, G. S.; Nitsche-Schmitz, D. P., Factors that cause trimethoprim resistance in Streptococcus pyogenes. *Antimicrob Agents Chemother* **2014**, *58* (4), 2281-8.
44. Bergmann, R.; Sagar, V.; Nitsche-Schmitz, D. P.; Chhatwal, G. S., first detection of trimethoprim resistance determinant dfrG in Streptococcus pyogenes clinical isolates in India. *Antimicrob Agents Chemother* **2012**, *56* (10), 5424-5.
45. Karpanoja, P.; Nyberg, S. T.; Bergman, M.; Voipio, T.; Paakkari, P.; Huovinen, P.; Sarkkinen, H.; Finnish Study Group for Antimicrobial, R., Connection between trimethoprim-sulfamethoxazole use and resistance in Streptococcus pneumoniae, Haemophilus influenzae, and Moraxella catarrhalis. *Antimicrob Agents Chemother* **2008**, *52* (7), 2480-5.
46. Dueger, E. L.; Asturias, E. J.; Matheu, J.; Gordillo, R.; Torres, O.; Halsey, N., Increasing penicillin and trimethoprim-sulfamethoxazole resistance in nasopharyngeal Streptococcus pneumoniae isolates from Guatemalan children, 2001--2006. *Int J Infect Dis* **2008**, *12* (3), 289-97.
47. Schmitz, F. J.; Perdikouli, M.; Beeck, A.; Verhoef, J.; Fluit, A. C.; European, S. p., Resistance to trimethoprim-sulfamethoxazole and modifications in genes coding for dihydrofolate reductase and dihydropteroate synthase in European Streptococcus pneumoniae isolates. *J Antimicrob Chemother* **2001**, *48* (6), 935-6.

48. Rudolph, K. M.; Parkinson, A. J.; Roberts, M. C., Mechanisms of erythromycin and trimethoprim resistance in the Alaskan *Streptococcus pneumoniae* serotype 6B clone. *J Antimicrob Chemother* **2001**, *48* (2), 317-9.
49. Lovgren, M.; Dell'Acqua, L.; Palacio, R.; Echaniz-Aviles, G.; Soto-Nogueron, A.; Castaneda, E.; Agudelo, C. I.; Heitmann, I.; Brandileone, M. C.; Zanella, R. C.; Rossi, A.; Pace, J.; Talbot, J. A., Determination of trimethoprim-sulfamethoxazole resistance in *Streptococcus pneumoniae* by using the E test with Mueller-Hinton agar supplemented with sheep or horse blood may be unreliable. The Pneumococcal Study Group. *J Clin Microbiol* **1999**, *37* (1), 215-7.
50. Huovinen, P., Trimethoprim resistance. *Antimicrob Agents Chemother* **1987**, *31* (10), 1451.
51. Bergmann, R.; van der Linden, M.; Chhatwal, G. S.; Nitsche-Schmitz, D. P., Factors That Cause Trimethoprim Resistance in *Streptococcus pyogenes*. *Antimicrob Agents Chemother* **2014**, *58* (4), 2281-2288.
52. Humphries, R. M.; Ambler, J.; Mitchell, S. L.; Castanheira, M.; Dingle, T.; Hindler, J. A.; Koeth, L.; Sei, K.; Development, C. M.; Standardization Working Group of the Subcommittee on Antimicrobial Susceptibility, T., CLSI Methods Development and Standardization Working Group Best Practices for Evaluation of Antimicrobial Susceptibility Tests. *Journal of clinical microbiology* **2018**, *56* (4), e01934-17.
53. Castor, M. L.; Whitney, C. G.; Como-Sabetti, K.; Facklam, R. R.; Ferrieri, P.; Bartkus, J. M.; Juni, B. A.; Cieslak, P. R.; Farley, M. M.; Dumas, N. B.; Schrag, S. J.; Lynfield, R., Antibiotic resistance patterns in invasive group B streptococcal isolates. *Infect Dis Obstet Gynecol* **2008**, *2008*, 727505-727505.
54. Hall, M. J.; Middleton, R. F.; Westmacott, D., The fractional inhibitory concentration (FIC) index as a measure of synergy. *Journal of Antimicrobial Chemotherapy* **1983**, *11* (5), 427-433.
55. Di Palo, B.; Rippha, V.; Santi, I.; Brettoni, C.; Muzzi, A.; Metruccio, M. M. E.; Grifantini, R.; Telford, J. L.; Paccani, S. R.; Soriani, M., Adaptive Response of Group B *Streptococcus* to High Glucose Conditions: New Insights on the CovRS Regulation Network. *PLOS ONE* **2013**, *8* (4), e61294.
56. Lamy, M. C.; Zouine, M.; Fert, J.; Vergassola, M.; Couve, E.; Pellegrini, E.; Glaser, P.; Kunst, F.; Msadek, T.; Trieu-Cuot, P.; Poyart, C., CovS/CovR of group B streptococcus: a two-component global regulatory system involved in virulence. *Molecular microbiology* **2004**, *54* (5), 1250-68.
57. Martin, J. K.; Sheehan, J. P.; Bratton, B. P.; Moore, G. M.; Mateus, A.; Li, S. H.-J.; Kim, H.; Rabinowitz, J. D.; Typas, A.; Savitski, M. M.; Wilson, M. Z.; Gitai, Z., A Dual-Mechanism Antibiotic Kills Gram-Negative Bacteria and Avoids Drug Resistance. *Cell* **2020**, *181* (7), 1518-1532.e14.

Chapter 4

Metabolomic interrogation of HMO-mediated antibacterial activity in group B

Streptococcus

4.1 Abstract

HMOs have significant antibacterial activity against GBS, but the cellular response to treatment with HMOs has not been previously characterized. Untargeted metabolomic analyses can provide information about antibiotic-induced changes to cellular metabolism. This chapter will detail our use of metabolomic analysis to investigate the HMO mechanism of action in GBS. We determine that upon HMO treatment, GBS lipid metabolism is most significantly impacted, with smaller changes also observed in purine and pyrimidine metabolism. These results demonstrate HMOs perturb lipid biosynthesis and organization within GBS, ultimately leading to growth inhibition.¹

4.2 Bacterial metabolism: an overview

Metabolism is broadly defined as the chemical reactions that occur within an organism to sustain life. Metabolism is responsible for converting nutrients into useable cellular energy and synthesizing molecules necessary for maintaining cell integrity and function. This includes the biosynthesis of lipids, proteins, and fatty acids. Subdivided under metabolism, catabolism is responsible for the breakdown of external molecules into useable biosynthetic building blocks, whereas anabolism is responsible for the buildup of molecules from acquired building blocks. Taken together, catabolism and anabolism perform the chemical reactions ultimately responsible for cellular survival.

Bacterial metabolism relies on sensing and responding to the surrounding environment and nutritional availability.² To sense such molecules, bacteria frequently harness two-component signal transduction systems (TCSs) (see section 1.6.3). Of critical importance to bacterial metabolism are pathways involved in carbohydrate acquisition, amino acid biosynthesis, lipid/fatty acid metabolism, and nucleotide biosynthesis.^{3, 4} Carbohydrate acquisition and metabolism acts as a vital carbon source for bacteria and contributes to the biosynthesis of short chain fatty acids (see section 3.3.1). Lipid and fatty acid metabolism are required for the formation of structural membranes, and amino acid biosynthesis is necessary for the formation of new proteins. Purine and pyrimidine metabolism are other essential pathways that generate nucleotides for DNA synthesis. These essential pathways and specific metabolites within will be detailed in further sections (see section 4.4), but their ubiquity across bacterial pathogens makes these metabolic pathways of prime interest for study.

4.3 Metabolomic analyses as methods for determining antibiotic mechanism of action

The well-studied metabolic pathways within bacterial cells makes metabolite-guided studies a robust tool in analyzing changes to bacteria and bacterial environments.^{5, 6} Global metabolomic profiling can be used to study bacterial survival in low-nutrient settings and the cellular effects of antibiotic treatments. Since clinically-used antibiotics affect known cellular targets and facilitate downstream changes to metabolic activity, metabolomic analyses have also been used to identify the mechanism of action of novel antibiotics.⁵⁻¹¹ One such example was the use of untargeted metabolomics in identifying the mechanism of action of the novel antibiotic pretomanid (**Figure 4.1**).⁹ Metabolomic

analysis revealed pretomanid treatment in *Mycobacterium smegmatis* caused metabolite accumulations within the pentose phosphate pathway (PPP). These accumulations increased downstream synthesis of methylglyoxal, to the point that overabundance of methylglyoxal became inhibitory to *M. smegmatis* growth. This study and others like it, demonstrate the powerful use of metabolomics to showcase cellular changes that occur upon antibiotic treatment.

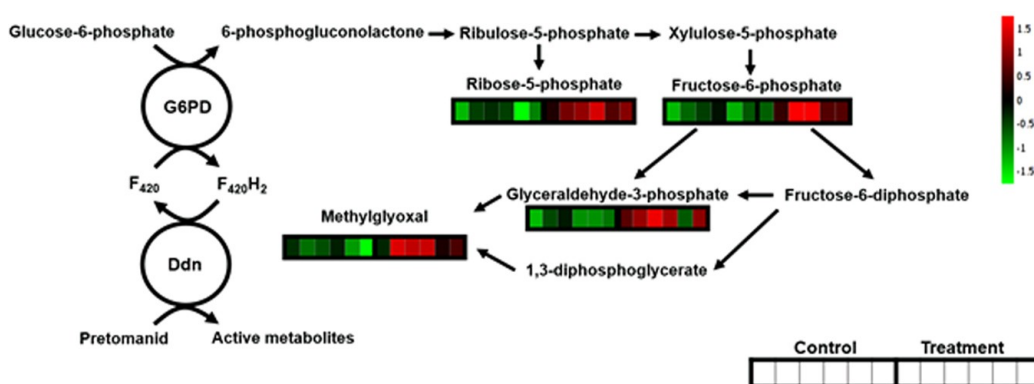


Figure 4.1 Accumulations of pentose phosphate pathway metabolites caused by pretomanid.⁹ The associated heatmap schematically depicts the relative concentration of each metabolite in six replicates of untreated controls and t = 6 h pretomanid-treated *Mycobacterium smegmatis* liquid cultures. Abbreviations: glucose-6-phosphate dehydrogenase (G6PD), deazaflavin dependent nitroreductase (Ddn).

4.4 Metabolomic analysis of HMO-induced perturbations in GBS: experimental design and rational

Our previous work using phenotypic microbial assays, demonstrated HMOs to be potent antibacterial agents against GBS and powerful tools to combat antifolate resistance (see **Chapter 3**). Nevertheless, little was understood about the precise mechanism of action of HMOs or the molecular changes HMOs caused within GBS. We proposed the use of

untargeted metabolomics to identify what metabolic pathways might be significantly affected by HMO treatment and to provide support for a potential mechanism of action. For our study, we partnered with the Vanderbilt Center for Innovative Technology (CIT) to observe and characterize the metabolomic profiles of two GBS populations: the first an untreated GBS control sample, the second a GBS sample treated with 1 mg mL⁻¹ HMOs (resulting in approx. 30% growth inhibition).¹² This HMO concentration was chosen to verify antibacterial activity, but still permit bacterial growth and metabolite isolation. The samples were grown in Todd-Hewitt broth (THB) which is traditionally used in the culture of GBS. This broth is highly supplemented and includes beef heart infusion, peptone, and glucose. The GBS strain GB2 was used for this study, as it was the most susceptible GBS strain to HMOs tested to-date (see **Table 3.2**).

Procedurally, metabolite isolates from both the untreated and HMO-treated cell cultures were subjected to either reverse-phase liquid chromatography (RPLC) or hydrophilic interaction liquid chromatography (HILIC). These LC purification methods were then followed by tandem mass spectrometry (MS/MS) and mass fragmentation analyses. From these data, individual mass spectra and fragmentation patterns were compared to known metabolite data bases to putatively identify metabolites and their relative abundance within samples.¹³⁻¹⁷ The identified metabolites and relative abundances for each sample type were then compared against one another, that is untreated GBS vs HMO-treated GBS. Upon analysis for statistically significant perturbations, the net metabolite profiles showed distinct differences between the HMO-treated and untreated GBS samples (**Figure 4.2A**). This indicated that there were global changes to the nature of GBS metabolism upon HMO-treatment. In total, approximately 900 metabolites were putatively

identified and saw statistically significant fold change (FC, $FC \geq |2|$) with a significant p-value ($p \leq 0.05$) (**Figure 4.2A/B**).

A.

Method	Pairwise Comparison		Total # of Compounds Observed CV<25%	Total # of Significant Compounds $p \leq 0.05$ and $FC \geq 2 $
	Untreated	Treated		
RPLCp	Untreated	Treated	3830	294
HILICp	Untreated	Treated	2866	599

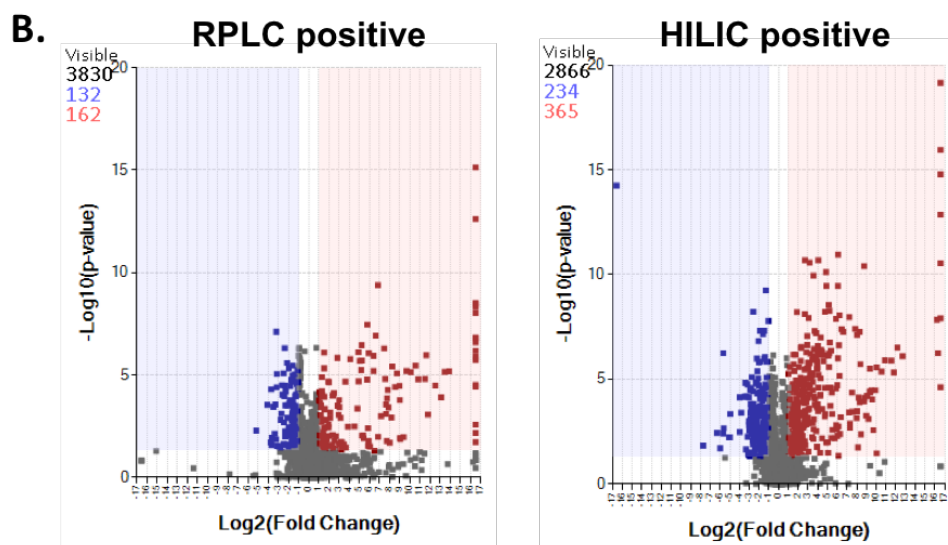


Figure 4.2 Pairwise comparisons of experimental conditions and significantly perturbed metabolites. (**A.**) Quantity of significant metabolites per LC purification method. (**B.**) Volcano plots of significantly perturbed metabolites per LC purification method.

4.5 GBS metabolic pathways perturbed upon HMO treatment

4.5.1 Global metabolic pathway analysis

With the identification of approximately 900 statistically significant metabolites, the putatively identified hits were then categorized according to their metabolic pathway of involvement. This gave a global pathway analysis of HMO-perturbations in GBS, from

which, we were able to determine which metabolic pathways had been most significantly perturbed. This analysis revealed the most statistically impacted pathways were those of linoleic acid metabolism, sphingolipid metabolism, and glycerophospholipid metabolism (**Table 4.1**). There were also significant effects observed in pyrimidine metabolism. Mapping these impacted pathways identified strong effects to GBS lipid metabolites and prompted us to look closer at the observed trends within these metabolic shifts.

Table 4.1. Pathway analysis of perturbed GBS metabolites

Metabolic Pathway	Hits / Total Metabolites	Raw p-value	Impact Factor
linoleic acid metabolism	6/15	2.05E-05	0.229
sphingolipid metabolism	6/25	5.81E-05	0.215
glycerophospholipid metabolism	4/39	1.33E-03	0.2403
pyrimidine metabolism	8/60	4.36E-03	0.238
pantothenate and CoA biosynthesis	3/27	0.116	0.135
lysine degradation	4/47	0.142	0.103
purine metabolism	6/92	0.204	0.062
cysteine and methionine metabolism	4/56	0.221	0.187

4.5.2 HMO-mediated perturbations to linoleic acid metabolites

4.5.2.1 Introduction: bacterial fatty acid synthesis and utilization of linoleic acid

Linoleic acid (LNA, **4.1**) is a polyunsaturated fatty acid most commonly biosynthesized by plants, but necessary for mammals.¹⁸⁻²⁰ Humans consume LNA in their diet, from which LNA is readily converted to a variety of other unsaturated fatty acids via enzymatic

oxidations and alkene isomerizations. These fatty acids and related metabolites are required in numerous biological processes, particularly the maintenance of cardiac cells and heart health. While the mammalian necessity for LNA is well understood, less is known about LNAs role in bacterial metabolism.

Bacterial fatty acids are necessary for the maintenance of cell membranes and for bacterial interactions with the host-immune response. Bacterial fatty acids are biosynthesized by the fatty acid synthase type II (FAS-II) system.²¹⁻²³ FAS-II within *Streptococcus* is regulated by the *fab* genes, where *fabA* is a critical dehydratase/isomerase enzyme for the formation of unsaturated fatty acids and *fabB* is an essential elongation enzyme.^{24, 25} In GBS, FAS-II has been shown to make both saturated and unsaturated fatty acids, including palmitic, palmitoleic, stearic, and octadecenoic acids.^{26, 27} GBS does not directly biosynthesize LNA. Nevertheless, it has been shown that GBS can uptake LNA for recruitment in anabolism of essential lipids. This was demonstrated by Brinster and coworkers, who showed that in the presence of exogenous LNA, GBS incorporates LNA into cell membrane structure, whereby approximately 20% of the total fatty acid composition is LNA-derived.²⁷ This indicates that GBS has acquired the ability to utilize exogenous fatty acids in lipid biosynthesis (see **Scheme 4.1**) and LNA is one such substrate.

4.5.2.2 Impact of HMOs on linoleic acid metabolites

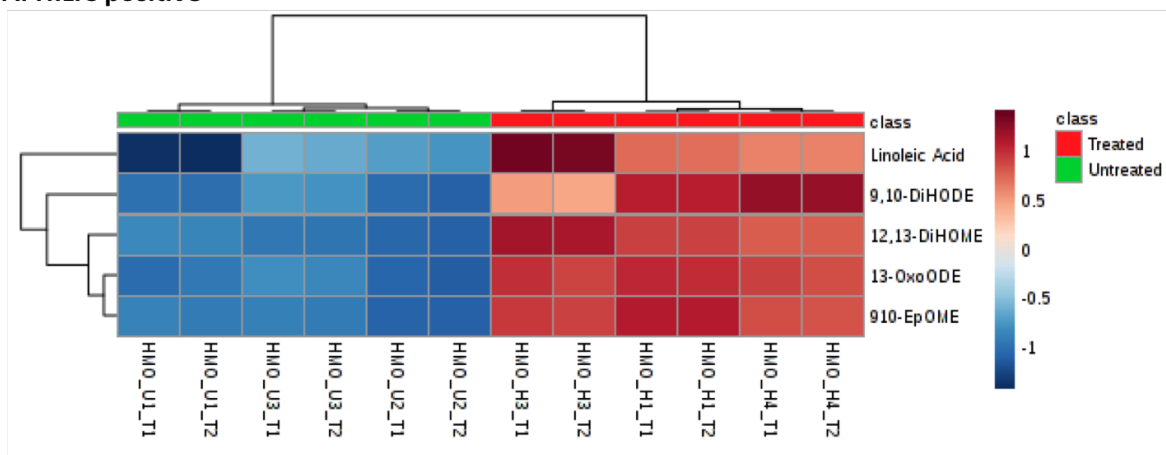
Through metabolomic analysis, we identified that HMOs impact linoleic acid metabolites significantly in GBS. As discussed, GBS does not biosynthesize LNA directly, so rather than correlating to a direct bacterial pathway, this result likely indicates a significant

change to how HMO-treated GBS cells uptake LNA. The presence of LNA metabolites is due to the beef heart tissues in Todd-Hewitt broth (THB) which was used for sample preparation.

At the specific metabolite level, every identified LNA metabolite was higher in abundance in the HMO-treated GBS sample relative to the untreated control (**Figures 4.3-4.4**). LNA (**4.1**) was identified with a FC > 9 ($p = 0.012$), indicating significant uptake from culture media. Additionally, several oxidized variants of polyunsaturated fatty acids were observed. These included 9,10-DiHODE (**4.2**, FC > 5, $p = 0.003$), 12(13)-EpOME (**4.3**, FC > 10, $p = 0.014$), and 9-OxoODE (**4.6**, FC > 10, $p = 0.003$). This increased abundance of oxidized LNA metabolites is most likely from similar GBS recruitment of exogenous fatty acids from growth media. Of note, the accumulation of epoxyoctadecanoic acids (EpOMEs) and dihydroxyoctadecanoic acids (DiHOMEs) has also been previously linked to changes in Na⁺ and K⁺ ion channels and downstream effects on cell membrane fluidity.¹⁸

Globally, the accumulation of these LNA associated metabolites suggests that HMO-treatment elicits defects within native GBS lipid biosynthesis. Resultantly, it can be postulated that GBS attempts to treat these defects by increased recruitment and catabolism of exogenous fatty acids. This metabolic shift might be an attempt to recruit exogenous fatty acids into the cellular membrane, which could also affect membrane integrity and lead to the resultant antibacterial activity of HMOs.

A. HILIC positive



B. RPLC positive

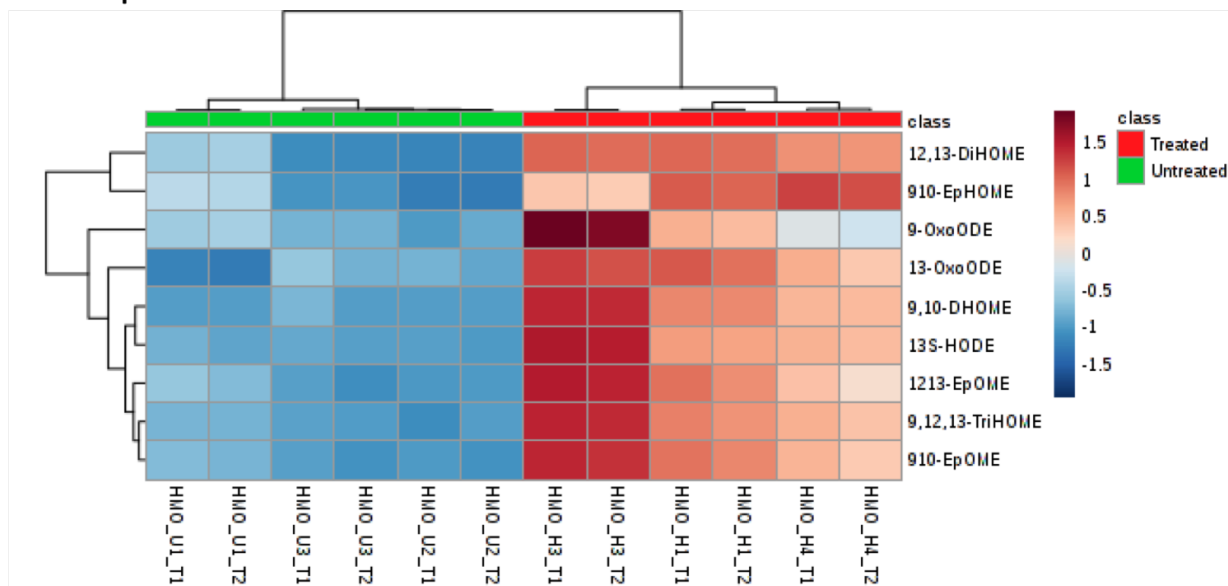


Figure 4.3 Heat-map representation of linoleic acid metabolites. **(A.)** HILIC positive LC-MS/MS analysis. **(B.)** RPLC positive LC-MS/MS analysis. Samples (columns) and features (rows) were processed using Euclidean Average clustering via Metaboanalyst 4.0. The heat map was generated for Pareto scaled, log transformed data, and colors are displayed by relative abundance, ranging from low (blue) to high (red) as shown in the legend. See **Table A4.2** for further details.

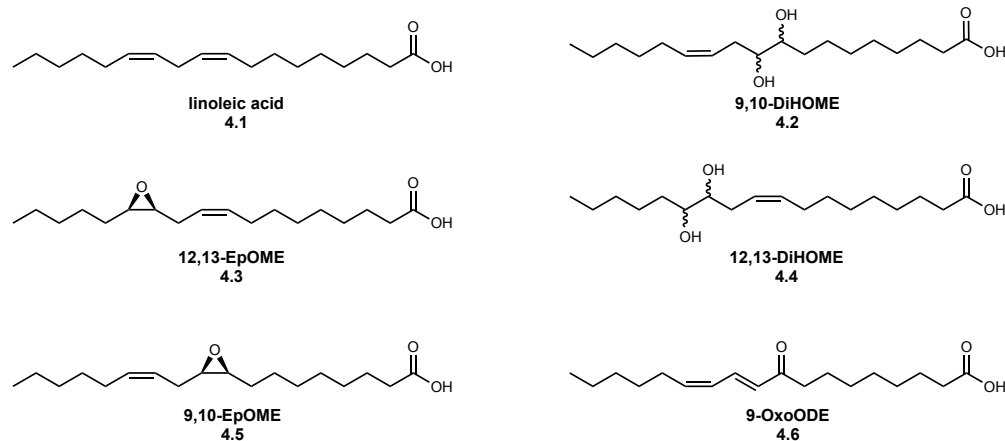


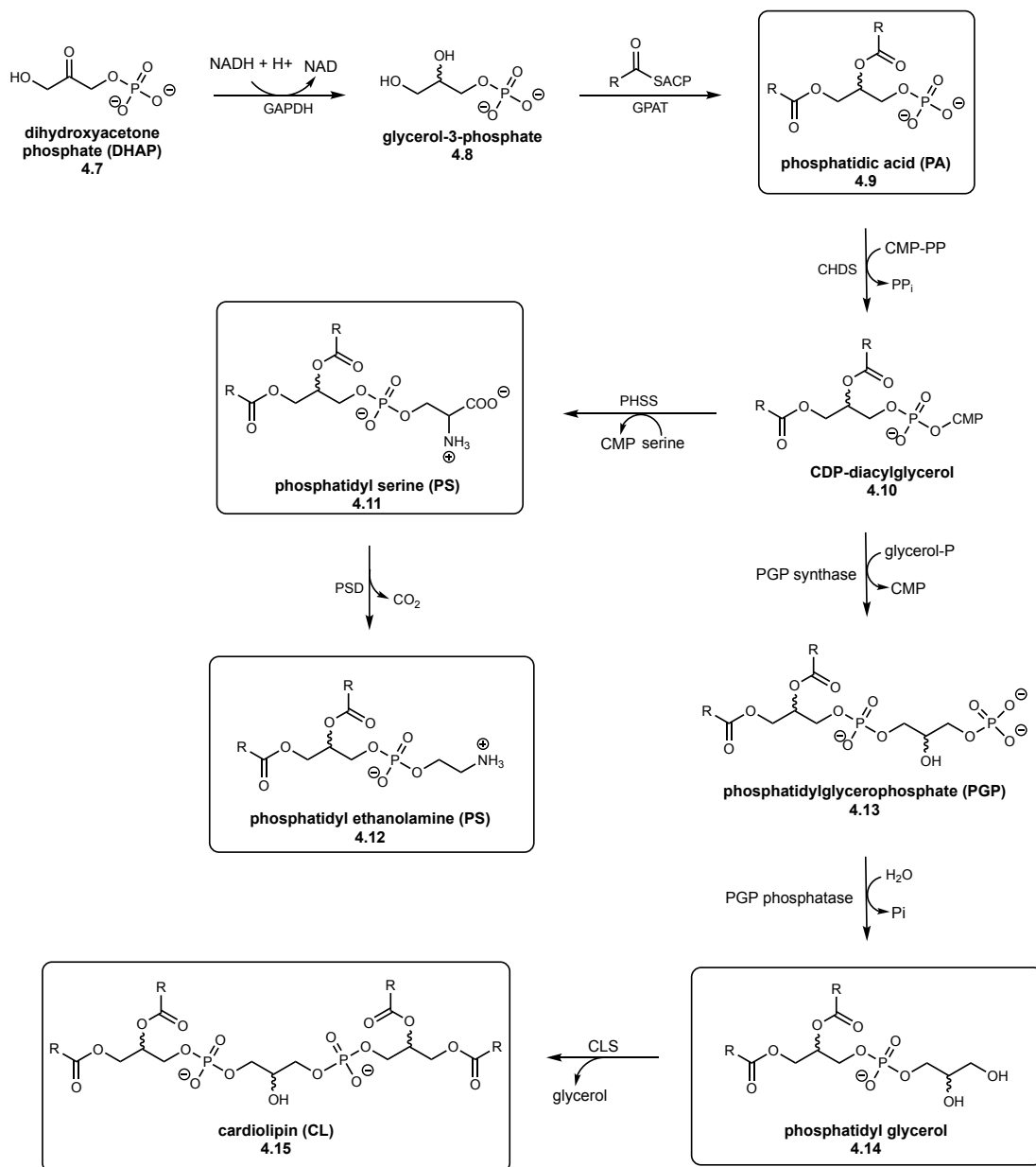
Figure 4.4 Representative structures of relevant LNA metabolites

4.5.3 HMO-induced perturbations to GBS glycerophospholipid metabolism

4.5.3.1 Introduction: bacterial glycerophospholipid metabolism

Fatty acids are essential for the cell membrane, since they act as metabolic precursors to the glycerophospholipids that ultimately form the intact membrane.²⁸⁻³⁰ Glycerophospholipids contain a negatively charged hydrophilic phosphonate group attached to a hydrophobic fatty acid chain. These polarity differences impart amphiphilic character that creates a cohesive membrane to protect cells from external degradation. Metabolically, glycerophospholipid biosynthesis first begins with the formation of phosphoglycerides (**Scheme 4.1**). Bacterial phosphoglycerides include phosphatidic acid (PA, **4.9**), phosphatidyl serine (PS, **4.11**), phosphatidyl ethanolamine (PE, **4.12**), phosphatidyl glycerol (**4.14**), and cardiolipin (CL, **4.15**) subclasses. Initial reduction of dihydroxyacetone phosphate (DHAP, **4.7**) yields **4.8** which acts as the critical substrate for fatty acid conjugation. From **4.8**, glycerol phosphate acyltransferase (GPAT) installs two fatty acid chains to generate the phosphatidic acid scaffold **4.9**. Of note, the fatty acid side chains can be either endogenous or exogenously derived, and the two sidechains

can be identical or mismatched. From **4.9**, conjugation of serine yields phosphatidyl serine variants (**4.11**) and subsequent decarboxylation gives phosphatidyl ethanolamine phosphoglycerides (**4.12**).



Scheme 4.1 Biosynthesis of phosphoglycerides. Abbreviations: dihydroxyacetone phosphate (DHAP), glycerol phosphate dehydrogenase (GAPDH), glycerol phosphate acyltransferase (GPAT), phosphatidic acid (PA), CDP-diglyceride synthase (CHDS), phosphatidylserine synthase (PHSS), phosphatidyl serine (PS), phosphatidylserine decarboxylase (PSD), phosphatidyl ethanolamine (PE), phosphatidylglycerolphosphate (PGP), cardiolipin synthase (CLS), cardiolipin (CL).

Alternatively, from **4.9** conjugation of glycerol yields phosphatidyl glycerol variants (**4.14**). **4.14** can then be catalyzed by cardiolipin synthase (CLS), to generate cardiolipin phosphoglycerides (**4.15**). Through the combination of bacterial phosphoglycerides and endogenous and exogenous fatty acids, bacteria synthesize a plethora of glycerophospholipids. From these, cells utilize complex machinery to assemble the cell membrane, through mechanisms that are still not well defined.³¹

4.5.3.2 Impact of HMOs on GBS glycerophospholipid metabolism

Our metabolomic study showed that HMO-treatment significantly affects GBS metabolism of glycerophospholipids (**Figures 4.5-4.6**). Overall, the metabolites identified were more abundant within the HMO-treated sample, similar to the accumulation seen in LNA metabolites (see section 4.5.2.2). Several metabolites associated with phosphoglyceride head groups were observed such as choline (**4.16**, FC > 1, p = 0.010), dihydroxyacetone phosphate (DHAP, **4.7**) (FC > 1, p = 0.181), and diethanolamine (**4.17**, FC > 2, p = 0.0003). Notably, DHAP (**4.7**) is the molecule of origin for glycerophospholipid anabolism. Further glycerophospholipid metabolites were identified with single intact fatty acid side chains, such as PE(O-18:1(9Z)/0:0) (**4.18**, FC > 50, p = 0.006), PE(P-16:0e/0:0) (**4.19**, FC > 27, p = 0.0005), and LysoPC(14:0/0:0) (**4.20**, FC > 16, p = 0.015). We hypothesize that the accumulation of these metabolites is from HMO-mediated stunting of glycerophospholipid anabolism. Altering reactions within this pathway might lead to increased quantity of metabolic intermediates. Uniquely, glycerophospholipid PE(19:1(9Z)/12:0) (**4.21**, FC > 2, p = 0.020) was identified as one of the few metabolites with lower relative abundance in the HMO-treated sample and further investigation might

identify reasons behind this unique metabolite profile. Globally, the identified glycerophospholipid metabolites indicate a conserved accumulation within the HMO-treated GBS sample and further support the hypothesis of HMO-mediated inhibition of native lipid biosynthesis.

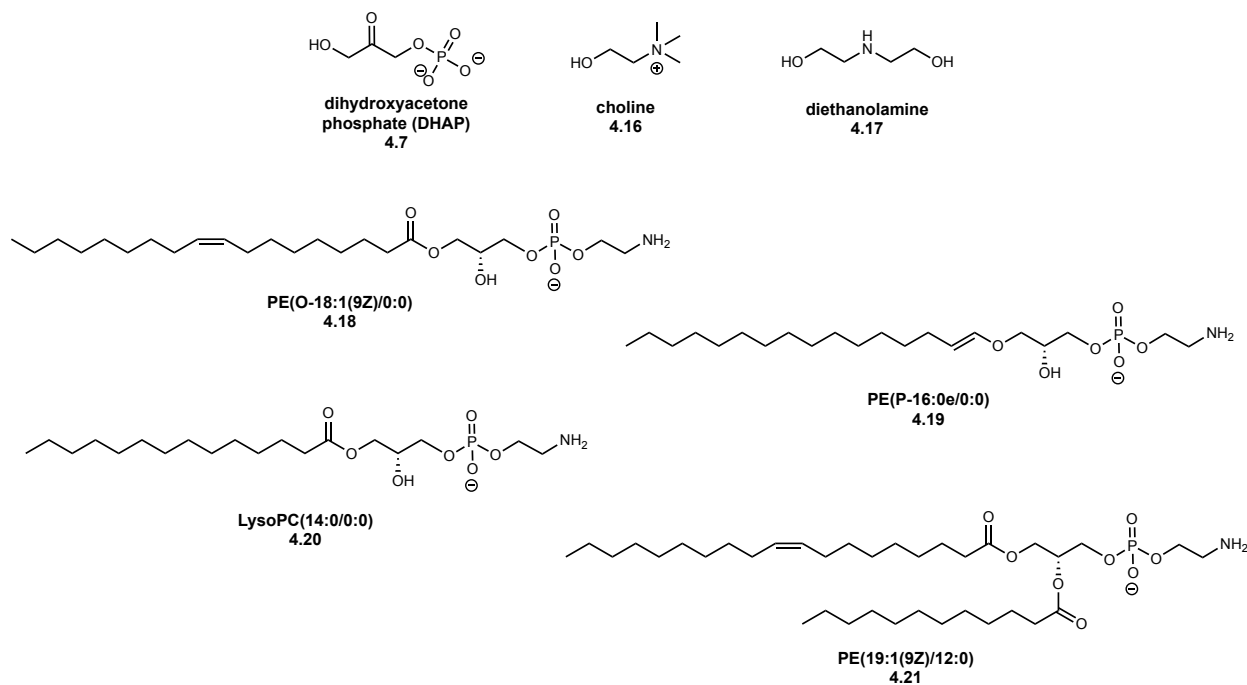
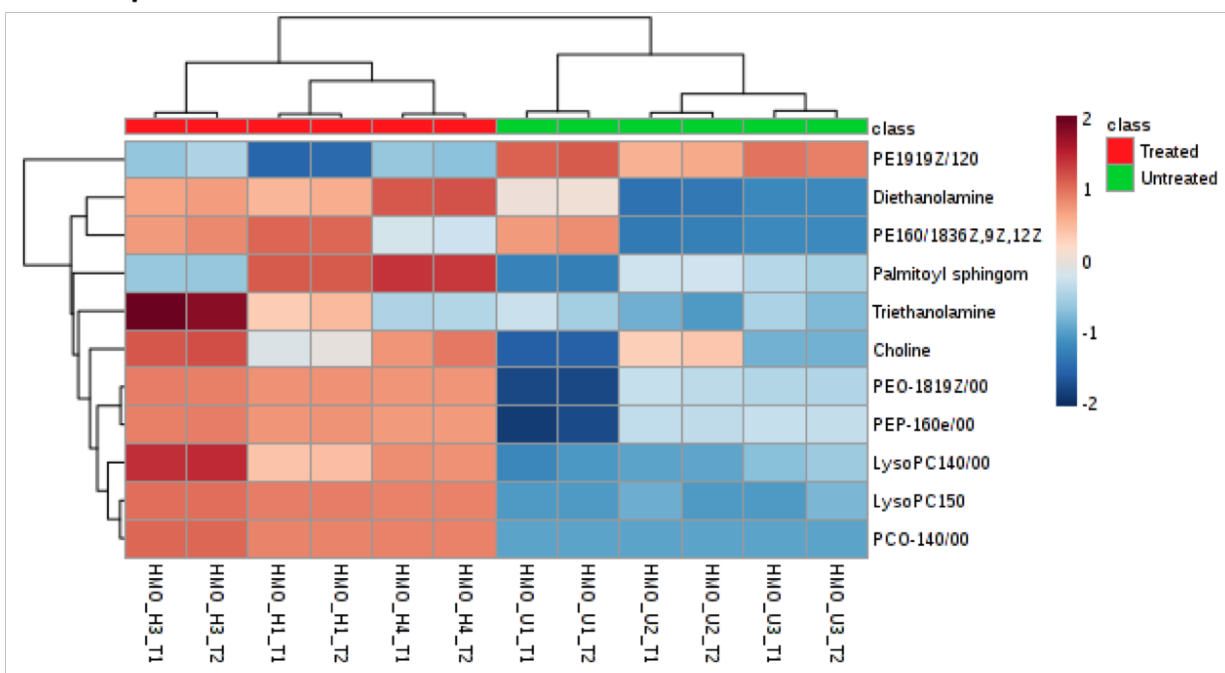


Figure 4.5 Representative structures of relevant glycerophospholipid metabolites

A. HILIC positive



B. RPLC positive

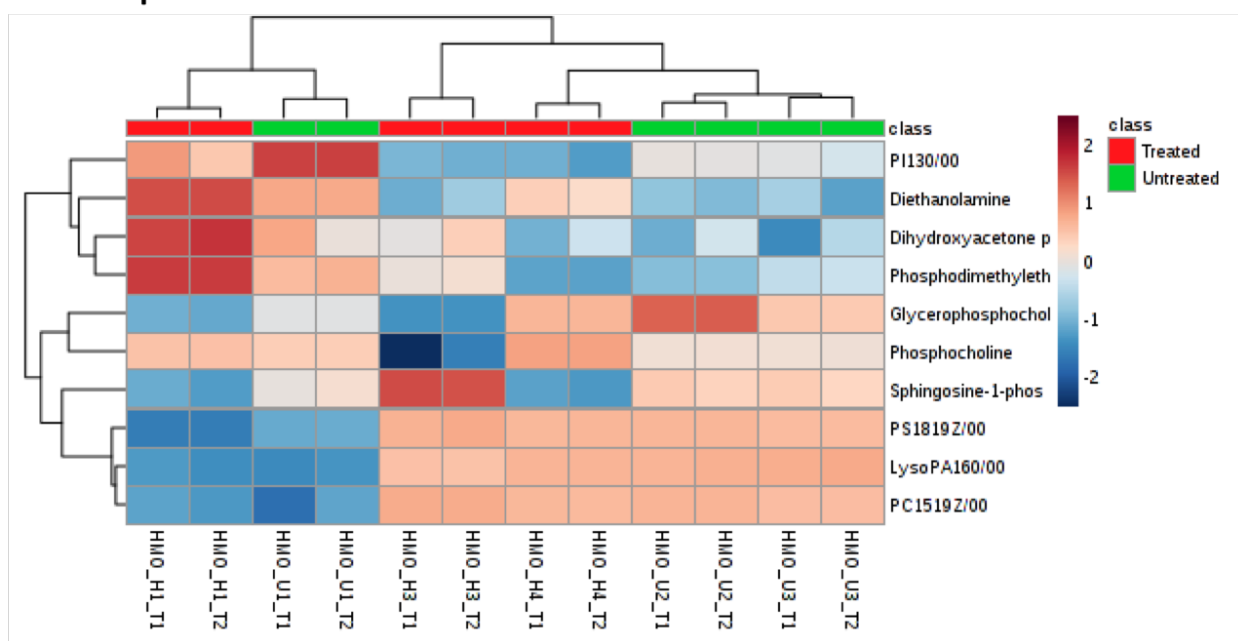


Figure 4.6 Heat map representation of glycerophospholipid metabolites. **(A.)** HILIC positive LC-MS/MS analysis. **(B.)** RPLC positive LC-MS/MS analysis. Samples (columns) and features (rows) were processed using Euclidean Average clustering via Metaboanalyst 4.0. The heat map was generated for Pareto scaled, log transformed data, and colors are displayed by relative abundance, ranging from low (blue) to high (red) as shown in the legend. See **Table A4.3** for further details.

4.5.4 Other HMO-induced changes to GBS metabolism

Our metabolomics study also identified significant changes to other metabolic pathways. In addition to the lipid metabolites discussed earlier, sphingolipid metabolism was also significantly affected by HMO treatment. Sphingolipids are biosynthesized by mammalian cells and, similar to LNA, are present within the growth media.^{32, 33} As in the case of LNA, GBS accumulates sphingolipids in response to HMO-treatment and these results further support the hypothesis that HMOs affect lipid biosynthesis and cell membrane assembly. Taken together, these impacts on exogenous fatty acid recruitment suggest that HMO treatment could also significantly impact GBS interactions with host-derived cells and metabolites.

Since our current results suggest HMOs increase GBS cell permeability, we also investigated if cell wall-affiliated metabolites were impacted by HMO treatment.¹¹ From our analysis, we were able to identify two cell wall-affiliated metabolites, both of which were higher in abundance within the HMO treated sample (**Figure 4.7**). These metabolites were UDP-MurNAc (FC > 19, p = 0.032) and UDP-GalNAc/GlcNAc (FC > 11, p = 0.175). Unfortunately, a higher experimental mass range would be needed to identify a more significant amount of these cell wall precursors and better identify a global trend.

HILIC positive

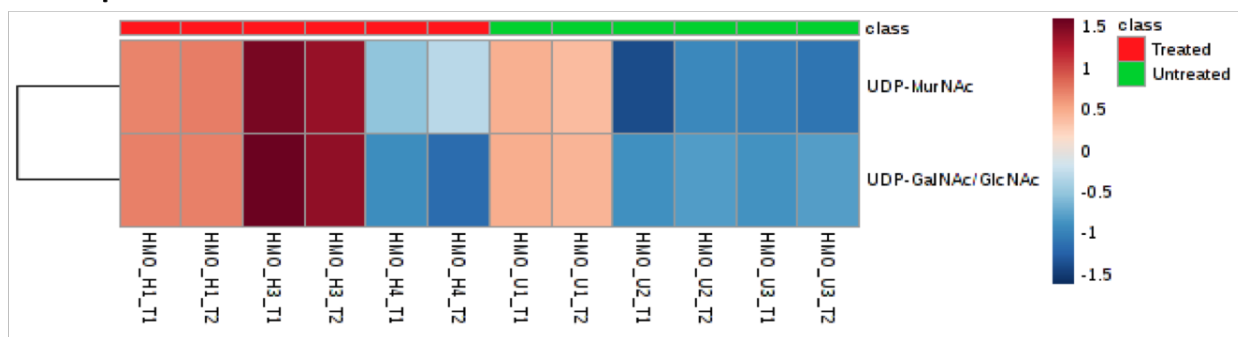


Figure 4.7 Heat map representation of cell wall metabolites from HILIC positive LC-MS/MS analysis. Samples (columns) and features (rows) were processed using Euclidean Average clustering via Metaboanalyst 4.0. The heat map was generated for Pareto scaled, log transformed data, and colors are displayed by relative abundance, ranging from low (blue) to high (red) as shown in the legend. See **Table A4.4** for further details.

4.6 Conclusion and future directions

The study conducted herein provided the first evaluation of the metabolic response of any cell type to HMO-mediated perturbations. From our metabolomics study, we were able to elucidate the metabolic impact HMOs have on GBS and identify significant changes to endogenous lipid metabolism and exogenous lipid recruitment. These effects indicate that HMOs significantly impact the catabolism and anabolism of essential cell membrane components, ultimately yielding an antibacterial effect.

Further analyses need to be conducted from our original experiments above, to better understand the global interactions of each impacted GBS metabolic pathway. Individual metabolites within glycerophospholipid metabolism should be mapped out and their relative abundances compared between the untreated and HMO-treated samples. This would provide a more detailed view of metabolite accumulation or depletion throughout the pathway and potentially identify specific metabolic reactions that are highly affected by HMOs. Since GBS tries to recruit exogenous fatty acids upon HMO treatment, we

anticipate HMOs directly impede endogenous fatty acid production and decrease activity in FAS-II. Changes within this production would necessitate increased use of exogenous fatty acids and induce changes to glycerophospholipid metabolism. Narrowing our analysis to the metabolite level will provide a more detailed understanding of which enzymatic reactions are being significantly impacted.

In addition to better investigating the single metabolite level, more work needs to be done to understand HMO effects on purine and pyrimidine biosynthesis and if these pathways also interact with lipid metabolism. While pyrimidine metabolism was the fourth-most affected GBS metabolic pathway, we did not fully analyze the metabolite identifications and fold changes that were observed. Analyzing this pathway further would demonstrate the changes to nucleotide biosynthesis that are observed upon HMO treatment. We hypothesize that HMOs do not directly inhibit purine and pyrimidine biosynthesis, but instead, as GBS struggles to make lipid metabolites in response to HMO treatment, significant downstream stress is placed on pyrimidine metabolism. Investigation into the nucleotide biosynthetic pathways and the perturbed metabolites within would better identify the interplay between various pathways in bacterial metabolism.

Most pertinent to future GBS metabolomic studies will be the experimental removal of exogenous fatty acids. This can be achieved by conducting similar metabolomic studies with GBS samples grown under minimal media conditions. Minimal media, or chemically-defined media, is culture media that contains only essential nutrients for bacterial growth, with known supplements of carbohydrate and amino acid sources if required. This change in growth media will eliminate the source of excess exogenous fatty acids from THB and disable GBS recruitment of such molecules. We anticipate that in the absence of these

exogenous LNA derivatives and sphingolipids, GBS growth will be inhibited more significantly by HMOs. Metabolically, this might result in even more pronounced changes to glycerophospholipid metabolism or other downstream pathways. Conducting such experiments in minimal growth media conditions would provide a better understanding of HMO-mediated effects on GBS without external fatty acid supplementation. This would better reveal the bacterial targets of HMOs and the corresponding antibiotic mechanism of action.

4.7 Experimental methods

Sample preparation for metabolomic analysis

Group B *Streptococcus* (*S. agalactiae* strain GB2, clinical isolate, Shannon Manning, Michigan State) was grown overnight as described above and used to inoculate 10 mL of fresh THB media to achieve 5×10^5 CFU mL⁻¹. Untreated GB2 in 10 mL of media served as a control, while other GB2 cultures were treated with HMOs at 1.00 mg mL⁻¹. After 24 hours, the samples were centrifuged at 1500 RPM for 20 min to generate a bacterial pellet. The media was removed and the pellet washed with 200 μ L of 50 mM ammonium formate buffer. The pellet was then resuspended in 200 μ L of 50 mM ammonium formate buffer and transferred to a sterile Eppendorf tube. This was then centrifuged at 1500 RPM for 10 min to generate a bacterial pellet. The buffer was removed and the pellet flash frozen in liquid N₂ and stored until use.

Bacterial cell pellets were lysed using 400 μ L ice cold lysis buffer (1:1:2, ACN:MeOH:ammonium bicarbonate 0.1M, pH 8.0, LC-MS grade) and vortexed. Individual samples were sonicated using a probe tip sonicator, 10 pulses at 30% power,

cooling down in ice between samples. A BCA protein assay was used to determine the protein concentration for each individual sample, and adjusted to a total amount of protein of 200µg total protein in 200 µL of lysis buffer. Isotopically labeled standard molecules, Phenylalanine-D8 (CDN Isotopes, Quebec, CA), and Biotin-D2 (CIL, MA, USA), were added to each sample to assess sample preparation reproducibility. Metabolites were extracted from untreated control and HMO treated cultures using protein precipitation by the addition of 800µL of ice-cold methanol (4x by volume) and incubated overnight at -80 °C. Following incubation, samples were centrifuged at 10,000 rpm for 10 min to eliminate precipitated proteins and the metabolite containing supernatant was dried in vacuo and stored at -80 °C until further UPLC-HRMS/MS analysis.

Global untargeted metabolomic analyses

Metabolite extracts were analyzed using reverse-phase liquid chromatography (RPLC) and hydrophilic interaction liquid chromatography (HILIC) followed by subsequent mass spectrometry analysis using a high-resolution Q-Exactive HF hybrid quadrupole-Orbitrap mass spectrometer (Thermo Fisher Scientific, Bremen, Germany) equipped with a Vanquish UHPLC binary system and autosampler (Thermo Fisher Scientific, Bremen, Germany). A quality control sample was prepared by pooling equal volumes of each sample. Isotopically labeled standards, Tryptophan-D3, Carnitine-D9 (CDN Isotopes, Quebec, CA), Valine-D8, and Inosine-4N15 (CIL, MA, USA), were added to each sample to assess MS instrument reproducibility.

Metabolite extracts (10 µL injection volume) were separated on a SeQuant ZIC-HILIC 3.5-µm, 2.1 mm × 100 mm column (Millipore Corporation, Darmstadt, Germany) held at 40 °C

for the HILIC analysis. Liquid chromatography was performed at $200 \mu\text{L min}^{-1}$ using solvent A (5mM ammonium formate in 90% water, 10% acetonitrile) and solvent B (5mM ammonium formate in 90% acetonitrile, 10% water) with the following gradient: 95% B for 2 min, 95-40% B over 16 min, 40% B held 2 min, and 40-95% B over 15 min, 95% B held 10 min (gradient length: 45 min). For the RPLC analysis metabolite extracts (10 μL injection volume) were separated on a Hypersil Gold, $1.9 \mu\text{m}$, $2.1\text{mm} \times 100 \text{mm}$ column (Thermo Fisher) held at $40 \text{ }^\circ\text{C}$. Liquid chromatography was performed at a $250 \mu\text{L min}^{-1}$ using solvent A (0.1% formic acid (FA) in water) and solvent B (0.1% FA in acetonitrile (ACN)) with the following gradient: 5% B for 1 min, 5-50% B over 9 min, 50-70% B over 5 min, 70-95% B over 5 min, 95% B held 2 min, and 95-5% B over 3 min, 5% B held 5 min (gradient length: 30 min).

MS analyses were acquired over a mass range of m/z 70-1050 using electrospray ionization positive mode. MS scans were analyzed at a resolution of 120000 with a scan rate of 3.5 Hz. The AGC target was set to 1×10^6 ions, and maximum ion IT was at 100 ms. Source ionization parameters were optimized, these include: spray voltage - 3.0 kV, transfer temperature - $280 \text{ }^\circ\text{C}$; S-lens - 40; heater temperature - $325 \text{ }^\circ\text{C}$; sheath gas - 40, aux gas - 10, and sweep gas flow - 1. Tandem spectra were acquired using a data dependent acquisition (DDA) in which one MS scan is followed by 2, 4 or 6 MS/MS scans. MS/MS scans are acquired using an isolation width of 1.3 m/z , stepped NCE of 20 and 40, and a dynamic exclusion for 6 s. MS/MS spectra were collected at a resolution of 15000, with an AGC target set at 2×10^5 ions, and maximum ion IT of 100 ms. Instrument performance and reproducibility in the run sequence was assessed by monitoring the retention times and peak areas for the heavy labeled standards added to the individual

samples prior to and during metabolite extraction to assess sample processing steps and instrument variability.

Metabolomics data processing

UPLC-HRMS/MS raw data were imported, processed, normalized and reviewed using Progenesis Q1 v.2.1 (Non-linear Dynamics, Newcastle, UK). All MS and MS/MS sample runs were aligned against a quality control (pooled) reference run, and peak picking was performed on individual aligned runs to create an aggregate data set. Following peak picking, unique spectral features (retention time and m/z pairs) were grouped based on adducts and isotopes, and individual features or metabolites were normalized to all features. Compounds with <25% coefficient of variance (%CV) were retained for further analysis. P-values were calculated by Progenesis Q1 using variance stabilized measurements achieved through log normalization, and metabolites with a $p < 0.05$ calculated by a one-way analysis of variance (ANOVA) test, and fold change (FC) $> |2|$ were considered significant.

Tentative and putative identifications were determined within Progenesis Q1 using accurate mass measurements (<5 ppm error), isotope distribution similarity, and fragmentation spectrum matching based on database searches against Human Metabolome Database (HMDB), Metlin, the National Institute of Standards and Technology (NIST) database and an in-house database.¹³⁻¹⁷ Annotations from both RPLC and HILIC analyses were performed for all significant compounds (p -value < 0.05 , FC $> |2|$). Annotations were further analyzed using pathway overrepresentation analysis using MetaboAnalyst 4.0.^{8, 34} The level system for metabolite identification confidence was

used. The level 3 (L3) of confidence for the metabolite identifications was assigned for those molecules that showed minimal experimental evidence than level 2 (L2), but do prioritize a top candidate. These are accepted by the metabolomics community and represent families of molecules that cannot be distinguished by the data acquired, predominantly because there are too many isomers as possible candidate metabolites.

4.8 References

1. This chapter is adapted from "A solution to antifolate resistance in group B Streptococcus: untargeted metabolomics identifies human milk oligosaccharide-induced perturbations that result in potentiation of trimethoprim" published in mBio and has been reproduced with the permission of the publisher and my co-authors including, Rebecca E. Moore, Kelly M. Craft, Steven D. Townsend, Jennifer A. Gaddy, Harrison C. Thomas, Rishub Das, Shannon D. Manning, Simona G. Codreanu, Stacy D. Sherrod, David M. Aronoff, and John A. McLean. Chambers SA, Moore RE, Craft KM, Thomas HC, Das R, Manning SD, Codreanu SG, Sherrod SD, Aronoff DM, McLean JA, Gaddy JA, Townsend SD. 2020. A solution to antifolate resistance in group B Streptococcus: untargeted metabolomics identifies human milk oligosaccharide-induced perturbations that result in potentiation of trimethoprim. mBio 11:e00076-20.
2. White, D.; Drummond, J.; Fuqua, C., *The physiology and biochemistry of prokaryotes*. Oxford University Press: New York, 2012.
3. Willenborg, J.; Goethe, R., Metabolic traits of pathogenic streptococci. *FEBS Letters* **2016**, *590* (21), 3905-3919.
4. Ferretti, J. J.; Stevens, D. L.; Fischetti, V. A., *Streptococcus pyogenes: Basic Biology to Clinical Manifestations*. University of Oklahoma Health Sciences Center © The University of Oklahoma Health Sciences Center.: Oklahoma City (OK), 2016.
5. Zampieri, M.; Szappanos, B.; Buchieri, M. V.; Trauner, A.; Piazza, I.; Picotti, P.; Gagneux, S.; Borrell, S.; Gicquel, B.; Lelievre, J.; Papp, B.; Sauer, U., High-throughput metabolomic analysis predicts mode of action of uncharacterized antimicrobial compounds. *Sci Transl Med* **2018**, *10* (429).
6. Vincent, I. M.; Ehmman, D. E.; Mills, S. D.; Perros, M.; Barrett, M. P., Untargeted Metabolomics To Ascertain Antibiotic Modes of Action. *Antimicrob Agents Chemother* **2016**, *60* (4), 2281-91.

7. Epand, R. M.; Walker, C.; Epand, R. F.; Magarvey, N. A., Molecular mechanisms of membrane targeting antibiotics. *Biochim Biophys Acta* **2016**, *1858* (5), 980-7.
8. Schrimpe-Rutledge, A. C.; Codreanu, S. G.; Sherrod, S. D.; McLean, J. A., Untargeted Metabolomics Strategies-Challenges and Emerging Directions. *J Am Soc Mass Spectrom* **2016**, *27* (12), 1897-1905.
9. Baptista, R.; Fazakerley, D. M.; Beckmann, M.; Baillie, L.; Mur, L. A. J., Untargeted metabolomics reveals a new mode of action of pretomanid (PA-824). *Sci Rep* **2018**, *8* (1), 5084.
10. Huang, J.; Li, S.; Li, L.; Wang, X.; Yao, Z.; Ye, X., Alarming regional differences in prevalence and antimicrobial susceptibility of group B streptococci in pregnant women: A systematic review and meta-analysis. *Journal of global antimicrobial resistance* **2016**, *7*, 169-177.
11. Dörries, K.; Schlueter, R.; Lalk, M., Impact of Antibiotics with Various Target Sites on the Metabolome of *Staphylococcus aureus*. *Antimicrob Agents Chemother* **2014**, *58* (12), 7151.
12. Chambers, S. A.; Moore, R. E.; Craft, K. M.; Thomas, H. C.; Das, R.; Manning, S. D.; Codreanu, S. G.; Sherrod, S. D.; Aronoff, D. M.; McLean, J. A.; Gaddy, J. A.; Townsend, S. D., A Solution to Antifolate Resistance in Group B *Streptococcus*: Untargeted Metabolomics Identifies Human Milk Oligosaccharide-Induced Perturbations That Result in Potentiation of Trimethoprim. *mBio* **2020**, *11* (2), e00076-20.
13. Wishart, D. S.; Tzur, D.; Knox, C.; Eisner, R.; Guo, A. C.; Young, N.; Cheng, D.; Jewell, K.; Arndt, D.; Sawhney, S.; Fung, C.; Nikolai, L.; Lewis, M.; Coutouly, M. A.; Forsythe, I.; Tang, P.; Shrivastava, S.; Jeroncic, K.; Stothard, P.; Amegbey, G.; Block, D.; Hau, D. D.; Wagner, J.; Miniaci, J.; Clements, M.; Gebremedhin, M.; Guo, N.; Zhang, Y.; Duggan, G. E.; Macinnis, G. D.; Weljie, A. M.; Dowlatabadi, R.; Bamforth, F.; Clive, D.; Greiner, R.; Li, L.; Marrie, T.; Sykes, B. D.; Vogel, H. J.; Querengesser, L., HMDB: the Human Metabolome Database. *Nucleic Acids Res* **2007**, *35* (Database issue), D521-6.
14. Wishart, D. S.; Knox, C.; Guo, A. C.; Eisner, R.; Young, N.; Gautam, B.; Hau, D. D.; Psychogios, N.; Dong, E.; Bouatra, S.; Mandal, R.; Sinelnikov, I.; Xia, J.; Jia, L.; Cruz, J. A.; Lim, E.; Sobsey, C. A.; Shrivastava, S.; Huang, P.; Liu, P.; Fang, L.; Peng, J.; Fradette, R.; Cheng, D.; Tzur, D.; Clements, M.; Lewis, A.; De Souza, A.; Zuniga, A.; Dawe, M.; Xiong, Y.; Clive, D.; Greiner, R.; Nazyrova, A.; Shaykhtudinov, R.; Li, L.; Vogel, H. J.; Forsythe, I., HMDB: a knowledgebase for the human metabolome. *Nucleic Acids Res* **2009**, *37* (Database issue), D603-10.
15. Wishart, D. S.; Jewison, T.; Guo, A. C.; Wilson, M.; Knox, C.; Liu, Y.; Djoumbou, Y.; Mandal, R.; Aziat, F.; Dong, E.; Bouatra, S.; Sinelnikov, I.; Arndt, D.; Xia, J.; Liu, P.; Yallou, F.; Bjorn Dahl, T.; Perez-Pineiro, R.; Eisner, R.; Allen, F.;

Neveu, V.; Greiner, R.; Scalbert, A., HMDB 3.0--The Human Metabolome Database in 2013. *Nucleic Acids Res* **2013**, *41* (Database issue), D801-7.

16. Wishart, D. S.; Feunang, Y. D.; Marcu, A.; Guo, A. C.; Liang, K.; Vazquez-Fresno, R.; Sajed, T.; Johnson, D.; Li, C.; Karu, N.; Sayeeda, Z.; Lo, E.; Assempour, N.; Berjanskii, M.; Singhal, S.; Arndt, D.; Liang, Y.; Badran, H.; Grant, J.; Serra-Cayuela, A.; Liu, Y.; Mandal, R.; Neveu, V.; Pon, A.; Knox, C.; Wilson, M.; Manach, C.; Scalbert, A., HMDB 4.0: the human metabolome database for 2018. *Nucleic Acids Res* **2018**, *46* (D1), D608-D617.

17. Smith, C. A.; O'Maille, G.; Want, E. J.; Qin, C.; Trauger, S. A.; Brandon, T. R.; Custodio, D. E.; Abagyan, R.; Siuzdak, G., METLIN: a metabolite mass spectral database. *Ther Drug Monit* **2005**, *27* (6), 747-51.

18. Ha, J.; Dobretsov, M.; Kurten, R. C.; Grant, D. F.; Stimers, J. R., Effect of Linoleic Acid Metabolites on Na⁺/K⁺ Pump Current in N20.1 Oligodendrocytes: Role of Membrane Fluidity. *Toxicology and Applied Pharmacology* **2002**, *182* (1), 76-83.

19. Devillard, E.; McIntosh, F. M.; Duncan, S. H.; Wallace, R. J., Metabolism of Linoleic Acid by Human Gut Bacteria: Different Routes for Biosynthesis of Conjugated Linoleic Acid. *J Bacteriol* **2007**, *189* (6), 2566.

20. Salsinha, A. S.; Pimentel, L. L.; Fontes, A. L.; Gomes, A. M.; Rodríguez-Alcalá, L. M., Microbial Production of Conjugated Linoleic Acid and Conjugated Linolenic Acid Relies on a Multienzymatic System. *Microbiology and Molecular Biology Reviews* **2018**, *82* (4), e00019-18.

21. Le Breton, Y.; Belew, A. T.; Valdes, K. M.; Islam, E.; Curry, P.; Tettelin, H.; Shirliff, M. E.; El-Sayed, N. M.; McIver, K. S., Essential Genes in the Core Genome of the Human Pathogen *Streptococcus pyogenes*. *Scientific Reports* **2015**, *5* (1), 9838.

22. Hooven, T. A.; Catomeris, A. J.; Akabas, L. H.; Randis, T. M.; Maskell, D. J.; Peters, S. E.; Ott, S.; Santana-Cruz, I.; Tallon, L. J.; Tettelin, H.; Ratner, A. J., The essential genome of *Streptococcus agalactiae*. *BMC Genomics* **2016**, *17*, 406-406.

23. Balemans, W.; Lounis, N.; Gilissen, R.; Guillemont, J.; Simmen, K.; Andries, K.; Koul, A., Essentiality of FASII pathway for *Staphylococcus aureus*. *Nature* **2010**, *463* (7279), E3-E3.

24. Lu, Y.-J.; Rock, C. O., Transcriptional regulation of fatty acid biosynthesis in *Streptococcus pneumoniae*. *Molecular microbiology* **2006**, *59* (2), 551-566.

25. Rock, C. O.; Jackowski, S., Forty Years of Bacterial Fatty Acid Synthesis. *Biochemical and Biophysical Research Communications* **2002**, *292* (5), 1155-1166.

26. Parsons, J. B.; Frank, M. W.; Subramanian, C.; Saenkham, P.; Rock, C. O., Metabolic basis for the differential susceptibility of Gram-positive pathogens to fatty acid

synthesis inhibitors. *Proceedings of the National Academy of Sciences* **2011**, 108 (37), 15378.

27. Brinster, S.; Lamberet, G.; Staels, B.; Trieu-Cuot, P.; Gruss, A.; Poyart, C., Type II fatty acid synthesis is not a suitable antibiotic target for Gram-positive pathogens. *Nature* **2009**, 458 (7234), 83-86.

28. Tocher, D. R., Chapter 6 Glycerophospholipid metabolism. In *Biochemistry and Molecular Biology of Fishes*, Hochachka, P. W.; Mommsen, T. P., Eds. Elsevier: 1995; Vol. 4, pp 119-157.

29. Dalebroux, Z. D., Cues from the Membrane: Bacterial Glycerophospholipids. *J Bacteriol* **2017**, 199 (13), e00136-17.

30. Zhang, Y.-M.; Rock, C. O., Thematic review series: Glycerolipids. Acyltransferases in bacterial glycerophospholipid synthesis. *J Lipid Res* **2008**, 49 (9), 1867-1874.

31. Silhavy, T. J.; Kahne, D.; Walker, S., The bacterial cell envelope. *Cold Spring Harb Perspect Biol* **2010**, 2 (5), a000414-a000414.

32. Heung, L. J.; Luberto, C.; Del Poeta, M., Role of Sphingolipids in Microbial Pathogenesis. *Infection and Immunity* **2006**, 74 (1), 28.

33. Heaver, S. L.; Johnson, E. L.; Ley, R. E., Sphingolipids in host-microbial interactions. *Current Opinion in Microbiology* **2018**, 43, 92-99.

34. Xia, J.; Wishart, D. S., Using MetaboAnalyst 3.0 for Comprehensive Metabolomics Data Analysis. *Curr Protoc Bioinformatics* **2016**, 55, 14 10 1-14 10 91.

Appendix A4

Supplementary metabolomics figures relevant to Chapter 4

Table A4.1 Quality metrics obtained for the heavy labeled standard molecules used for this study to assess the metabolite extraction, instrument performance and injection volume reproducibility.

Measurement	QC Pool Sample Assessment	RPLC	HILIC
		% CV	% CV
Process Variability	Biotin – D2	1.16	0.88
	Phenylalanine-D8	1.58	1.59
Instrument Variability	Carnitine – D9	1.95	4.32
	Valine – D8	1.55	3.76
	Tryptophan-D3	1.80	2.92
	Inosine – 4N15	4.99	3.20

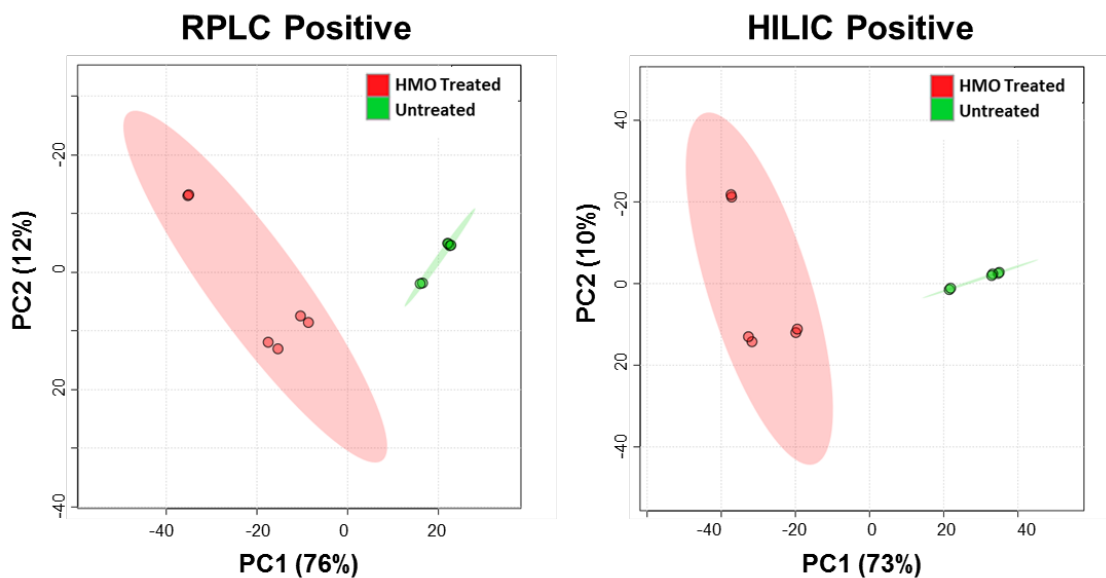


Figure A4.1 Global principal component analysis of the two different experimental sample groups, untreated vs HMO treated. Global principal component analysis of cellular extracted metabolites for the two biological conditions is illustrating a distinct shift in metabolic profiles between groups. Presenting the abundance data in PC space allows us to separate the run samples based on overall variability and shows clear separation of untreated samples vs HMO treated samples across the first PC dimension (x-axis).

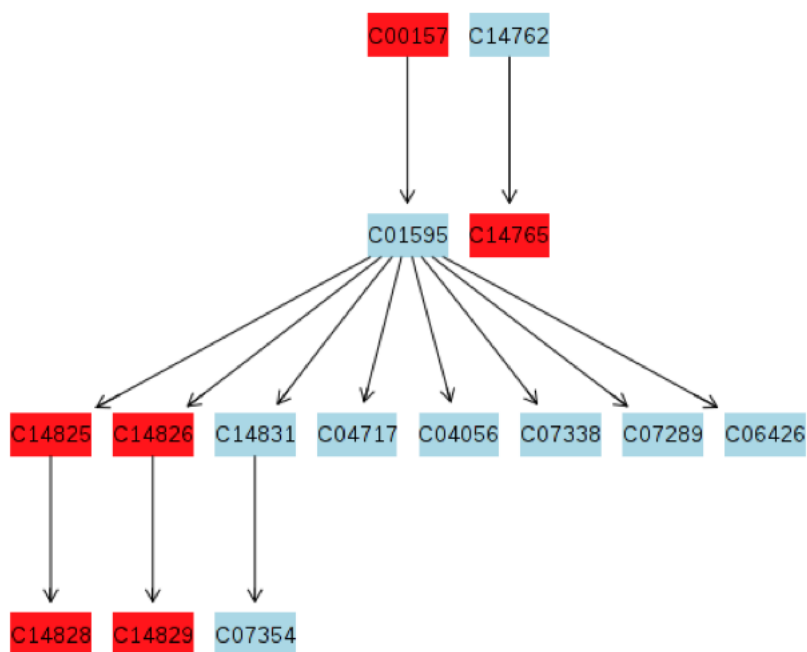
Table A4.2 Data table of linoleic acid metabolites, where “*” denotes significance with $p \leq 0.05$ and fold change $\geq |2|$.

HILIC positive

Compound ID	Accepted Description	Level	Anova (p)	Max Fold Change	Highest Mean	Lowest Mean
1.36_317.2086m/z	*13-OxoODE	L3	2.07E-11	6.54	Treated	Untreated
1.37_296.2351n	*9(10)-EpOME	L3	2.69E-11	9.06	Treated	Untreated
1.38_314.2457n	*12,13-DiHOME	L3	3.52E-10	29.71	Treated	Untreated
1.36_312.2301n	*9,10-DiHODE	L3	2.88E-07	5.04	Treated	Untreated
1.40_280.2403n	*Linoleic acid	L3	6.74E-06	9.67	Treated	Untreated

RPLC positive

Compound ID	Accepted Description	Level	Anova (p)	Max Fold Change	Highest Mean	Lowest Mean
15.20_314.2454n	*12,13-DiHOME	L3	1.22E-07	100.51	Treated	Untreated
14.10_315.2527m/z	*9,10-DHOME	L3	1.09E-06	3215.51	Treated	Untreated
16.77_295.2265m/z	*13-OxoODE	L3	1.48E-06	7.20	Treated	Untreated
16.89_295.2265m/z	*9,12,13-TriHOME	L3	1.70E-06	17.47	Treated	Untreated
17.24_296.2349n	*9(10)-EpOME	L3	1.97E-06	38.87	Treated	Untreated
16.22_279.2316m/z	*13S-HODE	L3	3.83E-06	308.84	Treated	Untreated
15.73_312.2297n	*9(10)-EpHOME	L3	2.05E-05	30.89	Treated	Untreated
17.33_297.2422m/z	*12(13)-EpOME	L3	2.11E-05	12.47	Treated	Untreated
17.01_295.2265m/z	*9-OxoODE	L3	0.003337	14.92	Treated	Untreated



Matched metabolites:

Pathway	Metabolites
Linoleic acid metabolism	9,10-Epoxyoctadecenoic acid; 12,13-EpOME; Linoleic acid; 13S-hydroxyoctadecadienoic acid; Phosphatidylcholine; 8(R)-Hydroperoxylinoleic acid; 9,10-DHOME; 12,13-DHOME; 13-OxoODE; 13-L-Hydroperoxylinoleic acid; Bovinic acid; (9Z,12Z)-(11S)-11-Hydroperoxyoctadeca-9,12-dienoic acid; (7S,8S)-DiHODE; Crepenynate; Gamma-Linolenic acid

Figure A4.2 Linoleic acid pathway. Red nodes reveal individual significant metabolites matched to the linoleic acid metabolic pathway. KEGG C# is shown within a node. The individual significant metabolites ($p < 0.05$) identified at confidence level L3 are highlighted in red for the linoleic acid metabolism generated by MetaboAnalyst 4.0 software.

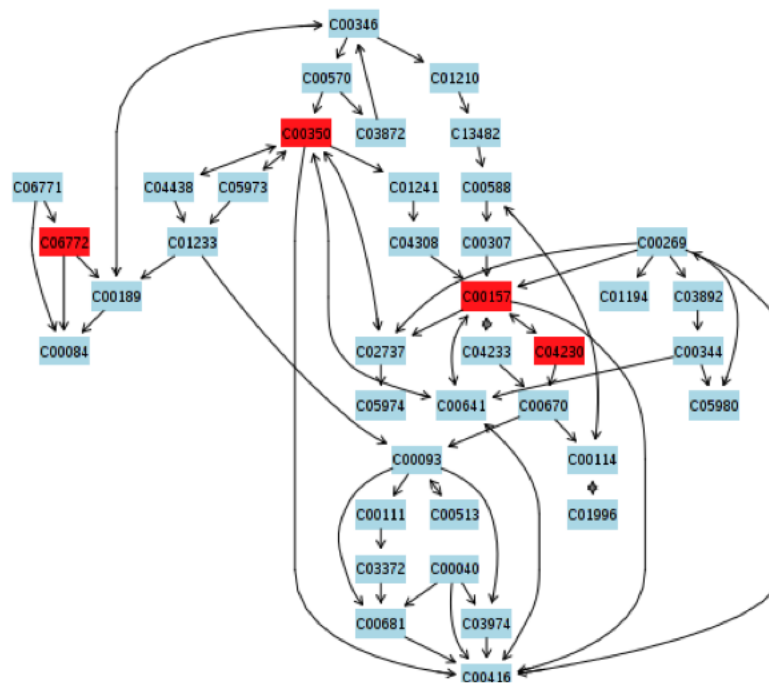
Table A4.3 Data table of glycerophospholipid metabolites, where “*” denotes significance with $p \leq 0.05$ and fold change $\geq |2|$.

HILIC positive

Compound ID	Accepted Description	Level	Anova (p)	Max Fold Change	Highest Mean	Lowest Mean
7.67_105.0790n	*Diethanolamine	L2	0.000329	2.13	Treated	Untreated
1.41_450.2978m/z	*LysoPC(14:0/0:0)	L3	6.23E-06	16.93	Treated	Untreated
2.80_464.3134m/z	*LysoPC(15:0)	L3	4.83E-06	3577.99	Treated	Untreated
3.88_703.5745m/z	*Palmitoyl sphingomyelin	L3	0.016365	4.74	Treated	Untreated
2.40_418.3061m/z	*PC(O-14:0/0:0)	L2	1.67E-15	Infinity	Treated	Untreated
2.78_714.5065m/z	*PE(16:0/18:3)	L3	0.04656	2.04	Treated	Untreated
2.84_676.4910m/z	*PE(19:1(9Z)/12:0)	L3	8.18E-06	2.33	Untreated	Treated
2.79_466.3291m/z	*PE(O-18:1(9Z)/0:0)	L3	0.006441	54.19	Treated	Untreated
2.89_438.2977m/z	*PE(P-16:0e/0:0)	L2	0.000454	27.73	Treated	Untreated
5.88_150.1125m/z	Triethanolamine	L3	0.017506	1.25	Treated	Untreated
6.18_104.1069m/z	Choline	L2	0.010304	1.34	Treated	Untreated

RPLC positive

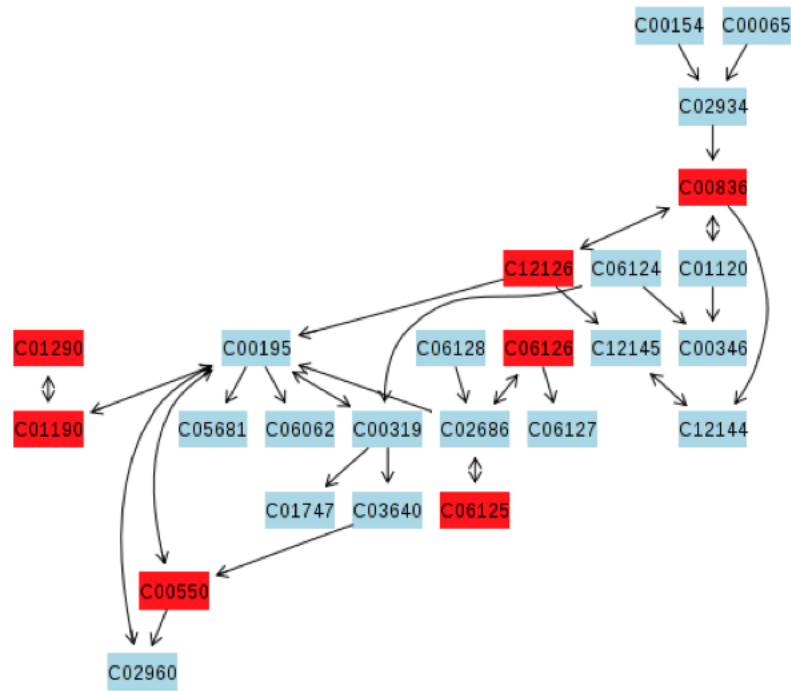
Compound ID	Accepted Description	Level	Anova (p)	Max Fold Change	Highest Mean	Lowest Mean
1.08_258.1099m/z	Glycerophosphocholine	L2	0.035	1.529	Untreated	Treated
1.87_495.2380m/z	PI(13:0/0:0)	L3	0.098	1.446	Untreated	Treated
4.40_449.2060m/z	LysoPA(16:0/0:0)	L3	0.923	1.336	Untreated	Treated
23.78_171.0055m/z	Dihydroxyacetone phosphate	L3	0.181	1.188	Treated	Untreated
1.05_106.0861m/z	Diethanolamine	L3	0.277	1.522	Treated	Untreated
3.10_134.0361m/z	Phosphodimethylethanol amine	L3	0.536	2.352	Treated	Untreated
17.94_429.3262m/z	Sphingosine-1-phosphocholine	L3	0.338	2.834	Treated	Untreated
1.06_206.0551m/z	Phosphocholine	L3	0.405	1.673	Treated	Untreated
5.86_562.2534m/z	PS(18:1(9Z)/0:0)	L3	0.516	1.231	Treated	Untreated
7.08_518.2640m/z	PC(15:1(9Z)/0:0)	L3	0.848	1.178	Treated	Untreated



Matched metabolites:

Pathway	Metabolites
Glycerophospholipid metabolism	<p>Phosphatidylethanolamine; Phosphatidylcholine; Glycerol 3-phosphate; Triethanolamine; Diethanolamine; Dihydroxyacetone phosphate; CDP-diacylglycerol; 2-Acyl-sn-glycerol 3-phosphate; Acyl-CoA; 2-Acyl-sn-glycero-3-phosphocholine; LysoPC(18:1(9Z)); 1,2-Diacyl-sn-glycerol; Citicoline; Phosphorylcholine; Choline; Acetylcholine ; O-Phosphoethanolamine; Ethanolamine; Phosphatidylglycerol; PA(16:0/16:0); PS(16:0/16:0); Glycerolphosphorylethanolamine; 1-Acyl-sn-glycerol 3-phosphate; CDP-Ethanolamine; L-Serine-phosphoethanolamine; Phosphatidylglycerophosphate; Glycerophosphocholine; N-Methylethanolamine phosphate; 1-Acyl-sn-glycero-3-phosphoethanolamine; Phosphodimethylethanolamine; 2-Acyl-sn-glycero-3-phosphoethanolamine; Dihydroxyacetone Phosphate Acyl Ester; CDP-glycerol; Phosphatidyl-N-dimethylethanolamine; Phosphatidyl-N-methylethanolamine; Acetaldehyde; 2-Acyl-sn-glycero-3-phosphoserine; 1-Phosphatidyl-D-myo-inositol; Cardiolipin</p>

Figure A4.3 Glycerophospholipid pathway. Red nodes reveal individual significant metabolites matched to the linoleic acid metabolic pathway. KEGG C# is shown within a node. The individual significant metabolites ($p < 0.05$) identified at confidence level L3 are highlighted in red for the linoleic acid metabolism generated by MetaboAnalyst 4.0 software.



Matched metabolites:

Pathway	Metabolites
Sphingolipid metabolism	Sphinganine ; Phytoceramide; Ceramide; Ceramide 1-phosphate; Sphingosine 1-phosphate; Sphinganine 1-phosphate; Dihydroceramide ; Phytosphingosine; SM ; Sphingosine; Palmitoyl-CoA; L-Serine; 3-Dehydrosphinganine; Galabiosylceramide ; Galactosylceramide; GM4; Lactosylceramide ; Glucosylceramide ; LysoSM(d18:1); 3-O-Sulfogalactosylceramide (d18:1/24:0) ; Ceramide 2-aminoethylphosphonate; Ceramide phosphoethanolamine; Digalactosylceramidesulfate; O-Phosphoethanolamine; Galactosylsphingosine

Figure A4.4 Sphingolipid pathway. Red nodes reveal individual significant metabolites matched to the linoleic acid metabolic pathway. KEGG C# is shown within a node. The individual significant metabolites ($p < 0.05$) identified at confidence level L3 are highlighted in red for the linoleic acid metabolism generated by MetaboAnalyst 4.0 software.

Table A4.4 Data table of cell wall metabolites, where “*” denotes significance with $p \leq 0.05$ and fold change $\geq |2|$.

HILIC positive

Compound ID	Accepted Description	Level	Anova (p)	Max Fold Change	Highest Mean	Lowest Mean
11.17_680.1096m/z	*UDP-MurNAc	L2	0.032	19.2	Treated	Untreated
10.70_608.0886m/z	UDP-GalNAc/GlcNAc	L3	0.175	11.2	Treated	Untreated

Chapter 5

Chemoproteomic target identification of human milk oligosaccharides in group B

Streptococcus

5.1 Abstract

HMOs have significant antibacterial effects against GBS, but the molecular interactions between HMOs and GBS remain unknown. Herein, we describe a methodology that enables the two-step derivatization of unprotected HMOs into a variety of bioorthogonal tool molecules. The probes are amenable for use in pull-down assays for chemoproteomic-based target identification and will be used to elucidate the bacterial targets of HMOs.¹

5.2 Chemoproteomic target identification

5.2.1 Using chemical biology to interrogate antibiotic mechanism of action: an introduction

The efficacy of antibiotics is driven by interactions between small molecules and bacterial cellular targets. By example, penicillin, trimethoprim, clindamycin, gentamycin, and nitrofurantoin all vary in their antibacterial mechanism of action, but universally the activity of each of these antibiotics is facilitated by their molecular interactions with a specific bacterial target (see section 1.7.1).^{2, 3} Penicillin interacts with transpeptidase enzymes to inhibit peptidoglycan formation.⁴ Trimethoprim binds to dihydrofolate reductase to prevent folate biosynthesis.⁵ Clindamycin and gentamycin interact with portions of the bacterial ribosome to stunt protein generation, and quinolones like nitrofurantoin bind to DNA

gyrase to halt DNA replication.⁶⁻⁸ Antibiotic activity is driven by molecular interactions between proteins and small molecules, and as such, research continues to develop methods for identifying them.

To determine antibacterial mechanisms of action, several methods can be exploited. These include the use of phenotypic biological assays (see **Chapter 3**), metabolomics (see **Chapter 4**), proteomics, as well as chemoproteomic-based target identification (ID). Target ID or “pull-down” assays are often used to identify small molecule-protein interactions.⁹⁻¹³ This is experimentally achieved by the covalent “linking” of small molecules and proteins, which can subsequently be isolated and analyzed. The workflow for these assays will be detailed below (see section 5.3), but the initial success of target ID techniques is largely dependent on the development and use of a multifunctional molecular probe.

5.2.2 Molecular probes for target ID

Chemoproteomic target ID uses molecular probes to capture native biological interactions between small molecules and bacterial targets. As a result, the use of multifunctional molecular probes is necessary to selectively modify and permit the isolation of meaningful binding events in complex biological systems. Molecular probes generally consist of three important units: an “active” molecule of interest, a cross-linking group to modify selective targets, and a purification tag for isolation and analysis (**Figure 5.1**).

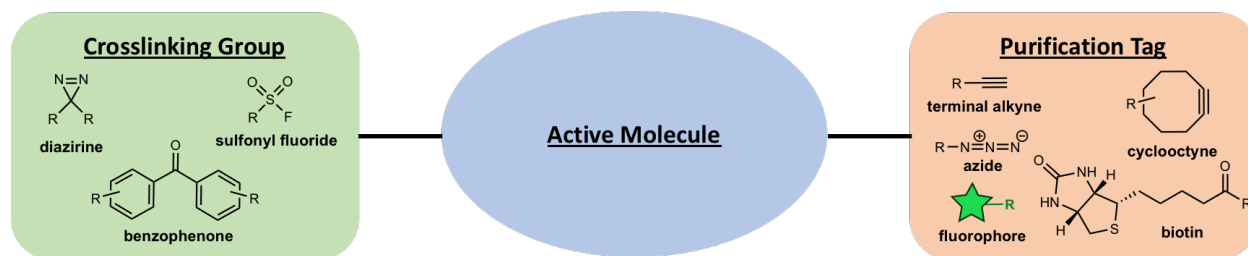


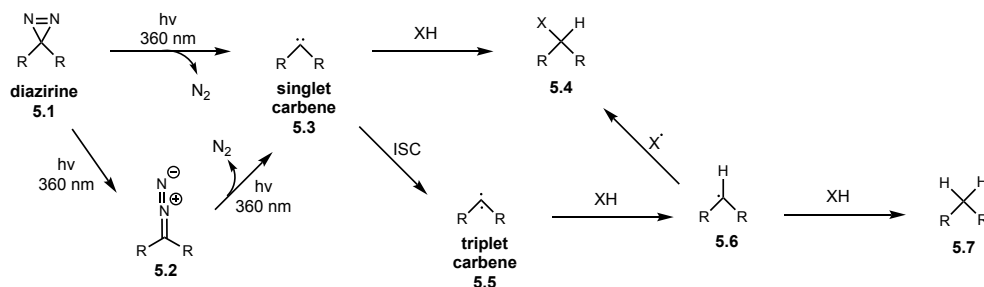
Figure 5.1 General molecular scaffold and functional groups useful in target ID studies

First and foremost, molecular probes begin with the identification of an active molecule of interest. These molecules can originate from a wide range of biological research areas and include novel antibiotic scaffolds, anti-cancer therapeutics, or inhibitors of protein interactions.

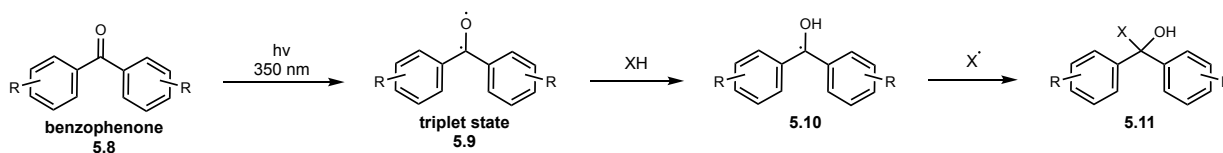
From there, the second unit of the molecular probe is a cross-linking group, capable of forming bonds with biological targets. Some cross-linking groups include photoactivatable motifs, such as diazirines **5.1** and benzophenones **5.8** (**Scheme 5.1**). These can be excited under ultra-violet (UV) light to produce reactive intermediates.¹⁴⁻¹⁶ From diazirine **5.1**, excitation permits the extrusion of nitrogen gas and the formation of a singlet carbene **5.3**. This can insert directly into X-H bonds to give **5.4**, where X = C, N, O, or S. Alternatively, intersystem crossing (ISC) can generate the triplet carbene **5.5**, which can undergo radical abstraction and recombination to give **5.4** or **5.7**. Similarly, benzophenone **5.8** can be excited under UV irradiation to give a reactive diradical triplet state **5.9** from which abstraction and recombination ultimately yields **5.11**. Through these mechanisms, diazirine and benzophenone functional groups are able to insert or radically capture neighboring bonds and, in biological settings, protein targets.^{15, 17-25} Electrophilic sulfonyl fluorides can also be used to cross-link nucleophilic amino acids residues, but do

not require photoactivation.²⁶ In general, the cross-linking group is responsible for covalently linking the active molecule of interest to its respective biological target.

A. Activation of diazirines



B. Activation of benzophenones



Scheme 5.1 Activation of various photoactivatable groups (A.) Activation of diazirines (B.) Activation of benzophenones

Finally, the third motif used in target ID probes is a purification tag that is amenable to derivatization, detection and purification. These motifs are often alkyne and azide handles, that can be subjected to click-chemistry with a variety of fluorophores and biotin derivatives.^{27, 28} The attachment of fluorophores and biotin scaffolds ultimately enables affinity purification of cross-linked small molecule-protein interactions. Bioorthogonal chemistries are continually developing to increase sensitivity and selectivity of these methods.^{27, 29-32} Such molecular scaffolds have been used to identify various small molecule-protein interactions across the field of chemical biology.

Nevertheless, when compared to other classes of natural products, the use of target ID methods in investigating carbohydrate interactions with proteins is particularly rare.^{21, 33} This is largely due to the inherent difficulty associated with capturing carbohydrate-protein interactions.³⁴⁻³⁶ Binding between carbohydrates and proteins is often weak in affinity and passive. Therefore, many carbohydrate binding events are multivalent in nature, where one protein binds many carbohydrates or vice versa. This multivalent presentation increases overall interaction time to yield meaningful biological responses. By example, the sialic acid residues involved in binding to siglecs during influenza infections, are only estimated to interact with a $K_d = 0.1-3\text{mM}$.³⁷⁻³⁹ Although, these single-binding events are low-affinity interactions, the abundance of siglecs available for binding cumulatively leads to the downstream host infection and response seen from influenza.

While a robust binding mode for biological impact, multivalent interactions present significant challenge for isolating single binding events between carbohydrates and proteins. These challenges are compounded by a lack of synthetic access to complex carbohydrates and functionalized derivatives. As such, further developments to target ID methodologies are needed to better capture low-affinity binding events and study biological interactions of carbohydrates.

5.3 Proposed workflow for using target ID to identify HMO interactions with GBS

Our earlier studies on the antibacterial activity of HMOs (see **Chapter 3** and **Chapter 4**) supports the hypothesis that HMOs increase GBS cell permeability through perturbations to lipid biosynthesis and utilization. This increased cell permeability inhibits GBS growth and can be harnessed in adjuvant therapies with antibiotics currently used in the clinic.

While our studies have supported this working hypothesis, the specific biological target of HMOs in GBS remains unknown.

Resultantly, we hypothesized that chemoproteomic target ID could be used to investigate specific HMO-GBS binding interactions (**Figure 5.2**). The proposed workflow would leverage well-precedented bioorthogonal chemistries for the novel study of these complex carbohydrate binding events. Generally, the proposed workflow begins with the incubation of an HMO molecular probe with GBS cells, whereby subsequent photoactivation facilitates cross-linking of the HMO to a specific biological target (**Figure 5.2, I-II**). Click reaction then attaches a biotin and/or fluorophore-containing purification handle (**Figure 5.2, III**).

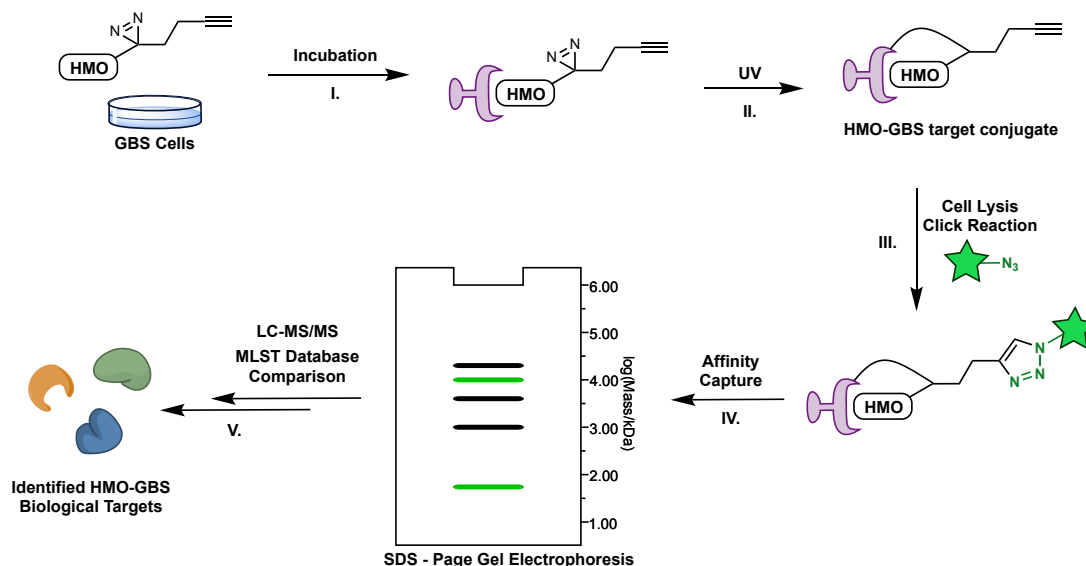


Figure 5.2 Proposed general workflow for chemoproteomic target ID of HMOs in GBS. (I.) Incubation of HMO probe with GBS cells and biological targets. (II.) UV irradiation and cross-linking of probe and biological target. (III.) GBS cell lysis and click reaction with fluorophore and/or biotin derivative. (IV.) Affinity capture and separation via gel electrophoresis. (V.) Mass spectrometry-guided identification of biological target of HMOs in GBS.

From here, affinity purification and fluorescence imaging would allow for isolation of select bacterial targets (**Figure 5.2, IV**). Ultimately, mass spectrometry guided analysis of isolated hits would identify GBS protein targets of HMOs (**Figure 5.2, V**). This workflow would permit the discovery of bacterial interactions with HMOs and contribute to our proposed HMO mechanism of action.

5.4 Rationale and design of HMO bioorthogonal probes

5.4.1 Identification of antibacterial single-entity HMOs

Chemoproteomic target ID begins with the development of amenable bioorthogonal tool compounds. There are several bioorthogonal motifs that can be used within target ID studies (**Figure 5.1**), but these additional functional groups must not affect the biological activity of the native molecule. As such, it is imperative that synthetic manipulations are minimal and do not impact molecular recognition elements of the native compound.

As we thought about synthesizing bioorthogonal HMO probes, we considered the most facile starting point. While pooled HMOs have significant inhibitory effects on GBS, these complex mixtures can contain over 200 different single-entity HMOs (see sections 3.2 and 3.3). The complex nature of HMO mixtures makes these solutions unideal for defined chemical derivatization. As a result, previous work was conducted to identify single-entity HMOs with significant antibacterial activity against GBS (**Table 5.1**).^{40, 41}

Table 5.1 Single-entity HMO antibacterial activity

HMO ^a	GB590		GB2	
	Average Growth Reduction	Average Viability Reduction	Average Growth Reduction	Average Viability Reduction
pooled HMOs	82%	23%	73%	24%
lactose (Lac)	3%	0%	0%	2%
2'-fucosyllactose (2'-FL)	8%	0%	9%	9%
3-fucosyllactose (3-FL)	15%	0%	0%	4%
difucosyllactose (DFL)	51%	17%	0%	11%
lacto- <i>N</i> -triose II (LNT II)	54%	12%	22%	8%
3'-sialyllactose (3'-SL)	13%	0%	0%	5%
6'-sialyllactose (6'-SL)	18%	0%	0%	4%
lacto- <i>N</i> -tetraose (LNT)	24%	11%	0%	0%
lacto- <i>N</i> -neotetraose (LNnT)	42%	13%	5%	4%
lacto- <i>N</i> -fucopentaose I (LNFP I)	1%	24%	0%	10%
lacto- <i>N</i> -fucopentaose II (LNFP II)	31%	15%	0%	9%
lacto- <i>N</i> -fucopentaose III (LNFP III)	26%	14%	0%	9%
LS-tetrasaccharide a (LST a)	38%	23%	42%	25%
LS-tetrasaccharide c (LST c)	15%	16%	35%	18%
disialyllacto- <i>N</i> -tetraose (DSLNT)	28%	18%	18%	21%

^aHMOs dosed at 5 mg mL⁻¹

Notably, difucosyllactose (DFL), lacto-*N*-triose II (LNT-II), and LS-tetrasaccharide A (LSTa) were determined to be antibacterial in GB590 with approximately 40-50% growth inhibition. Contrarily, lactose, 2'-fucosyllactose (2'-FL) and 3'-sialyllactose (3'-SL) were inactive (0-10% growth inhibition). Interestingly, these results indicate that there is variable antibacterial activity across single-entity HMOs with no clear correlation between overall fucosylation or sialylation patterns. That is, just because an HMO contains a fucose or sialic acid residue, does not indicate it will have antibacterial effects. Furthermore, smaller HMOs like LNT-II, are antibacterial in nature, indicating that more complexity in HMO structure might not be critical for activity against GBS.

Most importantly, lactose was shown to have no independent antibacterial activity against GBS. As each HMO biosynthetically originates from lactose and as such contains lactose at the reducing end (see section 3.2.2), this result led us to hypothesize the molecular interactions necessary for antibacterial activity occur at the non-reducing end of the HMO scaffold. Collectively, this initial activity screen offered key insights into the molecular structures that facilitate antibacterial effects against GBS and how we might synthesize bioorthogonal HMO probes.

5.4.2 Design of bioorthogonal HMO probes

To begin the development of chemoproteomic target ID studies, we proposed to synthesize a library of bioorthogonal HMOs probes (**Figure 5.3**). Since lactose alone has no antibacterial activity against GBS, we speculated that derivatization at the reducing end of the HMO scaffold might limit deleterious effects to biological function. From the previous study, we identified several initial antibacterial HMO scaffolds of interest,

including active HMOs LNT-II (**5.13**), DFL (**5.14**), and LSTa (**5.16**). We also wanted to synthesize inactive HMO probes for use as controls and selected 2'-FL (**5.12**) and LNT (**5.15**). This subset of single-entity HMOs represented both antibacterial and inactive HMOs with varying fucosylation and sialylation patterns.

From the core oligosaccharides, we then identified several bioorthogonal tags that had previously demonstrated success within target ID studies. These included diazirines **5.17** and **5.20**, benzophenones **5.18** and **5.22**, and sulfonyl fluoride **5.19**.^{42, 43} Additionally, we hoped to access fluorescent HMOs through conjugation of fluorophores such as rhodamine (**5.21**). The variety of bioorthogonal tags as well as the HMO scaffolds of interest prompted us to design a synthetic approach that was robust across carbohydrate scaffolds and functional groups.

We envisioned amide coupling between a carboxylic acid appended functionalized tag and an aminoglycoside would install the bioorthogonal motifs necessary for target ID. The aminoglycoside or aminoHMO used within the amide coupling, would then be accessed via Kochetkov amination.⁴⁴ This proposed two-step sequence would enable protecting-group free conversion of complex oligosaccharides into a variety of bioorthogonal tool molecules.

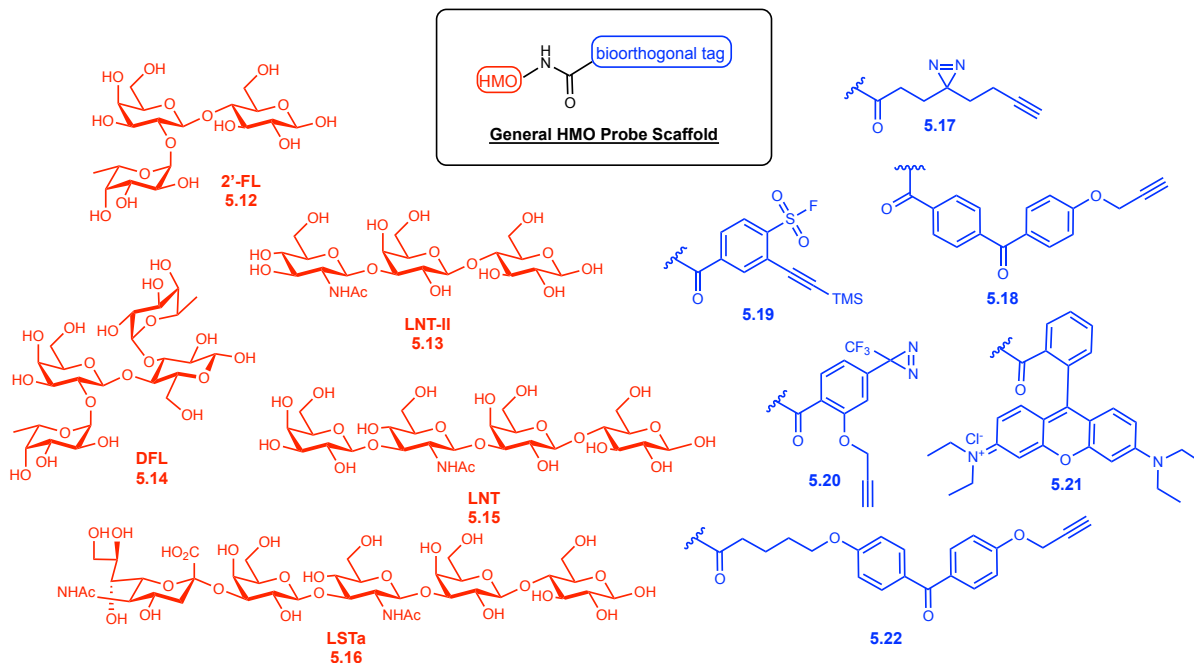
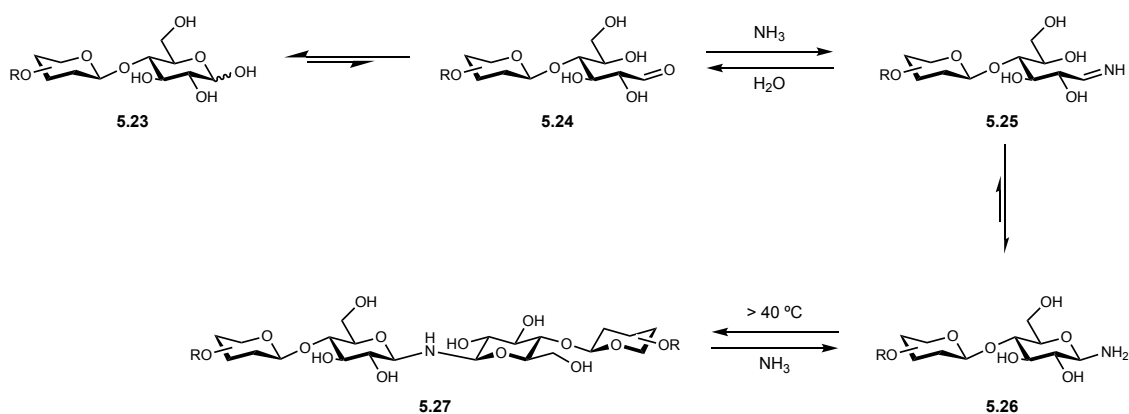


Figure 5.3 General proposed HMO probe scaffold including HMOs and bioorthogonal tags of interest

5.5 Kochetkov amination of HMOs

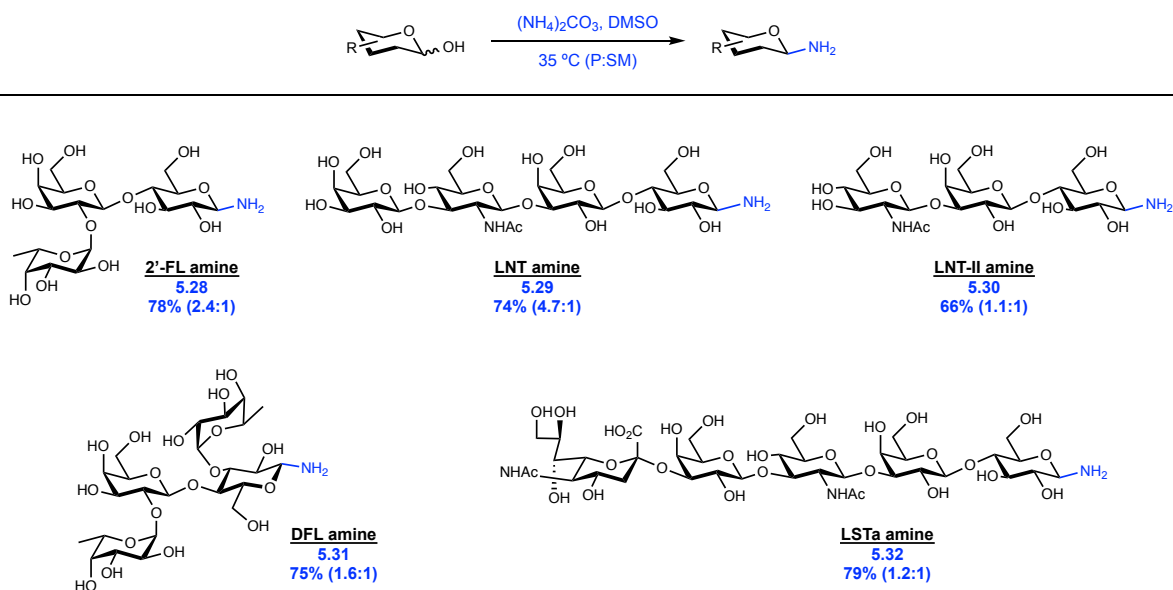
We first used the Kochetkov amination to convert deprotected HMOs into corresponding β -aminoHMOs.⁴⁴⁻⁴⁷ The reducing-end of carbohydrates is known to be in equilibrium with the open chain form (**Scheme 5.2**). This equilibrium can be harnessed synthetically to generate stereo-defined β -aminoglycosides in a reaction known as the Kochetkov amination.⁴⁸⁻⁵⁰ This reaction proceeds via condensation of ammonium onto the intermediate open-chain carbohydrate **5.24**, to form **5.26**. This condensation is most efficient under moderate thermal heating with excess ammonium carbonate. Higher temperatures can generate diglycosylamine byproducts **5.27**, while microwave-assisted methods are not amenable for amination of complex oligosaccharides. Resultantly, careful control of reaction conditions and the elimination of residual water are necessary to promote desired glycosyl amine formation in the highest yield and percent conversion.

Of note, the Kochetkov amination proceeds in a stereo-defined manner to produce almost exclusively the β -aminoglycoside, a phenomenon commonly attributed to the reverse anomeric effect (RAE).⁴⁸⁻⁵⁰



Scheme 5.2 Mechanism of the Kochetkov amination

Given these considerations, we were able to apply the Kochetkov amination to the synthesis of a variety of the desired β -aminoHMOs (**Scheme 5.3**).^{51, 52} We performed aminations under mild thermal heating at 35 °C in dimethyl sulfoxide (DMSO) to limit the presence of water and undesired diglycosylamine formation. These conditions gave high percent yields (70-80%) with substantial conversion to the desired glycosyl amines **5.28-5.32**. Each oligosaccharide sees inherent differences in amination conversion, likely owing to differing equilibrium rates between the open-chain and closed-chain forms. By example, LNT-II amine **5.30** sees a modest conversion ratio of 1.1:1 desired amine to starting HMO, while LNT amine **5.29** sees a conversion ratio of 4.7:1.



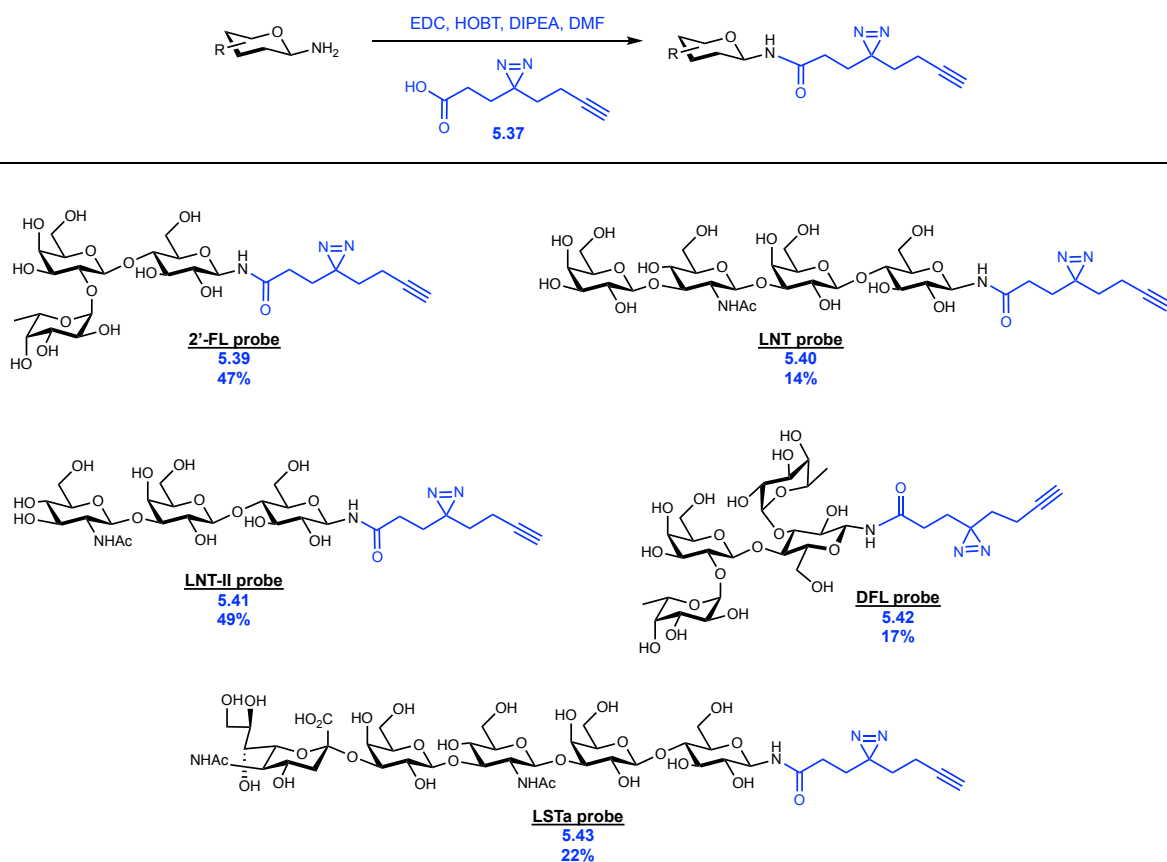
Scheme 5.3 Kochetkov amination of HMOs

5.6 Synthesis of diazirine-containing HMO bioorthogonal probes

From β -aminoHMOs **5.28-5.32**, we then envisioned subsequent amide coupling with a carboxylic acid appended bioorthogonal tag to yield the desired HMO probes. Initial work aimed to synthesize a small library of diazirine-containing HMO probes that might be used in target ID assays. Diazirines have gained popularity in chemoproteomic analyses as they are minimal in size and can be activated using commercial systems.^{18, 25, 42, 43}

Synthetically, diazirine **5.37** is accessible in 9 steps from ethylacetoacetate (**5.33**) (**Scheme 5.4**).¹⁸⁻²⁰ Treatment with excess LDA generates a Weiler-type dianion that is subsequently quenched with propargyl bromide to install the requisite alkyne functionality.⁵³ A three-step sequence of ketalization, LiAlH_4 mediated ester reduction, and ketal deprotection provides **5.35**, setting the stage for diaziridination. Treatment of **5.35** with liquid ammonia and hydroxylamine-*O*-sulfonic acid gives a diaziridine which is then oxidized upon exposure to iodine and NEt_3 to give diazirine **5.36**. Conversion of the

aminoHMO. This material can be recovered and re-subjected to the two-step Kochetkov amination/amidation sequence to ultimately limit net loss of material.

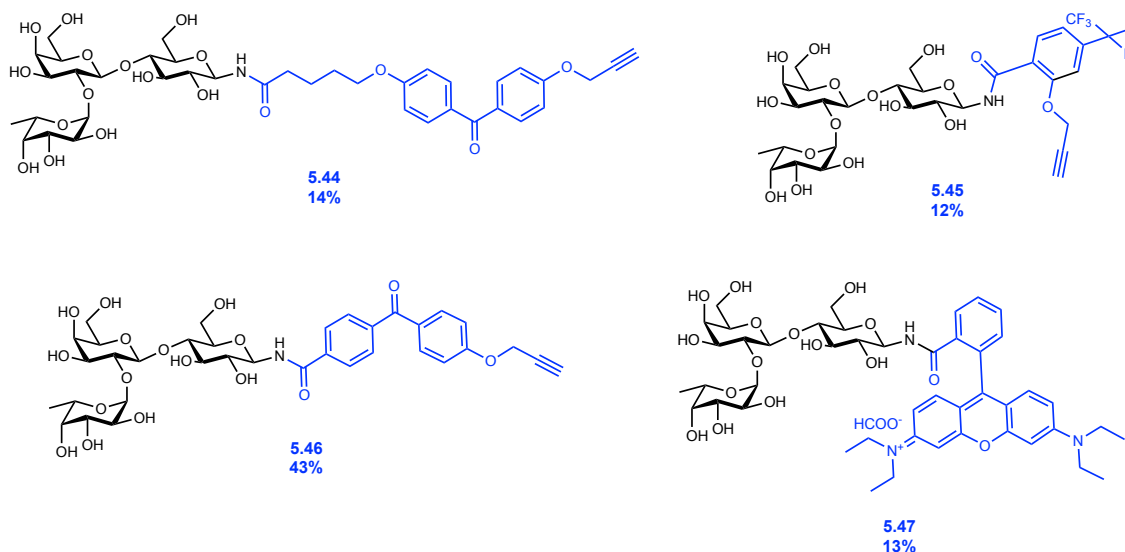
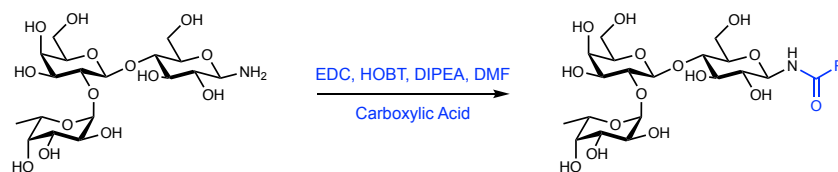


Scheme 5.5 Synthesis of diazirine-appended bioorthogonal HMO probes

In total, we successfully made five diazirine-appended HMOs, 2'-FL probe **5.39**, LNT probe **5.40**, LNT-II probe **5.41**, DFL probe **5.42**, and LSTa probe **5.43**. These derivatives are the first set of bioorthogonal HMO probes synthesized to date and set precedence for divergent syntheses of other oligosaccharide tool compounds.

5.7 Expansion of methodology: synthesis of additional HMO bioorthogonal tool compounds

Upon successful derivatization of HMOs with diazirine **5.37**, we then used our two-step conversion sequence to incorporate other tags and functionality (**Scheme 5.6**). This methodology expansion was conducted with 2'-FL as it is one of the most abundant HMOs in breast milk and has greater commercial accessibility. First, we used our methodology to generate the analogous aryl diazirine **5.45**. We then synthesized the benzophenone probes **5.44** and **5.46**, to demonstrate additional functional group tolerance and that larger tags could be appended successfully. Finally, we also synthesized a rhodamine labelled HMO **5.47**. This is the first fluorescently labelled HMO made within our program and offers potential for future use in microscopy imaging of HMOs in biological systems (see section 5.9). Our initial attempts to install sulfonyl fluoride containing bioorthogonal tag **5.19** proved largely unsuccessful, likely due to undesired reactivity of the sulfonyl fluoride handle with the deprotected oligosaccharide. Overall, we demonstrated this two-step conversion sequence is amenable to a variety of HMO scaffolds and bioorthogonal tags, highlighting the utility of this methodology.



Scheme 5.6 Synthesis of additional HMO bioorthogonal tool compounds

5.8 Validation of antibacterial properties of HMO probes

With the successful synthesis of a library of bioorthogonal HMO probes (**5.39-5.43**), we then needed to validate retained antibacterial activity of the HMO probes in GBS. To do this, we reproduced GBS growth assays analogous to the earlier single-entity studies.^{40,}

⁴¹ We conducted these assays in GB590 as it was the strain most susceptible to single-entity HMOs overall. Based on previous data, we anticipated 2'-FL (**5.12**) and LNT (**5.15**) would be inactive against GBS and LNT-II (**5.13**), DFL (**5.14**), and LSTa (**5.16**) would have antibacterial activity. We recapitulated these previous results (**Figure 5.4A**), where 2'-FL (**5.12**) and LNT (**5.15**) were shown to have no antibacterial activity and LNT-II (**5.13**), DFL (**5.14**), and LSTa (**5.16**) all saw ~30% growth inhibition over 24 hours. We then tested

our synthesized probes (5.39-5.43) in analogous assays (Figure 5.4B). Remarkably, the 2'-FL and LNT probes (5.39 and 5.40 respectively) remained inactive, while the LNT-II and DFL probes (5.41 and 5.42 respectively) retained their antimicrobial properties (~25% growth inhibition over 24 h). Additionally, these molecules did not significantly affect GBS viability profiles or biofilm formation (see Figures A5.44 and A5.45), indicating little change to bacterial phenotype from the native HMO structure. These results suggest that these bioorthogonal HMOs would be amenable for use in target ID studies and our synthesis did not impact native HMO function.

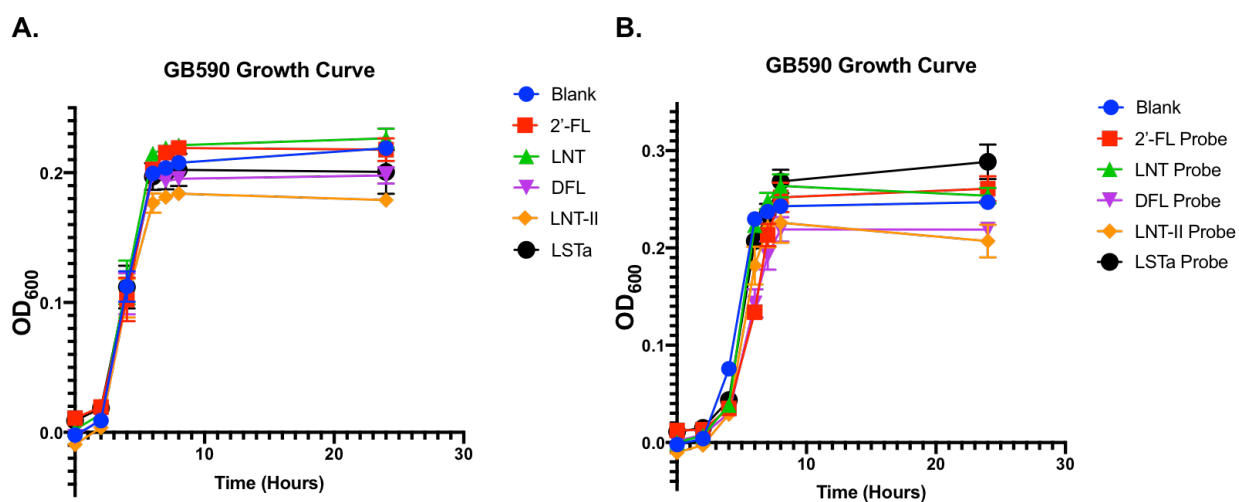


Figure 5.4 Growth curves of single-entity HMOs and HMO probes in GB590 when dosed at $\sim 5 \text{ mg mL}^{-1}$. Growth represented by OD_{600} reading taken at 0, 2, 4, 6, 8, and 24 hours over three biological replicates and three technical replicates with SEM depicted for each timepoint. (A.) Growth curve of single-entity HMOs in GB590. (B.) Growth curve of HMO probes in GB590.

Interestingly, the only HMO with an altered activity profile after adding the diazirine tag, was that of the LSTa probe 5.43. The original HMO had antibacterial activity ($\sim 30\%$ growth inhibition over 24 h), but that activity was lost upon addition of the diazirine tag. LSTa was the only sialylated HMO in our initial library, so this suggests a differing

mechanism of action for sialylated HMOs. Specifically, we hypothesize that the antibacterial activity of sialylated HMO variants is related to the charge about the sialic acid moiety. Our synthetic manipulations might have introduced various salts at the carboxylic acid moiety that undesirably disabled antibiotic activity. Future derivatization of sialylated HMOs should better account for these synthetic considerations and attempt to limit impacts to native sialylated HMO function.

Overall, we validated the retained antibacterial properties of several bioorthogonal HMO probes **5.39-5.42** as well as their limited effects on GBS viability or biofilm formation (see **Figures A5.44** and **A5.45**). These favorable results suggest these molecules are useful tools for antibacterial target ID and will also permit further use of bioorthogonal HMO scaffolds in chemical biology research areas.

5.9 Conclusion and future directions

With the successful design and synthesis of various bioorthogonal HMO probes, future work will be focused on the implementation of such molecules within target ID assays (**Figure 5.2**). Due to the retained biological activity of the HMO probes **5.39-5.42**, we believe conducting experiments in GBS cultures with these probes will permit the identification of HMO bacterial targets. The inactive HMO probes **5.39** and **5.40** will be of use in identifying non-specific binding interactions of HMOs. These are interactions that might not contribute to antibiotic efficacy, but are still of interest to determine the scope of binding interactions of HMOs. We anticipate there will be several nonspecific binding interactions between GBS and HMOs, as HMOs are known to interact with commensal bacterial cells in a variety of ways that do not inhibit growth.^{55, 56} Work to identify these

non-specific interactions will be imperative to filter for targets meaningful for antibiotic activity. The active HMO probes **5.41** and **5.42** can then be used to identify biological targets involved in the antibacterial activity of HMOs. Comparison to the inactive HMO controls will further aid in identification of relevant targets.

From an experimental standpoint, our early work in chemoproteomic target ID assay development optimized bacterial culture and lysis conditions for protein isolation in GBS. Cell lysis is more difficult in GBS than other cell types due to the gram-positive nature and thick peptidoglycan layer. We determined GBS lysis via wand sonication or boiling in sodium dodecyl sulfate (SDS) was not efficient enough and only yielded minimal amounts of soluble protein. Stepwise digestion of the cell wall proved most effective, whereby initial mutanolysin digest in the presence of a protease inhibitor generates GBS protoplasts.⁵⁷ The protoplasts can then be disrupted via rapid freeze/thaw cycling to release cytoplasmic proteins. From this protein isolation protocol, sufficient protein concentration was obtained and visualized in-gel. From here, immediate future experiments will need to be conducted to determine what incubation conditions, including time, temperature, and GBS cell state, are necessary for successful cross-linking of HMO probes.

To complement these target ID studies, global quantitative proteomics experiments could also be conducted. Similar to the metabolomics study we conducted (see **Chapter 4**), untargeted proteomic analyses could be used to observe proteomic perturbations between untreated and HMO treated GBS cultures.^{58, 59} Experiments like these would leverage technologies such as multi-dimensional protein identification technology (MudPIT) and stable isotope labeling with amino acids in cell culture (SILAC).^{60, 61} The comparison of proteomic profiles could reveal key proteins that are impacted by HMO

treatment and whether the identified proteins are significantly more or less abundant in the HMO-treated sample. These discoveries would complement chemoproteomic analyses, but could also provide a suitable backup experiment should target ID assays prove unsuccessful.

Additional complimentary experiments would contribute to further understanding HMO interactions with GBS and other biological systems. We validated our methodology could synthesize fluorescently labelled HMOs, but this work needs to be extended to include other HMOs scaffolds and a variety of fluorescent tags (e.g. BODIPY, TAMRA). These molecules then need to be studied for fluorescent activity in biological systems and stability, to identify which fluorescent dyes yield the highest intensity and best overall properties for imaging studies. These fluorescent HMO probes could then be used to visualize the localization of HMOs within bacterial systems. Confocal microscopy experiments would reveal if HMOs permeate into GBS cells or rather aggregate extracellularly. We hypothesize that HMOs do not penetrate GBS cells with high efficiency, but that HMO interactions at extracellular compartments damage cell membrane integrity and lead to increased intracellular localization over time. Future developments of novel HMO fluorescent probes could be used in time-lapsed confocal microscopy experiments to further investigate this hypothesis.

5.10 Experimental methods

General synthetic procedures and materials

All moisture-sensitive reactions were performed in flame-dried or oven-dried glassware under an atmosphere of argon. Oven-dried stainless-steel syringes or cannula were used

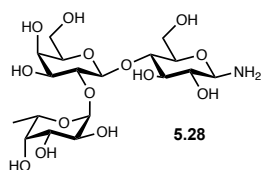
to transfer moisture- and air-sensitive liquids. Reaction temperatures were controlled and monitored using a hot plate stirrer with a thermocouple thermometer. Analytical thin-layer chromatography (TLC) was performed on Sorbtech Silica XHL UV254, glass-backed, 250 μm plated, and visualized using UV, cerium ammonium molybdate stain or ninhydrin stain. Yields were reported as purified, isolated compounds, with solvent impurities (DMSO) removed via calculation. Solvents were dried through a Braun MB-SPS solvent system and used immediately or stored over 3 \AA or 4 \AA molecular sieves. Diazirine **5.37** was either purchased from MilliporeSigma or prepared as reported by Yao et al.¹⁸ Pure single-entity HMOs were generously donated by the Danish biotech company, Glycom.

Instrumentation

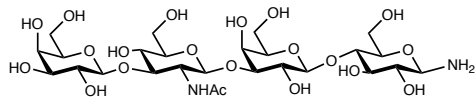
^1H NMR spectra were obtained on a Bruker 600 MHz spectrometer and are reported relative to deuterated solvent signals. Data for ^1H NMR spectra are presented as follows: chemical shift (δ ppm), multiplicity (s = singlet, d = doublet, t = triplet, q = quartet, p = pentet, m = multiplet, br = broad, app = apparent), coupling constants (Hz) and integration. Deuterated water was standardized to 4.79 ppm. Deuterated methanol was standardized to 3.31 ppm. Deuterated DMSO was standardized to 2.50 ppm. ^{13}C NMR spectra were obtained on a Bruker 150 MHz spectrometer and are reported relative to deuterated solvent signals. Deuterated methanol was standardized to 49.0 ppm. Deuterated DMSO was standardized to 39.52 ppm. High-resolution mass spectra (HRMS) were obtained from the Department of Chemistry, Vanderbilt University using a Synapt G2-S HDMS (Milford, Ma, USA) mass spectrometer. Low-resolution mass spectra (LRMS) were collected using a Thermo Fisher MSQ-Plus-40000 mass spectrometer.

General Kochetkov amination procedure

HMO (**5.12-5.16**, 100 mg) was dissolved in DMSO (1.0 M), ammonium carbonate (500 mg, 5 x mass of oligosaccharide) was added and the reaction stirred at 35 °C for 3 days. The solution of was then diluted in a minimal amount of water and lyophilized repeatedly (at minimum x3) until a constant mass of white solid was obtained. Ratio of conversion was determined by integration of C-1 anomeric protons of the starting material to that of the desired product. Mass of residual DMSO was accounted for in reported yields.

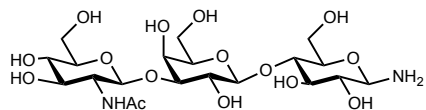


(2S,3S,4R,5S,6S)-2-(((2S,3R,4S,5R,6R)-2-(((2R,3S,4R,5R,6R)-6-amino-4,5-dihydroxy-2-(hydroxymethyl)tetrahydro-2H-pyran-3-yl)oxy)-4,5-dihydroxy-6-(hydroxymethyl)tetrahydro-2H-pyran-3-yl)oxy)-6-methyltetrahydro-2H-pyran-3,4,5-triol (5.28): 78%, 2.4:1 P:SM; ¹H NMR (600 MHz, D₂O) δ 5.32 (d, *J* = 3.9 Hz, 1H), 4.53 (d, *J* = 7.8 Hz, 1H), 4.25 (m, 1H), 4.10 (d, *J* = 8.8 Hz, 1H), 3.94 (dd, *J* = 11.9, 2.2 Hz, 1H), 3.94 – 3.85 (m, 3H), 3.86 – 3.65 (m, 10H), 3.63 – 3.55 (m, 1H), 3.45 (ddd, *J* = 10.0, 5.8, 2.1 Hz, 1H), 3.22 (t, *J* = 9.0 Hz, 1H), 1.24 (d, *J* = 6.6 Hz, 3H); ¹³C NMR (151 MHz, D₂O) δ 100.2, 99.3, 85.1, 76.2, 76.0, 75.2, 75.0, 74.0, 73.6, 71.6, 70.4, 69.6, 69.1, 68.1, 66.9, 61.1, 60.3, 15.2; HR-ESI-MS (*m/z*): calcd for C₁₈H₃₂NO₁₄⁻ (M-H)⁻ 486.1823, found 486.1816.



5.29

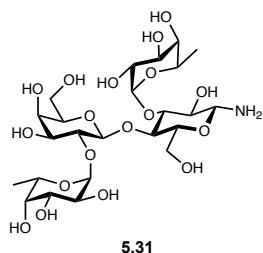
N-((2S,3R,4R,5S,6R)-2-(((2S,3R,4S,5S,6R)-2-(((2R,3S,4R,5R,6R)-6-amino-4,5-dihydroxy-2-(hydroxymethyl)tetrahydro-2H-pyran-3-yl)oxy)-3,5-dihydroxy-6-(hydroxymethyl)tetrahydro-2H-pyran-4-yl)oxy)-5-hydroxy-6-(hydroxymethyl)-4-(((2R,3R,4S,5R,6R)-3,4,5-trihydroxy-6-(hydroxymethyl)tetrahydro-2H-pyran-2-yl)oxy)tetrahydro-2H-pyran-3-yl)acetamide (5.29): 74%, 4.7:1 P:SM; ^1H NMR (600 MHz, D_2O) δ 4.72 (d, $J = 8.3$ Hz, 2H), 4.43 (d, $J = 7.7$ Hz, 2H), 4.14 (d, $J = 3.4$ Hz, 1H), 4.10 (d, $J = 8.8$ Hz, 1H), 3.89 (dd, $J = 16.0, 4.4$ Hz, 4H), 3.83 – 3.67 (m, 12H), 3.65 – 3.49 (m, 7H), 3.47 (ddd, $J = 9.9, 5.2, 2.3$ Hz, 1H), 2.02 (s, 3H); ^{13}C NMR (151 MHz, D_2O) δ 174.9, 103.5, 102.9, 102.5, 84.9, 82.0, 81.9, 78.6, 75.7, 75.2, 75.1, 75.1, 74.8, 73.9, 72.4, 70.6, 70.0, 68.5, 68.4, 68.3, 61.0, 60.9, 60.5, 60.2, 54.7, 22.2; HR-ESI-MS (m/z): calcd for $\text{C}_{26}\text{H}_{45}\text{N}_2\text{O}_{20}^-$ (M-H) $^-$ 705.2566, found 705.2552.



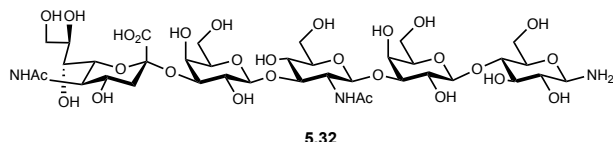
5.30

N-((2S,3R,4R,5S,6R)-2-(((2S,3R,4S,5S,6R)-2-(((2R,3S,4R,5R,6R)-6-amino-4,5-dihydroxy-2-(hydroxymethyl)tetrahydro-2H-pyran-3-yl)oxy)-3,5-dihydroxy-6-(hydroxymethyl)tetrahydro-2H-pyran-4-yl)oxy)-4,5-dihydroxy-6-(hydroxymethyl)tetrahydro-2H-pyran-3-yl)acetamide (5.30): 66%, 1.1:1 P:SM; ^1H NMR (600 MHz, D_2O) δ 4.66 (d, $J = 8.2$ Hz, 1H), 4.45 – 4.40 (m, 1H), 4.29 (d, $J = 8.9$ Hz, 1H), 4.13 (d, $J = 3.5$ Hz, 1H), 3.97-3.87 (m, 4H), 3.77 – 3.69 (m, 7H), 3.63 – 3.55 (m, 5H),

3.47 – 3.44 (m, 2H), 2.03 (s, 3H); ^{13}C NMR (151 MHz, D_2O) δ 174.9, 102.9, 102.8, 86.7, 81.9, 78.5, 78.3, 75.6, 74.8, 74.8, 74.3, 73.8, 73.5, 70.0, 69.7, 68.3, 60.9, 60.5, 55.6, 22.2; HR-ESI-MS (m/z): calcd for $\text{C}_{20}\text{H}_{35}\text{N}_2\text{O}_{15}^-$ (M-H) $^-$ 543.2037, found 543.2030.



(2S,3S,4R,5S,6S)-2-(((2R,3R,4R,5R,6R)-2-amino-5-(((2S,3R,4S,5R,6R)-4,5-dihydroxy-6-(hydroxymethyl)-3-(((2S,3S,4R,5S,6S)-3,4,5-trihydroxy-6-methyltetrahydro-2H-pyran-2-yl)oxy)tetrahydro-2H-pyran-2-yl)oxy)-3-hydroxy-6-(hydroxymethyl)tetrahydro-2H-pyran-4-yl)oxy)-6-methyltetrahydro-2H-pyran-3,4,5-triol (5.31): 75%, 1.6:1 P:SM; ^1H NMR (600 MHz, D_2O) δ 5.44 (d, J = 4.1 Hz, 1H), 5.25 (d, J = 3.7 Hz, 1H), 4.45 (q, J = 9.3, 8.6 Hz, 1H), 4.23 (dt, J = 16.4, 8.2 Hz, 1H), 4.05 (d, J = 8.9 Hz, 1H), 3.94 (dd, J = 10.2, 3.5 Hz, 2H), 3.87 – 3.53 (m, 13H), 3.63 – 3.52 (m, 2H), 3.38 (d, J = 9.0 Hz, 2H), 1.23 (overlapping doublets, J = 6.6 Hz, 6H). ^{13}C NMR (151 MHz, D_2O) δ 100.1, 99.3, 98.3, 85.2, 77.8, 76.6, 76.3, 75.8, 74.8, 73.6, 72.9, 72.0, 71.7, 69.7, 69.2, 68.7, 68.2, 68.0, 66.8, 66.5, 61.5, 61.4, 15.5, 15.5; HR-ESI-MS (m/z): calcd for $\text{C}_{24}\text{H}_{42}\text{NO}_{18}^-$ (M-H) $^-$ 632.2402, found 632.2389.



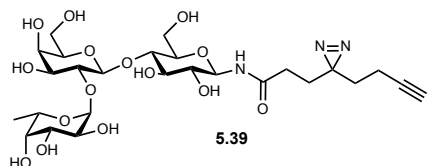
(2S,4S,5R,6R)-5-acetamido-2-(((2R,3R,4S,5S,6R)-2-(((2S,3R,4R,5S,6R)-3-acetamido-2-(((2S,3R,4S,5S,6R)-2-(((2R,3S,4R,5R,6R)-6-amino-4,5-dihydroxy-2-(hydroxymethyl)tetrahydro-2H-pyran-3-yl)oxy)-3,5-dihydroxy-6-(hydroxymethyl)tetrahydro-2H-pyran-4-yl)oxy)-5-hydroxy-6-(hydroxymethyl)tetrahydro-2H-pyran-4-yl)oxy)-3,5-dihydroxy-6-(hydroxymethyl)tetrahydro-2H-pyran-4-yl)oxy)-4-hydroxy-6-((1R,2R)-1,2,3-

trihydroxypropyl)tetrahydro-2H-pyran-2-carboxylic acid (5.32): 79%, 1.2:1 P:SM; ¹H NMR (600 MHz, D₂O) δ 4.74 (d, *J* = 8.5 Hz, 2H), 4.51 (d, *J* = 7.8 Hz, 1H), 4.46 – 4.41 (m, 1H), 4.15 (d, *J* = 3.6 Hz, 1H), 4.11 (d, *J* = 8.8 Hz, 1H), 4.08 (dd, *J* = 9.9, 3.2 Hz, 1H), 3.94 (d, *J* = 3.3 Hz, 2H), 3.90 – 3.49 (m, 30H), 2.03 (d, *J* = 1.8 Hz, 6H), 1.78 (t, *J* = 12.1 Hz, 1H). ¹³C NMR (151 MHz, D₂O) δ 174.9, 174.9, 173.8, 103.4, 102.9, 102.9, 102.5, 99.6, 84.9, 82.1, 81.9, 78.6, 78.3, 75.7, 75.6, 75.2, 75.1, 75.1, 74.9, 72.8, 71.8, 70.0, 69.1, 68.4, 68.3, 68.3, 68.0, 67.2, 62.5, 61.0, 61.0, 60.5, 54.6, 51.7, 39.8, 22.3, 22.1; HR-ESI-MS (*m/z*): calcd for C₃₇H₆₂N₃O₂₈⁻ (M-H)⁻ 996.3520, found 996.3482.

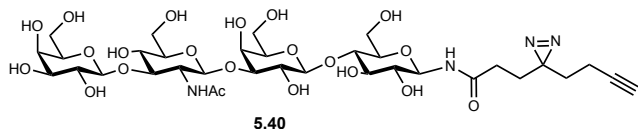
General amidation procedure

To glycosyl amine (10 mg, 1 equiv.) in DMF (0.1 M), EDC (1.25 equiv), DIPEA (1.25 equiv.), HOBT (1.25 equiv.), and carboxylic acid (1.25 equiv.) were added and the resulting slurry stirred at RT in the dark. The reaction mixture was tested by TLC for remaining glycosyl amine (60:30:5:1 DCM:MeOH:H₂O:AcOH, ninhydrin stain). Upon consumption, the reaction was concentrated *in vacuo*. The resulting solid was dissolved

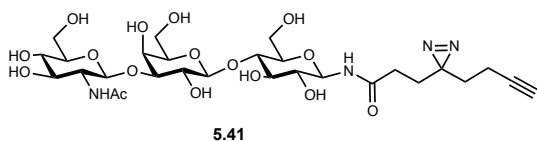
in 10% MeCN/H₂O and purified by reverse phase preparative HPLC (5%-40% MeCN/H₂O over 30 min; Hypersil GOLD 150 mm x 10 mm). The purified fractions were detected by mass spectrometry then lyophilized to yield the products as white solids, which were stored at -20 °C in the dark until use.



3-(3-(but-3-yn-1-yl)-3H-diazirin-3-yl)-N-((2R,3R,4R,5S,6R)-5-(((2S,3R,4S,5R,6R)-4,5-dihydroxy-6-(hydroxymethyl)-3-(((2S,3S,4R,5S,6S)-3,4,5-trihydroxy-6-methyltetrahydro-2H-pyran-2-yl)oxy)tetrahydro-2H-pyran-2-yl)oxy)-3,4-dihydroxy-6-(hydroxymethyl)tetrahydro-2H-pyran-2-yl)propenamide (5.39): 47%; ¹H NMR (600 MHz, D₂O) δ 5.34 (d, *J* = 3.6 Hz, 1H), 4.98 (d, *J* = 9.2 Hz, 1H), 4.56 (d, *J* = 7.8 Hz, 1H), 4.26 (d, *J* = 6.7 Hz, 1H), 3.96 (dd, *J* = 12.2, 2.1 Hz, 1H), 3.94 – 3.86 (m, 2H), 3.86 – 3.57 (m, 13H), 3.46 (t, *J* = 9.3 Hz, 1H), 2.28 – 2.18 (m, 2H), 2.10 – 2.04 (m, 2H), 1.84 (td, *J* = 7.5, 1.6 Hz, 2H), 1.71 (t, *J* = 7.2 Hz, 2H), 1.27 (d, *J* = 6.6 Hz, 3H); ¹³C NMR (151 MHz, D₂O) δ 176.5, 100.2, 99.3, 79.2, 76.8, 76.2, 75.2, 75.1, 73.6, 71.6, 71.5, 69.6, 69.1, 68.1, 66.9, 61.1, 59.9, 30.9, 29.7, 28.6, 27.8, 15.2, 12.4; HR-ESI-MS (*m/z*): calcd for C₂₆H₄₀N₃O₁₅⁻ (*M*-H)⁻ 634.2459, found 634.2443.

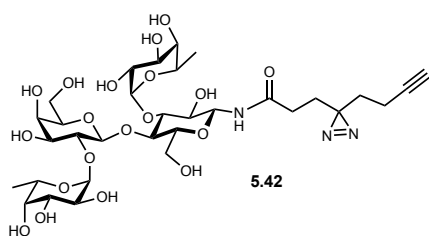


N-((2R,3R,4R,5S,6R)-5-(((2S,3R,4S,5S,6R)-4-(((2S,3R,4R,5S,6R)-3-acetamido-5-hydroxy-6-(hydroxymethyl)-4-(((2R,3R,4S,5R,6R)-3,4,5-trihydroxy-6-(hydroxymethyl)tetrahydro-2H-pyran-2-yl)oxy)tetrahydro-2H-pyran-2-yl)oxy)-3,5-dihydroxy-6-(hydroxymethyl)tetrahydro-2H-pyran-2-yl)oxy)-3,4-dihydroxy-6-(hydroxymethyl)tetrahydro-2H-pyran-2-yl)-3-(3-(but-3-yn-1-yl)-3H-diazirin-3-yl)propanamid (5.40): 14%; ^1H NMR (600 MHz, D_2O) δ 4.99 (d, $J = 9.3$ Hz, 1H), 4.74 (d, $J = 8.5$ Hz, 1H), 4.46 (dd, $J = 7.8, 5.7$ Hz, 2H), 4.16 (d, $J = 3.4$ Hz, 1H), 3.97 – 3.88 (m, 4H), 3.86 – 3.47 (m, 18H), 3.44 (t, $J = 9.1$ Hz, 1H), 2.26 – 2.17 (m, 2H), 2.06 (t, $J = 7.2$ Hz, 2H), 2.04 (s, 3H), 1.84 – 1.81 (m, 2H), 1.70 (t, $J = 7.2$ Hz, 2H); ^{13}C NMR (151 MHz, D_2O) δ 176.4, 175.0, 103.5, 102.8, 102.5, 82.0, 81.9, 79.1, 77.7, 76.3, 75.3, 75.2, 75.1, 74.9, 72.4, 71.4, 70.7, 70.0, 68.5, 68.4, 68.3, 61.0, 61.0, 60.5, 59.8, 54.7, 31.5, 31.1, 30.9, 29.7, 28.6, 27.8, 22.2, 12.4; HR-ESI-MS (m/z): calcd for $\text{C}_{34}\text{H}_{53}\text{N}_4\text{O}_{21}^-$ ($\text{M}-\text{H}$) $^-$ 853.3202, found 853.3181.

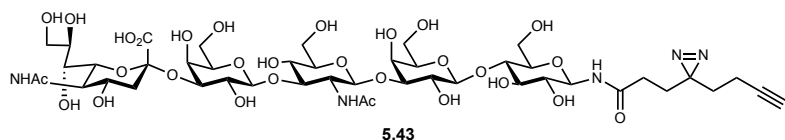


N-((2R,3R,4R,5S,6R)-5-(((2S,3R,4S,5S,6R)-4-(((2S,3R,4R,5S,6R)-3-acetamido-4,5-dihydroxy-6-(hydroxymethyl)tetrahydro-2H-pyran-2-yl)oxy)-3,5-dihydroxy-6-(hydroxymethyl)tetrahydro-2H-pyran-2-yl)oxy)-3,4-dihydroxy-6-(hydroxymethyl)tetrahydro-2H-pyran-2-yl)-3-(3-(but-3-yn-1-yl)-3H-diazirin-3-yl)propanamide (5.41): 49%; ^1H NMR (600 MHz, D_2O) δ 4.99 (d, $J = 9.3$ Hz, 1H), 4.69

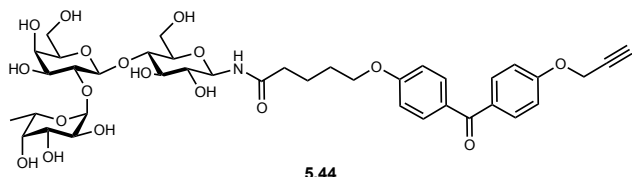
(d, $J = 8.4$ Hz, 1H), 4.46 (d, $J = 7.9$ Hz, 1H), 4.16 (d, $J = 3.4$ Hz, 1H), 3.97 – 3.88 (m, 2H), 3.84 – 3.66 (m, 11H), 3.63 – 3.54 (m, 2H), 3.51 – 3.41 (m, 4H), 2.25-2.18 (m, 2H), 2.07-2.05 (m, 5H), 1.82 (t, $J = 7.5$ Hz, 2H), 1.70 (t, $J = 7.2$ Hz, 2H); ^{13}C NMR (151 MHz, D_2O) δ 176.4, 175.0, 102.8, 81.9, 79.1, 77.6, 76.3, 75.6, 75.1, 74.9, 73.5, 71.4, 70.0, 69.7, 68.4, 61.0, 60.5, 59.8, 55.6, 30.9, 29.7, 28.6, 27.8, 22.1, 12.4; HR-ESI-MS (m/z): calcd for $\text{C}_{28}\text{H}_{43}\text{N}_4\text{O}_{16}^-$ (M-H) $^-$ 691.2674, found 691.2653.



3-(3-(but-3-yn-1-yl)-3H-diazirin-3-yl)-N-((2R,3R,4R,5R,6R)-5-(((2S,3R,4S,5R,6R)-4,5-dihydroxy-6-(hydroxymethyl)-3-(((2S,3S,4R,5S,6S)-3,4,5-trihydroxy-6-methyltetrahydro-2H-pyran-2-yl)oxy)tetrahydro-2H-pyran-2-yl)oxy)-3-hydroxy-6-(hydroxymethyl)-4-(((2S,3S,4R,5S,6S)-3,4,5-trihydroxy-6-methyltetrahydro-2H-pyran-2-yl)oxy)tetrahydro-2H-pyran-2-yl)propenamide (5.42): 17%; ^1H NMR (600 MHz, D_2O) δ 5.47 (d, $J = 4.0$ Hz, 1H), 5.29 (d, $J = 3.6$ Hz, 1H), 4.97 (d, $J = 9.3$ Hz, 1H), 4.88 (q, $J = 6.6$ Hz, 2H), 4.52 (d, $J = 7.8$ Hz, 1H), 4.27 (q, $J = 6.7$ Hz, 1H), 3.99 (dd, $J = 10.3, 3.5$ Hz, 2H), 3.93 – 3.70 (m, 11H), 3.67 – 3.57 (m, 3H), 3.57 – 3.51 (m, 1H), 2.25-2.18 (m, 2H), 2.07-2.03 (m, 2H), 1.82 (t, $J = 7.9$ Hz, 2H), 1.79 – 1.66 (m, 2H), 1.30 (d, $J = 6.7$ Hz, 3H), 1.26 (d, $J = 6.6$ Hz, 3H); ^{13}C NMR (151 MHz, D_2O) δ 176.5, 100.1, 99.3, 98.3, 79.3, 77.8, 77.2, 76.3, 74.9, 73.6, 73.1, 72.2, 72.0, 71.6, 69.7, 69.2, 68.7, 68.2, 68.0, 66.9, 66.6, 61.5, 59.7, 30.9, 30.8, 29.8, 28.6, 28.2, 27.8, 15.4, 15.4, 12.4; HR-ESI-MS (m/z): calcd for $\text{C}_{32}\text{H}_{50}\text{N}_3\text{O}_{19}^-$ (M-H) $^-$ 780.3039, found 780.3008.



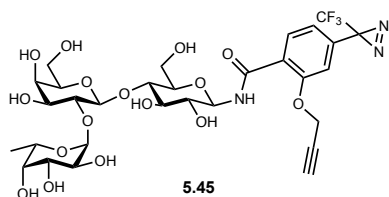
(2S,4S,5R,6R)-5-acetamido-2-(((2R,3R,4S,5S,6R)-2-(((2S,3R,4R,5S,6R)-3-acetamido-2-(((2S,3R,4S,5S,6R)-2-(((2R,3S,4R,5R,6R)-6-(3-(3-(but-3-yn-1-yl)-3H-diazirin-3-yl)propanamido)-4,5-dihydroxy-2-(hydroxymethyl)tetrahydro-2H-pyran-3-yl)oxy)-3,5-dihydroxy-6-(hydroxymethyl)tetrahydro-2H-pyran-4-yl)oxy)-5-hydroxy-6-(hydroxymethyl)tetrahydro-2H-pyran-4-yl)oxy)-3,5-dihydroxy-6-(hydroxymethyl)tetrahydro-2H-pyran-4-yl)oxy)-4-hydroxy-6-((1R,2R)-1,2,3-trihydroxypropyl)tetrahydro-2H-pyran-2-carboxylic acid (5.43): 22%; ^1H NMR (600 MHz, D_2O) δ 4.99 (d, $J = 9.2$ Hz, 1H), 4.75 (d, $J = 8.4$ Hz, 2H), 4.52 (d, $J = 7.9$ Hz, 1H), 4.46 (d, $J = 7.8$ Hz, 1H), 4.16 (d, $J = 3.4$ Hz, 1H), 4.09 (dd, $J = 9.8, 3.2$ Hz, 1H), 3.96 – 3.47 (m, 22H), 3.44 (t, $J = 8.9$ Hz, 1H), 3.39 (t, $J = 7.0$ Hz, 1H), 2.77 (dd, $J = 12.4, 4.6$ Hz, 1H), 2.41 (t, $J = 7.0$ Hz, 1H), 2.25-2.18 (m, 1H), 2.13 (t, $J = 7.5$ Hz, 1H), 2.12 – 2.02 (m, 6H), 2.01 (t, $J = 7.6$ Hz, 1H), 1.85 – 1.66 (m, 7H); ^{13}C NMR (151 MHz, D_2O) δ 176.4, 175.0, 174.9, 173.9, 103.4, 102.8, 102.5, 99.6, 82.1, 81.8, 79.1, 77.7, 76.3, 75.6, 75.2, 75.1, 74.9, 72.8, 71.8, 71.4, 70.0, 69.1, 68.5, 68.4, 68.3, 68.0, 67.2, 62.4, 61.0, 61.0, 60.5, 59.8, 54.6, 51.6, 39.7, 38.7, 30.9, 29.7, 28.6, 27.8, 22.3, 22.0, 12.4, 12.4; HR-ESI-MS (m/z): calcd for $\text{C}_{45}\text{H}_{70}\text{N}_5\text{O}_{29}^-$ ($\text{M}-\text{H}$) $^-$ 1144.4156, found 1144.4113.



5.44

N-((2R,3R,4R,5S,6R)-5-(((2S,3R,4S,5R,6R)-4,5-dihydroxy-6-(hydroxymethyl)-3-(((2S,3S,4R,5S,6S)-3,4,5-trihydroxy-6-methyltetrahydro-2H-pyran-2-yl)oxy)tetrahydro-2H-pyran-2-yl)oxy)-3,4-dihydroxy-6-(hydroxymethyl)tetrahydro-2H-pyran-2-yl)-5-(4-(4-(prop-2-yn-1-yloxy)benzoyl)phenoxy)pentanamide (5.44):

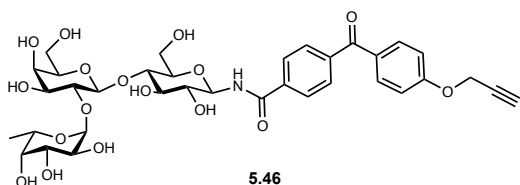
14%; ¹H NMR (600 MHz, MeOD) δ 7.79 – 7.74 (m, 4H), 7.12 (d, *J* = 8.8 Hz, 2H), 7.07 – 7.03 (m, 2H), 5.26 (d, *J* = 3.6 Hz, 1H), 4.50 (d, *J* = 7.1 Hz, 1H), 4.22 – 4.16 (m, 2H), 4.15 – 4.08 (m, 3H), 3.89 – 3.65 (m, 12H), 3.61 – 3.48 (m, 1H), 3.35 (t, *J* = 9.2 Hz, 2H), 2.49 (t, *J* = 7.0 Hz, 1H), 2.36 (q, *J* = 7.4 Hz, 2H), 2.25 (t, *J* = 7.4 Hz, 1H), 1.91 – 1.83 (m, 3H), 1.26 – 1.19 (m, 3H), 0.10 (d, *J* = 3.3 Hz, 2H); ¹³C NMR (151 MHz, MeOD) δ 210.1, 162.6, 133.4, 133.2, 132.4, 115.6, 115.2, 101.7, 78.7, 77.4, 75.4, 73.6, 71.7, 69.0, 68.2, 62.6, 56.8, 30.7, 29.7, 23.1, 16.7; HR-ESI-MS (*m/z*): calcd for C₃₉H₅₀NO₁₈⁻ (M-H)⁻ 820.3028, found 820.3016.



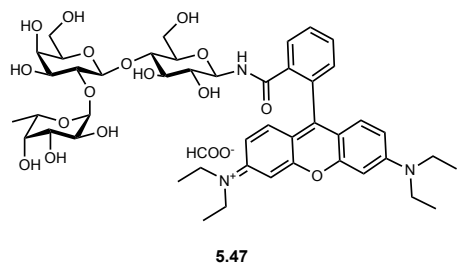
5.45

N-((2R,3R,4R,5S,6R)-5-(((2S,3R,4S,5R,6R)-4,5-dihydroxy-6-(hydroxymethyl)-3-(((2S,3S,4R,5S,6S)-3,4,5-trihydroxy-6-methyltetrahydro-2H-pyran-2-yl)oxy)tetrahydro-2H-pyran-2-yl)oxy)-3,4-dihydroxy-6-(hydroxymethyl)tetrahydro-2H-pyran-2-yl)-2-(prop-2-yn-1-yloxy)-4-(3-(trifluoromethyl)-3H-diazirin-3-

yl)benzamide (5.45): 12%; ^1H NMR (600 MHz, MeOD) δ 8.02 – 7.96 (m, 1H), 7.11 – 7.00 (m, 1H), 6.96 (d, $J = 7.6$ Hz, 1H), 5.27 (td, $J = 7.8, 7.1, 3.7$ Hz, 1H), 5.15 – 5.08 (m, 1H), 4.98 (d, $J = 2.2$ Hz, 1H), 4.54 – 4.45 (m, 3H), 4.24 – 4.15 (m, 2H), 3.97 – 3.44 (m, 20H), 3.22 – 3.08 (m, 2H), 1.26 – 1.18 (m, 5H); ^{13}C NMR (151 MHz, MeOD) δ 133.2, 120.7, 120.2, 113.6, 102.5, 101.8, 78.9, 78.7, 78.2, 77.3, 77.0, 75.4, 73.6, 71.7, 70.7, 68.3, 62.5, 58.0, 57.7, 30.8, 23.7, 16.7, 14.4; HR-ESI-MS (m/z): calcd for $\text{C}_{30}\text{H}_{37}\text{F}_3\text{N}_3\text{O}_{16}^-$ (M-H) $^-$ 752.2126, found 752.2113.



N-((2R,3R,4R,5S,6R)-5-(((2S,3R,4S,5R,6R)-4,5-dihydroxy-6-(hydroxymethyl)-3-(((2S,3S,4R,5S,6S)-3,4,5-trihydroxy-6-methyltetrahydro-2H-pyran-2-yl)oxy)tetrahydro-2H-pyran-2-yl)oxy)-3,4-dihydroxy-6-(hydroxymethyl)tetrahydro-2H-pyran-2-yl)-4-(4-(prop-2-yn-1-yloxy)benzoyl)benzamide (5.46): 43%; ^1H NMR (600 MHz, MeOD) δ 8.04 (t, $J = 8.6$ Hz, 2H), 7.85 – 7.79 (m, 4H), 7.16 – 7.10 (m, 2H), 5.28 (d, $J = 3.7$ Hz, 1H), 5.16 (d, $J = 8.6$ Hz, 1H), 4.53 (d, $J = 7.4$ Hz, 1H), 4.24 – 4.13 (m, 3H), 3.92 – 3.46 (m, 15H), 1.25 (d, $J = 6.6$ Hz, 3H), 1.21 (t, $J = 6.4$ Hz, 2H); ^{13}C NMR (151 MHz, MeOD) δ 133.5, 133.4, 130.5, 130.1, 130.0, 128.7, 115.8, 115.7, 102.4, 101.6, 81.7, 78.6, 77.5, 77.0, 75.3, 73.5, 73.3, 71.6, 70.5, 68.2, 62.5, 56.8, 16.6; HR-ESI-MS (m/z): calcd for $\text{C}_{35}\text{H}_{42}\text{NO}_{17}^-$ (M-H) $^-$ 748.2453, found 748.2440.



N-(6-(diethylamino)-9-(2-(((2R,3R,4R,5S,6R)-5-(((2S,3R,4S,5R,6R)-4,5-dihydroxy-6-(hydroxymethyl)-3-(((2S,3S,4R,5S,6S)-3,4,5-trihydroxy-6-methyltetrahydro-2H-pyran-2-yl)oxy)tetrahydro-2H-pyran-2-yl)oxy)-3,4-dihydroxy-6-(hydroxymethyl)tetrahydro-2H-pyran-2-yl)carbamoyl)phenyl)-3H-xanthen-3-ylidene)-N-ethylethanaminium chloride (5.47): 13%; $^1\text{H NMR}$ (600 MHz, MeOD) δ 7.88 (d, $J = 7.6$ Hz, 1H), 7.55 (dtd, $J = 29.3, 7.5, 1.1$ Hz, 2H), 7.06 (d, $J = 7.7$ Hz, 1H), 6.58 (d, $J = 8.9$ Hz, 1H), 6.51 (d, $J = 8.8$ Hz, 1H), 6.43 – 6.30 (m, 4H), 5.06 (d, $J = 3.7$ Hz, 1H), 4.59 (t, $J = 9.2$ Hz, 1H), 4.41 (d, $J = 7.3$ Hz, 1H), 3.97 (d, $J = 9.3$ Hz, 1H), 3.77 – 3.56 (m, 12H), 3.50 (q, $J = 14.2, 7.2$ Hz, 2H), 3.42-3.34 (m, 5H), 3.20 (t, $J = 9.1$ Hz, 2H), 1.16 (t, $J = 7.0$ Hz, 9H), 1.09 (d, $J = 6.6$ Hz, 3H), 0.90 (t, $J = 6.9$ Hz, 3H). LR-ESI-MS (m/z): calcd for $\text{C}_{46}\text{H}_{62}\text{N}_3\text{O}_{16}^+$ ($\text{M}-(\text{HCOO}^-)^+$) 912.4, found 912.2.

Bacterial strains and culture conditions

GBS strain *S. agalactiae* GB590 (clinical isolate, Shannon Manning, Michigan State) was grown on tryptic soy agar plates supplemented with 5% sheep blood (blood agar plates) at 37 °C in ambient air overnight. Strains were sub-cultured from blood agar plates into 5 mL of Todd-Hewitt broth (THB) and incubated under shaking conditions at 180 rpm at 37 °C in ambient air overnight. Following overnight incubation, bacterial density was quantified through absorbance readings at 600 nm (OD_{600}) using a Promega GloMax-

Multi Detection System plate reader. Bacterial numbers were determined using the predetermined coefficient of $1 \text{ OD}_{600} = 10^9 \text{ CFU mL}^{-1}$.

Bacterial growth and viability assays

Test strains were grown as described above and used to inoculate fresh THB or THB supplemented with $\sim 5 \text{ mg mL}^{-1}$ HMO or HMO probe. Inoculation was completed at a multiplicity of infection (MOI) of 5×10^5 CFUs per $100 \mu\text{L}$ of growth medium in 96-well tissue culture treated, sterile polystyrene plates (Corning, Inc.). Cultures were grown under static conditions at $37 \text{ }^\circ\text{C}$ in ambient air. Growth was quantified through spectrophotometric reading at OD_{600} . Viability was assessed through serial dilution and plating onto blood agar plates followed by quantification of viable CFU mL^{-1} .

Bacterial biofilm assays

Test strains were grown as described above and used to inoculate fresh THB or THB supplemented with $\sim 5 \text{ mg mL}^{-1}$ HMO. Inoculation was performed at a multiplicity of infection (MOI) of 5×10^5 CFUs per $100 \mu\text{L}$ of growth medium in 96-well tissue culture treated, sterile polystyrene plates (Corning, Inc.). Cultures were incubated under static conditions at $37 \text{ }^\circ\text{C}$ in ambient air for 24 h. Following spectrophotometric reading at OD_{600} , culture media was removed, and the wells were gently washed once with phosphate-buffered saline (PBS, pH 7.4) to remove non-adherent cells. Adherent cells were stained

with a 10% crystal violet solution for 10 min. Excess stain was discarded, and the wells were gently washed with PBS followed by drying at room temperature for 30 min. The crystal violet stain was solubilized with an 80% ethanol/20% acetone solution and biofilm formation quantified through spectrophotometric reading at OD₅₆₀.

Statistical analysis

All data shown signify three independent experiments each with three technical replicates. Data are expressed as the mean \pm SEM. Statistical analyses were performed in GraphPad Prism Software v. 7.0c. Statistical significance for biofilm production was determined using one-way ANOVA with post hoc Dunnett's multiple comparison test comparing biofilm production in the presence of HMOs to biofilm production in media alone.

5.11 References

1. This chapter is adapted from "Bioorthogonal human milk oligosaccharide probes for antimicrobial target identification within *Streptococcus agalactiae*" published in Carbohydrate Research and "Two-step conversion of unprotected oligosaccharides to generate bioorthogonal oligosaccharide tool compounds" published in MethodsX and has been reproduced with the permission of the respective publishers and my co-author Steven D. Townsend. Schuyler A. Chambers and Steven D. Townsend. (2020). "Bioorthogonal human milk oligosaccharide probes for antimicrobial target identification within *Streptococcus agalactiae*." Carbohydrate Research. 488: 107895. Schuyler A. Chambers and Steven D. Townsend. (2020). "Two-step conversion of unprotected oligosaccharides to generate bioorthogonal oligosaccharide tool compounds." MethodsX. 100996.
2. Kapoor, G.; Saigal, S.; Elongavan, A., Action and resistance mechanisms of antibiotics: A guide for clinicians. *J Anaesthesiol Clin Pharmacol* **2017**, 33 (3), 300-305.

3. Hooper, D. C., Mechanisms of Action of Antimicrobials: Focus on Fluoroquinolones. *Clinical Infectious Diseases* **2001**, 32 (Supplement_1), S9-S15.
4. Yocum, R. R.; Rasmussen, J. R.; Strominger, J. L., The mechanism of action of penicillin. Penicillin acylates the active site of *Bacillus stearothermophilus* D-alanine carboxypeptidase. *J Biol Chem* **1980**, 255 (9), 3977-86.
5. Gleckman, R.; Blagg, N.; Joubert, D. W., Trimethoprim: mechanisms of action, antimicrobial activity, bacterial resistance, pharmacokinetics, adverse reactions, and therapeutic indications. *Pharmacotherapy* **1981**, 1 (1), 14-20.
6. Dhawan, V. K.; Thadepalli, H., Clindamycin: a review of fifteen years of experience. *Reviews of infectious diseases* **1982**, 4 (6), 1133-53.
7. Gonzalez, L. S., 3rd; Spencer, J. P., Aminoglycosides: a practical review. *Am Fam Physician* **1998**, 58 (8), 1811-20.
8. Aldred, K. J.; Kerns, R. J.; Osheroff, N., Mechanism of quinolone action and resistance. *Biochemistry* **2014**, 53 (10), 1565-1574.
9. Schenone, M.; Dančík, V.; Wagner, B. K.; Clemons, P. A., Target identification and mechanism of action in chemical biology and drug discovery. *Nature chemical biology* **2013**, 9 (4), 232-240.
10. Ziegler, S.; Pries, V.; Hedberg, C.; Waldmann, H., Target Identification for Small Bioactive Molecules: Finding the Needle in the Haystack. *Angewandte Chemie International Edition* **2013**, 52 (10), 2744-2792.
11. Su, Y.; Ge, J.; Zhu, B.; Zheng, Y.-G.; Zhu, Q.; Yao, S. Q., Target identification of biologically active small molecules via in situ methods. *Curr Opin Chem Biol* **2013**, 17 (5), 768-775.
12. Chen, X.; Wang, Y.; Ma, N.; Tian, J.; Shao, Y.; Zhu, B.; Wong, Y. K.; Liang, Z.; Zou, C.; Wang, J., Target identification of natural medicine with chemical proteomics approach: probe synthesis, target fishing and protein identification. *Signal Transduction and Targeted Therapy* **2020**, 5 (1), 72.
13. Pan, S.; Zhang, H.; Wang, C.; Yao, S. C.; Yao, S. Q., Target identification of natural products and bioactive compounds using affinity-based probes. *Nat Prod Rep* **2016**, 33 (5), 612-20.
14. Ge, S.-S.; Chen, B.; Wu, Y.-Y.; Long, Q.-S.; Zhao, Y.-L.; Wang, P.-Y.; Yang, S., Current advances of carbene-mediated photoaffinity labeling in medicinal chemistry. *RSC Advances* **2018**, 8 (51), 29428-29454.
15. Smith, E.; Collins, I., Photoaffinity labeling in target- and binding-site identification. *Future Med Chem* **2015**, 7 (2), 159-183.

16. Murale, D. P.; Hong, S. C.; Haque, M. M.; Lee, J.-S., Photo-affinity labeling (PAL) in chemical proteomics: a handy tool to investigate protein-protein interactions (PPIs). *Proteome Science* **2017**, *15* (1), 14.
17. Mackinnon, A. L.; Taunton, J., Target Identification by Diazirine Photo-Cross-linking and Click Chemistry. *Current protocols in chemical biology* **2009**, *1*, 55-73.
18. Li, Z.; Hao, P.; Li, L.; Tan, C. Y.; Cheng, X.; Chen, G. Y.; Sze, S. K.; Shen, H. M.; Yao, S. Q., Design and synthesis of minimalist terminal alkyne-containing diazirine photo-crosslinkers and their incorporation into kinase inhibitors for cell- and tissue-based proteome profiling. *Angew Chem Int Ed Engl* **2013**, *52* (33), 8551-6.
19. Pan, S.; Jang, S. Y.; Wang, D.; Liew, S. S.; Li, Z.; Lee, J. S.; Yao, S. Q., A Suite of "Minimalist" Photo-Crosslinkers for Live-Cell Imaging and Chemical Proteomics: Case Study with BRD4 Inhibitors. *Angew Chem Int Ed Engl* **2017**, *56* (39), 11816-11821.
20. Li, Z.; Wang, D.; Li, L.; Pan, S.; Na, Z.; Tan, C. Y.; Yao, S. Q., "Minimalist" cyclopropene-containing photo-cross-linkers suitable for live-cell imaging and affinity-based protein labeling. *J Am Chem Soc* **2014**, *136* (28), 9990-8.
21. Wu, H.; Kohler, J., Photocrosslinking probes for capture of carbohydrate interactions. *Current Opinion in Chemical Biology* **2019**, *53*, 173-182.
22. Rowland, M. M.; Bostic, H. E.; Gong, D.; Speers, A. E.; Lucas, N.; Cho, W.; Cravatt, B. F.; Best, M. D., Phosphatidylinositol 3,4,5-trisphosphate activity probes for the labeling and proteomic characterization of protein binding partners. *Biochemistry* **2011**, *50* (51), 11143-11161.
23. Cisar, J. S.; Cravatt, B. F., Fully Functionalized Small-Molecule Probes for Integrated Phenotypic Screening and Target Identification. *Journal of the American Chemical Society* **2012**, *134* (25), 10385-10388.
24. Sumranjit, J.; Chung, S. J., Recent advances in target characterization and identification by photoaffinity probes. *Molecules (Basel, Switzerland)* **2013**, *18* (9), 10425-10451.
25. Yamamoto, N.; Bernardi, F.; Bottoni, A.; Olivucci, M.; Robb, M. A.; Wilsey, S., Mechanism of Carbene Formation from the Excited States of Diazirine and Diazomethane: An MC-SCF Study. *Journal of the American Chemical Society* **1994**, *116* (5), 2064-2074.
26. Narayanan, A.; Jones, L. H., Sulfonyl fluorides as privileged warheads in chemical biology. *Chemical Science* **2015**, *6* (5), 2650-2659.
27. Nguyen, S. S.; Prescher, J. A., Developing bioorthogonal probes to span a spectrum of reactivities. *Nature Reviews Chemistry* **2020**, *4* (9), 476-489.

28. Agard, N. J.; Prescher, J. A.; Bertozzi, C. R., A Strain-Promoted [3 + 2] Azide–Alkyne Cycloaddition for Covalent Modification of Biomolecules in Living Systems. *J Am Chem Soc* **2004**, *126* (46), 15046-15047.
29. Sletten, E. M.; Bertozzi, C. R., Bioorthogonal chemistry: fishing for selectivity in a sea of functionality. *Angewandte Chemie (International ed. in English)* **2009**, *48* (38), 6974-6998.
30. Ramil, C. P.; Lin, Q., Bioorthogonal chemistry: strategies and recent developments. *Chemical Communications* **2013**, *49* (94), 11007-11022.
31. Yang, P.; Liu, K., Activity-Based Protein Profiling: Recent Advances in Probe Development and Applications. *ChemBioChem* **2015**, *16* (5), 712-724.
32. Wang, S.; Tian, Y.; Wang, M.; Wang, M.; Sun, G.-B.; Sun, X.-B., Advanced Activity-Based Protein Profiling Application Strategies for Drug Development. *Front Pharmacol* **2018**, *9*, 353-353.
33. Paulson, J. C.; Blixt, O.; Collins, B. E., Sweet spots in functional glycomics. *Nat Chem Biol* **2006**, *2* (5), 238-48.
34. Williams, S. J.; Davies, G. J., Protein-carbohydrate interactions: learning lessons from nature. *Trends in Biotechnology* **2001**, *19* (9), 356-362.
35. Zhang, Y.; Luo, S.; Tang, Y.; Yu, L.; Hou, K.-Y.; Cheng, J.-P.; Zeng, X.; Wang, P. G., Carbohydrate–Protein Interactions by “Clicked” Carbohydrate Self-Assembled Monolayers. *Analytical Chemistry* **2006**, *78* (6), 2001-2008.
36. Wittmann, V.; Pieters, R. J., Bridging lectin binding sites by multivalent carbohydrates. *Chemical Society Reviews* **2013**, *42* (10), 4492-4503.
37. Crocker, P. R.; Paulson, J. C.; Varki, A., Siglecs and their roles in the immune system. *Nature Reviews Immunology* **2007**, *7* (4), 255-266.
38. Crocker, P. R.; Varki, A., Siglecs in the immune system. *Immunology* **2001**, *103* (2), 137-145.
39. Bochner, B. S.; Zimmermann, N., Role of siglecs and related glycan-binding proteins in immune responses and immunoregulation. *J Allergy Clin Immunol* **2015**, *135* (3), 598-608.
40. Craft, K. M.; Thomas, H. C.; Townsend, S. D., Sialylated variants of lacto-N-tetraose exhibit antimicrobial activity against Group B Streptococcus. *Org Biomol Chem* **2018**, *17* (7), 1893-1900.
41. Craft, K. M.; Thomas, H. C.; Townsend, S. D., Interrogation of Human Milk Oligosaccharide Fucosylation Patterns for Antimicrobial and Antibiofilm Trends in Group B Streptococcus. *ACS Infect Dis* **2018**, *4*, 1755-1765.

42. Bond, M. R.; Zhang, H.; Vu, P. D.; Kohler, J. J., Photocrosslinking of glycoconjugates using metabolically incorporated diazirine-containing sugars. *Nature Protocols* **2009**, *4*, 1044.
43. McCombs, J. E.; Zou, C.; Parker, R. B.; Cairo, C. W.; Kohler, J. J., Enhanced Cross-Linking of Diazirine-Modified Sialylated Glycoproteins Enabled through Profiling of Sialidase Specificities. *ACS Chemical Biology* **2016**, *11* (1), 185-192.
44. Likhoshesterov, L. M.; Novikova, O. S.; Derevitskaja, V. A.; Kochetkov, N. K., A new simple synthesis of amino sugar β -d-glycosylamines. *Carb Res* **1986**, *146* (1), C1-C5.
45. Kallin, E.; Lönn, H.; Norberg, T.; Elofsson, M., Derivatization Procedures for Reducing Oligosaccharides, Part 3: Preparation of Oligosaccharide Glycosylamines, and Their Conversion Into Glycosaccharide - Acrylamide Copolymers. *Journal of Carbohydrate Chemistry* **1989**, *8* (4), 597-611.
46. Liu, X.; Zhang, G.; Chan, K.; Li, J., Microwave-assisted Kochetkov amination followed by permanent charge derivatization: a facile strategy for glycomics. *Chem Commun (Camb)* **2010**, *46* (39), 7424-6.
47. Moore, R. E.; Craft, K. M.; Xu, L. L.; Chambers, S. A.; Nguyen, J. M.; Marion, K. C.; Gaddy, J. A.; Townsend, S. D., Leveraging Stereoelectronic Effects in Biofilm Eradication: Synthetic β -Amino Human Milk Oligosaccharides Impede Microbial Adhesion As Observed by Scanning Electron Microscopy. *The Journal of Organic Chemistry* **2020**.
48. Lemieux, R. U.; Morgan, A. R., The Abnormal Conformations of Pyridinium α -glycopyranosides. *Canadian Journal of Chemistry* **1965**, *43* (8), 2205-2213.
49. Paulsen, H.; Györgydeák, Z.; Friedmann, M., Konformationsanalyse, V. Einfluß des anomeren und inversen anomeren Effektes auf Konformationsgleichgewichte von N-substituierten N-Pentopyranosiden. *Chemische Berichte* **1974**, *107* (5), 1590-1613.
50. West, A. C.; Schuerch, C., Reverse anomeric effect and the synthesis of α -glycosides. *Journal of the American Chemical Society* **1973**, *95* (4), 1333-1335.
51. Chambers, S. A.; Townsend, S. D., Bioorthogonal human milk oligosaccharide probes for antimicrobial target identification within *Streptococcus agalactiae*. *Carbohydr Res* **2020**, *488*, 107895.
52. Chambers, S. A.; Townsend, S. D., Two-step conversion of unprotected oligosaccharides to generate bioorthogonal oligosaccharide tool compounds. *MethodsX* **2020**, 100996.
53. Huckin, S. N.; Weiler, L., Alkylation of dianions of β -keto esters. *J Am Chem Soc* **1974**, *96* (4), 1082-1087.

54. Villadsen, K.; Martos-Maldonado, M. C.; Jensen, K. J.; Thygesen, M. B., Chemoselective Reactions for the Synthesis of Glycoconjugates from Unprotected Carbohydrates. *ChemBioChem* **2017**, *18* (7), 574-612.
55. Chambers, S. A.; Townsend, S. D., Like mother, like microbe: human milk oligosaccharide mediated microbiome symbiosis. *Biochemical Society Transactions* **2020**, *48* (3), 1139-1151.
56. Bode, L., The functional biology of human milk oligosaccharides. *Early Hum Dev* **2015**, *91* (11), 619-622.
57. Kling, D. E.; Madoff, L. C.; Michel, J. L., Subcellular fractionation of group B Streptococcus. *BioTechniques* **1999**, *27* (1), 24-6, 28.
58. Schirmer, E. C.; Yates, J. R., 3rd; Gerace, L., MudPIT: A powerful proteomics tool for discovery. *Discovery medicine* **2003**, *3* (18), 38-9.
59. Tsakou, F.; Jersie-Christensen, R.; Jenssen, H.; Mojsoska, B., The Role of Proteomics in Bacterial Response to Antibiotics. *Pharmaceuticals (Basel)* **2020**, *13* (9), 214.
60. Ong, S.-E.; Mann, M., A practical recipe for stable isotope labeling by amino acids in cell culture (SILAC). *Nature Protocols* **2006**, *1* (6), 2650-2660.
61. Chen, X.; Wei, S.; Ji, Y.; Guo, X.; Yang, F., Quantitative proteomics using SILAC: Principles, applications, and developments. *Proteomics* **2015**, *15* (18), 3175-92.

Appendix A5

Data and NMR spectra relevant to Chapter 5

Figure A5.1 ¹H NMR (600 MHz, D₂O) of 5.28

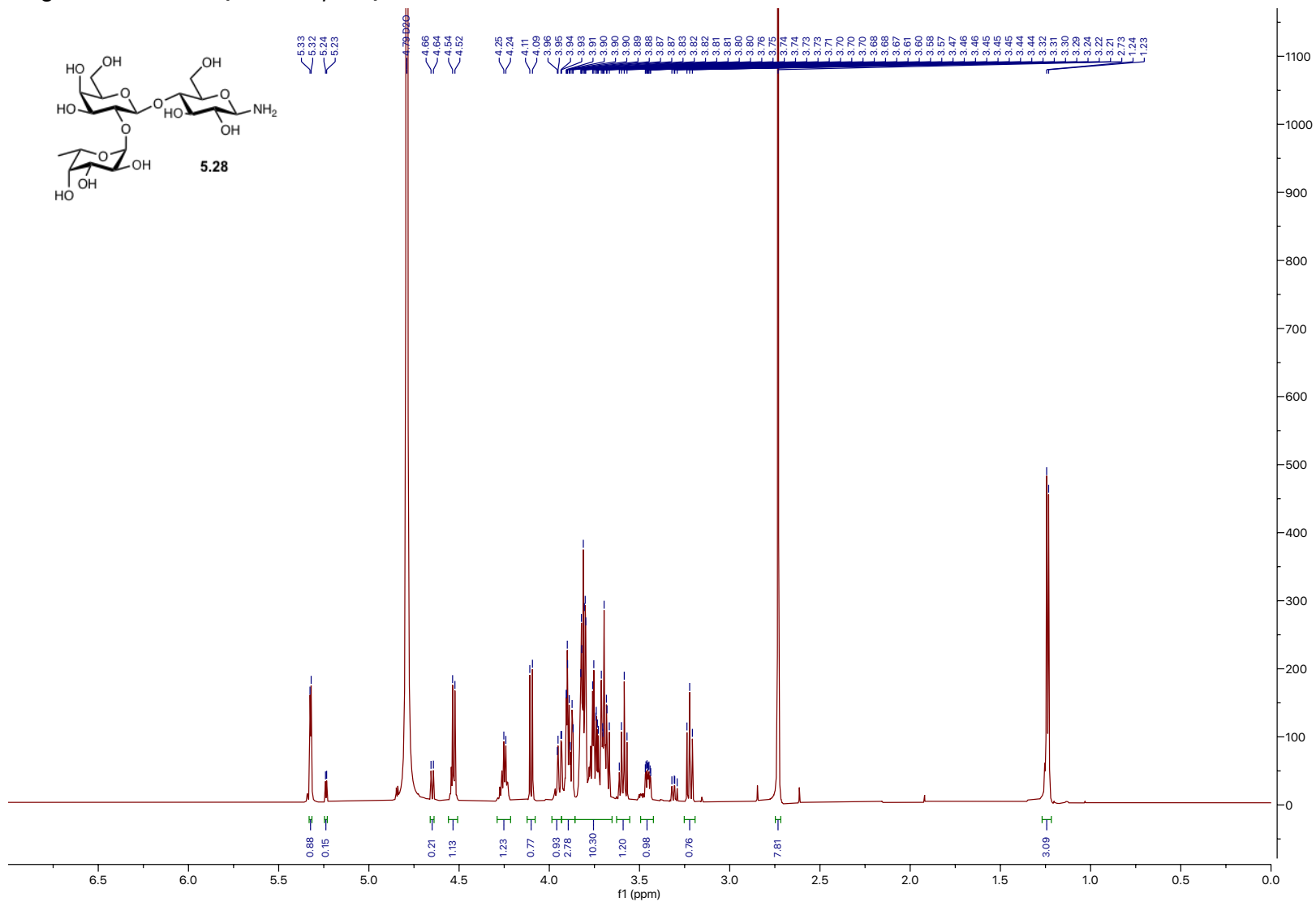


Figure A5.2 ^{13}C NMR (151 MHz, D_2O) of 5.28

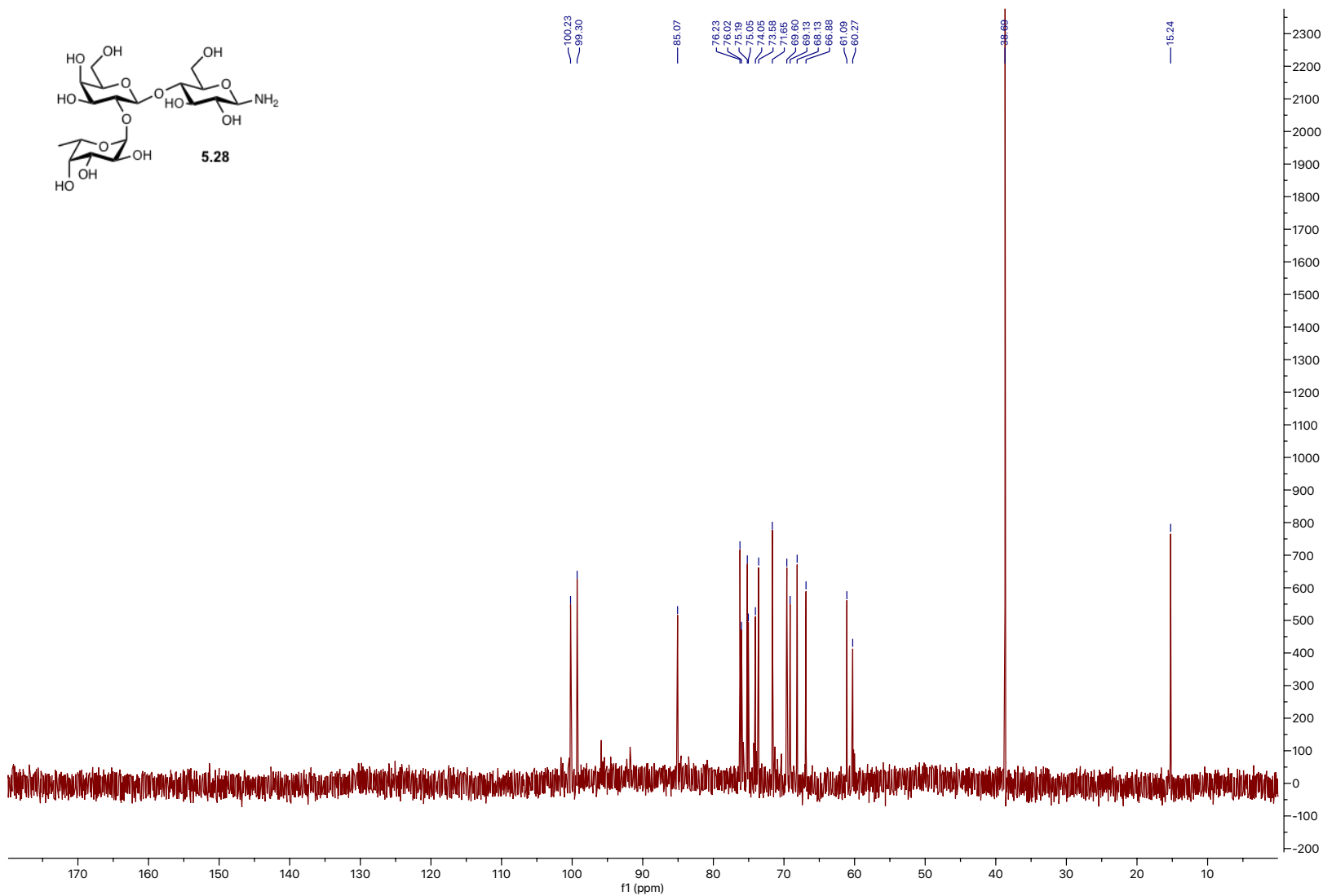


Figure A5.3 ¹H NMR (600 MHz, D₂O) of 5.29

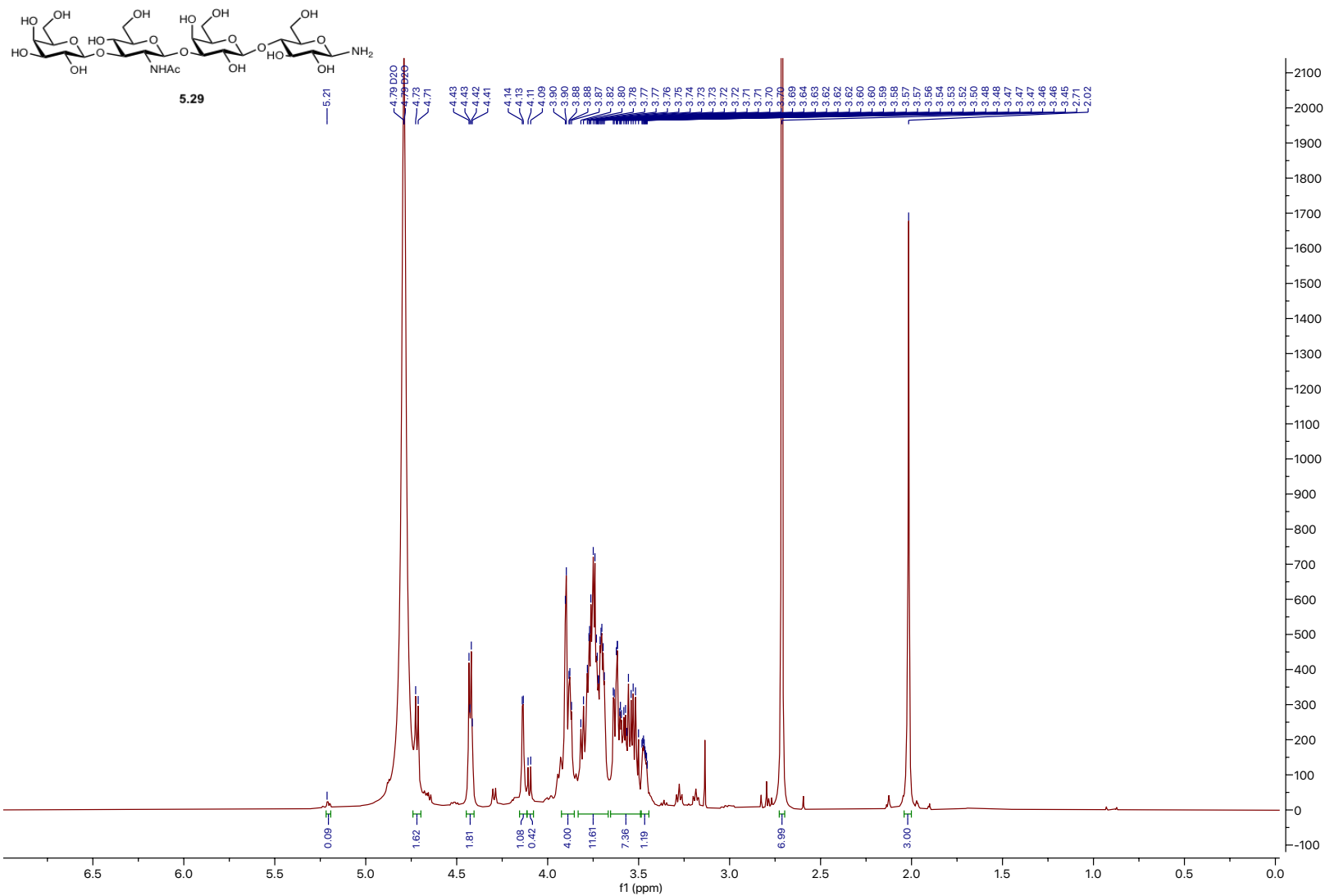
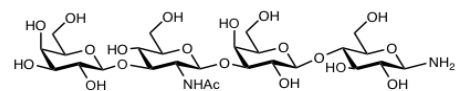


Figure A5.4 ^{13}C NMR (151 MHz, D_2O) of 5.29



5.29

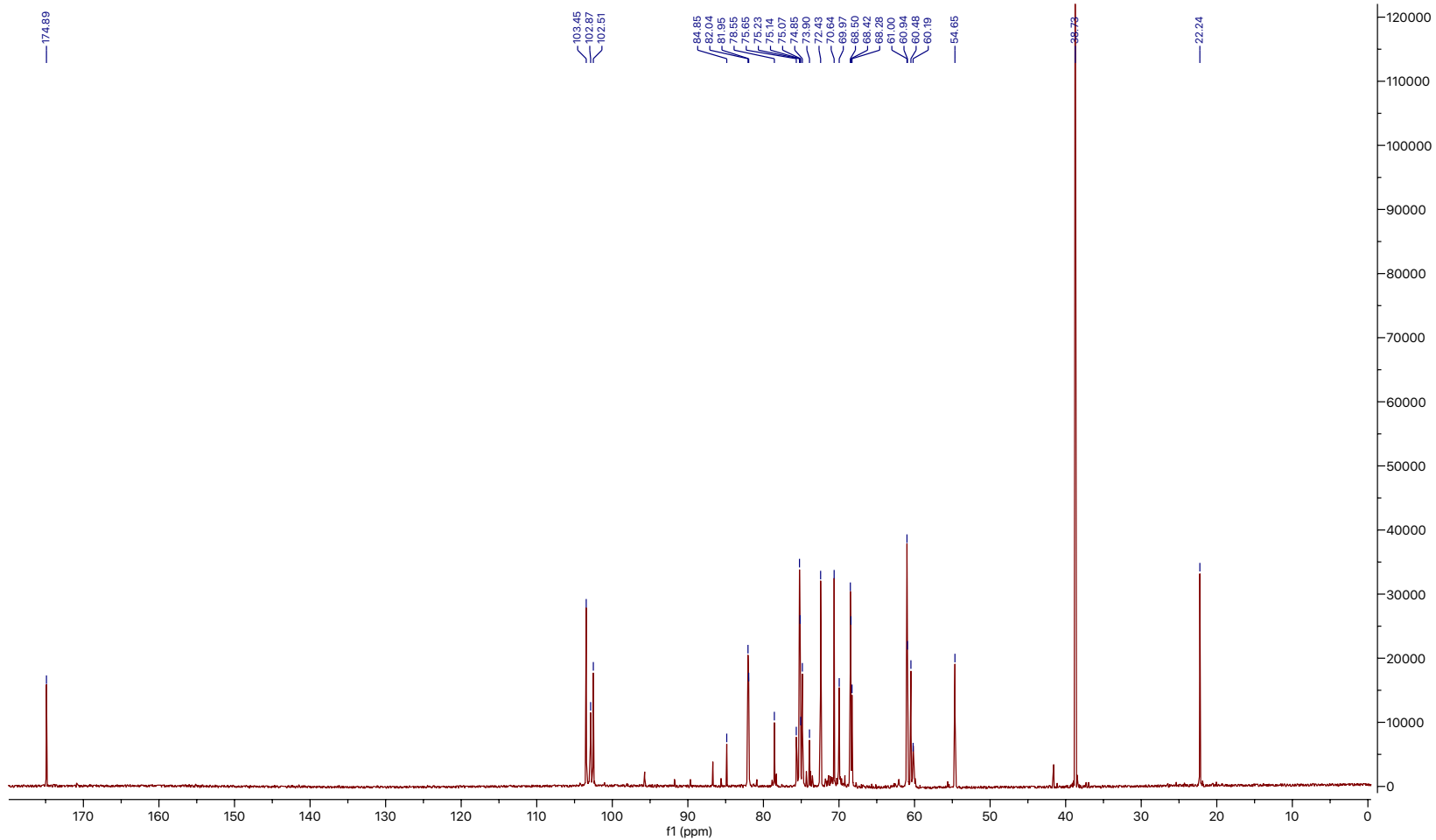


Figure A5.5 ¹H NMR (600 MHz, D₂O) of 5.30

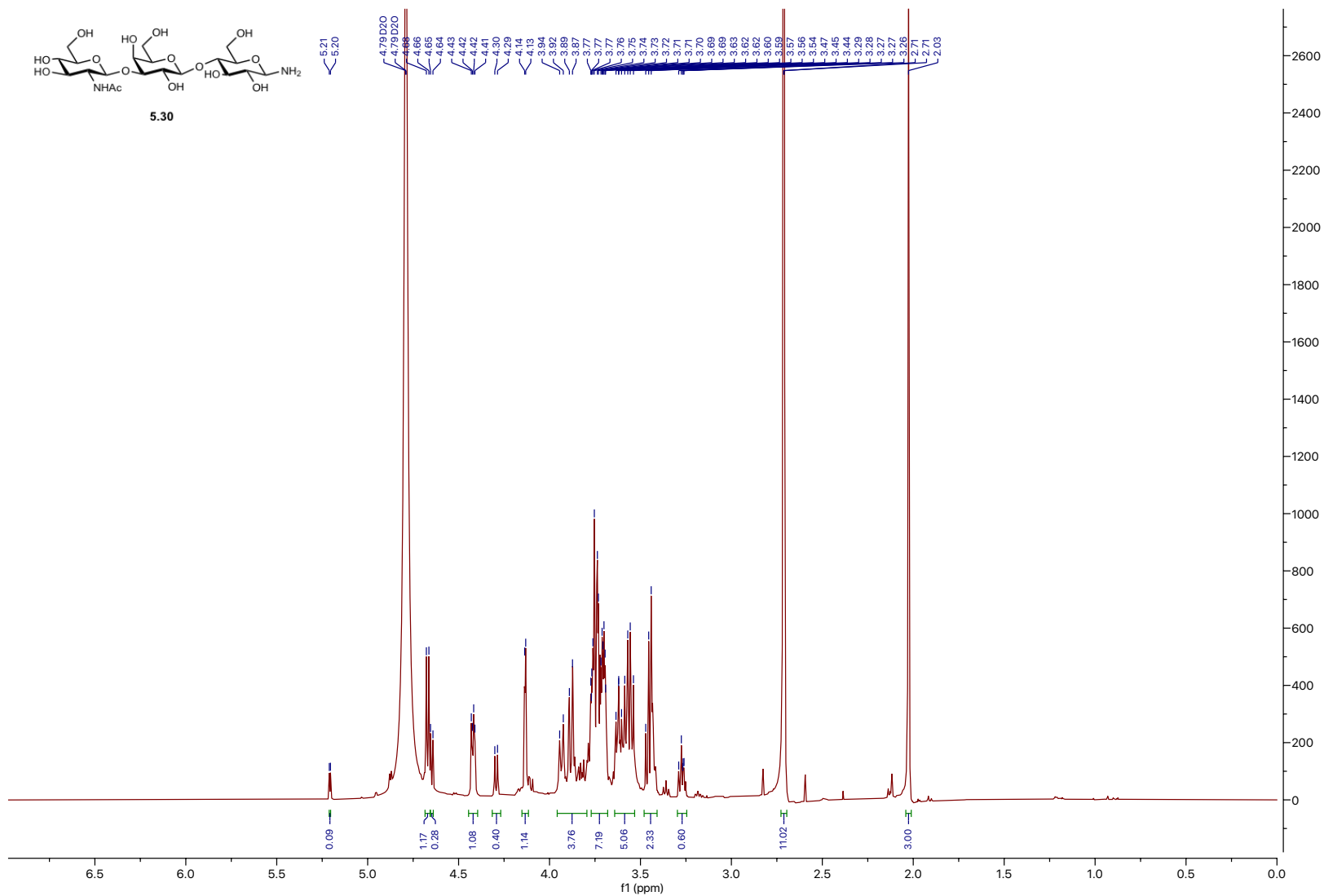


Figure A5.6 ^{13}C NMR (151 MHz, D_2O) of 5.30

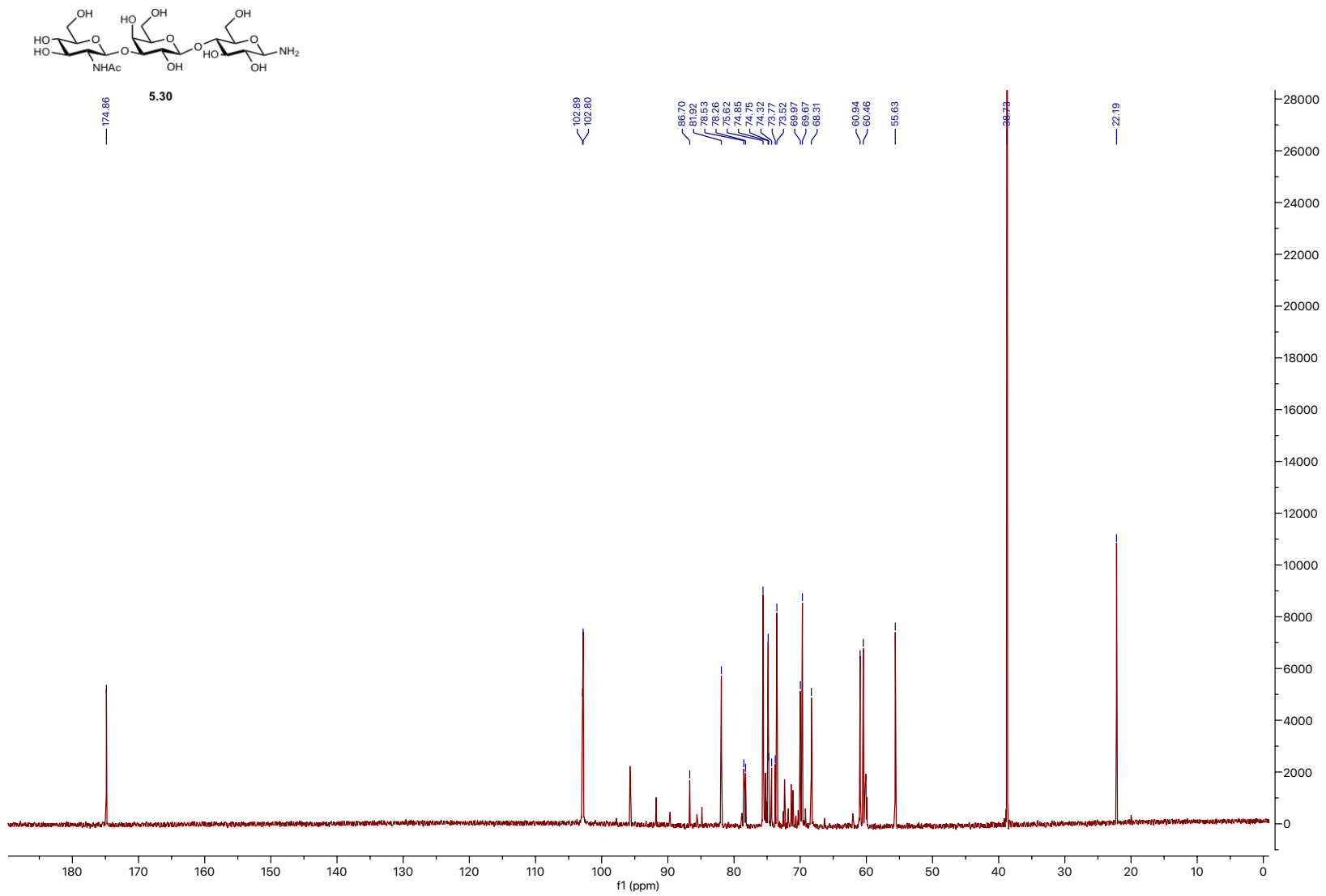


Figure A5.7 ^1H NMR (600 MHz, D_2O) of 5.31

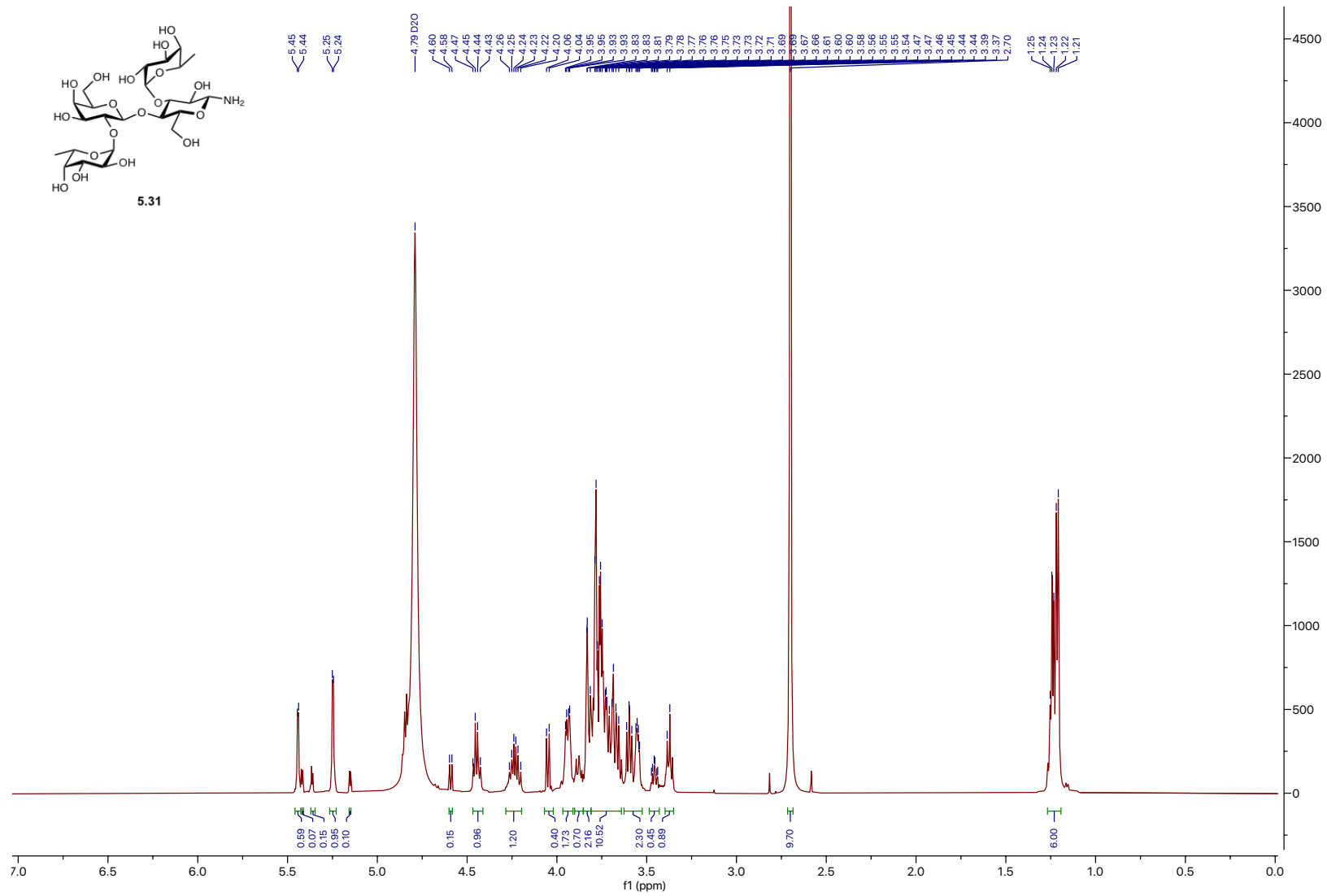


Figure A5.8 ^{13}C NMR (151 MHz, D_2O) of 5.31

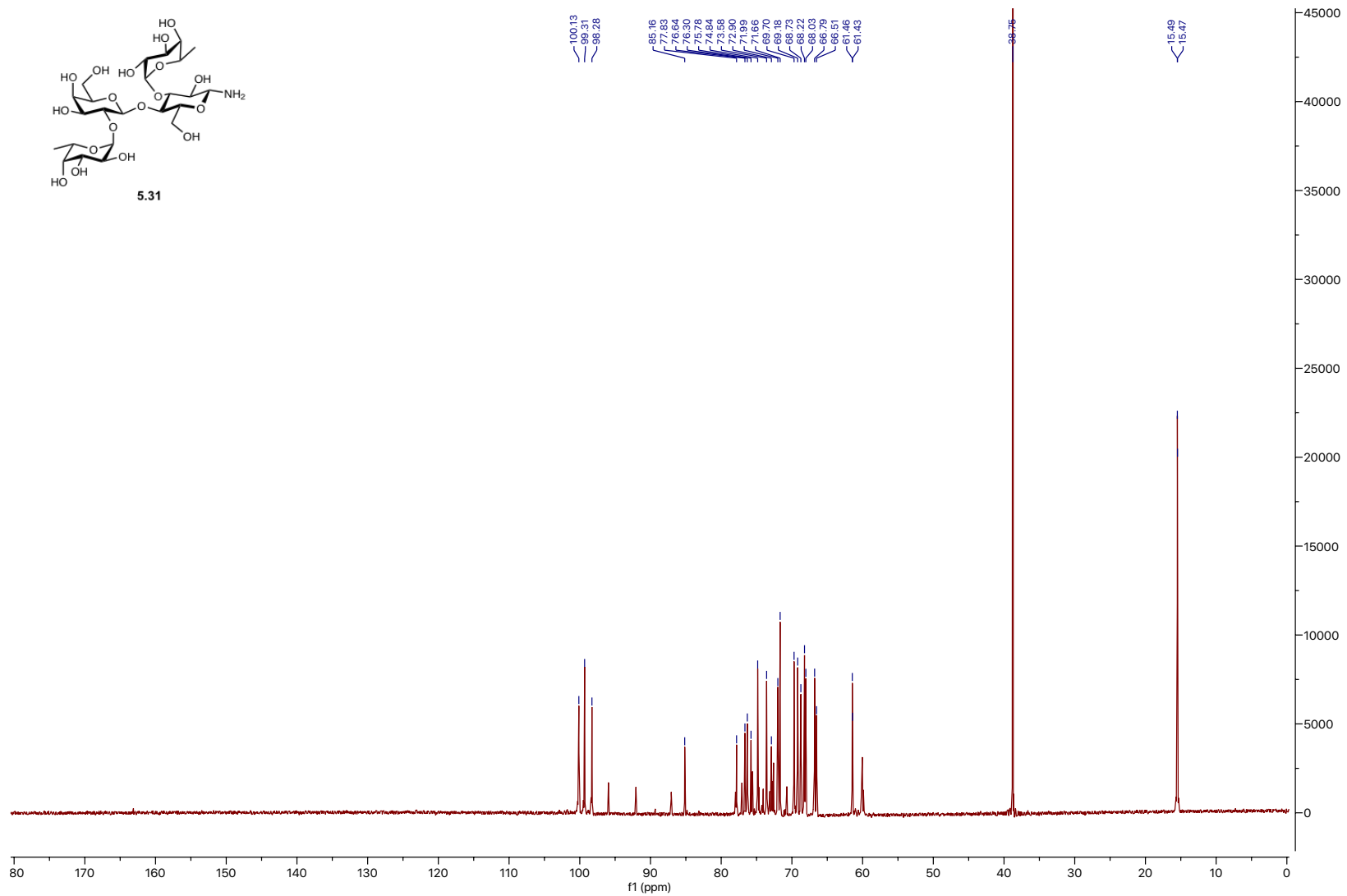


Figure A5.9 ¹H NMR (600 MHz, D₂O) of 5.32

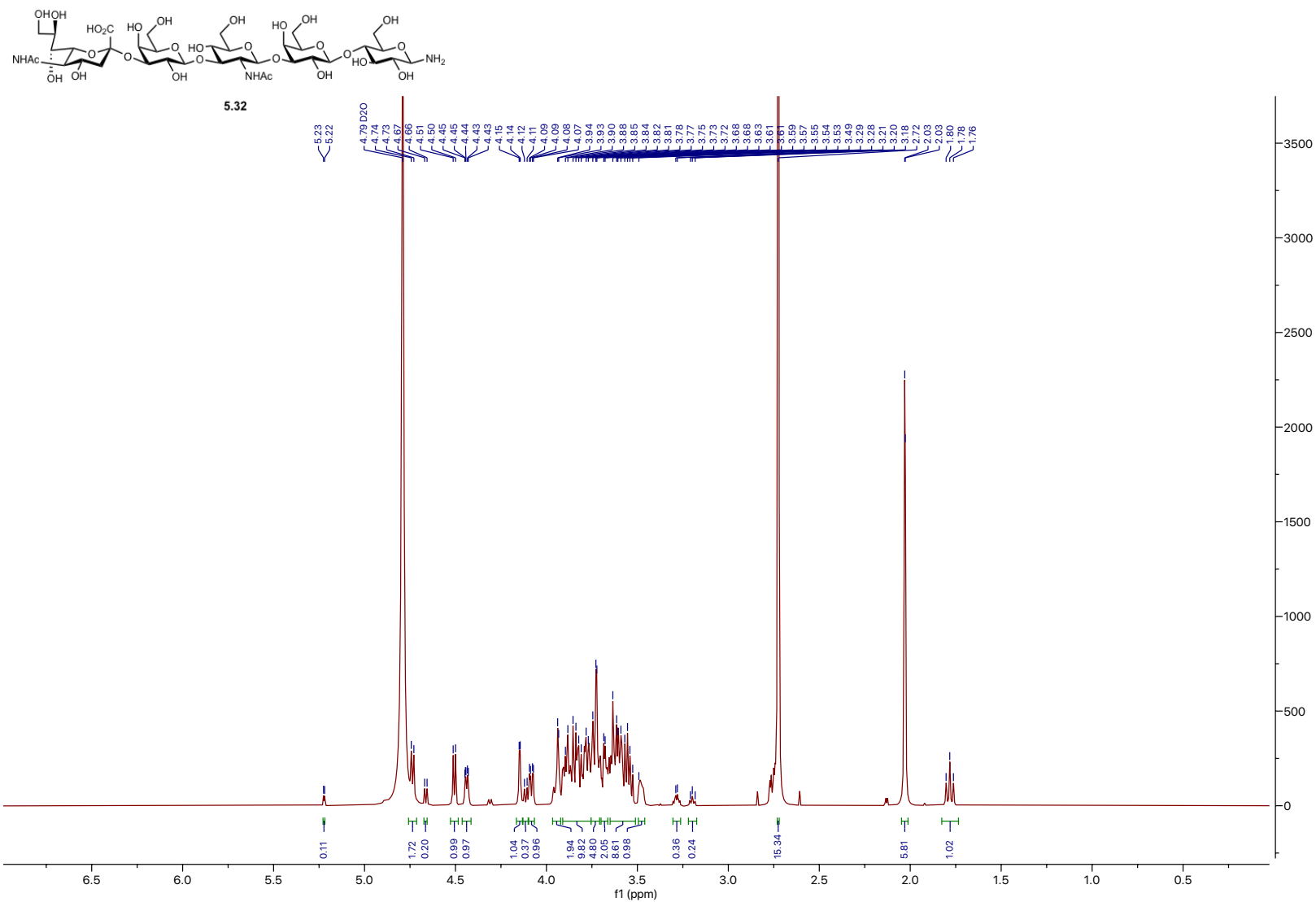


Figure A5.10 ¹³C NMR (151 MHz, D₂O) of 5.32

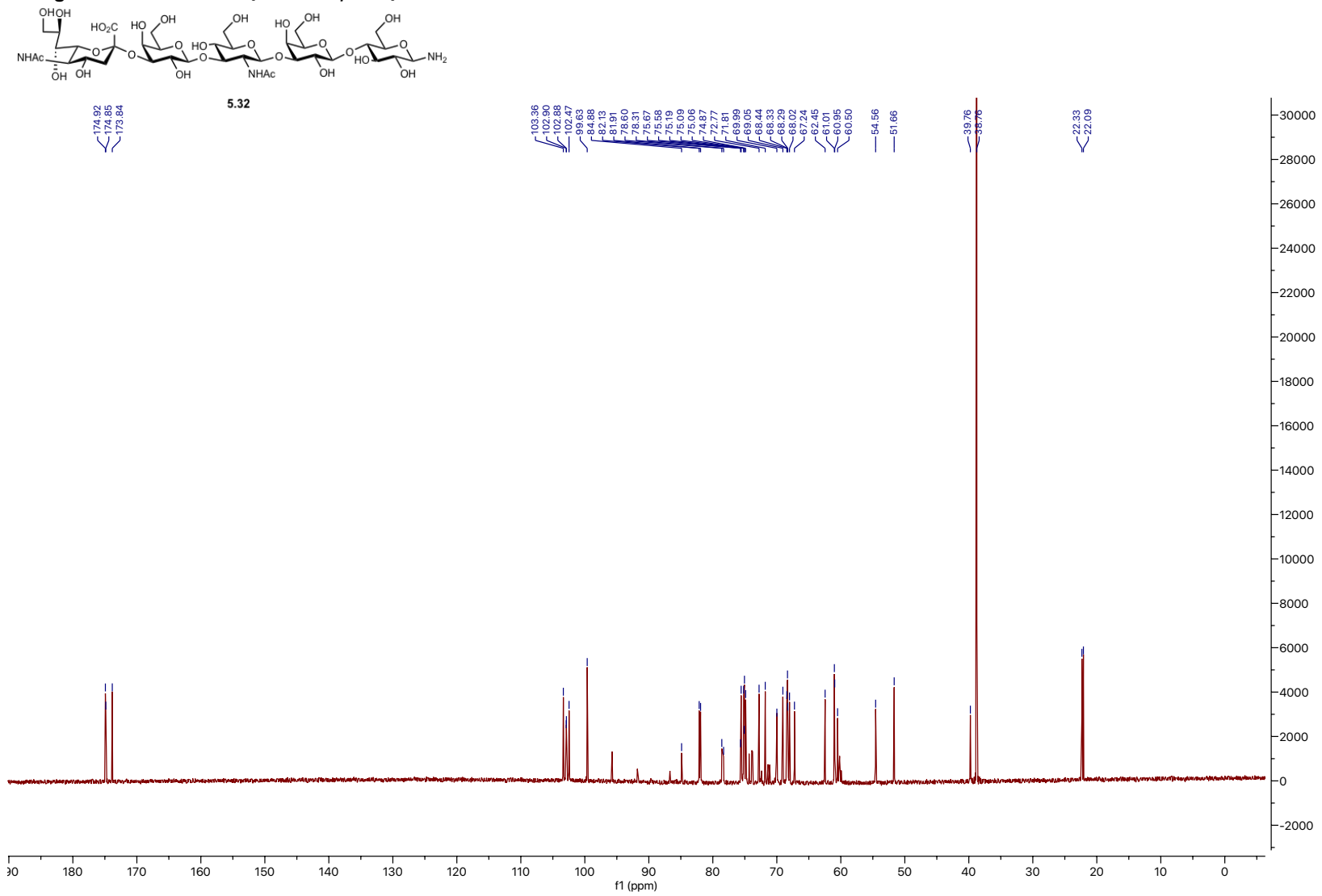


Figure A5.11 ¹H NMR (600 MHz, D₂O) of 5.39

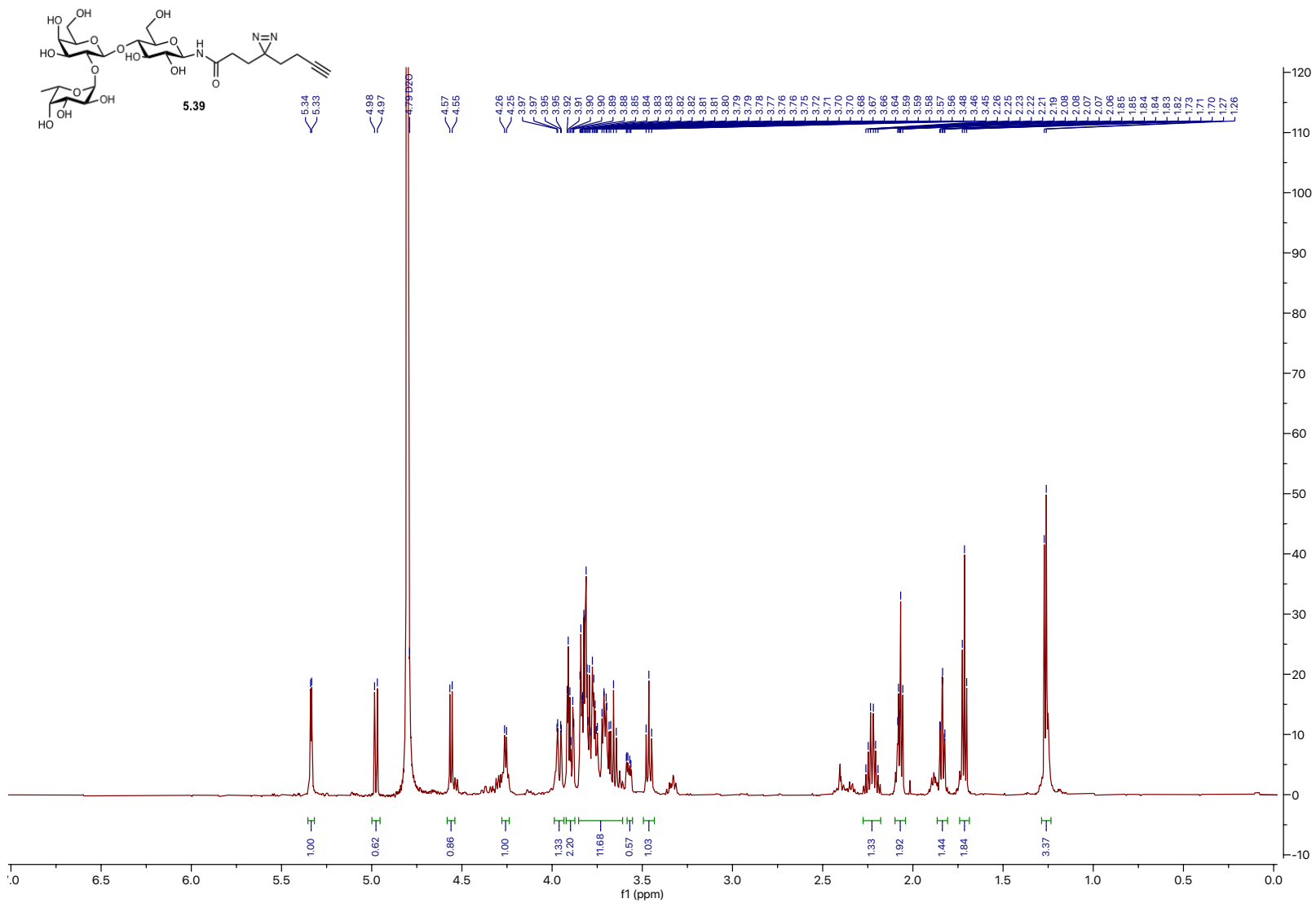


Figure A5.12 ¹³C NMR (151 MHz, D₂O) of 5.39

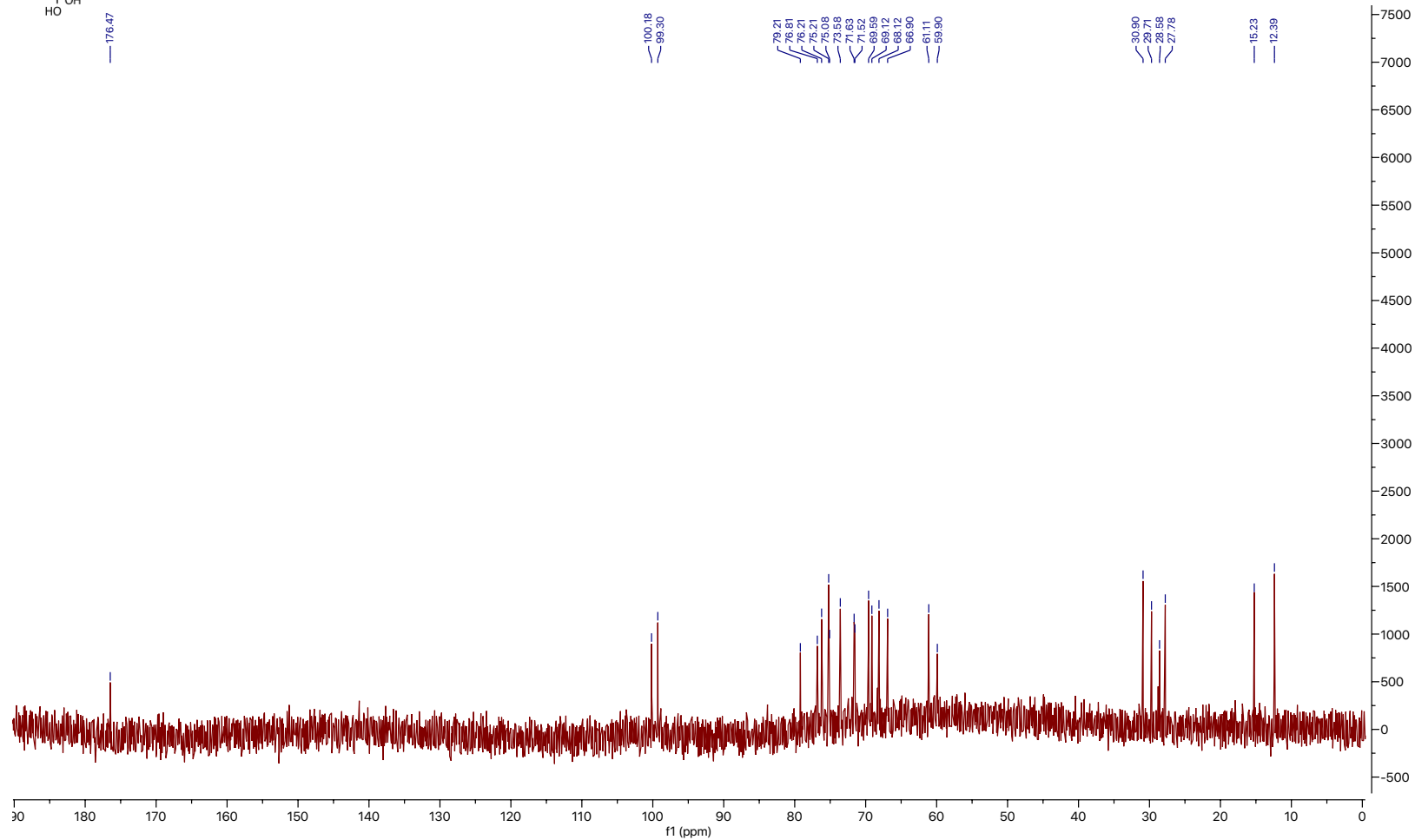
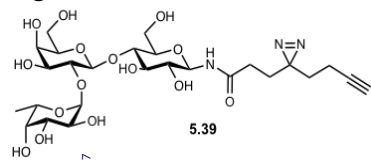


Figure A5.13 HSQC (600 MHz, D₂O) of 5.39

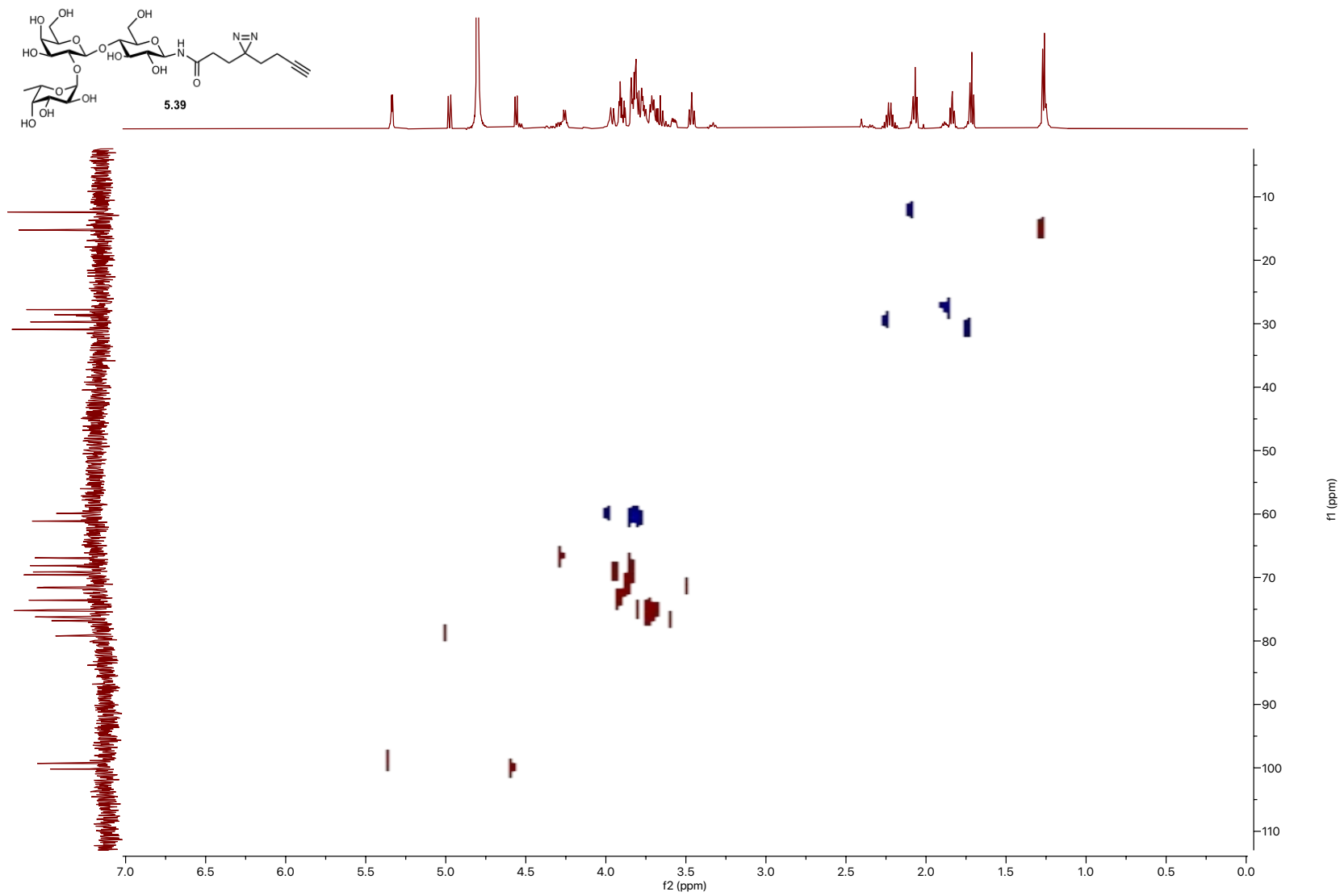


Figure A5.14 COSY (600 MHz, D₂O) of 5.39

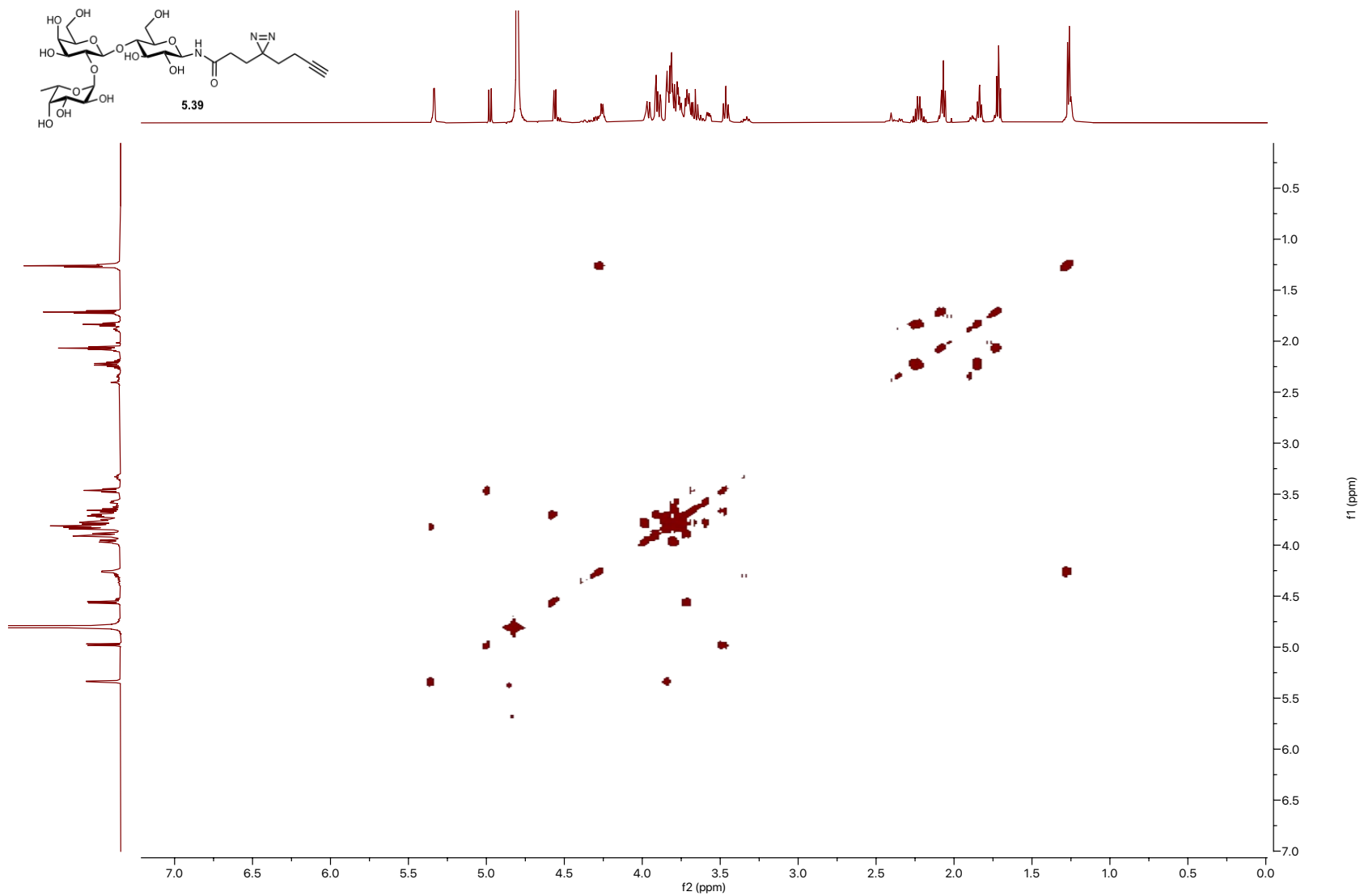


Figure A5.15 HMBC (600 MHz, D₂O) of 5.39

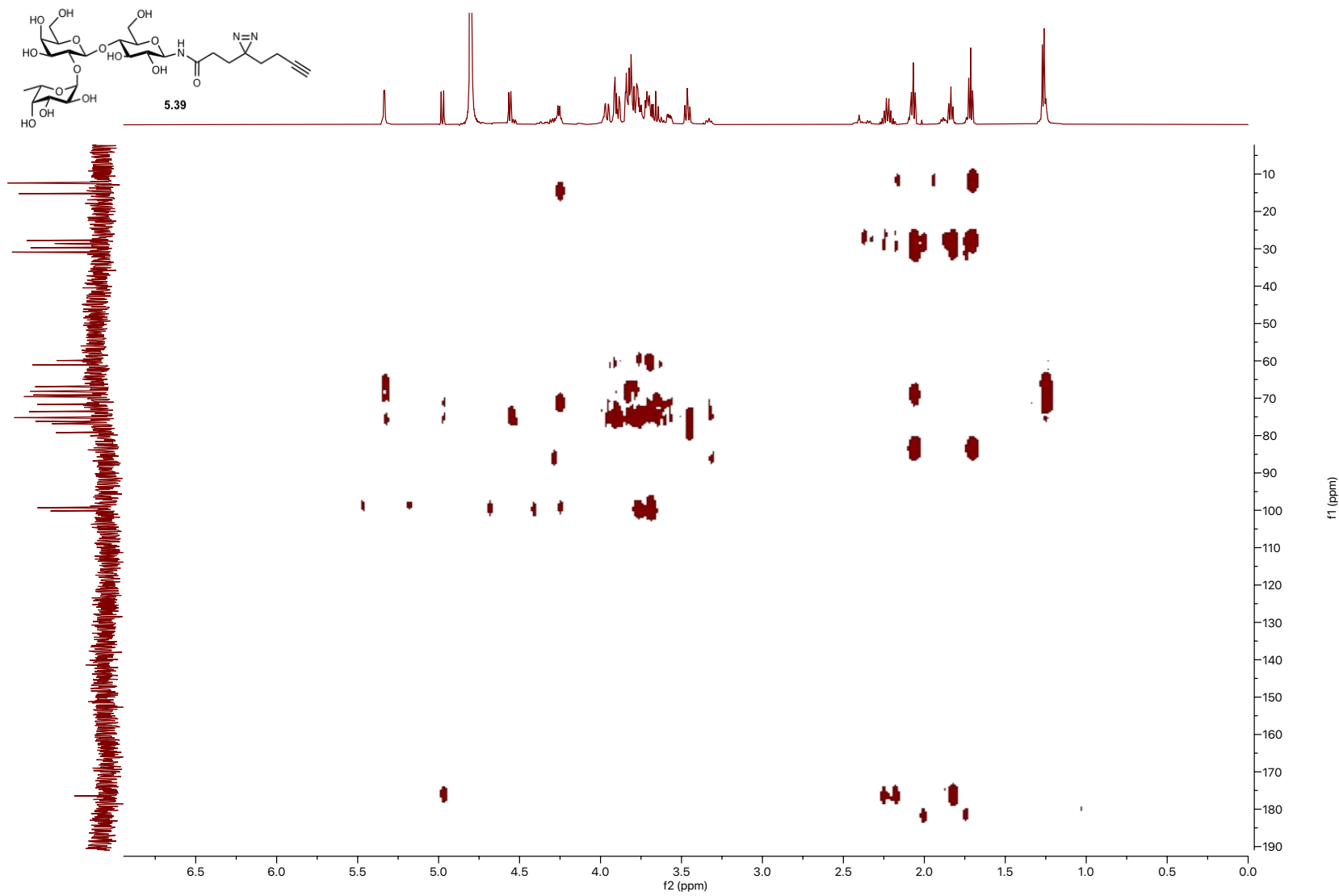


Figure A5.16 ¹H NMR (600 MHz, D₂O) of 5.40

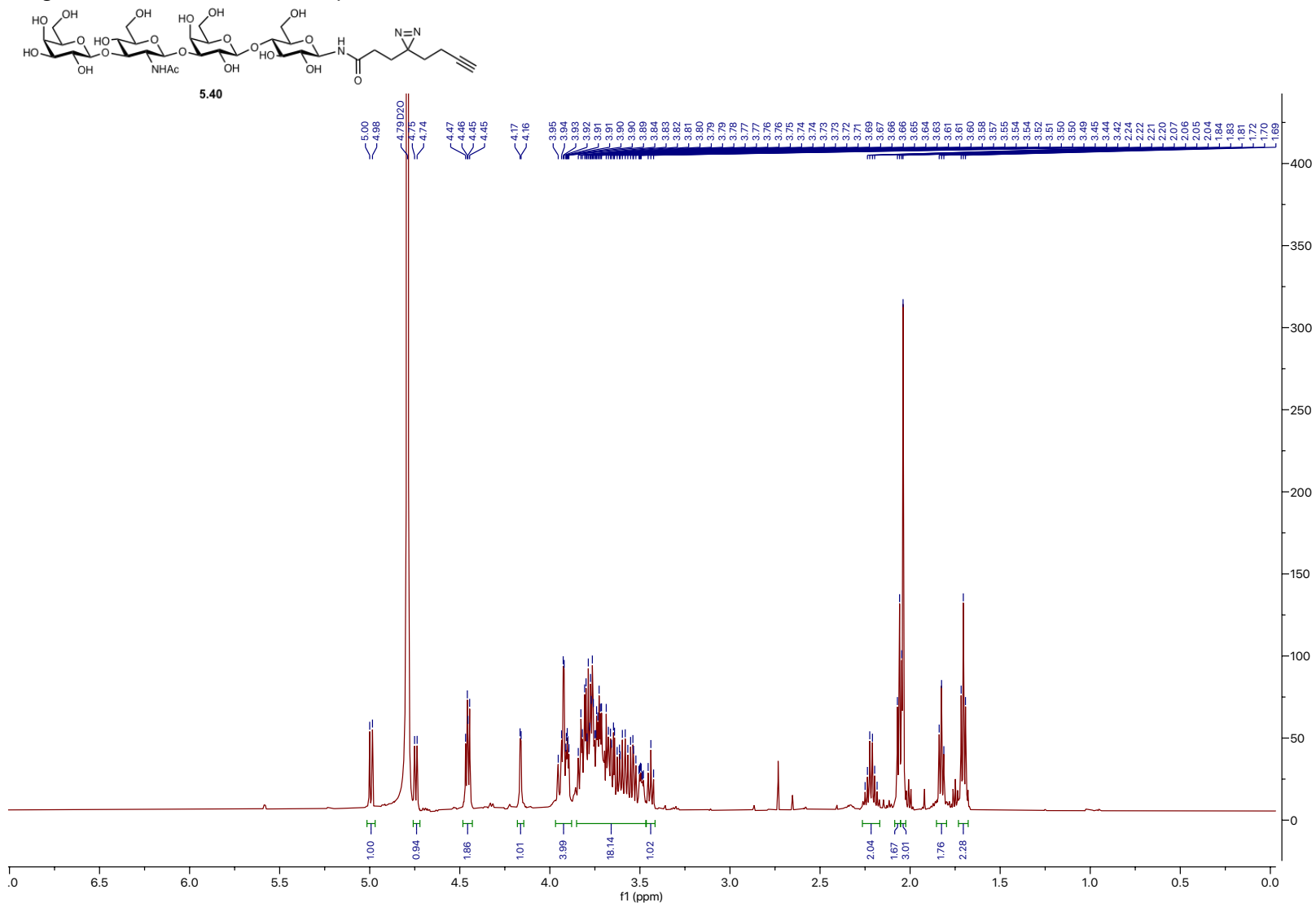


Figure A5.17 ¹³C NMR (151 MHz, D₂O) of 5.40

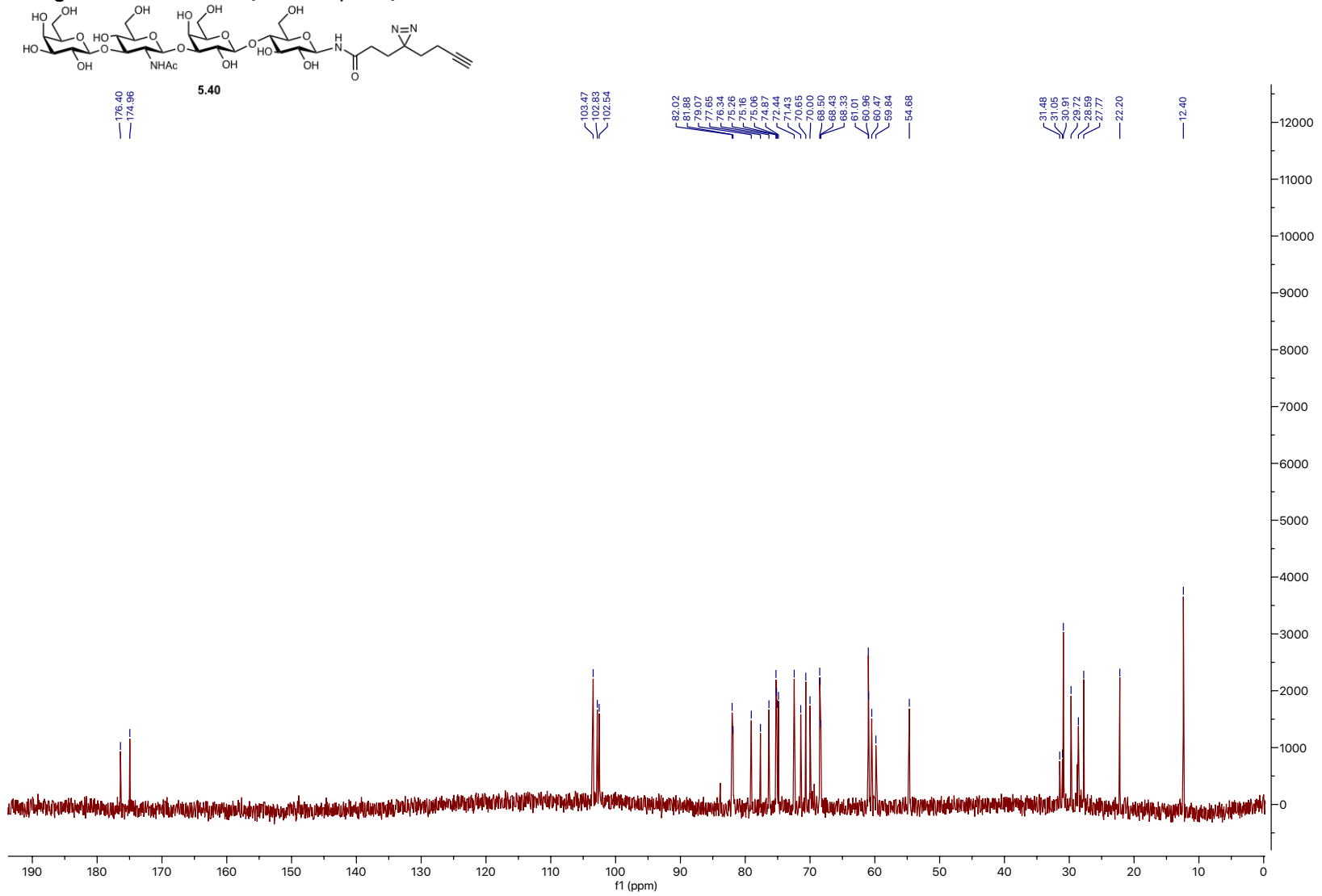


Figure A5.18 HSQC (600 MHz, D₂O) of 5.40

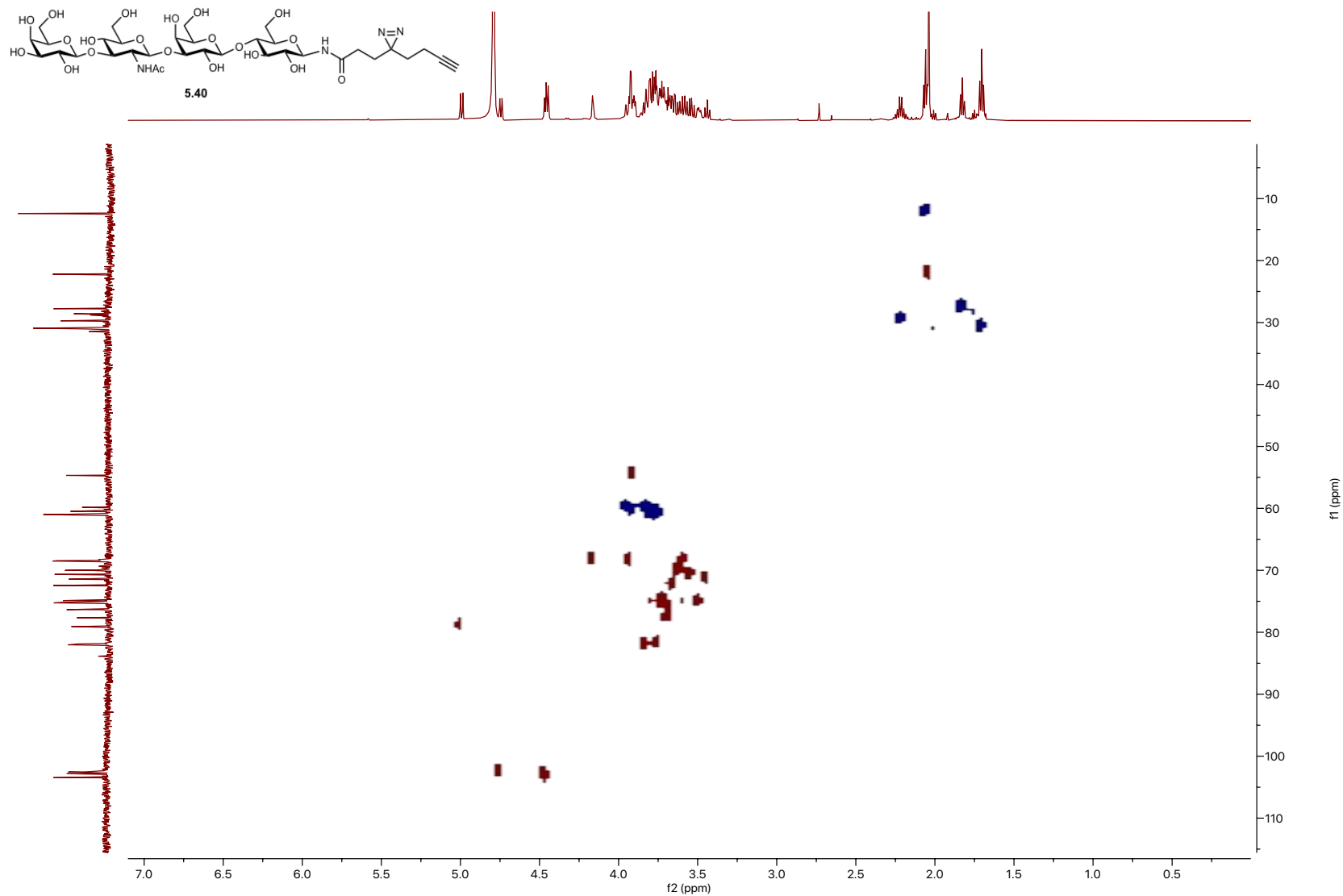


Figure A5.19 COSY (600 MHz, D₂O) of 5.40

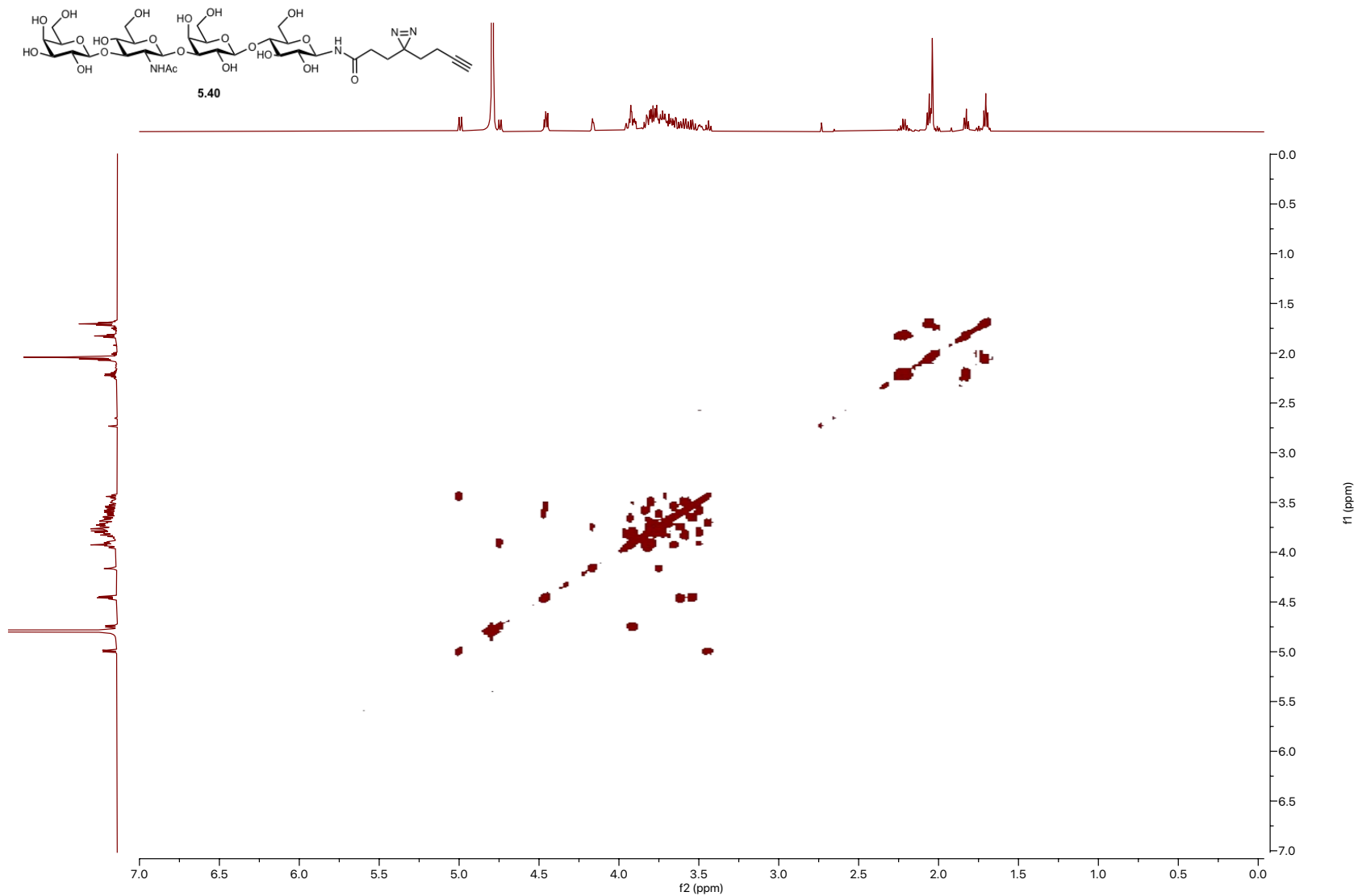


Figure A5.20 HMBC (600 MHz, D₂O) of 5.40

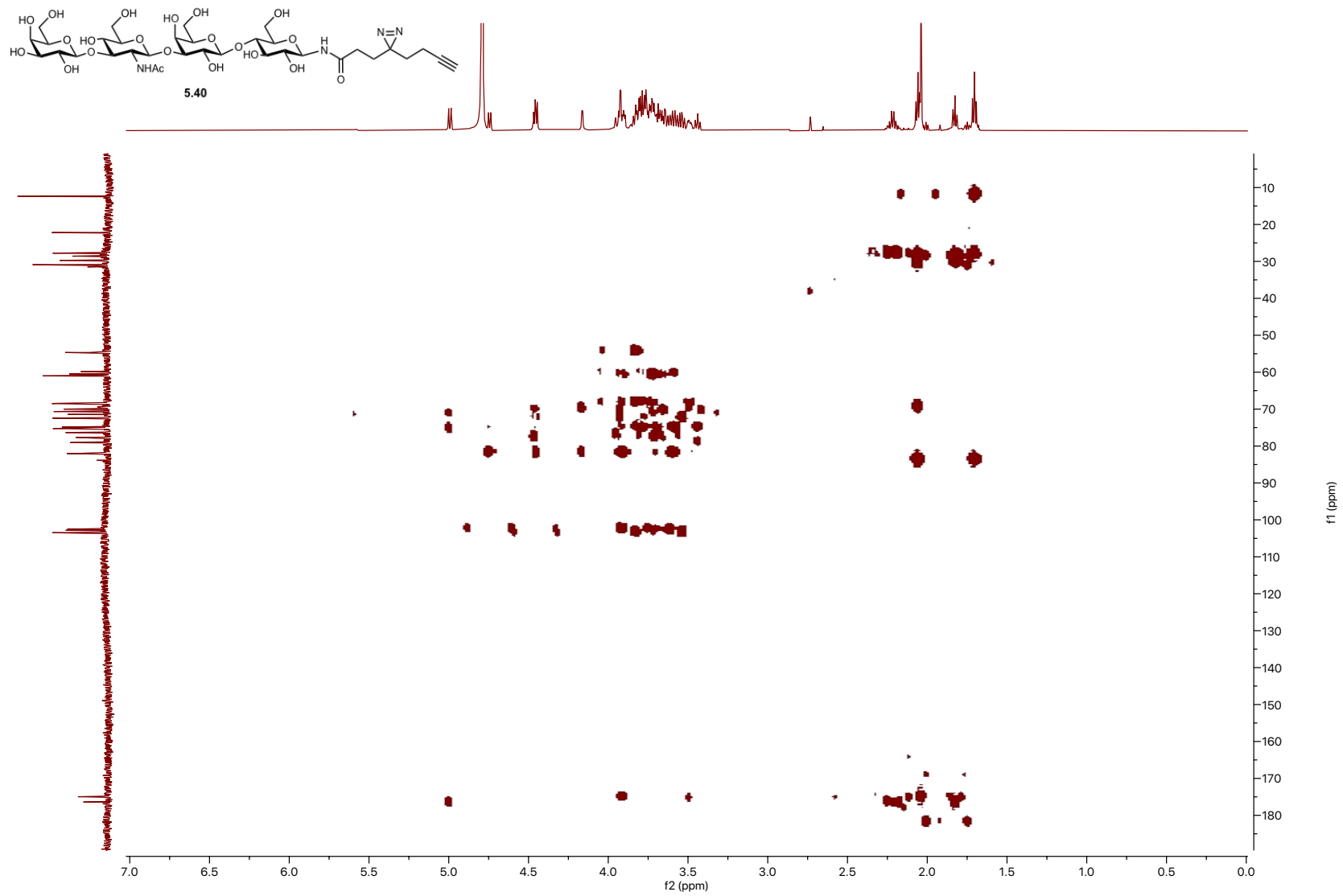


Figure A5.21 ¹H NMR (600 MHz, D₂O) of 5.41

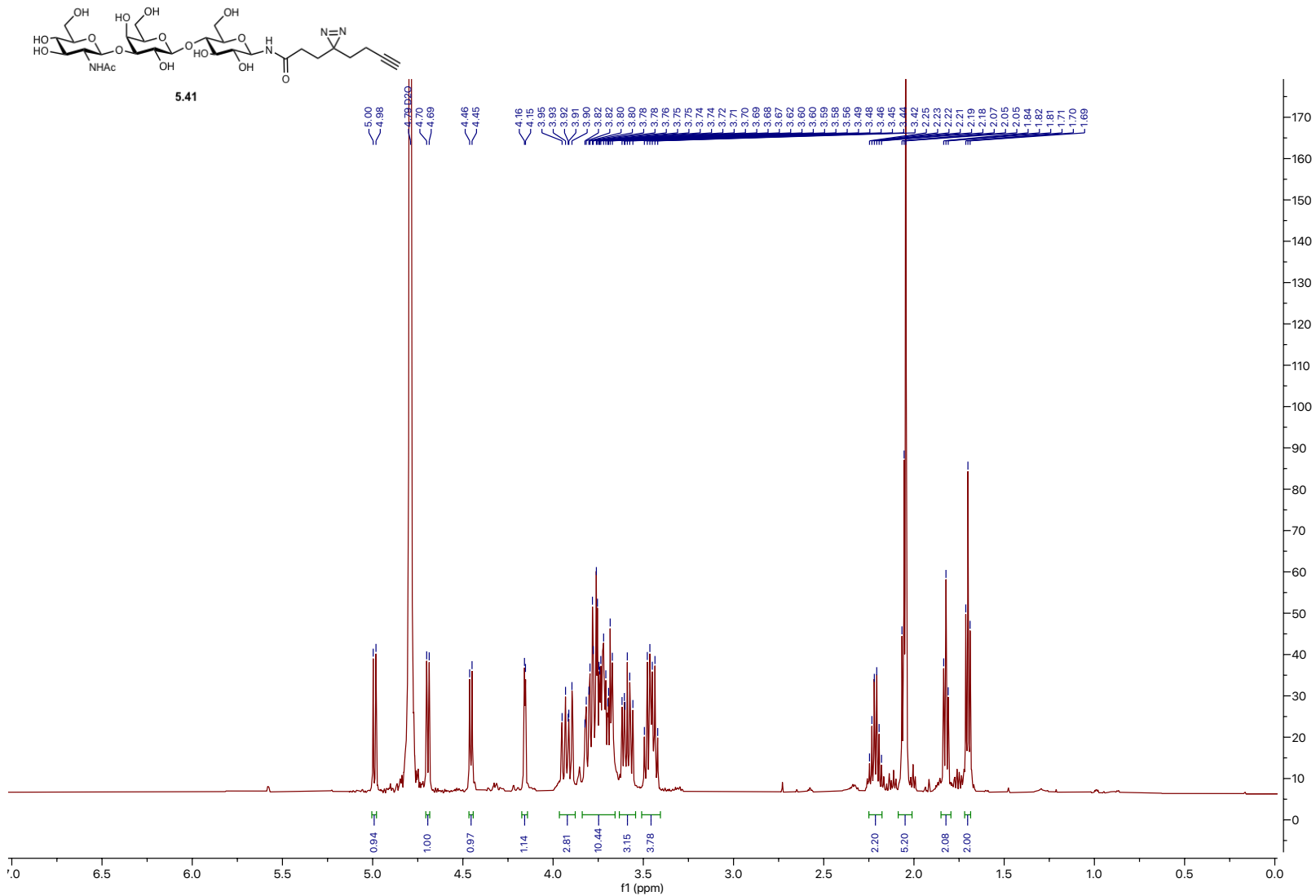


Figure A5.22 ¹³C NMR (151 MHz, D₂O) of 5.41

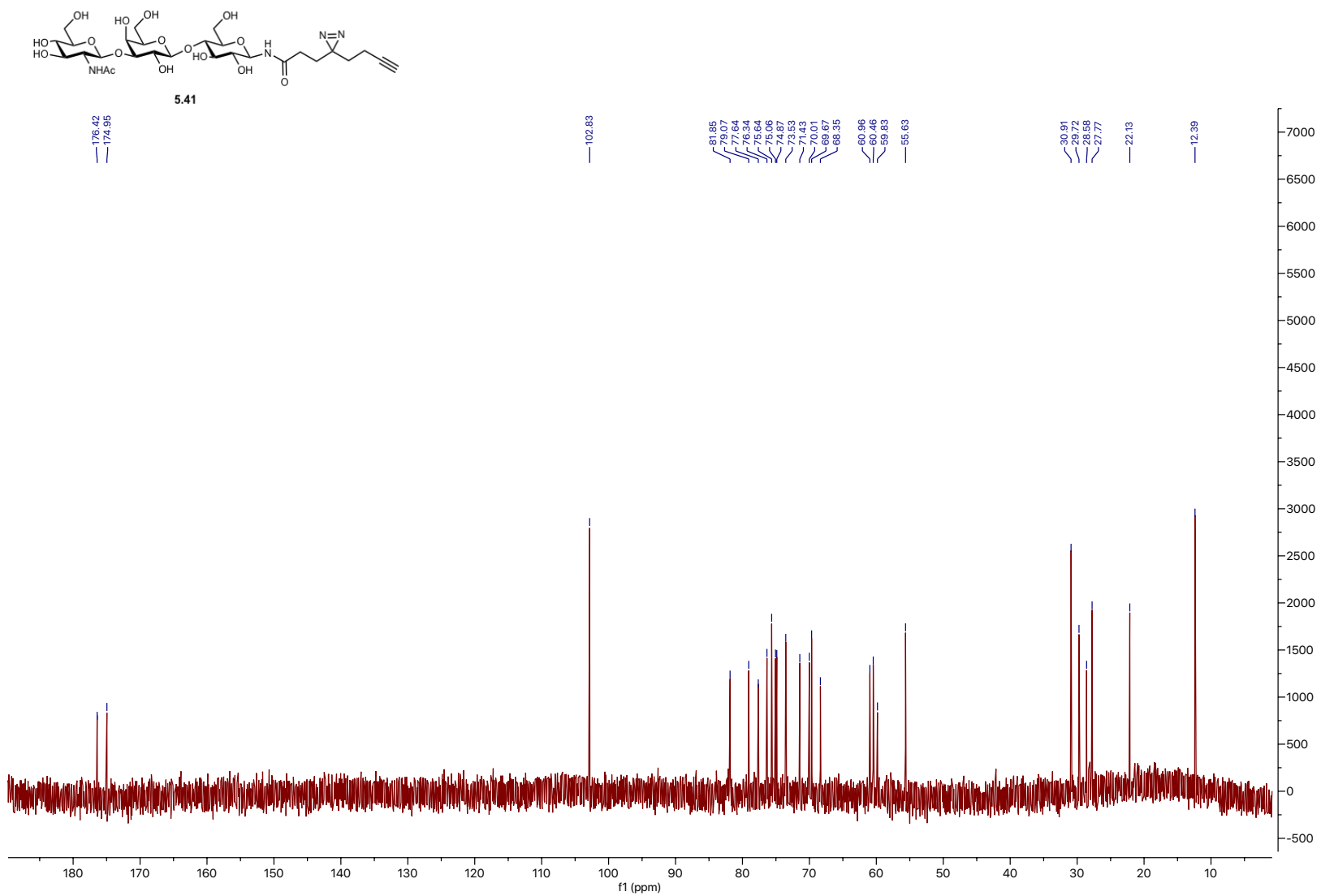


Figure A5.24 COSY (600 MHz, D₂O) of 5.41

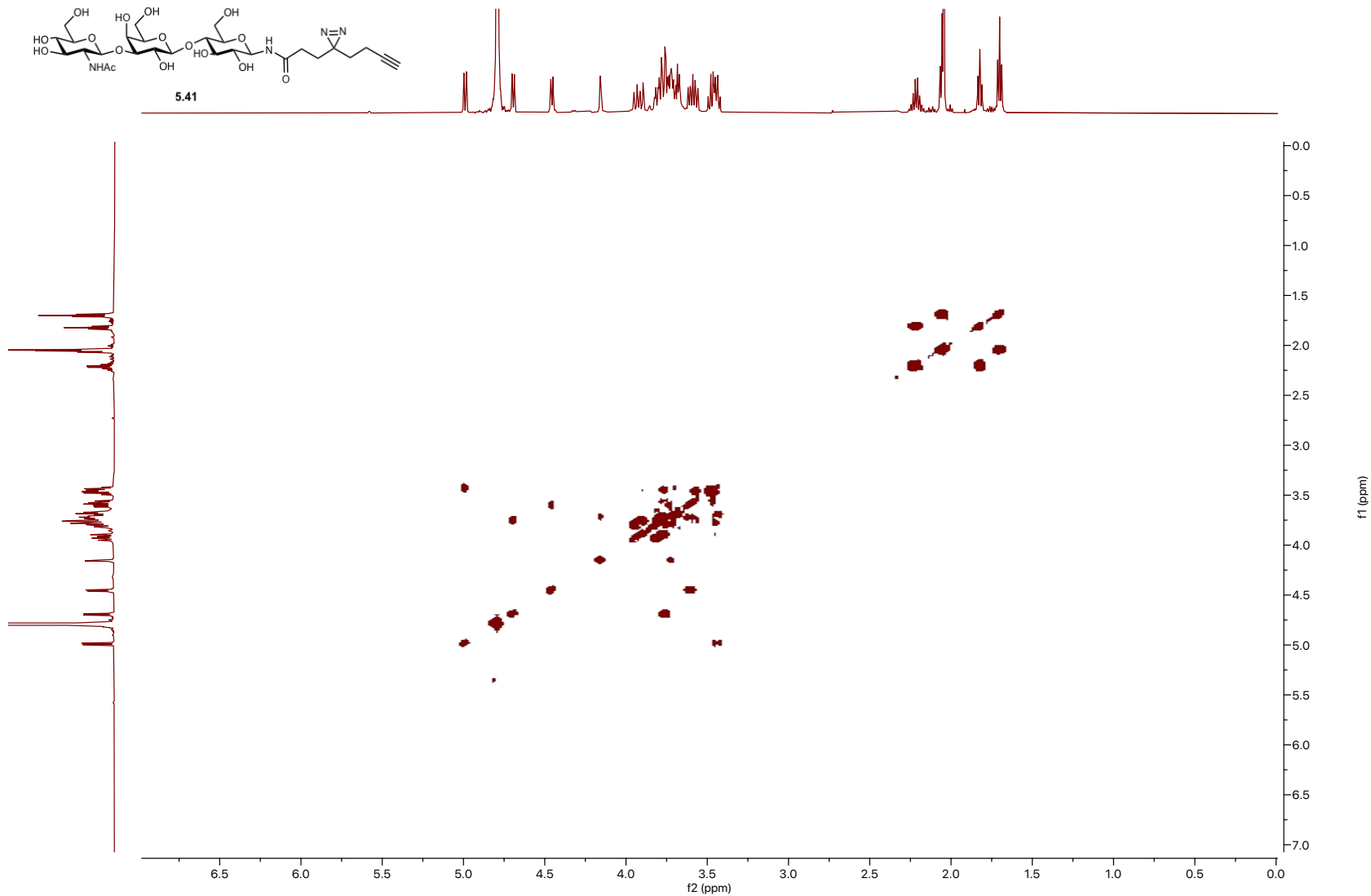


Figure A5.26 ¹H NMR (600 MHz, D₂O) of 5.42

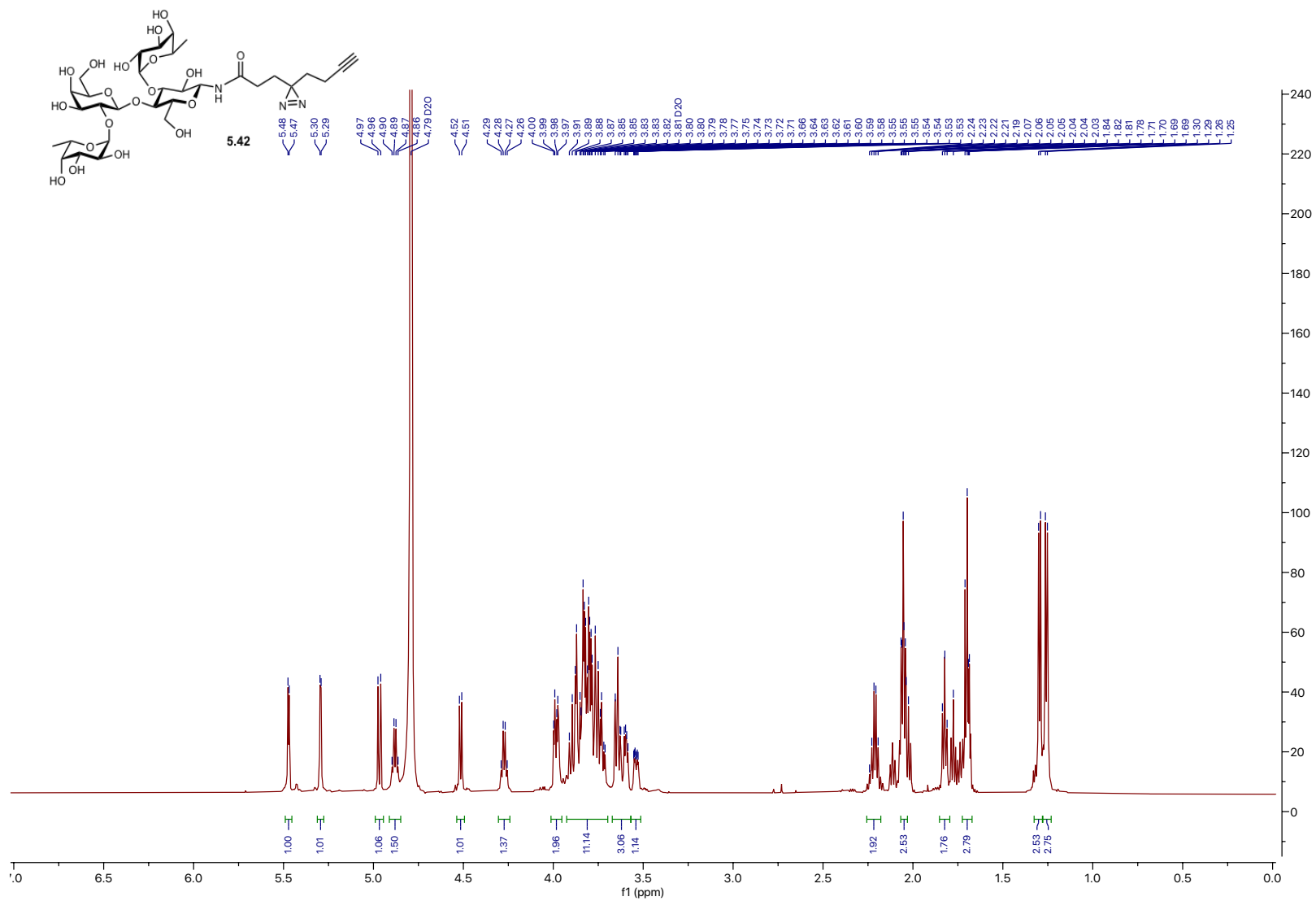


Figure A5.27 ^{13}C NMR (151 MHz, D_2O) of 5.42

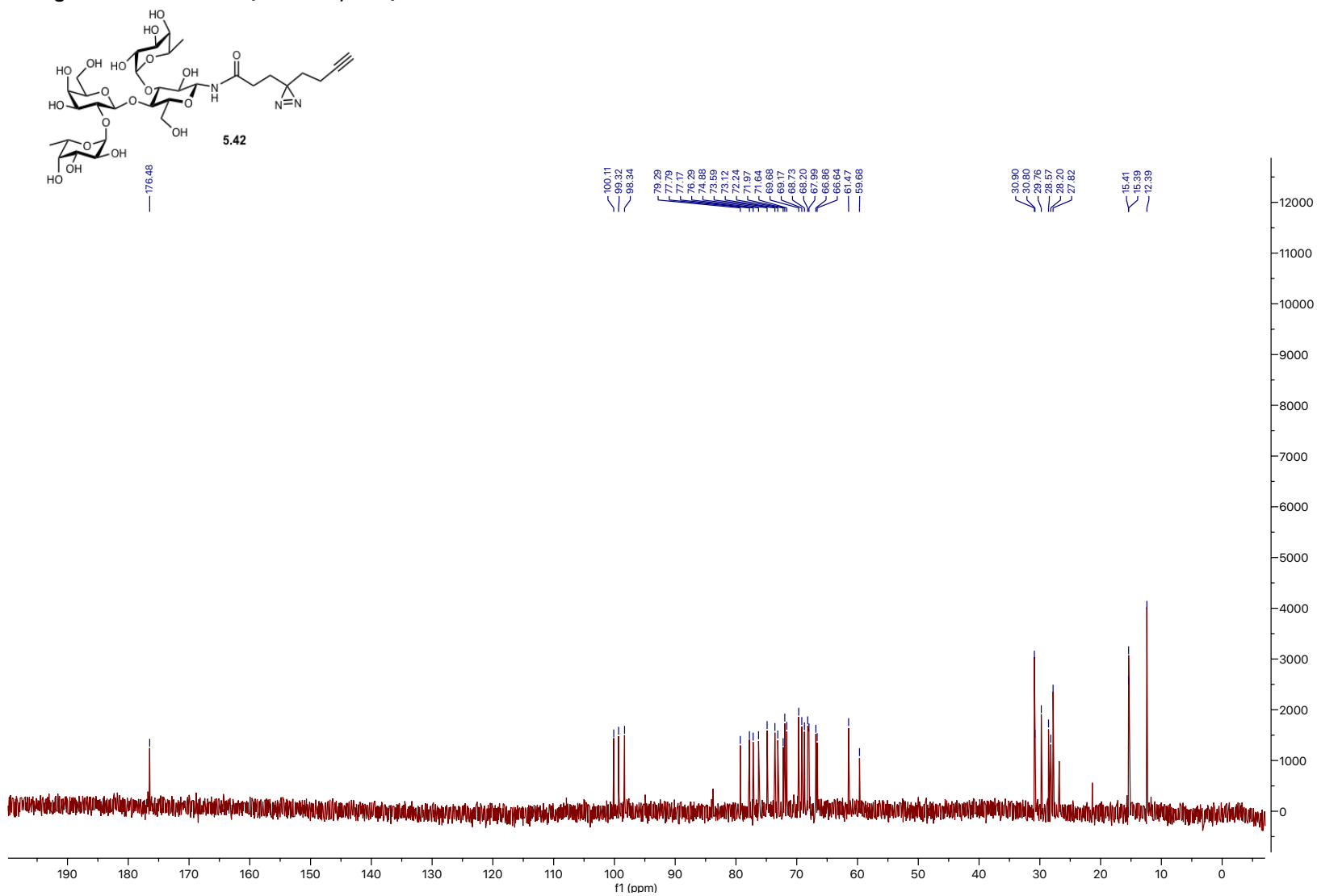


Figure A5.28 HSQC (600 MHz, D₂O) of 5.42

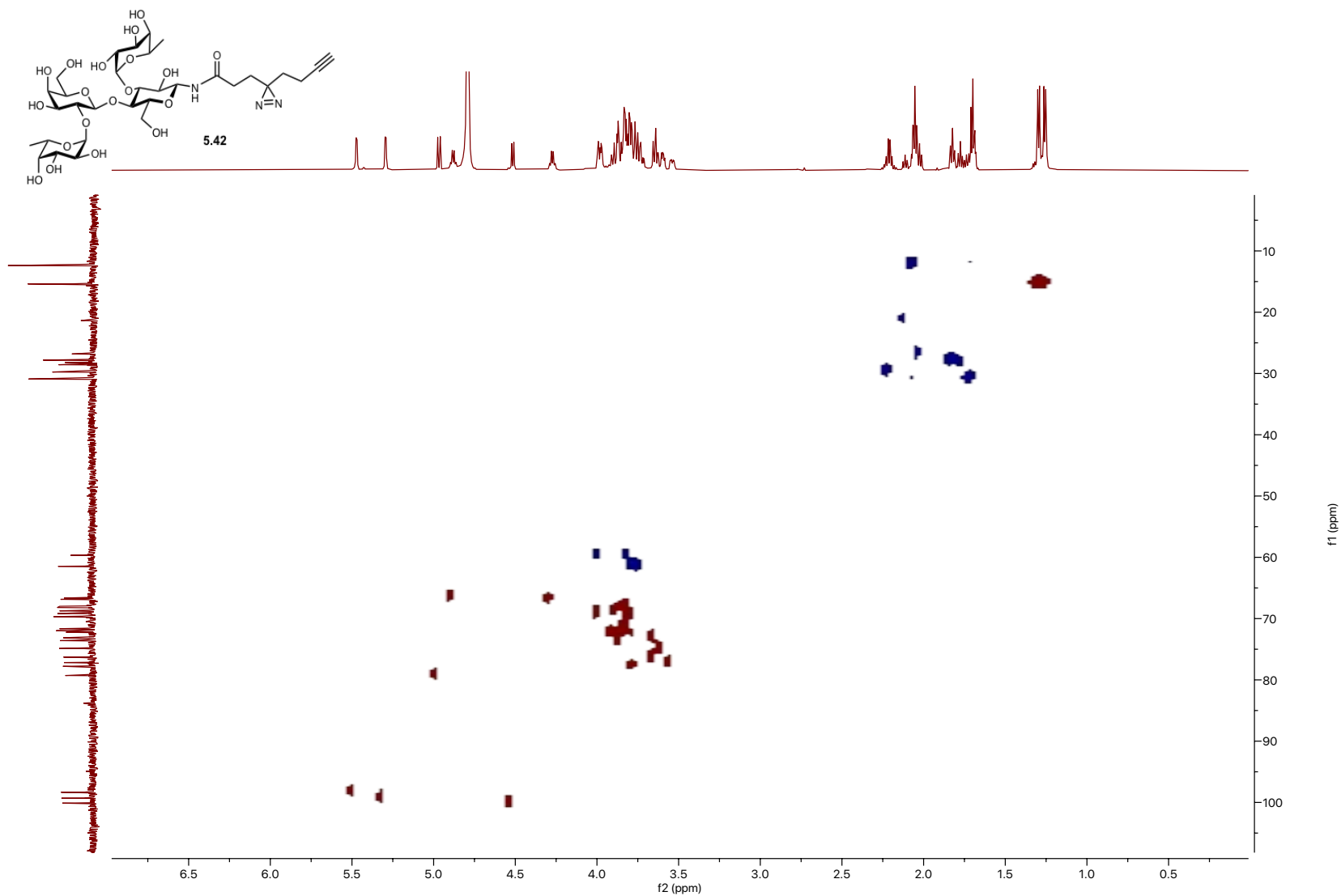


Figure A5.29 COSY (600 MHz, D₂O) of 5.42

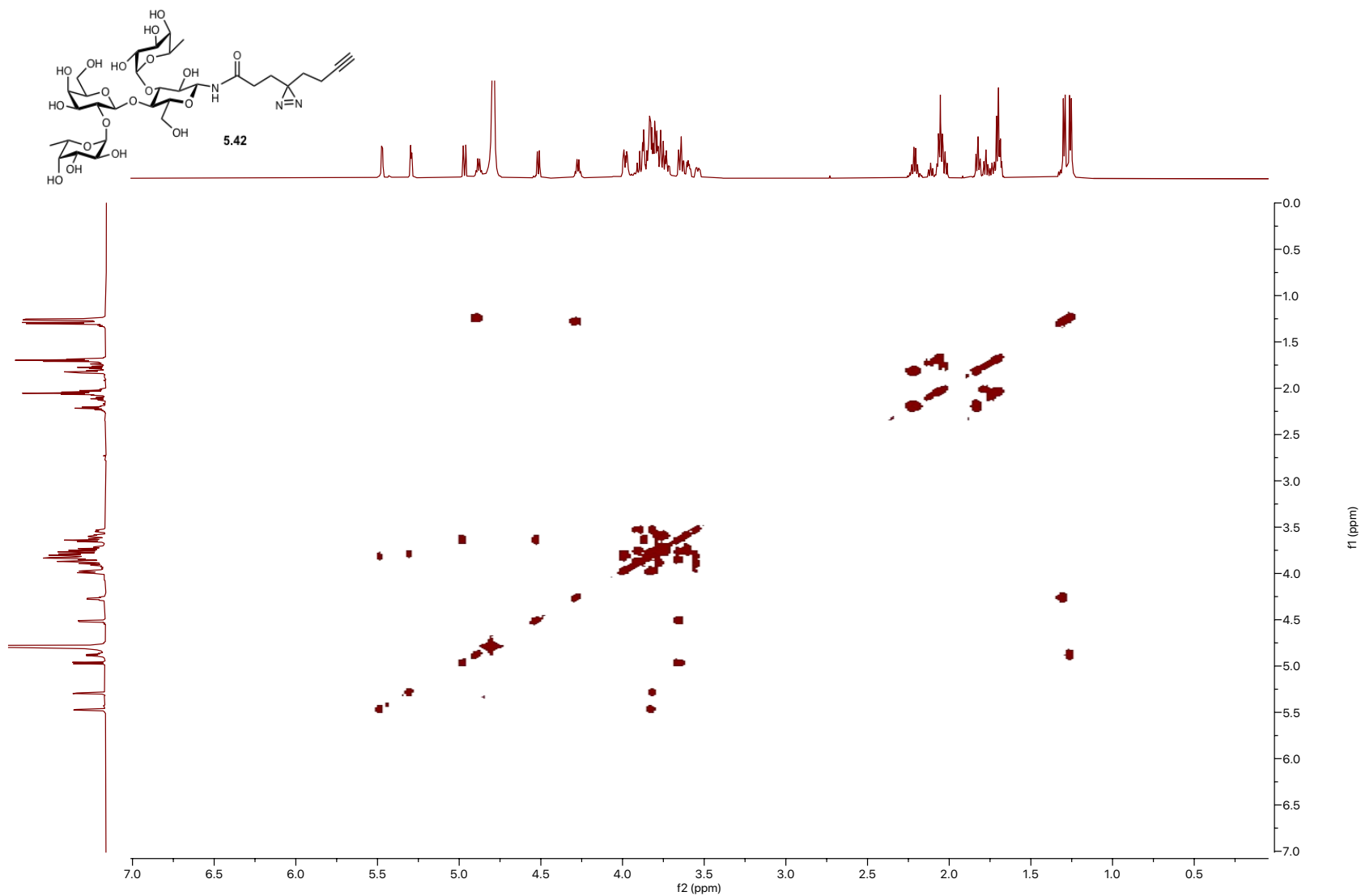


Figure A5.30 HMBC (600 MHz, D₂O) of 5.42

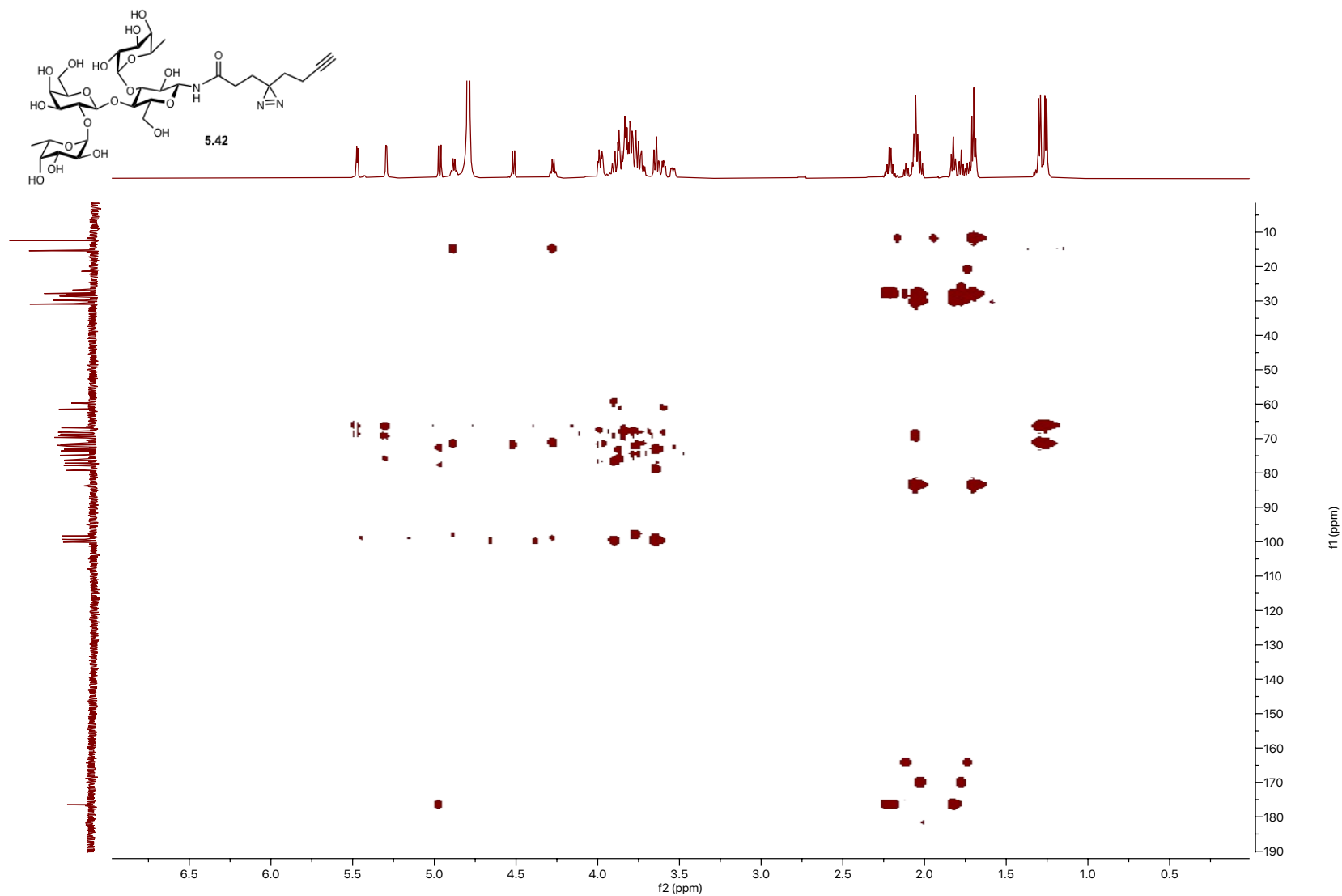


Figure A5.31 ¹H NMR (600 MHz, D₂O) of 5.43

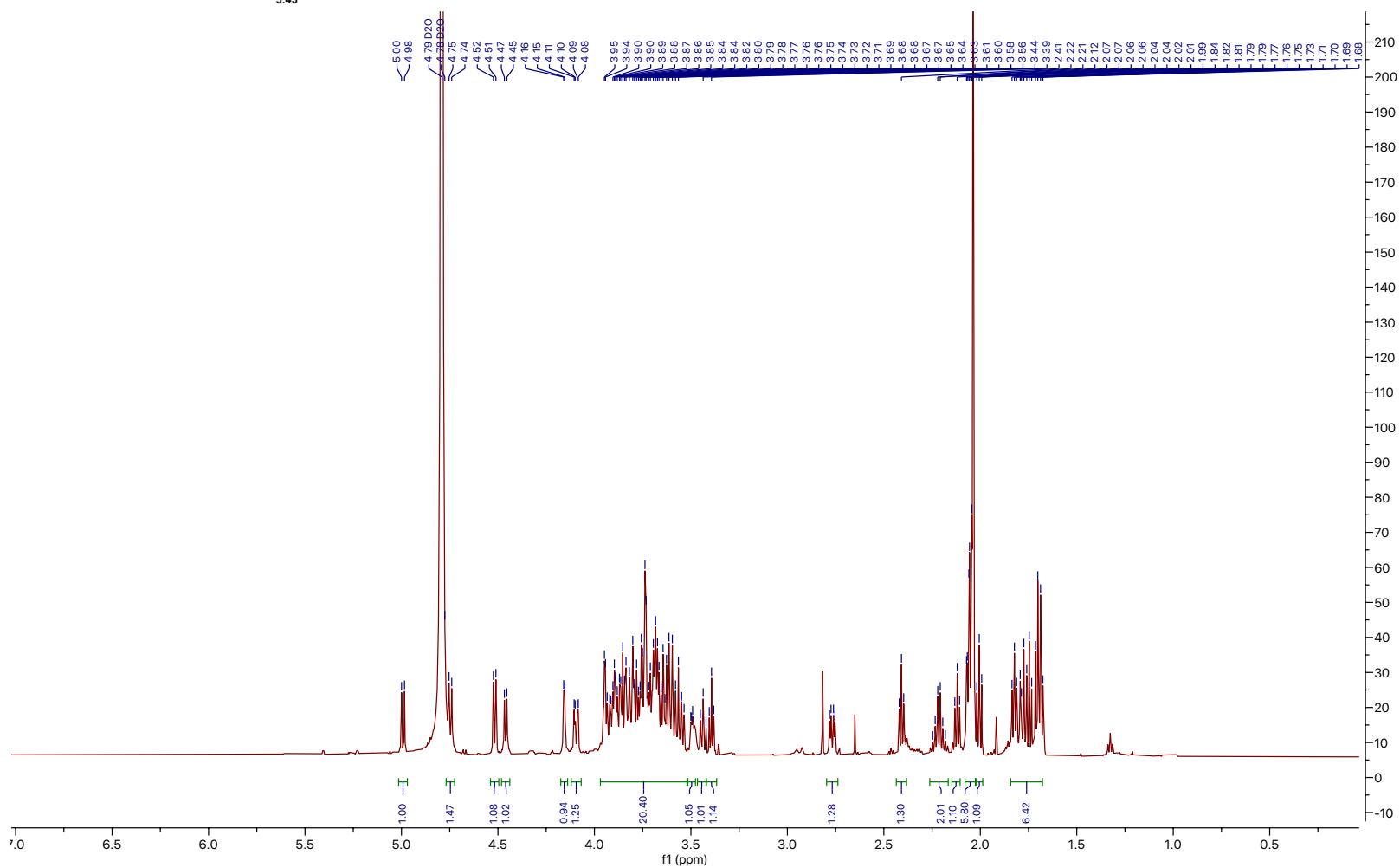
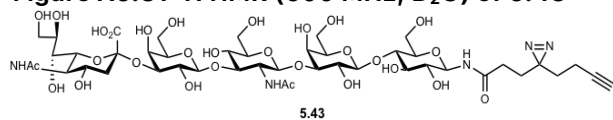


Figure A5.32 ¹³C NMR (151 MHz, D₂O) of 5.43

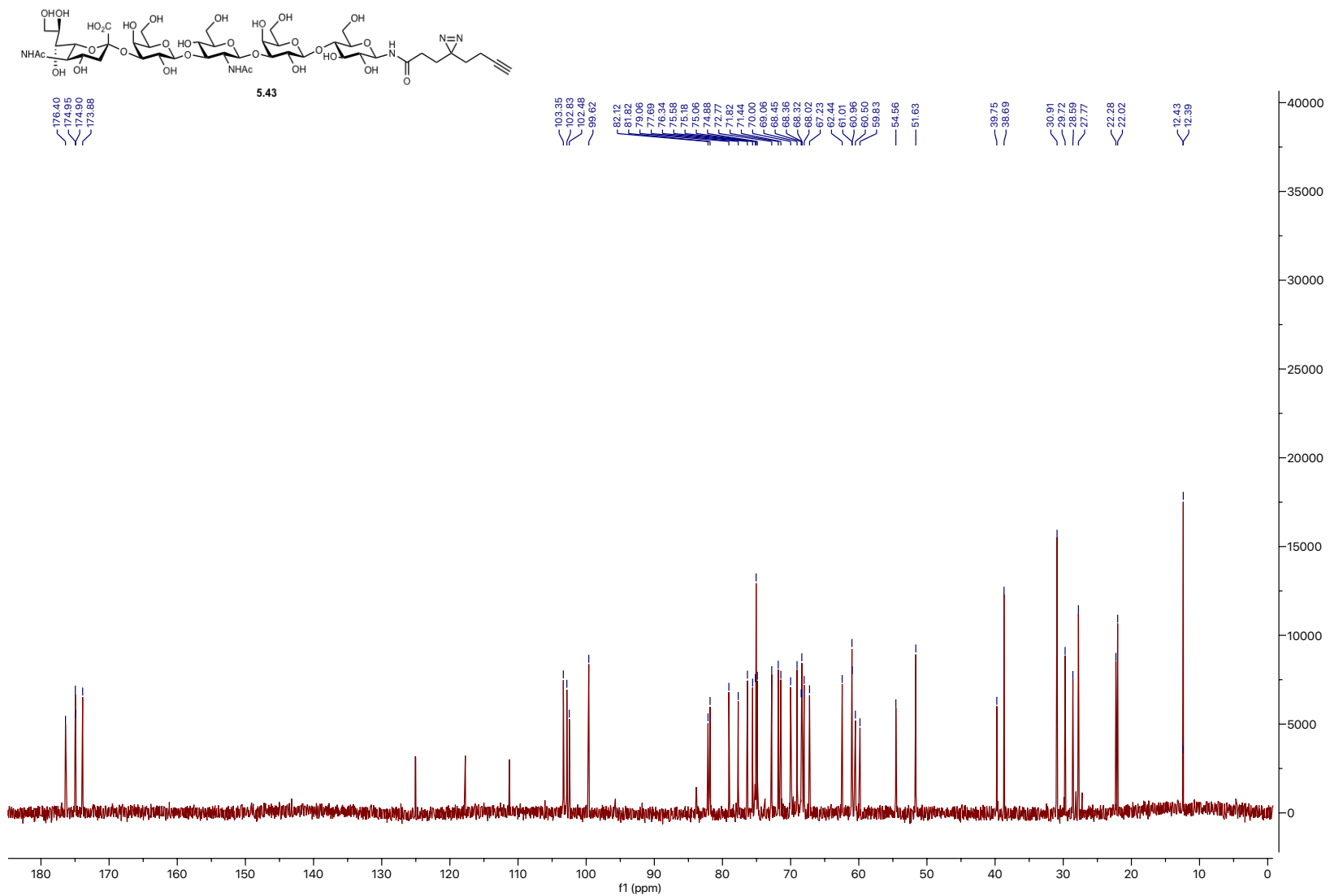


Figure A5.33 HSQC (600 MHz, D₂O) of 5.43

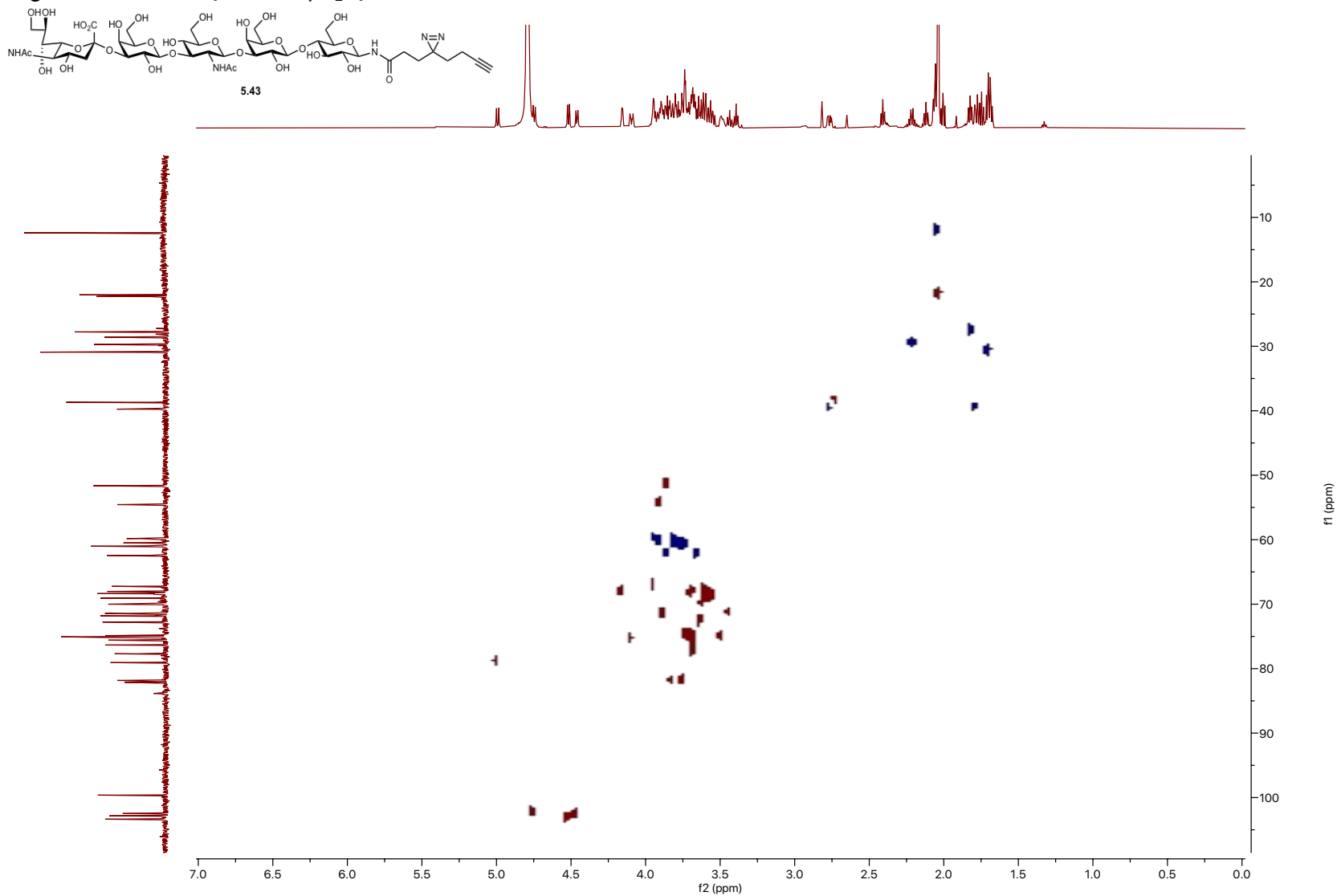


Figure A5.34 COSY (600 MHz, D₂O) of 5.43

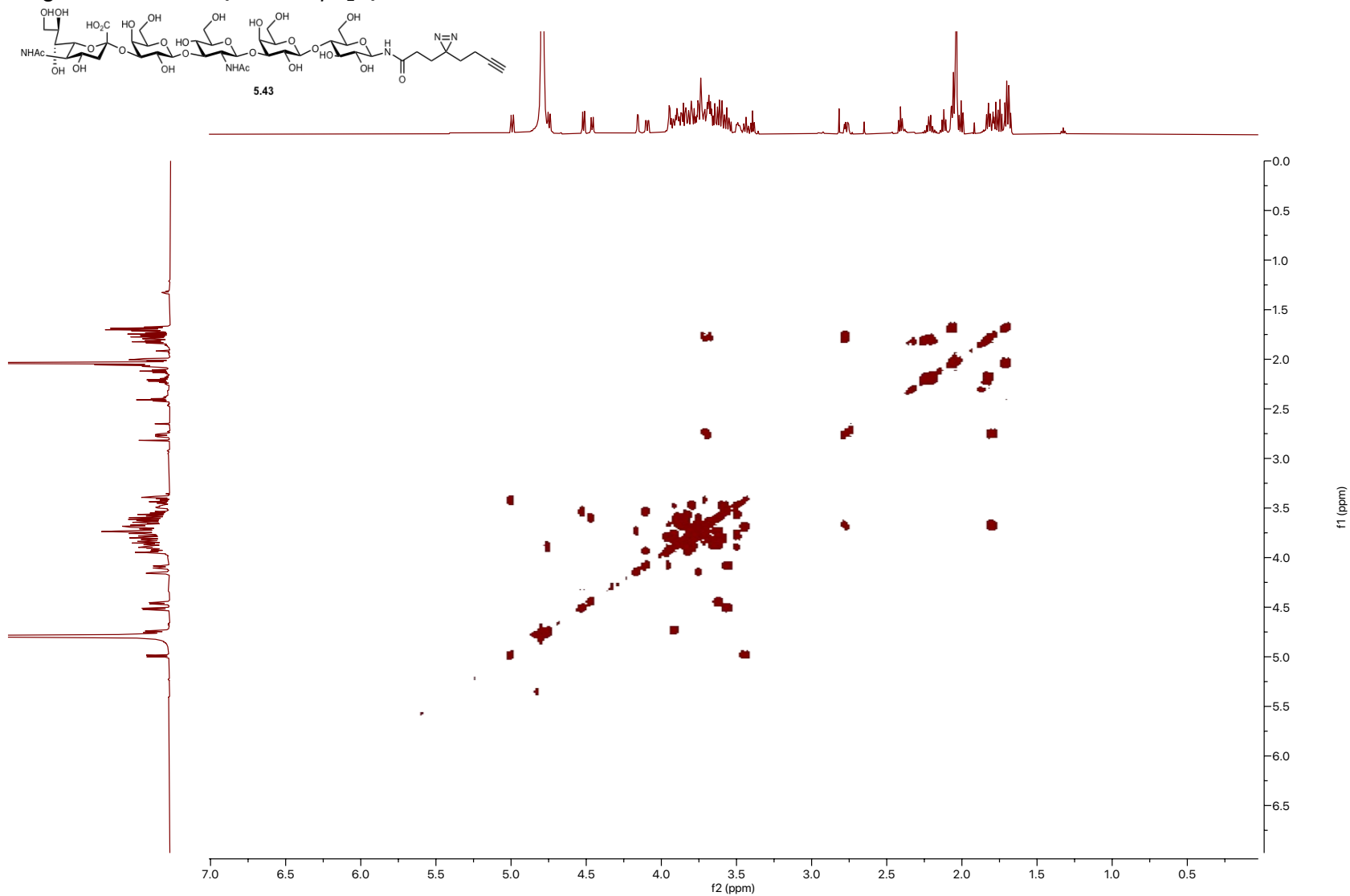


Figure A5.35 HMBC (600 MHz, D₂O) of 5.43

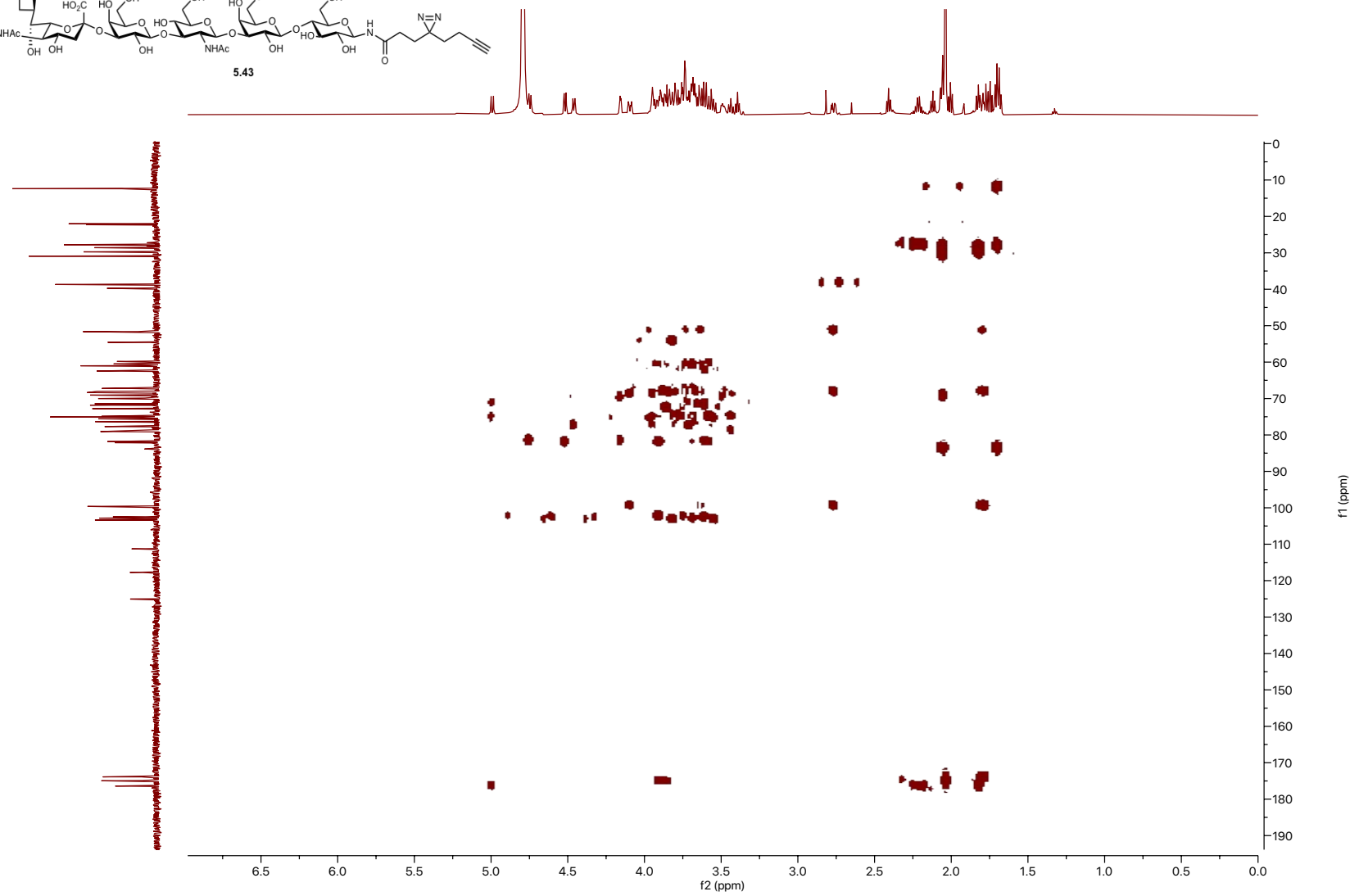
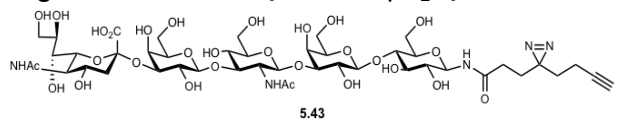


Figure A5.36 ¹H NMR (600 MHz, MeOD) of 5.44

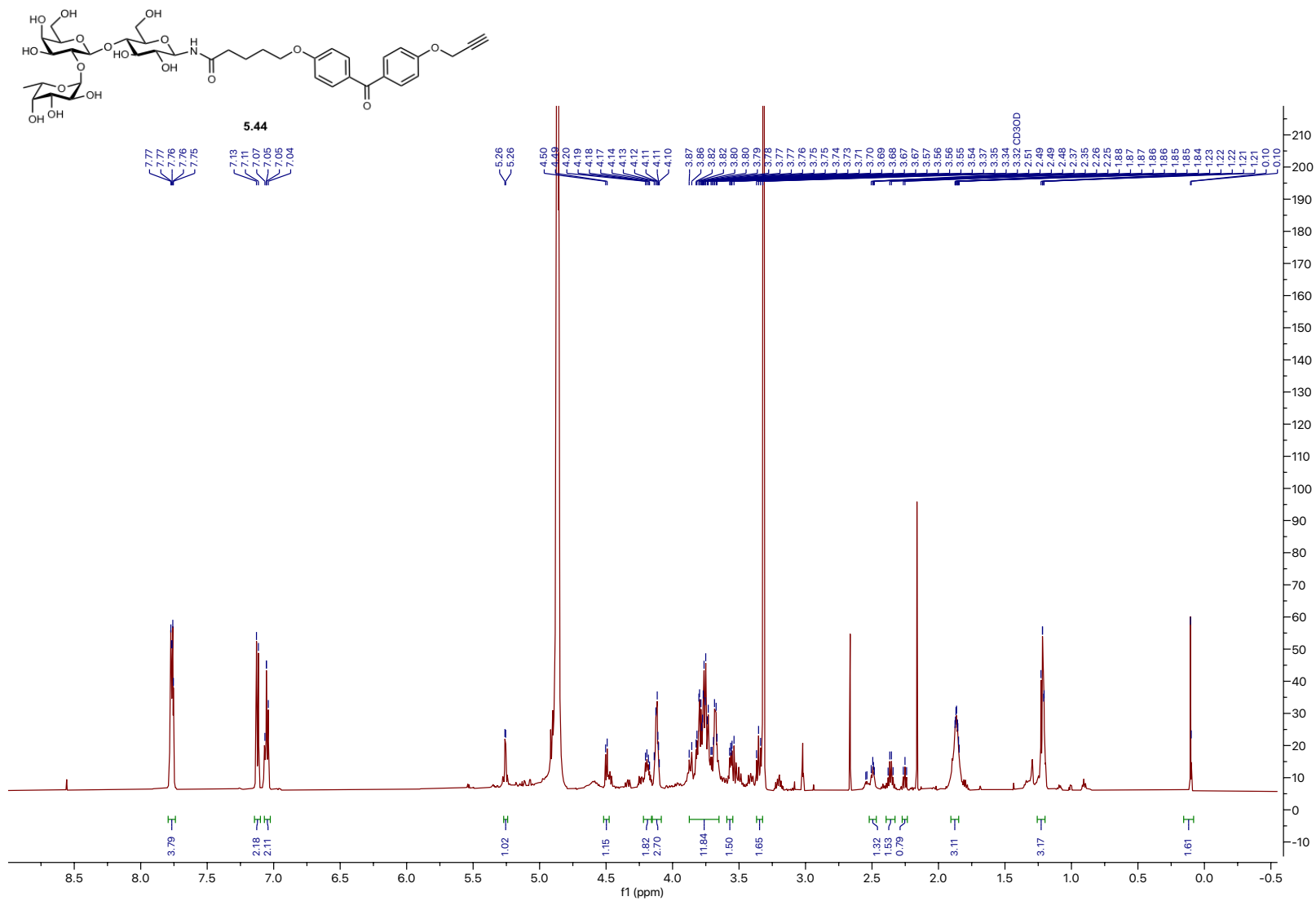


Figure A5.37 ¹³C NMR (151 MHz, MeOD) of 5.44

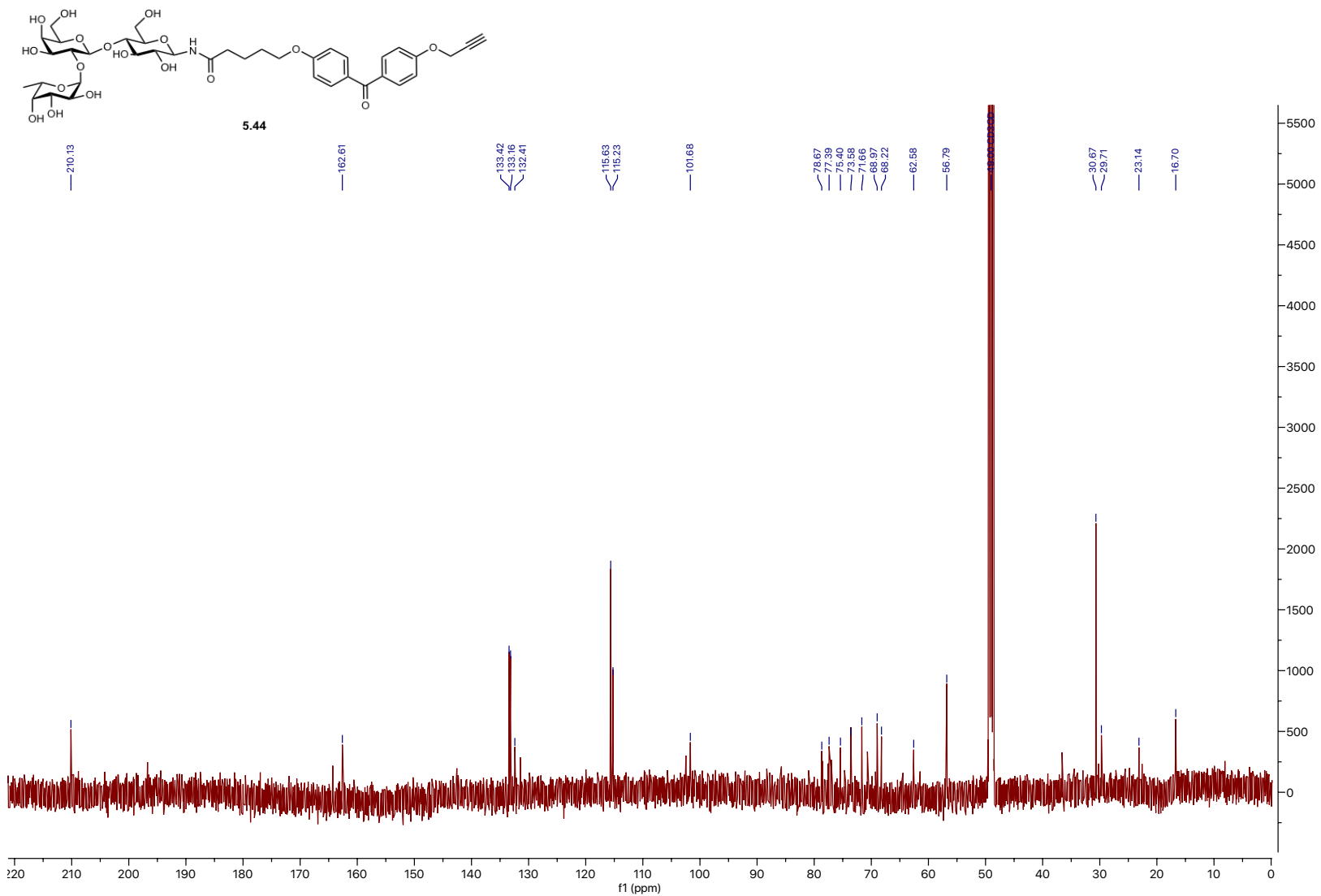


Figure A5.38 ¹H NMR (600 MHz, MeOD) of 5.45

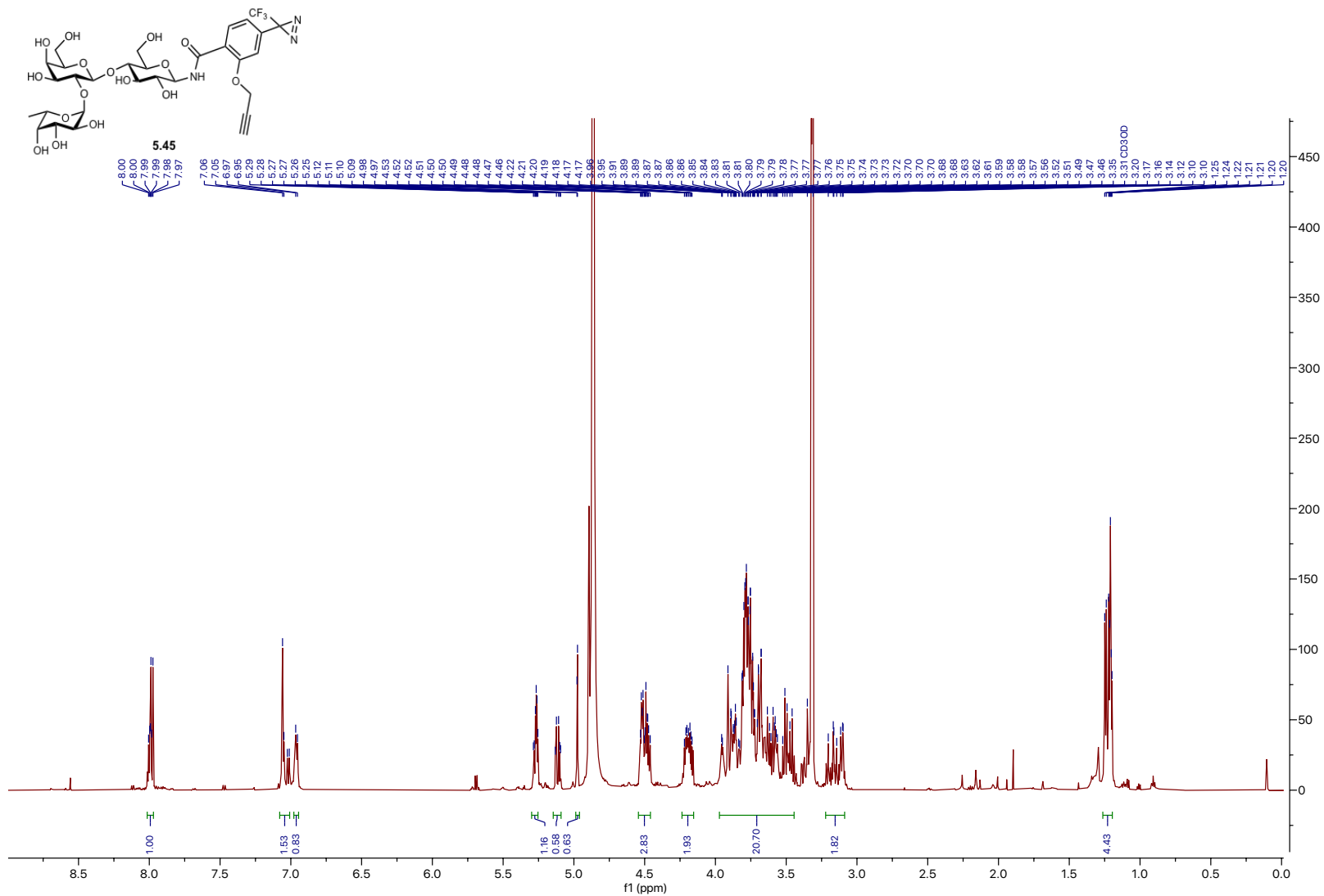


Figure A5.39 ¹³C NMR (151 MHz, MeOD) of 5.45

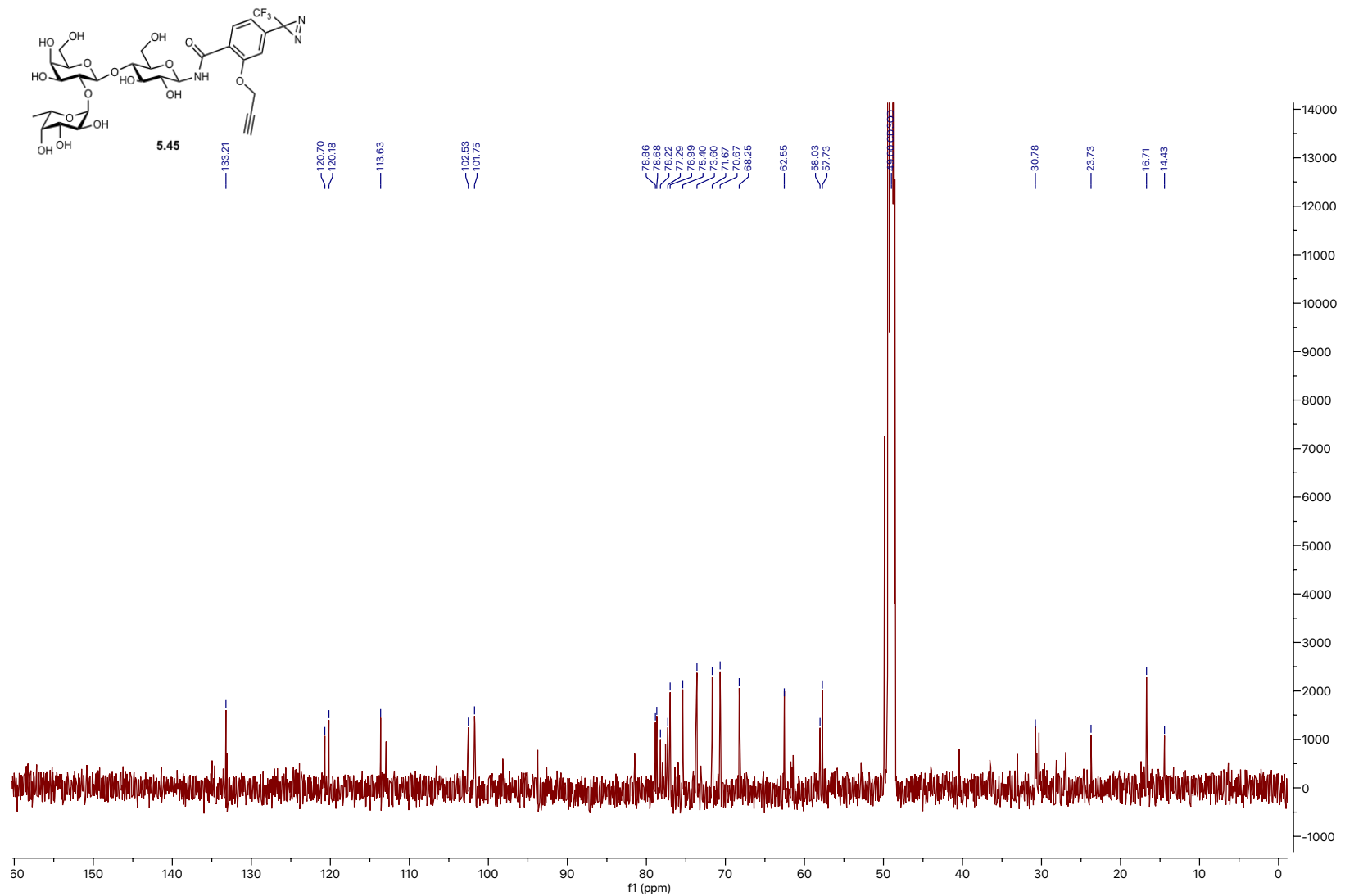


Figure A5.40 ¹H NMR (600 MHz, MeOD) of 5.46

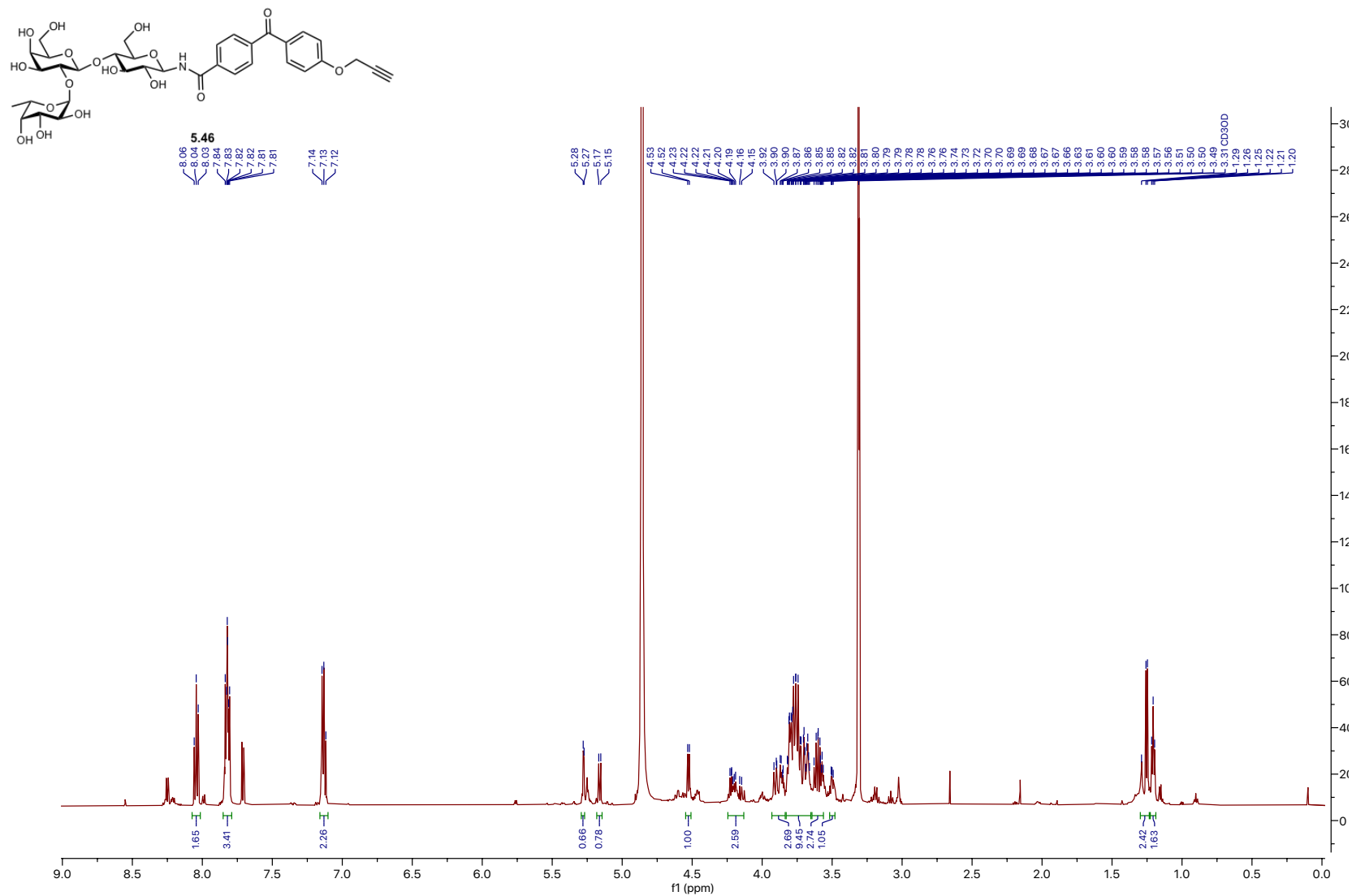


Figure A5.41 ¹³C NMR (151 MHz, MeOD) of 5.46

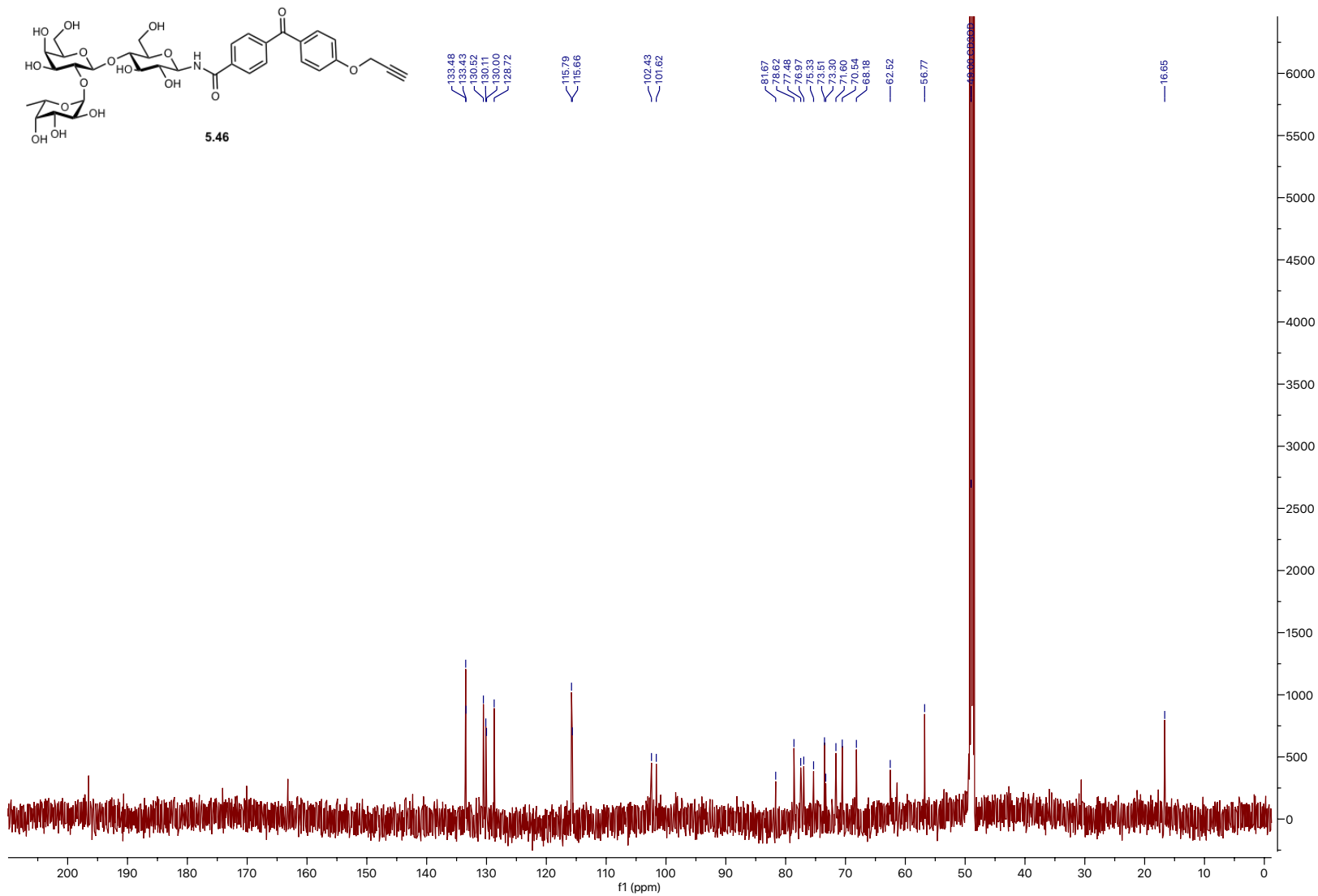


Figure A5.42 ¹H NMR (600 MHz, MeOD) of 5.47

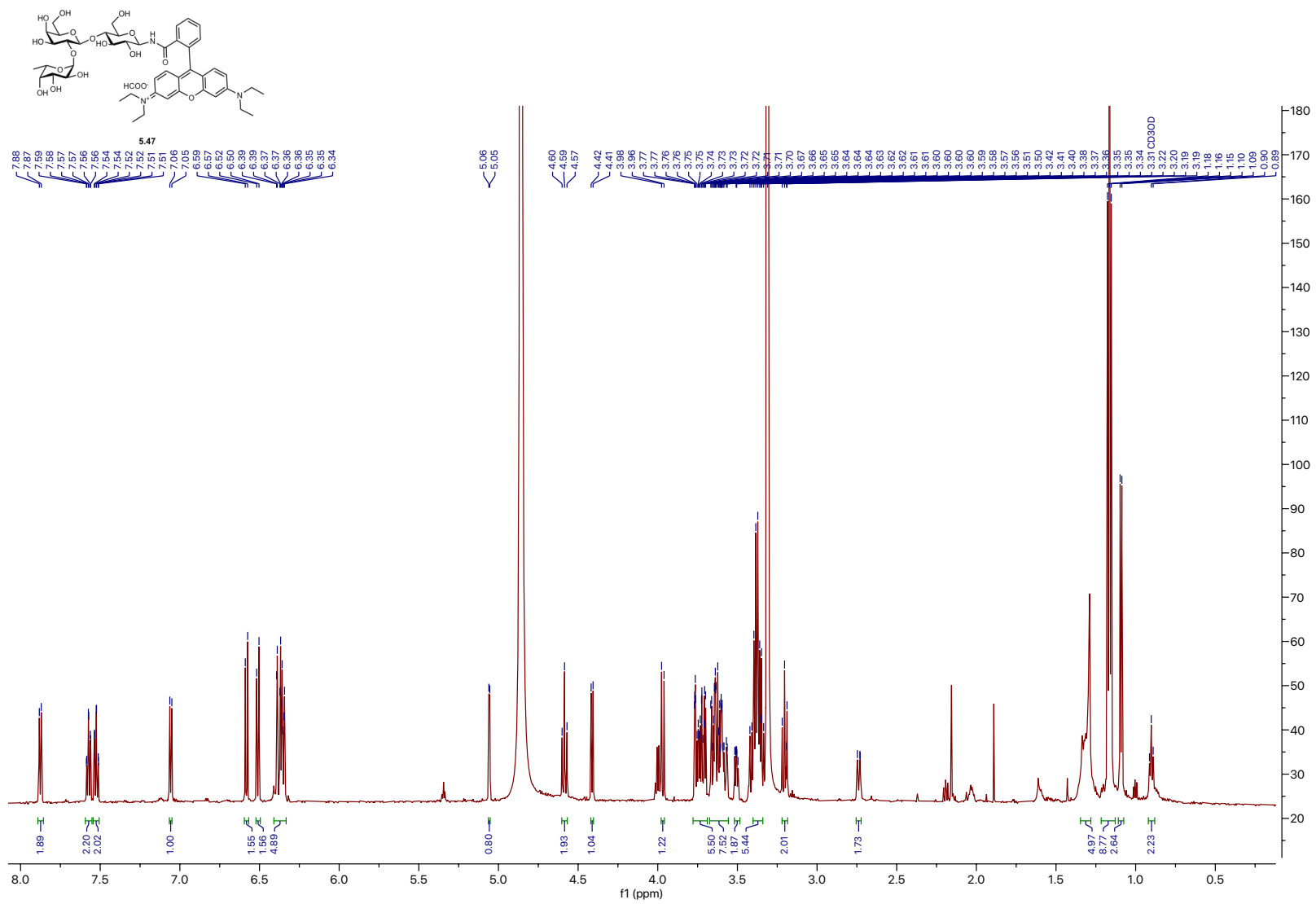
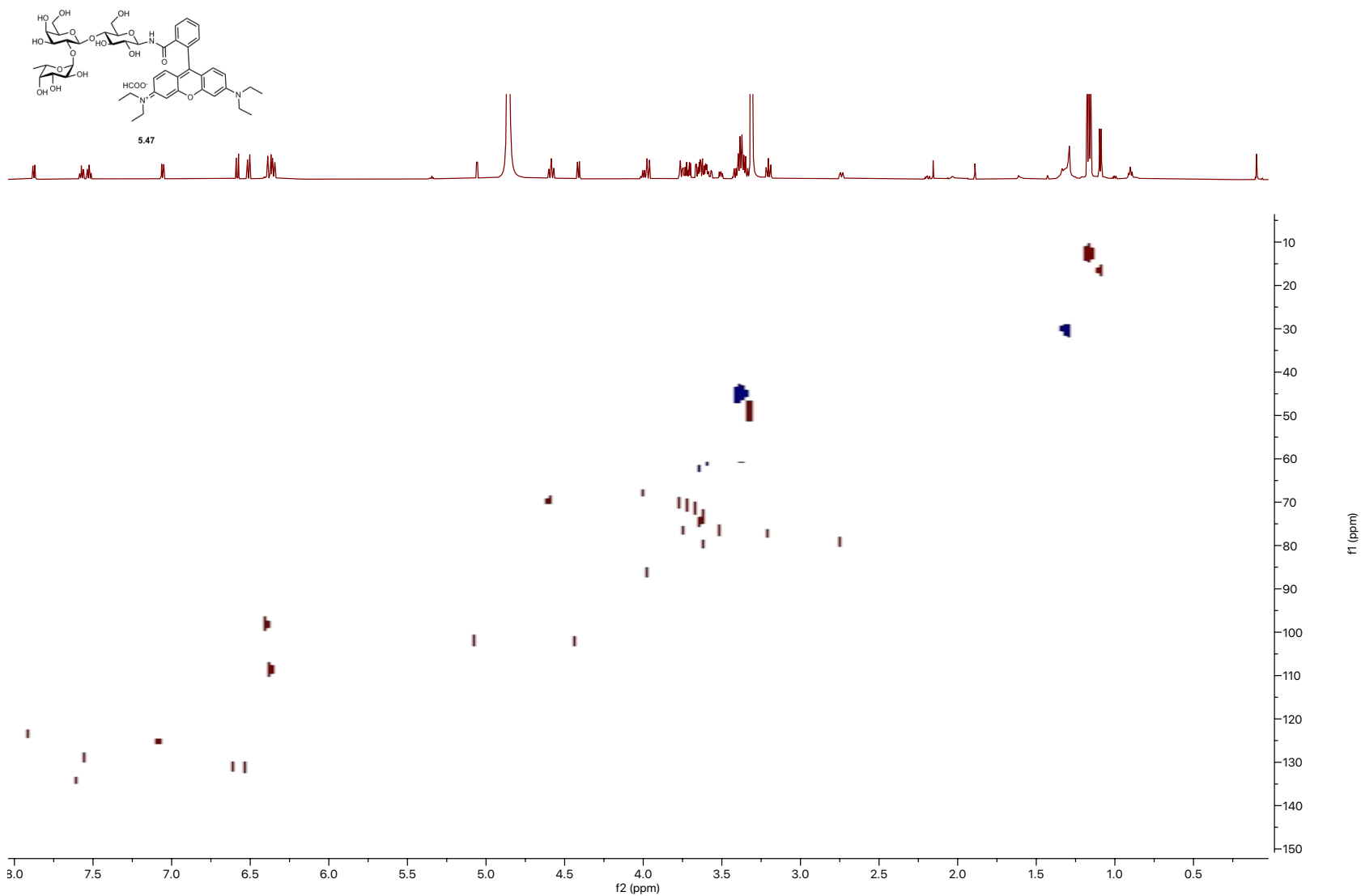


Figure A5.43 HSQC (600 MHz, MeOD) of 5.47



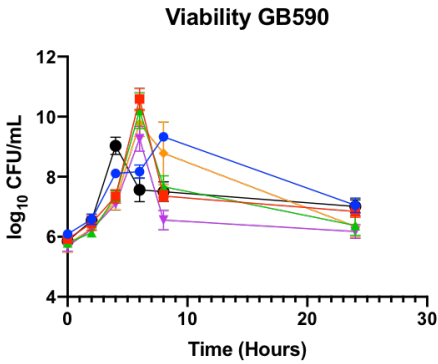
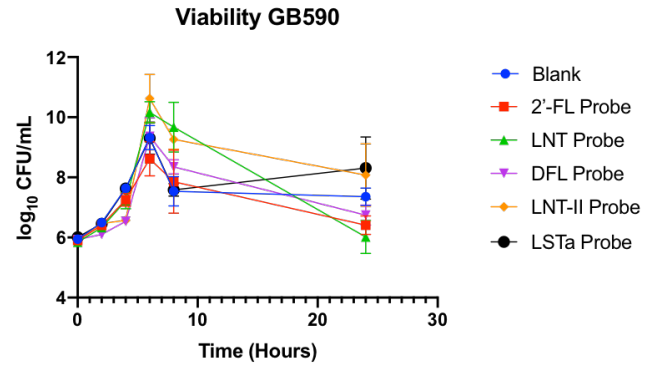
A.**B.**

Figure A5.44. Viability was assessed by enumeration of CFU mL⁻¹ performed at 0, 2, 4, 6, 8, and 24 h. Log₁₀ CFU mL⁻¹ for each HMO and time point are indicated by the corresponding symbols. **(A.)** Viability of GB590 (log₁₀ CFU mL⁻¹) corresponding to the OD values graphed in Figure 5.4A. **(B.)** Viability of GB590 (log₁₀ CFU mL⁻¹) corresponding to the OD values graphed in Figure 5.4B. Data displayed represent the mean log₁₀ CFU mL⁻¹ ± SEM of at least three independent experiments, each with three technical replicates.

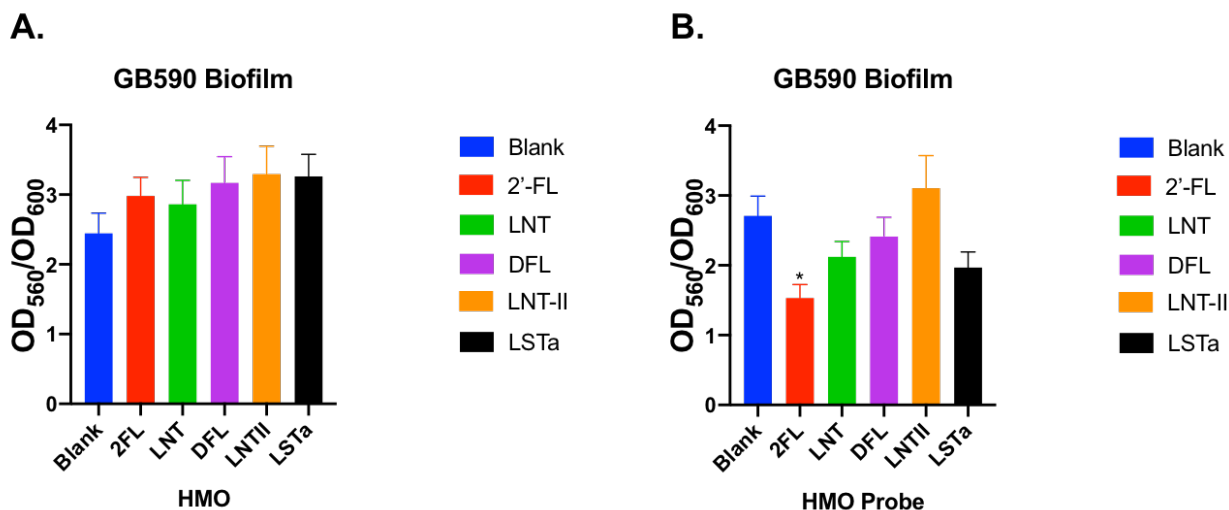


Figure A5.45. Effects of single-entity HMO and HMO probes at $\sim 5 \text{ mg mL}^{-1}$ on GBS biofilm production in THB after 24 h of growth. **(A.)** Biofilm production, denoted by the ratio of biofilm/biomass ($\text{OD}_{560}/\text{OD}_{600}$), by GB590 in the presence of single-entity HMOs relative to biofilm production in THB alone. Data displayed represent the relative mean biofilm/biomass ratio \pm SEM of at least three independent experiments, each with three technical replicates. **(B.)** Biofilm production, denoted by the ratio of biofilm/biomass ($\text{OD}_{560}/\text{OD}_{600}$), by GB590 in the presence of HMO probes relative to biofilm production in THB alone. Data displayed represent the relative mean biofilm/biomass ratio \pm SEM of at least three independent experiments, each with three technical replicates. * represents $p < 0.05$ by one-way ANOVA, $F = 3.140$ with post hoc Dunnett's multiple comparison test comparing biofilm production of GB590 in each HMO supplementation condition to biofilm production of GB590 in media alone.

Chapter 6

Summary: dissertation findings and future perspectives

This dissertation work has contributed to the discovery and development of new antibiotic interventions in the treatment and prevention of group B streptococcal infections. In **Chapter 1**, we introduce group B *Streptococcus* (GBS), the clinical burden associated with GBS infections, the virulence factors that contribute to pathogenicity, and current antibiotic strategies and limitations. Of significant importance, we highlight that current antibiotic interventions are losing efficacy due to the development of antibiotic resistance and other issues associated with antibiotic perturbation of the neonatal microbiome.

Chapter 2 details the synthesis and evaluation of ellagic acid glycosides as antibiofilm agents against GBS. We successfully synthesize three ellagic acid glycosides containing xylose, arabinose, and rhamnose residues. We identify that arabinosyl ellagic acid inhibits early adhesion mechanisms of GBS cells and prevents biofilm maturation. These findings indicate ellagic acid glycosides can be used to prevent GBS biofilm formation and decrease bacterial virulence.

In **Chapter 3** we identify that human milk oligosaccharides (HMOs) can be used to increase the antibiotic efficacy of clinically-relevant antibiotics. We demonstrated that HMO treatment can overcome antifolate resistance mechanisms of GBS and restore antibiotic efficacy of trimethoprim. We also show that the synergistic relationship between HMOs and trimethoprim is likely facilitated by the CovRS two-component signal transduction system. This work identifies HMOs as powerful molecules capable of overcoming antibiotic resistance mechanisms within GBS.

Chapter 4 interrogates the metabolomic changes induced in GBS upon treatment with HMOs. We discover that HMOs facilitate significant changes to lipid metabolites and specifically leads to the accumulation of glycerophospholipid metabolites. It is also shown that the recruitment of exogenous fatty acids is increased upon HMO treatment, indicating that HMOs likely inhibit the biosynthesis and assembly of cell membrane affiliated lipids. In **Chapter 5**, we design and synthesize a variety of bioorthogonal HMO tool molecules. We develop a two-step derivatization of unprotected HMOs that can be used to append bioorthogonal handles, such as diazirines, benzophenones, and fluorophores. These developments will enable chemoproteomic target identification studies to determine the biological targets of HMOs in GBS.

Together, this work has developed several novel antibiotic treatments and strategies for the prevention of GBS infections. While the molecules studied herein inhibit GBS growth and virulence, both ellagic acid glycosides and HMOs are prebiotics for other neonatal commensals. This dual activity identifies these compounds as potentially advantageous modulators of the infant microbiome and valuable scaffolds for continued research. Of particular importance, will be future identification of the bacterial targets of HMOs. It is my sincere hope that the work developed herein, will enable the discovery of the antibiotic mechanism of action of HMOs and propel future efforts towards bettering neonatal health and wellness through the prevention of GBS transmission.